MODELING HUMAN GENETIC KIDNEY MALFORMATIONS CAUSED BY *HNF1B* MUTATION USING PLURIPOTENT STEM CELLS

A thesis submitted to the University of Manchester for the degree of Doctor of Philosophy (PhD)
in the Faculty of Biology, Medicine and Health

2019

Tengku Muhamad Faris Syafiq

School of Biological Sciences

Division of Cell Matrix Biology & Regenerative Medicine

CONTENTS

Total word count: 57,454

LIST OF FIGURES

LIST OF TABLES

LIST OF ABBREVIATIONS

AQP1	Aquaporin 1
AQP2	Aquaporin 2
BMP4	Bone Morphogenetic Protein 4
BMP7	Bone Morphogenetic Protein 7
BRACHYURY	T, Brachyury Homolog
C-MYC	V-Myc Avian Myelocytomatosis Viral Oncogene Homolog
DAPI	4',6-diamidino-2-phenylindole
Dkk1	Dickkopf WNT Signaling Pathway Inhibitor 1
Dll1	Delta-Like 1
ECAD	Cadherin 1, Type 1, E-Cadherin
EYA1	Eyes Absent Homolog 1
EtV4	Ets Variant Gene 4 (E1A Enhancer-Binding Protein, E1AF)
FXYD2	FXYD Domain Containing Ion Transport Regulator 2
FGF8	Fibroblast Growth Factor 8
FOXD1	Forkhead Box Protein D1
GATA3	GATA Binding Protein 3
GDNF	Glial Cell Line Derived Neurotrophic Factor
HOXB7	Homeobox B7
HNF1A	Hepatocyte Nuclear Factor 1-Alpha
HNF1B	Hepatocyte Nuclear Factor 1-Beta
HOX11	T-Cell Leukemia Homeobox 1
JAG1	Jagged 1
KLF4	Kruppel-Like Factor 4
Lef1	Lymphoid Enhancer-Binding Factor 1
LHX1	Lim Homeodomain Transcription 1
Lmx1b	LIM Homeobox Transcription Factor 1, Beta
MIXL	Mix Paired-Like Homeobox
NANOG	Nanog Homeobox
Notch2	Neurogenic Locus Notch Homolog Protein 2
NPHS1	Nephrosis 1, Congenital, Finnish Type (Nephrin)
OSR1	Odd-skipped-related 1
OCT4	POU Class 5 Homeobox 1
PAX2	Paired Box 2
PBMC	Peripheral blood mononuclear cells
Pdgfr	Platelet-Derived Growth Factor Receptor
PODXL	Podocalyxin
PDGFrB	Platelet-Derived Growth Factor Receptor Beta Polypeptide
PKD1	Polycystic Kidney Disease 1 (Autosomal Dominant)
Ret	Receptor Tyrosine Kinase
RCAD	Renal cysts and diabetes syndrome
RTM	Renal tract malformations
SIX1	Sine Oculis Homeobox Homolog 1
SALL1	Spalt-Like Transcription Factor 1
SYNPO	Synaptopodin
Sox8	SRY (Sex Determining Region Y)-Box 8
Vegfa	Vascular Endothelial Growth Factor A
WNT9B	Wingless-Type MMTV Integration Site Family, Member 9B
WNT4	Wingless-Type MMTV

ABSTRACT

Some human renal tract malformations (RTMs) are caused by mutations of genes active during formation of the metanephric kidney, so these are direct outcomes of perturbed kidney differentiation. Indeed, classic dissections by Edith Potter, 60 years ago, showed human dysplastic kidney cysts are dilated segments of poorly branched collecting ducts derived from the ureteric bud (UB). How these genes drive specific stages of human kidney development is unclear. Moreover, the precise biological aberrations in human RTMs associated with defined mutations are unknown. Critically, for translational medicine, such insights would facilitate designing novel therapies to enhance differentiation. One can not necessarily extrapolate from animal studies (i.e. mouse or zebrafish) due to differences in metabolic pathways and drug metabolites that can lead to variation in efficacy and toxicity so human models are urgently required. Recently, several new pluripotent stem cell (PSCs) protocols have been developed to generate human cells of the major kidney lineages, generating nephrons and collecting tubule structures. These protocols have been refined in Professor Kimber's Laboratory (Takasato et al., 2016). Kidney disease is a major problem for health services, and so it may be possible to develop genetically defined RTM models using PSCs differentiated to kidney progenitors. Such model may be used to study pathobiology and design of new biological therapies. RTM patients with 'renal cysts and diabetes syndrome' (RCAD) caused by heterozygous hepatocyte nuclear factor 1-beta (HNF1B) mutations, identified by Professor Woolf, are ideal subjects for this research. HNF1B mutation can cause dysplastic kidney malformations containing poorly branched collecting ducts terminating in cysts, and lack of functional nephrons. I hypothesise that hPSCs carrying HNF1B mutation can be differentiated towards nephron progenitors *in vitro* expressing kidney transcriptional genes. These progenitors are expected to differentiate into a more complex 3D structure containing multiple cell types that can self-organise thereby can be used to recapitulate some morphological and functional aspect of the kidney as seen in the patient with cystic kidney disease. Towards this aim, I derived hiPSC lines from two siblings each born with bilateral cystic dysplastic kidneys and each harbouring heterozygous *HNF1B* mutation. I differentiated unaffected and mutant hiPSCs by inducing them to form kidney precursors over 7 days in 2D culture (CHIR99021 followed by FGF9/heparin), then pulsing them with CHIR99021 and maintaining them in 3D on transwells at an air-media interface for 18 days. Here, I reported that *de novo* generation of 3D kidney organoids *in vitro* via directed differentiation of HNF1B-derived iPSC lines resulted in lesser degree of structure complexity, increased diameter per organoid and lower expression of key kidney marker genes as compared to healthy organoids that contained epithelial nephron-like structures expressing markers of podocyte (WT1, NPHS1, NPHS2 and SYNPO) and surrounded by a Bowman space and capsule that resembles nephron *in vivo*. Deeper in the generated kidney organoid, I detected a variety of tubules, often $HNF1B^+/CDH1^+$ and $PAX2^+/CDH1^+$. Some were most likely to be in the ureteric bud/collecting duct lineage (e.g. $GATA3^+/CDH1^+$), while others were proximal tubules ($HNF1A^+/CUBN^+$) or loops of Henle ($UMOD^+$) in the nephron lineage. Functional assay on $CUBN^+$ proximal tubules revealed transporter capability to facilitate uptake of organic anion, 6CF but not cations, intracellularly in both HNF1B-affected and healthy organoids. Also, challenging organoids with cAMP has demonstrated tubule dilatation which is a normal feature in healthy organoids and the fact that it is severely decreased in HNF1B-affected organoids which indicated that those nephron tubules, although present, are lacking in functionality. To conclude, this research has partially proved the hypothesis that hPSCs can be utilised to study early kidney developmental program. The results has indicated phenotypic and functional aberrations in HNF1B-derived organoids that can be optimised in near future thereby making them appropriate models to study molecular and cellular pathobiology with a view to finding new therapies.

DECLARATION

No portion of the work referred to in the thesis has been submitted in support of an application for another degree or qualification of this or any other university or other institute of learning.

COPYRIGHT STATEMENT

i. The author of this thesis (including any appendices and/or schedules to this thesis) owns certain copyright or related rights in it (the "Copyright") and s/he has given The University of Manchester certain rights to use such Copyright, including for administrative purposes.

ii. Copies of this thesis, either in full or in extracts and whether in hard or electronic copy, may be made only in accordance with the Copyright, Designs and Patents Act 1988 (as amended) and regulations issued under it or, where appropriate, in accordance with licensing agreements which the University has from time to time. This page must form part of any such copies made.

iii. The ownership of certain Copyright, patents, designs, trademarks and other intellectual property (the "Intellectual Property") and any reproductions of copyright works in the thesis, for example graphs and tables ("Reproductions"), which may be described in this thesis, may not be owned by the author and may be owned by third parties. Such Intellectual Property and Reproductions cannot and must not be made available for use without the prior written permission of the owner(s) of the relevant Intellectual Property and/or Reproductions.

iv. Further information on the conditions under which disclosure, publication and commercialisation of this thesis, the Copyright and any Intellectual Property University IP Policy (see http://documents.manchester.ac.uk/display.aspx?DocID=24420, in any relevant Thesis restriction declarations deposited in the University Library, The University Library's regulations (see http://www.library.manchester.ac.uk/about/regulations/) and in The University's policy on Presentation of Theses.

DEDICATION

To my beloved mum, Khasia'ah Yaacob, my dad Tengku Zakaria

Best partner-in-parenting, my wife Nurzafirah Zamharir

Special gifts during my studies, Tengku Noah and Tengku Musa

ACKNOWLEDGEMENTS

The kidney, due to cellular complexities and functional diversities, has been regarded as the most remarkable organ in our body. To create a new kidney would be ambitiously challenging but a realistic vision. Through this scientific journey, there are several people needs to be acknowledged. I would like to express my heartiest appreciation to my supervisor, Prof Susan J Kimber, for nurturing me along this scientific exploration, infinite guidance and continually conveyed a spirit of adventure in regard to my research throughout these 49 months. Prof Adrian S Woolf for amazing support, HNF1B blood samples, analysis of immunological sections and ethical approval which without his persistent support and critical comments throughout 132 serial meetings, this thesis will not have been possible. I am grateful to my advisor Prof Rachel Lennon for her advices, suggestions and COL4A3 antibodies. Also, Dr Caroline Milner, my PG tutor for keeping me on track. I wish to express my sincere thanks to Dr Ioannis Bantounas, senior postdoc in the lab for continuous technical help since day one, optimising renal differentiation, characterisation of pluripotent stem cells and genomic DNA primer design. I am grateful to Dr Steven Woods for guiding me on derivation of induced pluripotent stem cell lines from human dermal fibroblast and venous blood samples. To Dr Sara Cuvertino who assisted me on protein extraction and Sendai virus PCR. To Dr Chris Smith for statistical analysis and proofreading, Dr Phil Lewis for his help on the karyotyping analysis of MAN13 and LV-MAN13 lines, and Dr Edina Silajdzic for pluripotency assessment by flow cytometry. I am indebted to Nicola Bates for karyotyping, iPSC passaging, feedings and her precise yet concise advices on technical issues regarding cell cultures. To Qi Wang for purchasing chemicals, reagents and providing necessary facilities. To fellow colleagues from Renal biology group, Dr Parisa Ranjzad for immunostainings of E14 kidney sections and TRPV5 antibodies, Dr Neil Roberts for training on immunohistochemistry, Filipa Lopes for providing me the wild type CD-1 E14 and E15 fetal mouse kidneys, Dr Emma Hilton and Karl Chopra for their assistance during kidneys dissections. Also, to Dr Jila Adjeian for her kindness sharing SeV primers. Not to forget the Core Technology facilities staffs from Bioimaging unit, Dr Steven Marsden for guiding me using widefield and inverted confocal microscope. Dr Peter March for image processing and Dr Roger Meadows for panaromic slide scanning. To Histology unit, Dr Peter Walker and Grace Bako for assisting me during processing and sectioning of paraffin-embedded mouse kidneys. Thanks also go to phenomenal PhD students, Paweena Uppanan, Paul Humpreys, Maribel Montufar, Julietta O'Flaherty, Miguel Ferreira, Mark Naven, Erum Hayder, Kirsty Rooney and essentially all Kimber lab members (2015-present). I would like to thank Doctoral Academy especially Christine Burns, for scholarship and visa matters. Thanks to Kidney Research UK, Medical Research Council and Kidneys for life, for funding the project. I would also like to acknowledge Malaysian Ministry of Higher Education and Department of Basic Medical Sciences, Kulliyyah of Nursing, International Islamic University Malaysia for granting the fellowships. As always, special thanks to my parents, wife, my little one, Noah and siblings for their unconditional love and obvious compassion. It would be impossible to complete this thesis without their unceasing love and encouragements. Thanks a lot (more).

Chapter 1 Introduction

1.1 General overview

Kidneys are essential excretory organs that are involved in the regulation of fluid and acid-base balance, osmolarity, pH, filtration of blood and excretion of waste products. Unlike the mature mouse kidney that contains ~13,000 nephrons, each human kidney comprises 0.2-1.8 million of nephrons (Cullen-Mcewen et al., 2003; Hughson et al., 2003; Yu et al., 2007). The nephron consists of filtering glomerulus and segments (i.e proximal tubule, loop of Henle and distal tubule) that perform specialised functions in transporting glucose and solutes, and regulation of acid-base balance (Heliot et al., 2013) whereas the collecting duct (CD) further controls pH, reclaims free water and drains the urine into the renal pelvis. Human RTMs involve under the development of kidney with absent or abnormal nephrons and CDs structures. Underdeveloped kidney morphology during early embryogenesis has been commonly associated with numerous congenital renal phenotypes includeing renal dysplasia. HNF1β, a homeobox-containing transcription factor, controls normal kidney development. Heterozygous mutations of *HNF1B* are the most common known monogenic cause of human RTMs (Madariaga et al., 2013; Thomas et al., 2011). In normal human embryonic kidneys, *HNF1B* transcripts are prominently expressed in UB branches differentiating into CDs and, at a lower level, in nephron precursor epithelia (Kolatsi-Joannou et al., 2001). The former observation is consistent with Potter's observation that CDs is the key lineage involved in dysplastic pathogenesis (Potter, 1972). In mice CDs, genetic deletion of *Hnf1b* is cystogenic (Gresh et al., 2004). These *Hnf1b* mutant mice, however, lack the profoundly abnormal early kidney development which characterises human renal dysplasia, so human *HNF1B* mutant cells probably have additional aberrations of further signalling pathways operating in UB differentiation (Woolf and Davies, 2012).

Marked differences between human and other species suggest that the morphogenesis and molecular events in kidney development may differ although several developmental key genes may be expressed and functions in similar ways. Understanding of cellular and molecular pathways in kidney development will provide means of improved diagnostics of people with renal anomalies and in the treatment of RTMs especially in child. Current advances in stem cell research have provided new avenues to construct disease model, manipulate and target faulty genes. Differentiation of human pluripotent stem cells (hPSCs) to kidney lineages is of urgent importance to better understand how mutations cause RTMs. The current breakthrough in genome editing through innovation of novel genome 'scissor', the CRISPR/Cas system, makes it possible for precise gene targeting for various purposes

including deletion, silencing, substitution and mutation of gene construct. Hence, I will use an *in vitro* RTM model to better understand normal and abnormal kidney development and mechanisms of how mutations in *HNF1B* may cause RTMs.

1.2 Development of the human kidney

Kidney development is a multi-stage process that involves complex interactions between epithelial and mesenchymal cells which give rises to coordinated growth and differentiation of highly specialized vascular, stromal and epithelial cell types. Kidney development begins with derivation of intermediate mesoderm (layer of mammalian embryo that formed during gastrulation) followed by MET (i.e. nephrogenesis) and branching morphogenesis (Pope et al., 1999). Generally, kidney development can be divided into five main stages; the primary UB, the cap mesenchyme (CM), mesenchymal-epithelial transition or MET (developmental process that determine cell fate), glomerulogenesis and tubulogenesis and the interstitial cells (Faa et al., 2012). From anatomical view, the nephrogenic cords, intermediate mesoderm and the lateral plate mesoderm, establish the basis of the genitourinary system and sequentially direct formation of three successive excretory systems; the pronephros, mesonephros, and metanephros (Woolf and Jenkins, 2006).

The human pronephros, the initial anlage from the most rostral part of nephrogenic cord, consists of few rudimentary tubules. During its degenerations, the pronephric duct remains and survives as the mesonephric duct (Wolffian duct). The human mesonephros begins to develop from day 24 of gestation and grows to form the urogenital ridge that bulges into the coelomic cavity. Formation of vesicle-like structures give rise to primitive nephrons with glomeruli. At this stage, the nephron units resemble those in metanephros but without a loop of Henle (Woolf and Jenkins, 2006). The mesonephric tubules involute by the end of the first trimester, with some residual remnants (Harding et al., 2011). In males, remnants of caudal mesonephric tubules develop as efferent ducts of epididymis, whereas in female, the whole mesonephros degenerates (during third month of gestation) except for few vestigial and inconstant structures such as epoophoron, paroophoron and Gartner duct. Both the transitory pronephros and mesonephros involute prior formation of the permanent kidney, the metanephros (Woolf and Jenkins, 2006).

The human metanephros, on the other hand, can be divided into two major parts; the metanephric mesenchyme (MM) and UB. The MM is located dorsally and immediately adjacent to the caudal end of the mesonephric duct. During nephrogenesis, this mesenchyme differentiates into nephrons each of which contains a glomerulus, proximal tubule, loop of Henle and a distal tubules (Harding et al., 2011). The UB branches from the mesonephric duct and then serially bifurcates into

UB tips. This lineage forms the CDs, renal pelvis and ureter which collect urine from the nephrons (Costantini and Kopan, 2010; Woolf and Jenkins, 2006). The human metanephros appears at five weeks of gestation (Bayley and Hunt, 1974). The UB/MM interactions mark the initial development of the mature kidney. Perturbations in signals governing these primary interactions lead to renal agenesis (Boyden, 1932; Gruenwald, 1939), dysplastic and hypoplastic RTMs (Woolf et al., 2004). Figure 1.1 shows schematic embryonic development of three successive excretory systems in mouse kidney relative to human.

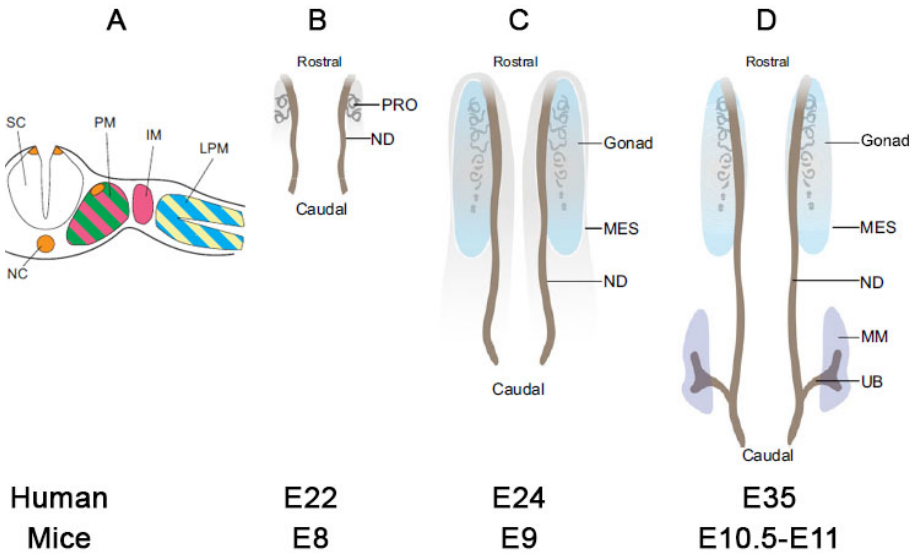

Figure 1.1 Derivatives of intermediate mesoderm. (A) Cross-section of the mammalian embryo. The kidney arises from the intermediate mesoderm (IM), between the lateral plate mesoderm (LPM) and paraxial mesoderm (PM) (B) Pronephros (PRO) stage: The nephric duct (ND) is apparent at E22 (or E8 in mice) which extends caudally by proliferation and extension. This rudimentary PRO regresses and survives as mesonephric tubules (C) At 24th day of gestation (or 9th day in mice), mesonephric (MES) tubules reaches the cloaca with more developed mid-thoracic region, vascularized glomeruli and convoluted tubules draining into ND. (D) Primary ureteric bud (UB) branches off Wolffian duct at the posterior end and invades adjacent metanephric mesenchyme (MM) that flanks the nephric duct caudally. UB bifurcates into several branches (UB tips) that induce formation of condensed mesenchyme surrounding them. Abbreviations: E, embryonic stage (days after gestation); NC, notochord; SC, spinal cord (Takasato et al., 2015).

At day 28 of human gestation, the primary UB arises from the posterior end of mesonephric duct. This UB progressively bifurcates into UB tips after invading the MM, thus inducing the nephron formation (Watanabe and Costantini, 2004; Yosypiv, 2008). Further maturation of these branches will then give rise to CDs, renal pelvis and ureter (Reidy and Rosenblum, 2009). Once the UB invades MM, it provides a permissive signal that stimulates the condensation and aggregation of metanephric mesenchymal cells around the UB tips forming cap mesenchyme (CM). This CM undergoes MET of mesenchymal cells and lumen formation to form epithelia of the nephron (Carroll et al., 2005; Sariola, 2002; Stark et al., 1994).

Further development of the nephron can be divided into four main stages; Stage I, renal vesicle transformation from pretubular aggregates (PTA); Stage II, comma- and S-shaped bodies; Stage III, capillary loops and Stage IV, maturing nephrons. In

humans, nephrogenesis ceases at 34-36 weeks of gestation (anatomically equivalent to 14th days of postnatal in mouse). In the first stage, the mesenchymal cells of self-renewing CM progenitors form PTA *via* MET that differentiate into a roundish epithelial structures each with a central lumen called the renal vesicle (RV). In the second stage, the RV extends towards UB epithelium and then progressively segments into a comma-shaped body (CSB) divided into a proximal and a distal segment. Later, regionalised S-shaped bodies (SSB) are formed and organised distally to give rise to early distal tubule; medially to form immature loop of Henle (LOH) and the proximal tubule that consists of parietal (Bowman's capsule) and visceral (podocyte) layers (Hartman et al., 2007; Heliot et al., 2013). In the third stage, which is the capillary loop stage, glomerular capillary and presumptive endothelial of renal corpuscle are generated (Ferraz et al., 2008). The final mature nephron stage involves the differentiation of glomerulus, podocytes and capsules, and tubular segments such as proximal tubules, LOH and distal tubules. Appearance of juxtaglomerular complex components (such as mesangium, macula densa and the juxtaglomerular apparatus in the afferent arteriole) and differentiation of interstitial cells (into cortical, medullary, nephrogenic zone interstitium and perihilar) are observed at this stage (Little et al., 2007). In humans, the whole process finishes around 34 weeks of gestation (Potter, 1972). Figure 1.2 illustrated the development of kidney using the mouse as a simple mammalian model.

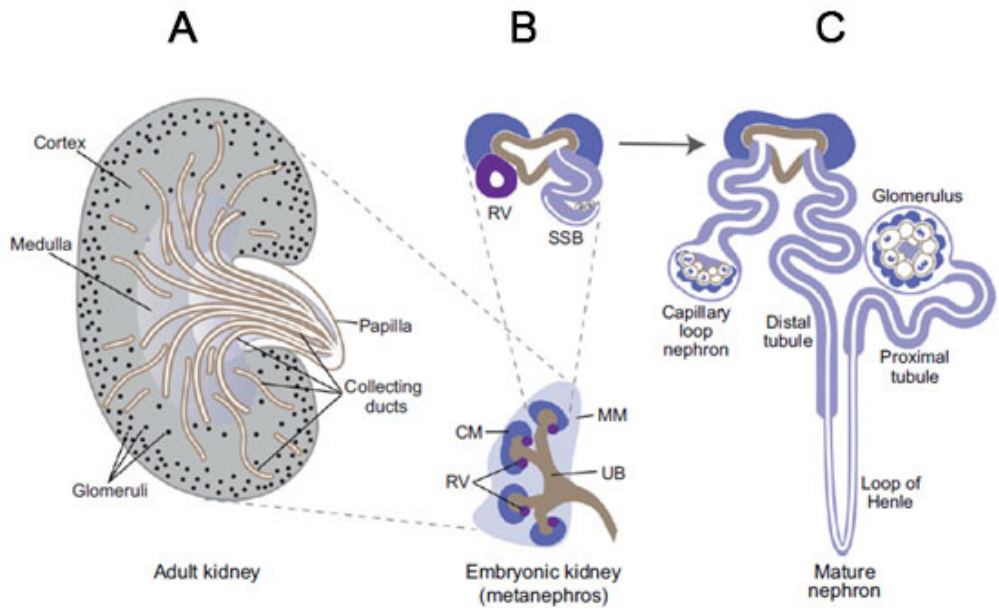

Figure 1.2 The developing kidney in mouse model. (A) The adult kidney matures with distinct structures of glomeruli-containing cortex, medulla and papilla which drains the collecting ducts (B) Ureteric bud (UB, in brown) branches and interact with the metanephric mesenchyme (MM, in light blue). Mesenchymal cells surrounding UB tips forms the cap mesenchyme (CM, dark blue). This CM differentiates into renal vesicle (RV, in purple) *via* mesenchymal-to-epithelial transition. The RVs elongates and undergo segmentation to comma-shaped (CSB, not shown) and S-shaped bodies (SSB). (C) Further elongation forms the capillary loop of nephron before development of more complex structures of mature nephrons (Takasato and Little, 2015).

1.3 Molecular mechanisms of human kidney development

Several studies have been carried out to determine the key molecular players during normal kidney development in human and other species (i.e rodents, *Xenopus*, zebrafish, chicks and Drosophila spp). This section aims to discuss the molecular pathways governing kidney organogenesis in human and related genes from other species. Highly coordinated growth and differentiation of specialized cell types (i.e epithelial, vascular and stromal) begin with the complex signalling cascade between mesenchymal and epithelial cells. The regulation of key genes in generation of the kidney can be divided into six main checkpoints namely; (i) intermediate mesoderm (IM) (ii) the branching of primary UB; (iii) the invasion of MM and CM formation; (vi) the MET; (v) the nephron maturation into tubules and glomeruli; and (vi) the formation of interstitium.

The Osr1 transcription factor is the principal cellular regulator in the intermediate mesoderm (IM) that regulates *Osr*$^{+}$ cells such as nephron, vascular and interstitial cell, and nephric duct. These cellular components form the basis of metanephric kidney (Mugford et al., 2008). The IM is also characterized by the expression of *Lhx1, Pax2* and *Gata3* (Barnes et al., 1994; Dressler, 2009). *Pax2* and *Gata3* acts downstream (β-catenin signalling), relative to *Osr1* expression, to give rise to the UB and prevents ectopic induction of metanephric kidney (Torres et al., 1995) whereas *Lhx1* directs caudal extension and the duct development (Tsang et al., 2000).

In humans, the first branching of UB begins at 28th day of gestation. Elongation and bifurcation are regulated by multiple inducers such as *PAX2, PAX8, Ret, GDNF, SOX8, SOX9, EtV4, EtV5, Wnt11,* Angiotensin II, *FGF8*, p53, *AT1R, AT2R, FGFR1, FGFR2, MMP-9,* Cofilin I and Destrin, whereas UB growth is inhibited by *Spry1, FoxC1, FoxC2, BMP4, Slit2, Robo2* and Class 3 semaphorins (Yosypiv, 2008). GDNF/c-Ret/Wnt1 pathways establish the primary signalling pathways in UB development. GDNF secretion by MM is controlled by PAX2, whereas SOX genes (SOX8/9) are the key players in controlling c-RET signalling. Knockout of both GDNF and RET in mice has implicated in inhibition of UB development and renal hypoplasia (and agenesis), respectively (Brophy et al., 2001). PAX2/PAX8 expression are critical during early nephric duct development, morphogenesis and maintenance of nephron progenitors' survival during nephrogenesis (Benetti et al., 2007; Grote et al., 2006). FGF receptors (FGFRs) promote UB development, and impaired FGF signalling will result in UB elongation, renal agenesis, dysgenetic effects and cysts formation (Hains et al., 2008).

In the MM, expression of *Osr1, Wt1, HOX* genes (*Hoxa11, Hoxc11 and Hoxd11*), *Sall1, Six1* and *Eya1* are evident. Of these, *Osr1*, *Six1, Eya1* and *Hox11* paralogs

specify MM cell fates from the IM (Wellik et al., 2002) whereas *Wt1* within IM functions in the early MM development (Kreidberg et al., 1993). *Sall1, Eya1* and *Six1* determines metanephric specification and function, particularly during early cell interaction that leads to UB bifurcations (Sato et al., 2003). Sall1, a zinc finger protein is crucial during invasion of UB into the MM and are constitutively expressed in MM by renal progenitors, when stimulated by Wnt4 (Nishinakamura, 2003). Knockout of *Sall1* in mice promotes renal agenesis (Nishinakamura and Takasato, 2005). These Sall1-expressing renal progenitor cells are also mediated by *Six2* expression that maintains the progenitor state, and *Six2* knockout leads to premature differentiation of mesenchymal cells into epithelia, reduced MM precursors and renal hypoplasia (Self et al., 2006). *Pax2* and *Wnt4* drive the differentiation of MM into CM with the former are of highly importance in the UB branching and also expressed in condensed mesenchyme and RV (Batchelder et al., 2009). Wnt9b, induces formation of MM and promotes *in vitro* mesenchymal aggregation but does not affect the UB branching (Carroll et al., 2005; Park et al., 2007). Undifferentiated mesenchymal cells of MM give rise to stromal cells that express Foxd1 *via* non-nephron lineage. The upregulation of *Foxd1*$^{+}$ cells leads to formation of self-renewing progenitors of medullary interstitium, RV, mesangial cells and pericytes (Kobayashi et al., 2008). Figure 1.3 illustrates the lineage relationship of intermediate mesoderm derivatives and the mammalian metanephros.

During MET, disordered spindle-shaped mesenchymal cells are transformed into organized epithelial structures. This process evident in the CM surrounding UB tips. Mesenchymal cells of MM condensate and form aggregates of CM that express Wnt4 signalling molecules whereas some other mesenchymal cells remain gives rise to stromal lineage. Wnt4 drives the transformation of CM to polarized epithelial cells *via* formation of RV (Stark et al., 1994). The stromal cells that express genes outside CM such as *Foxd1*, retinoic acid receptor (RAR) and transcription factor Tcf21 (also known as Pod1) also facilitate MET through promotion of epithelial cell proliferation and survival (Dudley et al., 1999; Hatini et al., 1996). Additional signalling, such as *Fgf8* and *Bmp7,* maintains mesenchymal polarization and prevention of apoptosis in CM in the nephrogenic zone (Grieshammer et al., 2005). In RV, *Lhx1*, *Papss2, Greb1, Pcsk1* and *Pou3f3* are apparent in the distal region, whereas *Wt1* and *Tmem100* are expressed more proximally. Genes that are expressed distally, such as Notch (*Jag1, Dll1*), Wnt (*Wnt4, Lef1, Dkk1*) and *Bmp2,* determine cellular activity and identity throughout the distal-proximal axis (Georgas et al., 2009; Dressler et al., 2006; Mugford et al., 2009). For instance, *Lhx1* involved in the nephron patterning of distal tubules whereas *Notch2* determines its proximal fates (the proximal tubules epithelium and podocyte) (Cheng et al. 2007; Kobayashi et al. 2005).

At the stage of CSB, E-cadherin (*Cdh1*) and cadherin-6 adhesion molecules are also prominent which marked the segmentation of tubules to proximal and distal fates. Also, at this stage, CSB expressed *Foxc2*, the podocyte-specific gene. At SSB stage, further differentiation separates epithelial cell morphology to parietal layer of Bowman's capsule and podocyte-containing visceral epithelium which is marked by expression of *Podx1, Nphs1, Nphs2* and *Lmx1b* (Takemoto et al. 2006). The capillary bed that surrounds the glomeruli expresses *Vegfa* which attracts angioblast from the interstitium (Eremina et al. 2003). Continuous expression of *Vegfa* with Wt1 maintains podocyte's structure. In podocytes, *Bmp4* and *PdgfB/Pdgfrb* pathway promotes glomeruli development and mesangial cell recruitment, respectively (Lindahl et al. 1998; Ueda et al. 2008). Thus, regulation of multiple gene networks across kidney development are essential for the establishment of a functioning nephron. Perturbations in any of these signals may impede normal cellular growth, successive MM invasion, MET, UB branching ability, nephron patterning and overall structural organization. Table 1.1 summarizes the genes involved in the early stage of kidney development.

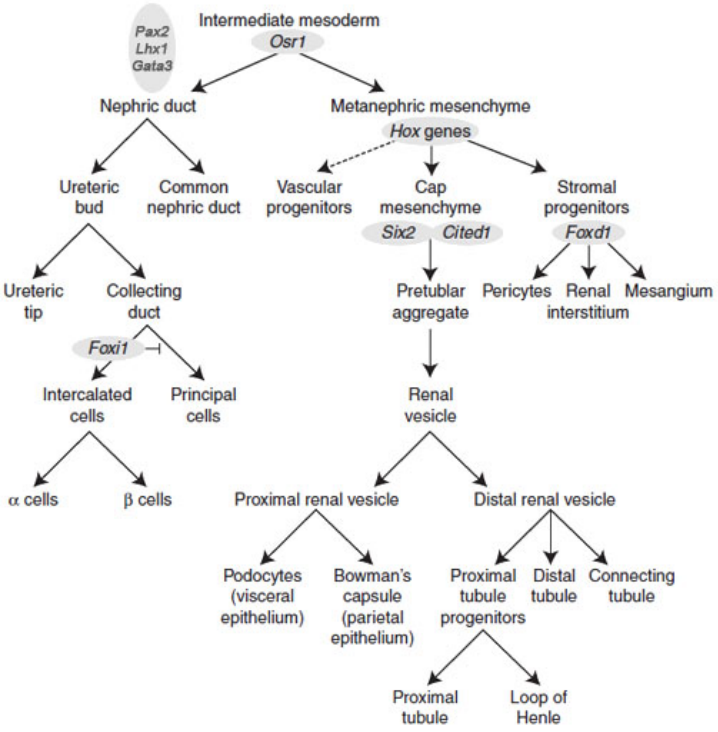

Figure 1.3 Developing metanephric kidneys from intermediate mesoderm. The intermediate mesoderm is derived from the posterior primitive streak after gastrulation. Intermediate mesoderm develops into two distinct structures, the metanephric mesenchyme and nephric duct. Metanephric mesenchyme forms the excretory components (nephrons) whereas nephric duct further develops into drainage systems consisting collecting duct and the ureter. Establishment of interaction framework by *Osr*+ IM derivatives give rise to *Pax2*$^{+}$, *Lhx1*$^{+}$ and *Gata3*$^{+}$ nephric ducts. Ureteric bud branching depend on *Six2*$^{+}$ and *Cited1*$^{+}$ MM induction that further forms the RV. *Foxd1*$^{+}$ MM subcompartments develop into pericytes and mesangial cells. The *Flk*+ *(Kdr/Vegfr2*) cells of MM promote vascularization and maintain ureteric bud outgrowth (Little and Mcmahon, 2012).

Regulation of gene expression by micro RNAs (miRNA) also plays an indispensable role during early kidney development. miRNA are referred to endogenous short non-coding RNA that consists of 21-25 nucleotides which alters post-transcriptional activity by binding to 3' –untranslated region (UTR) of target mRNA to inhibit/activate protein translation. miRNA functions in renal development, physiological functions and homeostasis (Kawahara, 2014; Q. Wei et al., 2013). miRNAs such as mir-23b, mir-24, mir-26a and mir-30 family has been associated with several kidney phenotypes. miR-10a, miR-106b and miR-17-5p had found to protect nephron progenitors of CM *via* downregulation of Bim, a pro-apoptotic protein thus reducing the amount of nephron death at birth (Ho et al., 2010). In mice, knockout of Dicer, an RNase III type enzyme, has found to implicate developmental phenotypes. For instance, Dicer inactivation in podocytes cause foot process effacement, glomerulosclerosis, proteinuria and tubulointerstitial fibrosis at 2-4 weeks after birth and leads to fatality due to severe renal failure (Harvey et al., 2008; Ho et al., 2008; Shi et al., 2008).

Similarly, Drosha deletion (a RNase III-like protein) leads to collapsing glomerulopathy, indicating crucial regulatory function of miRNA in normal kidney component development (Zhdanova et al., 2011). miRNA has been found to modulate expression profiles of RTM-associated genes. For instance, alteration in mir-17 that regulates anti-cystic genes, the PKD1 and PKD2, has been linked to autosomal dominant polycystic kidneys (Sun et al., 2010). In a *PKD* mouse model, deletion of mir-17-92 in renal tubules retarded cyst development (Patel et al., 2013). Loss of heterozygosity (heterozygous deletion alone is sufficient to promote tumor) of mir-562 has been linked to *Wilms* tumor (Drake et al., 2009). Aberrant mir-330 and mir-125b-5p regulation fails to maintain smooth muscle phenotype in juxtaglomerular cells (Medrano et al., 2012). Thus, understanding of functional regulatory roles of miRNAs, its biogenesis and expressions in renal tubules is of importance in determining its implications on RTMs.

Table 1.1 Genes that regulate early stage in kidney development in mammals (Dressler, 2009).

Gene	Expression	Mutant phenotype (knockout)
Early mesodermal regionalization		
Osr1	LPM, IM	Posterior nephric structures fail to develop
Lhx1	LPM, ND	No nephric duct, no kidneys
Pax2	IM, ND	No mesonephric tubules, no metanephros
Pax2/Pax8	IM	No nephric duct, no kidneys
UB formation		
c-Ret	UB	Block development of UB, no branching
GDNF	UB	Renal hypoplasia or agenesis
PAX2	UB	Apoptosis in UB tips; aberrant nephron regeneration
FGFR1, FGFR2	UB	Embryonic lethal, dysgenetic effects, cysts, no UB elongation, agenesis
Metanephric development		
Wt1	IM, MM	Fewer mesonephric tubules, apoptosis of mesenchyme
Foxd1	MM, SC	Developmental arrest, few nephrons, limited branching
Hoxa11 , Hoxd11	MM	No metanephros
Eya1	MM	No induction of mesenchyme
Six1	MM	No UB, no induction
Six2	MM, CM	Premature differentiation of CM, no self-renewal
Sall1	MM UB	invasion but no branching, no induction
Wnt9b	UB	Failure to induce the MM
Nephron patterning		
Wnt4	CM	No polarization of CM, developmental arrest
Fgf8	MM, CM	Cell death, few renal vesicles, developmental arrest
Bmp7	UB, MM	Developmental arrest post-induction, some branching, few nephrons
Notch2	RV, SSB	Deletion of proximal nephron
Tcf21 (*Pod1*)	SC, PC	Poorly differentiated podocytes
Pdgfr	PC	No vascularization of glomerular tuft

Abbreviations: LPM, lateral plate mesoderm; IM, intermediate mesoderm; SC, stromal cells; ND, nephric duct; MM, metanephric mesenchyme; CM, cap mesenchyme; UB, ureteric bud; RV, renal vesicle; SSB, S-shaped bodies; PC, podocyte cells.

The establishment of The GenitoUrinary Development Molecular Anatomy Project (GUDMAP, www.gudmap.org) acts as a convenient platform for researchers to search for updated gene expression for the developing organs of the GenitoUrinary tract with emphasis of mechanism that control tubular morphogenesis, nephron polarity and specialization of kidney progenitors. This initiative leads to the characterization and identification of molecular markers governing early stages of GU system (Brunskill et al. 2008; Thiagarajan et al. 2011) with provision of high resolution molecular anatomy of the GU system and rapid access to primary data *via* the GUDMAP database.

1.4 Human RTMs: Anatomical variation and genetic mutations

Renal tract malformations (RTMs) are congenital structural anomalies of the kidneys and/or lower urinary tract. RTMs are the commonest cause of end stage renal disease (ESRD) in children (i.e. the patient needs renal replacement therapy in the form of dialysis and transplantation) (Kerecuk et al., 2008). RTMs constitute almost 20–30% of all congenital malformations with prevalence of three to six per 1,000 births (Brown et al., 1987; Queisser-Luft et al., 2002; Sanna-Cherchi et al., 2007). Some mild RTMs are asymptomatic but other patients may develop hypertension, renal impairment and proteinuria (Wühl et al., 2013). These RTM defects begin during the formation of human metanephros in early kidney development. Failure of the UB to invade the cause the most severe form of RTM, the complete absence of kidney or agenesis, when the UB fails to generate ureter, collecting duct and renal pelvis and the MM does not form the nephrons. There are several types of malformation ranging

from the most severe renal agenesis and multicystic dysplastic kidney (kidney is present but contains undifferentiated cells) to the milder cases of hypoplasia (kidney is present but contains too few nephrons) (Figure 1.4) (Kerecuk et al., 2008).

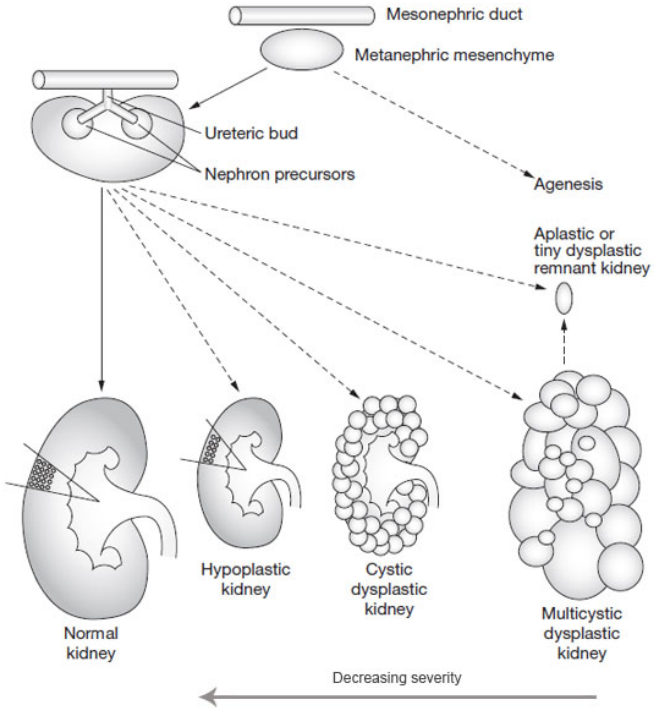

Figure 1.4 Diagram of normal and abnormal kidney development. The Wolffian body/nephric duct of the mesonephros gives rise to metanephric mesenchyme that in turn induces ureteric bud tip branching. Normal transcriptional regulations governing differentiation process develops nephrogenic precursors that promotes ureteric bud (UB) branching. Invasion of UB into the metanephric mesenchyme give rise to functional healthy kidney with several layers of nephrons (solid arrow). Aberrant signalling causes several forms of human RTMs (dotted arrows). No primary growth is observed in aplastic kidneys and the similar phenotype is seen in the organ remnant left after the spontaneous involution of a multicystic dysplastic kidney. Renal agenesis is the most severe type of RTM. The multicystic dysplastic kidney is devoid of excretory function and its pelvis is absent or severely disorganized. Cystic dysplastic kidneys generated malformed tubules with small cysts but generally retain the excretory function. Hypoplastic kidneys have lower number of nephron units than normal but retain a moderate degree of excretory function (Kerecuk et al., 2008).

'Dysplastic kidney' refers to the defective and incomplete development though the organs are present (Kerecuk et al., 2008). These kidneys are characterized by incomplete bifurcations of ureteric ducts that derive from the UB-collecting duct lineage and the malformed tubules become surrounded by undifferentiated and metaplastic (muscle-like) stroma. With little or no excretory function, dysplastic kidneys are often accompanied by a nonpatent ureters (Potter, 1972; Risdon, 1971). According to Potter (1972), cysts in dysplastic kidneys resulted from abnormal development whereas those in polycystic kidneys arise from pre-existing nephrons and CDs. The multicystic dysplastic kidney, a familiar variant of kidney dysplasia has no excretory function and a severely disorganized pelvis (Kerecuk et al., 2008). They can involute during gestation postnatally and this is accompanied by fulminant apoptosis (Belk et al., 2002; Hiraoka et al., 2002; Winyard et al., 1996). Hypoplastic kidneys have limited number of nephron units as compared with normal kidneys but

retain moderate excretory function. A severe form of kidney hypoplasia, 'oligomeganehronia', is characterized by 80% reduction in nephron number, one-eighth to one-half of normal kidney mass with hypertrophy of glomeruli (Kerecuk et al., 2008; Thorner, 1995). Other RTMs include congenital pelviureteric junction obstruction (Sanna-Cherchi et al., 2007), primary vesicoureteric reflux (VUR), horseshoe kidney, megaureter, ectopic ureter, and duplex collecting system (Nicolaou et al., 2015). 'Renal tubular dysgenesis' describes incomplete differentiation of proximal tubular nephron segments (Bernstein and Barajas, 1994).

A family history of renal abnormalities is present in ~10% RTM patients (Stoll et al., 2014). RTMs however, could be familial, oligogenic or monogenic in nature (Kerecuk et al., 2008; Vivante et al., 2014). The disease phenotype might differ between individuals, between and within families, even if they possess similar underlying mutations. Monogenic causes of some human RTMs have been determined. Other studies have indicated the environmental and epigenetic modifying influences (Nicolaou et al., 2015). Dominant renal hypodysplastic phenotype was commonly found in mutated regulators. Familiar examples of monogenic diseases include; *PAX2* mutation that causes renal-coloboma syndrome, vesicoureteric reflux and renal hypoplasia (Sanyanusin et al., 1995).; *SALL1,* Townes-Brocks syndrome; *EYA1* and *SIX1,* branchio-oto-renal syndrome. Variants of UB genes such as *GDNF/RET* and *ROBO2/SLIT2* have been implicated in vesicoureteric reflux. Mutation in these genes inhibited ureteric bifurcations resulting in kidney agenesis and associated Hirschprung's disease (Jain, 2009; Manié et al., 2001). Table 1.2 illustrates the genetic mutation and syndromes associated with RTMs. Some of these human genetic RTMs mirror the aberrant phenotypes as seen in mutant mouse models. For example, *Pax2* null mice devoid of nephric duct; *Gdnf* and *c-Ret* knockout in mice has implicated in inhibition of UB development and renal hypoplasia (and agenesis), respectively (Brophy et al., 2001); knockout of *Sall1* in mice promotes renal agenesis (Nishinakamura and Takasato, 2005); Interactions between *Eya1* and *Six1* commonly associated with branchio-oto-renal (BOR) syndrome in human, characterized by uni- or bilateral renal hypoplasia, agenesis, dysplasia, craniofacial fistulas and cochlear malformations (Kochhar et al., 2007). However, these phenotypes does not necessarily resembles as those seen in human because gene variation and expressions patterns are unique across species.

Table 1.2 Associated gene mutations of human RTMs, syndromes and symptoms (Kerecuk et al., 2008; Nicolaou et al., 2015)

Genes	Syndrome	Sign and symptoms
Autosomal dominant		
EYA1 and *SIX1*	Branchio-oto-renal (BOR)	Deafness and neck fistulas and/or sinuses
GATA3	Hypoparathyroidism, sensorineural deafness, and renal dysplasia	Hypoparathyroidism, sensorineural deafness, and renal dysplasia
WNT4	Mayer–Rokitansky–Küster–Hauser	Absence of upper vagina and uterus
PAX2	Renal coloboma	Optic nerve coloboma
SALL1	Townes–Brocks	Anal atresia, triphalangeal thumbs and sensorineural hearing loss
Autosomal recessive		
Several identified (some encode centrosomal/ primary cilium associated proteins)	Bardet–Biedl	Obesity, retinal degeneration and polydactyly
FRAS1 and *FREM2*	Fraser	Soft tissue syndactyly and cryptophthalmos
IFT80	Jeune	Constricted thoracic cage, retinal degeneration and polydactyly
MKS1 and *MKS3*	Meckel– Gruber	Encephalocele, polydactyly and ductal plate malformations of the liver
CHRM3	Prune belly	Abdominal wall musculature deficiency and cryptorchidism
HPSE2 and LRIG2	Urofacial syndrome	Grimace upon smiling
X-linked		
KAL1 (encodes a cell adhesion molecule)	Kallmann	Anosmia and hypogonadotrophic hypogonadism
GPC3	Simpson–Golabi–Behmel	Somatic overgrowth and tumors

1.5 Human *HNF1B* mutations and the role of *HNF1B* in kidney development

In the last decade, it has become clear that mutations of *HNF1B* are the commonest genetically defined causes of human RTMs. Heterozygous mutations in this gene causes multisystem disorder that has been commonly linked to renal cysts and diabetes syndrome (RCAD), associated RTMs (Woolf et al., 2002), early onset of gout and hyperuricemia (Bingham et al., 2003), hypomagnesemia and renal magnesium wasting (Adalat et al., 2009). Patients with or without diabetes-associated renal disease were found to suffer from microdeletions at chromosome position 17q12. Microdeletion of this genomic locus mostly leads to earlier onset of renal multicystic dysplastic kidneys (Mefford et al., 2007). Renal functions can be compromised in *HNF1B*-associated disease, ranging from normal to ESRD (Faguer et al., 2011). Eight (n=99) of children with dysplastic or hypoplastic RTMs have *HNF1B* variants (Weber et al., 2006). Furthermore, *HNF1B* variants are commonest in cystic RTMs. This implies that existence of *HNF1B* mutants is more common in hypoplastic or dysplastic patients with cysts or bilateral disease (Ulinski et al., 2006a).

The *HNF1B* gene, located on human chromosome 17q12, encodes for a divergent homeobox transcription factor, HNF1B which is developmentally expressed in early induction of kidney development, specifically in the collecting duct of metanephroi with lower expression in glomeruli (Cereghini et al., 1992; Kolatsi-Joannou et al., 2001; Massa et al., 2013). The HNF1B transcription factor is also expressed in the

developing liver, pancreas, stomach, intestines, thymus, gonads and lung. HNF1B is required for is required for visceral endoderm specification (Barbacci et al., 1999) and postmitotic reprogramming of numerous gene expression associated with cystic kidney disease (Verdeguer et al., 2010).

The *HNF1A* gene, which is located on human chromosome 12q, shares similar DNA sequence as *HNF1B* (>80% homology). The HNF1A transcription factor is highly expressed in the liver and heterodimerization has been associated with monogenic form maturity-onset diabetes of the young (MODY) which caused by autosomal dominant beta cell dysfunction (Bingham and Hattersley, 2004). Sequence homology has rendered *HNF1B* as a good candidate gene for MODY cases since its discovery in a Japanese family in 1997 (Horikawa et al., 1997). Both *HNF1A* and *HNF1B* are normally expressed in liver, gut, intestines and pancreas and the secreted proteins bind to DNA as homodimer or as heterodimer (Mendel et al., 1991). Despite the sequence homology, *HNF1B* expressions are different from *HNF1A* in developmental timing and localization. For instance, *HNF1B* expression is involved in the early renal developments whereas *HNF1A* expression is initiated later during organogenesis (Cereghini et al., 1992).

The human *HNF1B* contain 9 exons and splice sites with four functional domains, namely the dimerization domain, DNA binding domains (POU_S and POU_H) and a transactivation domain (Clissold et al., 2015). Mutations predominantly occupy the first 5 exons which include frameshift, splice site, missense and nonsense mutation (Bingham et al., 2003; Clissold et al., 2015; Horikawa et al., 1997; Iwasaki et al., 2001). In fact, genetic alteration such as base substitutions and small indels occur at 41% in adult and 44% in younger patients and foetus. Whole gene deletion occur at 59% and 56% in adults and children, respectively (Clissold et al., 2015). To date, 50 different mutations have been identified in *HNF1B* (Clissold et al., 2015). Exon 1-4 recorded the highest frequency of mutation that potentially halts dimerization and DNA binding potential leading to changes in gene transcriptions. RTMs are commonly caused by mutation that occurs at exon 2, 4 and intron 2 splice donor sites. Exon 2, which controls transcription, encodes pseudo-POU domain that controls DNA binding for normal genitourinary development. Serine-to-proline conversion (missense) in exon 2 (S151P proband) and single base pair deletion (frameshift) at codon 243 of exon 3 (Q243fsdelC proband) leads to cystic and single functioning kidneys, respectively (Bingham et al., 2002). However, there is no association exist between mutation position to any particular clinical features that consistent with haploinsufficiency as the underlying disease mechanism (Edghill et al., 2006). In addition, *HNF1B* mutation was found to mediate transactivation of *FXYD2* gene, mutation of which causes autosomal dominant hypomagnesemia and hypocalciuria,

suggesting a role for *HNF1B* in regulating tubular function (Adalat et al., 2009). Figure 1.5 shows the spectrum mutations of intragenic *HNF1B*.

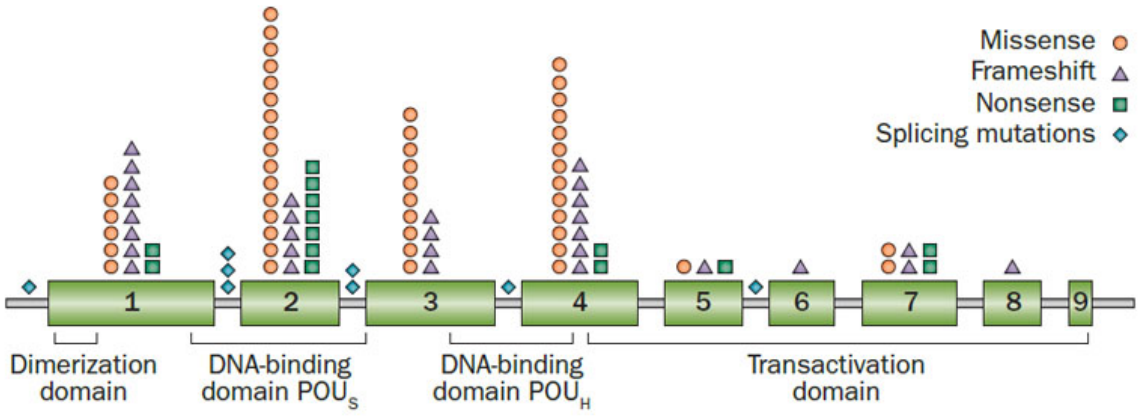

Figure 1.5 Distribution of *HNF1B* mutations. Mutations are grouped within nine exons and splice sites. The numbered green boxes refer to the exons. *HNF1B* mutations involve missense, splice sites, nonsense or frameshifts. HNF1B proteins comprise four functional domains; the dimerization domain, DNA binding domain (POU_S and POU_H) and transactivation domain. Symbols indicate separate mutation, not an individual subject. Abbreviations: HNF1B, hepatocyte nuclear factor 1β; POUS, Pit-1Oct-1/2Unc-86 specific; POUH, Pit-1Oct-1/2Unc86 homeodomain (Clissold et al., 2015).

Several functional studies on HNF1B have been carried out in mouse, *Xenopus* and zebrafish which are relevant to humans because of the conserved molecular interactions across species. In *Xenopus*, intact DNA binding activity of wild type Hnf1b proteins allow dimerization and transactivation of the reporter gene whereas lack of DNA binding and/or absence of transactivation potential in mutants leads to enlarged, partial or complete agenesis of pronephros (Bohn et al., 2003; Wild et al., 2000). Similarly, insertional mutagenesis in zebrafish leads to undeveloped pancreas, liver and formation of cysts in pronephros (Sun and Hopkins, 2001). Renal-specific inactivation of *Hnf1b* caused reduced transcriptional activation of *Umod, Pkhd1* and *Pkd2,* the anti-cystic genes (Gresh et al., 2004). In humans, autosomal recessive mutation of *PKHD1* lead to polycystic kidney whereas in transgenic mice, dominant-negative expression of a *Hnf1b* mutation leads to cysts in glomeruli and renal tubules (Hiesberger et al., 2004). This is due to evolutionary conserved *Pkhd1* binding site at the promoter region (Bingham and Hattersley, 2004).

HNF1B plays key role in UB branching and early nephrogenesis in mice. Other genes such as *Lfng, Dll1, Jag1* and the *Irx1/2* factors which are activated *via* Notch signalling also mediate renal tubular segmentation and glomerular formation (Cheng et al., 2007; Heliot et al., 2013). Inactivation of *Hnf1b* leads to absence of the proximal, loop of Henle, distal tubules and drastic distortion of nephron precursors. Downregulation of *Dll1* and *Notch* inactivation distorts compartmentalization of comma- and S-shaped bodies (Massa et al., 2013). Evidently, overexpression of *Hnf1b* in the *Xenopus* embryo reduced proximal and intermediate pronephric segment markers. *In vivo* assessment has also indicated co-expression of

transcription factors *Hnf1b* and *Pax2* in the Wolffian duct and UB which govern kidney development and differentiation of the ureter (Paces-Fessy et al., 2012). Thus, it could be summarized that *HNF1B* plays a crucial role in early kidney specification, segmentation of proximo-intermediate renal tubules, differentiation of ureter and nephron development in vertebrates, of which mutations may cause various phenotypes (Adalat et al., 2009; Barbacci et al., 1999; Heliot et al., 2013; Paces-Fessy et al., 2012).

1.6 Derivation of hPSCs and regulation of pluripotency

Pluripotency refers to the capacity to give rise to all cells of the mature organism after stimulation by developmental cues. In 1998, James Thomson and colleagues derived the first human embryonic stem cells (hESCs) from the inner cell mass (ICM) of preimplantation human blastocysts. These cell display capacity to proliferate indefinitely as undifferentiated cells (self-renewal) and differentiate into three germ layers, the mesoderm, endoderm and ectoderm (pluripotency) (Evans and Kaufman, 1981; Thomson et al., 1998). ESCs can be characterized by its origin (derivation from pre- or periimplantation embryos), prolonged undifferentiated proliferation and stability in developing the three embryonic germ layers (Thomson and Marshall, 1997). ESC features unlimited proliferative capacity due to high methylation in the genome (Meissner et al. 2008).

Mouse embryonic stem cell (mESCs) and hESCs are both derived from ICM and share similar mechanism to maintain self-renewal. Both however rely on different growth factor to maintain the stem cell fate and express different cell surface markers characteristic of ICM of their own species. hESCs require fibroblast growth factor 2 (FGF2) to maintain the undifferentiated state and ACTIVIN/NODAL signalling for self-renewal whereas mouse counterpart rely on bone morphogenetic protein (BMP) and Leukemia inhibitory factor (LIF) (Thomson et al., 1998; Vallier et al., 2005). PSCs can also be derived from the post-implantation (day 5.5/6 embryo) epiblast to produce Epi stem cells (EpiSC), or from primordial germ cells of (midgestation embryos) and adult germ lines (spermatogonial cells) (Matsui et al., 1992; Surani, 1999; Tesar et al., 2007). Unlike mESCs, EpiSC and hESCs share similar gene expression, morphology and signalling pathways involved in self-renewal.

Transcription factors play an indispensable role in governing pluripotency. Several studies have demonstrated pluripotent markers such as Nanog, Sox2, Oct4, SSEA3/4, Tra1-60 and Tra1-81 consistently expressed in hESCs and induced pluripotent stem cells (iPSCs) (Chamberlain et al., 2010; Keramari et al., 2010; Takasato et al., 2014a; Wang et al., 2012). The Nanog, Oct4 and Sox2 are regarded as the core factors of pluripotency that bind to DNA promoter region and activate or

repress transcription (Silva and Smith, 2008). They are the key regulators of pluripotency and predominantly expressed in PSCs. Activation of Oct4 or POU domain, class 5, transcription factor 1 (Pou5f1) promote differentiation into primitive endoderm and mesoderm whilst downregulation inappropriately differentiate ICM and ES cells into trophectoderm (Nichols et al., 1998). Sox2 functions to maintain pluripotency and lineage specification with expressions not limited to pluripotent cells (e.g. expression also observed in neural lineages) (Avilion et al., 2003). In mouse, loss of Nanog expression leads to differentiation of primitive endoderm (ICM derivatives of developing blastocyts) whereas overexpression promotes self-renewal in absence of leukemic inhibitory factor (LIF) that activates Stat3 transcription factor (Chambers et al., 2003; Matsuda et al., 1999). Although these three key regulators functions *via* distinct pathways, the interplay between them is crucial to govern early cell fate decisions. Table 1.3 described the gene expression analysis of Oct4, Nanog and Sox2.

Table 1.3 Gene expression analysis of transcription factors in ES cell pluripotency (Boyer et al., 2006).

Transcription factor	Protein family	Expression pattern	Loss-of-function phenotype		Gain-of-function phenotype in ES cells
			Embryonic development	ES cells	
Oct4	Pit–Oct–Unc protein family	Oocytes, fertilized embryo, ICM, epiblast, ES cells, embryonic carcinoma cells, germ cells	Embryonic lethal (blastocyst stage), differentiation of epiblast into trophectoderm lineage	Loss of pluripotency, differentiation into trophectoderm lineage	Differentiation into primitive endoderm and mesoderm
Nanog	Novel homeodomain protein	Morula, ICM, epiblast, ES cells, embryonic carcinoma cells, germ cells	Embryonic lethal (E5.5), lack of epiblast, differentiation of ICM into primitive endoderm	Loss of pluripotency, differentiation into primitive endoderm	LIF–Stat3-independent self-renewal, resistance to retinoic acid-induced differentiation
Sox2	SRY-related HMG box protein	Oocytes, ICM, epiblast, germ cells, multipotent cells of extraembryonic ectoderm, cells of neural lineage, brachial arches, gut endoderm	Embryonic lethal (E6.5), failure to maintain epiblast	Unknown	Unknown

1.7 Reprogramming of hiPSCs

The discovery of iPSCs in 2006 had violated the earlier believe claiming that terminally differentiated cell are restricted and have lost the potential to generate other cell types. The new era of biology witnessed profound breakthrough by Yamanaka to the fact that cell fates is reversible using different approaches such as somatic cell nuclear transfer (SCNT), direct reprogramming and cell fusion (Huang, 2009; Yildirim, 2012). SCNT involved insertion of somatic cell nuclear into enucleated oocyte whereas Yamanaka technique begins with screening of 24 pluripotency-associated genes that are transfected into murine fibroblasts. After selection, colonies with characteristics of ESCs emerged. He found that retroviral-mediated delivery of four transgenes (*Oct4, Sox2, Klf4 and c-Myc*) was required for reprogramming of these terminally differentiated murine fibroblasts into an ES-like pluripotent cell named induced pluripotent stem cell (iPSC) albeit with very low efficiency (Takahashi and Yamanaka, 2006). In addition, James Thomson and colleagues generated iPSCs

using lentiviral system to deliver different gene combinations viz. Oct4 (or POU5F1), Sox2, Nanog and Lin28 (Yamanaka, 2012). Although both reprogramming tools slightly differs to that of authentic ESC, which remain the gold standard, utilization of iPSCs to study tissue-specific differentiation could bypass the limited success of cloning and ethical concern because iPSCs are more feasible, inexpensive and efficient.

Unlike in mouse iPSCs (miPSC), human induced pluripotent stem cells (hiPSCs) requires the four factors (Oct4, Sox2, Klf4 and c-Myc) but with slight modification by substituting Klf4 and c-Myc with Nanog and Lin28a (Takahashi et al., 2007; Yu et al., 2007). In fact, after removal of c-Myc, Oct4 and Sox2 together with Nanog are capable of reprogramming human fibroblast (Nakagawa et al., 2008; Monserrat., 2013). Preinfection of slc7a1, a retroviral receptor facilitated the delivery of the four factors in human fibroblast by lentiviral transfection. Since the first derivation of iPSCs, the equivalence issues between hESCs and hiPSCs remains controversial. Both ESCs and iPSCs share similar morphology, proliferation and can form teratomas experimentally (Hanley et al., 2010). However, several studies have reported that they differ in expression levels (Chin et al., 2009), DNA methylation control (Doi et al., 2009), efficiency of production of chimeras (Okita et al., 2007), *in vitro* differentiation (Hu et al., 2010) and teratoma formation (Miura et al., 2009). In fact, it remains uncertain whether the differences between hESCs and hiPSCs are caused by inherited differences or *de novo* changes during differentiation, although several lab have reported the influence of inter- or intra-lab variation (Newman and Cooper, 2010), cell-line passage number (Chin et al., 2009), viral genome integration (Soldner et al., 2009) and genetic background (Stadtfeld et al., 2010) on functionality and expressions of pluripotent cells. Single nucleotide polymorphism assay (SNP) and exon sequencing have revealed copy number variation and point mutation in iPSCs of three independent studies, respectively.

Previous reprogramming protocols using lentiviral delivery, non-integrating plasmids and synthetic RNA have limited its application for therapeutic purposes due to integration into the host genome (Yu et al., 2009). Current reprogramming method using a non-integrating RNA Sendai virus (SeV) has however found to efficiently generate transgene-free iPSCs (Lieu et al., 2013). Recent research has shifted to the use of episomal plasmids, non-integrating adenovirus, excisable transposons (i.e *PiggyBac*), mRNA or recombinant proteins (Si-Tayeb et al., 2010). Unfortunately, comparison of between techniques of non-integrating reprogramming such as episomal (Epi), SeV and mRNA transfection mRNA methods have significant differences in reprogramming efficiency, aneuploidy rates, reliability and workload although all of these methods have generated high-quality human iPSCs (hiPSCs)

(Schlaeger et al., 2014). Table 1.4 summarizes the earlier and current vector technology to overexpress reprogramming factors.

Table 1.4 Vector technologies to deliver reprogramming factors in iPSCs (Bellin et al., 2012; De Lázaro et al., 2014).

Vector technology	Virus	Non-viral
Integrating	Retrovirus Lentivirus Inducible lentivirus	PiggyBac transposon
Non-integrating	Adenovirus Sendai virus	mRNA miRNA Small molecules Episomal vectors Protein

Abbreviations: mRNA, messenger RNA; miRNA, microRNA

Both hESCs and hiPSCs share the self-renewal and pluripotency properties, and in theory, can be differentiated into various type of cells. In fact, study by Choi et al. (2015) has reported that both cell types are molecularly and functionally equivalent with similar gene expression signatures which supports earlier study that suggest chromatin state of both cell types are consistent (Plath et al., 2011). Also, both hiPSCs and hESCs have found to express 2390 common genes with only 684 and 249 genes exclusively expressed by hiPSCs and hESCs, respectively (Wang et al., 2010). However, studies have also suggested essential differences in gene expressions of these two cell sources (Bock et al., 2011). Reported random differentiation propensities of hiPSCs to cardiovascular, hematopoetic and neural lineages have complicated disease modelling attempts (Narsinh et al., 2011). Derivation of hESCs are challenging and controversial due to limited supply of donor human embryos and *ex utero* destruction of human embryos. Although not economical, the hiPSCs are relatively less controversial and cell lines can be easily derived from donor with various genetic background. This approach can be utilised to create patient-specific hiPSC lines and bypassed the immunorejection issues which would then be beneficial for studying genetic disorders.

1.8 Comparison of differentiation protocol to direct hPSCs differentiation into renal progenitors

Kidney development began with formation of intermediate mesoderm (IM) from posterior primitive streak. IM further differentiates into metanephric mesenchyme (MM) and ureteric bud (UB) that give rise to nephrons and CD system, respectively. Directed differentiation of hESCs *via* primitive streak and IM resulted in synchronous induction of MM and UB that formed self-organizing structure under defined conditions (Rumballe et al., 2011; Tam and Loebel, 2007). Thus, a three-stage framework has been defined for hESCs differentiation (the induction of primitive streak, then formation of IM and finally nephrons). Some early studies attempt to drive differentiation of hPSCs into several kidney tissues such as proximal tubules

and podocytes (Narayanan et al., 2013; Song et al., 2012), but fails to describe comprehensive intervention steps along the differentiation. Most of recent study, however had recently suggested a stepwise differentiation concept. In this regard, three independent studies have been undertaken and compared (Xia et al., 2013; Takasato et al., 2014; Taguchi et al., 2014).

Xia et al. (2013) have generated UB progenitor-like epithelial cells from hPSCs within 4 days. Addition of BMP4 and FGF2 induces the T^+ mesoderm. Further additions of retinoic acid (RA), BMP2 and activin A expresses UB and nephric duct-associated genes, the PAX2, PAX8, OSR1, GATA3 and LHX1. When these progenitors are co-cultured within mESCs, an observable integration was seen which is evident by formation of $CK8^+$ epithelium and surrounded by mESCs collecting duct (Xia et al., 2013). Taguchi and colleagues have generated MM within 23 days. He begins with formation of BMP4-dependent embryoid bodies which subsequently forms epiblast after induction of activin A/FGF2. Following additions of BMP4 and the WNT agonist, CHIR99021, epiblast has transformed to nascent mesoderm, marked by expression of T and CDX2 (caudal type homeobox 2). Continuous activation by activin A/BMP4/RA/CHIR99021 expresses caudal IM-related genes, the OSR1 and PAX2 but not T and CDX2. This population sequentially give rise to nephrogenic mesenchyme and further forms nephrons with podocyte-containing glomeruli after additions of FGF9. Amazingly, incorporation of mESCs into recipient mouse promotes vascularization in the host glomeruli (Taguchi et al., 2014).

A study by Takasato et al. (2014a) performed differentiation using a monolayer culture of a MIXL1-GFP reporter hESCs line that reflects the primitive streak (Davis et al., 2008). He begins with CHIR99021 or activin A/BMP4 that generates the posterior primitive streak, marked by expressions of MIXL1 (Mix1 homeobox-like 1) and T. The addition of FGF9 or combinations of FGF9/RA/BMP7 simultaneously differentiates IM ($LHX1^+$, $PAX2^+$) into UB and MM progenitors. After 4 days, PAX2+ population undergoes MET to develop $GATA3^+PAX2^+ECAD^+$ (cadherin 1, CDH1) that reflects UB identity. Notably, these UB tissues are surrounded by a $SIX2^+WT1^+HOXD11^+$ MM. He concluded that the protocols mediate nephrogenesis *via* UB/MM reciprocal interactions (Takasato et al., 2015). Other similar studies have also reported the ability of hESCs and hiPSCs to differentiate into several kidney lineages. For example, following stimulation by two IM inducers called the retinoids (AM580 and TTNPB), an efficient and rapid differentiation of hESCs and hiPSCs towards nephrogenic IM has been established (Toshikazu et al., 2013). A robust induction protocol of hPSCs differentiation to IM produces 90% of OSR^+ cells (Shin-Ichi et al., 2013). An *in vivo* lineage-tracing study coupled with an *in vitro*-directed differentiation systems derives metanephric nephron progenitors or MM from hiPSCs

and mESCs (Atsuhiro et al., 2013) whereas directed differentiation of hPSCs give rise to UB progenitor-like cells (Yun et al., 2013).

In another study, hPSCs were treatment with glycogen synthase kinase-3β inhibitor (GSK-3βi), the CHIR99021 which promoted differentiation of $BRACHYURY^{+}MIXL1^{+}$ mesendoderm with 100% efficiency. Continuous culture of CHIR99021 with additions of fibroblast growth factor 2 (FGF2) and retinoic acid (RA) generates $PAX^{+}LHX1^{+}$ IM cells. Interestingly, these $PAX^{+}LHX1^{+}$ cells further differentiate into cap mesenchyme nephron progenitor cells upon stimulation by activin and FGF9, evidenced by expression of SALL1, SIX2 and WT1 markers (Albert et al., 2014). In addition, undifferentiated hESC (HUES-7) culture in renal epithelial growth medium for 20 days were reported to develop into functional renal proximal tubular-like cells expressing aquaporin 1 (*AQP1*) marker (Karthikeyan et al, 2013). A study from Nishinakamura revealed that nephron progenitors can epithelialize when co-cultured with murine embryonic spinal cord on polycarbonate filter generating early nephron structures expressing tubular (CDH1 and CDH6) and podocyte identity (NPHS1 and WT1). However, these immature structure still co-express PAX2 and SALL1 thereby suggesting the need for further refinement. Figure 1.6 described the different protocols to generate kidney organoids. Table 1.5 summarizes commonly used growth factors in differentiation protocols. Table 1.6 summarizes the specific renal cell types for appropriate targeting.

Table 1.5 Growth factors involved in regionalization and patterning during kidney development (Takasato et al., 2015)

Growth factors	**Developmental regulations**
RA, activin A, FGF2, WNT3A	Primitive streak formation
RA, FGF2/9, WNT3A/5A	A-P mesodermal patterning
BMP4, activin A, FGFs	M-L mesodermal patterning
RA, activin A	Nephric duct identity
WNTs, BMP7, FGF2/9	MM fate
FGF2/9, BMP2/7	MM survival

Abbreviations; RA, retinoic acid; FGF, fibroblast growth factor; WNT, wingless-type MMTV integration site family; BMP, bone morphogenetic protein; A-P, anterio-posterior; M-L, medio-lateral.

Table 1.6 Appropriate targets of various renal cell types to resemble disease model (Hendry et al., 2012)

Renal diseases	Podocyte[a]	Pan-nephron epithelial progenitor[a]	Proximal tubular epithelium[a]	Distal tubular/ LOH tubular epithelium[a]	Collecting duct epithelium	Mesangial cell
Polycystic kidney disease (ADPKD, ARPKD)						
Alport syndrome, nephrotic syndrome (NPHS1/2), other podocyte defects						
Cystic diseases; ciliopathies						
Dent's disease, cystinosis, Lowe syndrome						
Gitelman syndrome, distal tubular acidosis						
Diabetes insipidus						
Denys Drash syndrome; Frasier syndrome, other inherited forms of FSGS or MS						

Abbreviations: ARPKD, autosomal recessive polycystic kidney disease; FSGS, focal segmental glomerulosclerosis; ADPKD, autosomal dominant polycystic kidney disease; LOH, loop of Henle; MS, mesangial sclerosis. Shaded grey boxes indicate the intended cell types to be generated through reprogramming for therapeutic purposes. [a]Derived from cap mesenchyme or nephron progenitors

Despite this successful differentiation, the generation of kidney progenitors seems very complex due to the presence of 20 different cell types and distinct temporospatial demarcation between intricate structures such as collecting duct and nephrons. Although previous papers have mentioned the independent differentiation of hPSCs into either only ureteric epithelium or nephron progenitors, Takasato and colleagues have found that collecting duct and nephrons' progenitor are induced at the same time. Also, it was reported that the nephron-associated collecting duct forms a network surrounded by endothelial cells and renal interstitium resembling mature adult kidney (Takasato et al., 2014a). His breakthrough has further generated near-functional kidney organoids (Takasato et al., 2015). Another important point to consider is the determination of specific cell type targets for renal diseases because different renal mutations affect distinct cell types.

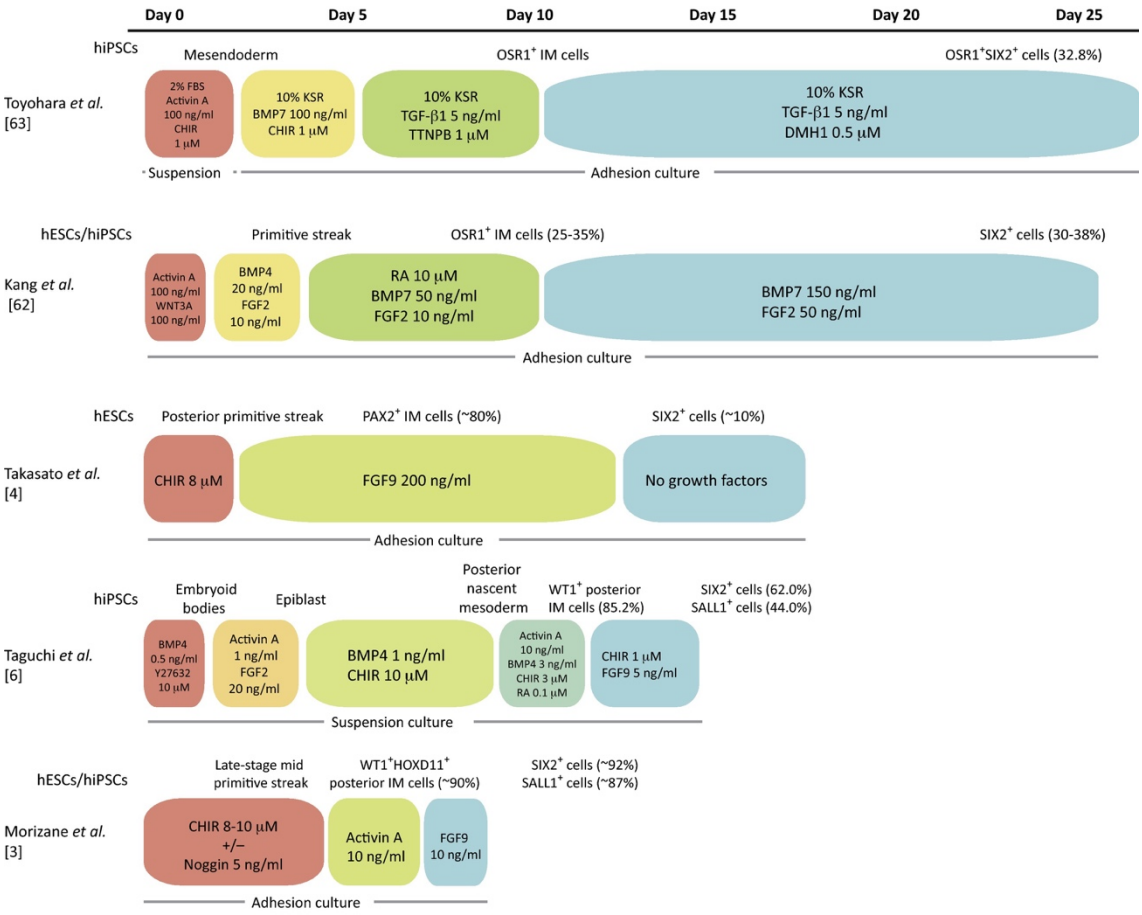

Figure 1.6 Comparison between differentiation protocols to kidney lineages from hPSCs. Colored boxes indicated chemical factors, duration and concentrations. Culture method indicated at the bottom of each protocol whereas resulting cell types were displayed on the top. IM, intermediate mesoderm, CHIR, CHIR99021, FBS, fetal bovine serum, KSR, knockout serum replacement, TGF, transforming growth factor, BMP, bone morphogenetic protein, TTNPB, 4-[(E)-2-(5,6,7,8-Tetrahydro-5,5,8,8-tetramethyl-2-naphthalenyl)-1- propenyl]benzoic acid (a retinoic acid receptor agonist), DMH1: 4-[6-(4-Isopropoxyphenyl)pyrazolo[1,5-a]pyrimidin-3-yl]quinoline,4-[6-[4-(1- Methylethoxy) phenyl]pyrazolo [1,5-a]pyrimidin-3-yl]-quinoline (a selective inhibitor of BMP ALK2 receptor), FGF, fibroblast growth factor, Wnt3a, wingless-type MMTV integration site family, member 3A, OSR1, odd-skipped related transcription factor 1, RA, retinoic acid, Y27632, a selective p160ROCK inhibitor, PAX2, paired box 2, WT1, Wilms tumor 1, SIX2, SIX homeobox 2, HOXD11: homeobox D11, SALL1, spalt like transcription factor 1.

1.9 Disease modelling using hiPSC-derived kidney organoids

Generation of custom-tailored cells (hiPSCs) from somatic cells using selected reprogramming factors are useful in modelling human disease, study of gene-drug interactions and may potentially lead to discovery of novel drugs to treat multiple disorders. The ability to induce pluripotency in somatic cells make it possible for generating cell lines that contain genome which are predisposed to disease, particularly genetically inherited disease where the aberrant tissues can be easily accessed (Tiscornia et al., 2011). Several terminally differentiated iPSC has been found to genetically resemble inherited and sporadic diseases in human (Wu and Hochedlinger, 2011). However, several key points should be considered before executing the modelling experiments such as (i) the choice of disease (i.e early of late onset, polygenic or monogenic ethiology), (ii) selection of cell type to reprogram

(i.e. early or late passage, hematopoietic or fibroblast), (iii) reprogramming methods (i.e non-integrating plasmids, retroviral, transcription factors), (iv) characterization of hiPSCs (i.e. pluripotency, epigenetic and genetic analysis, teratoma assay), (v) differentiation protocol to the desired cell types, (vi) characterization of disease phenotype (i.e. gene expression, molecular characterization, RNAi knockdown, genetic rescue) and (vii) drug target screening (i.e. small molecule effectors).

Successful differentiation was reported in multiple studies in modeling disease features. For instance, iPSCs that are generated from patient with Hutchinson-Gilford progeria who suffered from vascular defects has revealed differentiated smooth muscle senescence *in vitro* (Zhang et al., 2011). iPSC with glutaminergic neurons with fewer synapses reflected the phenotype of methyl CpG binding protein 2 (MeCP2)-deficient female patients with RETT syndrome (Marchetto et al., 2010). hiPSCs derived from patient with long QT syndrome indicated electrophysiological characteristics such as prolonged duration of action potential and arrhythmia (Moretti et al., 2010). These examples are the proof-of-concept for modelling disease using iPSC technology. However, its safety/efficiency balance remains controversial and has forced extensive pre-clinical and clinical testing for therapeutic purposes (De Lázaro et al., 2014). Once established, clinical grade iPSCs could be tested to reverse the disease-specific phenotype and to search for drug targets.

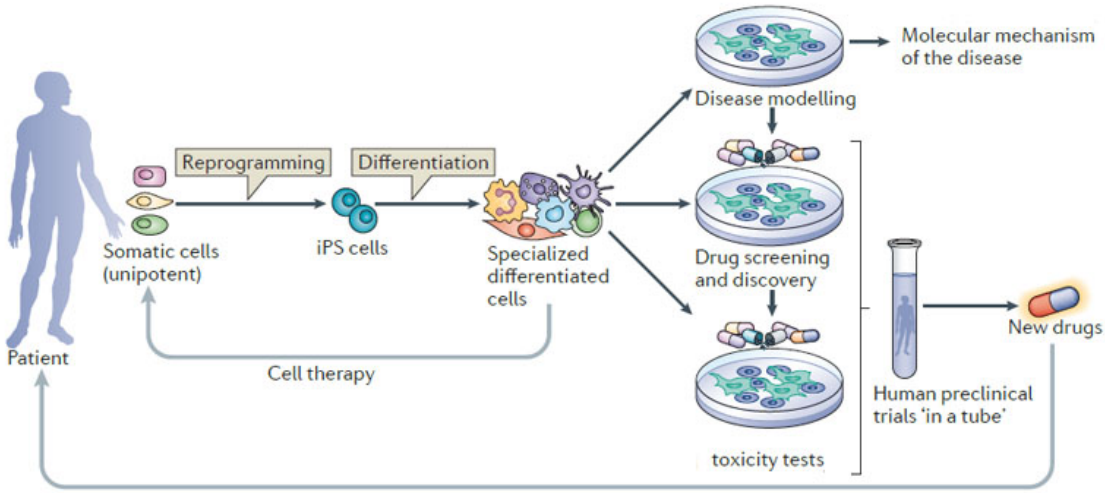

1.7 hiPSCs' derivation, differentiation and applications. Unipotent adult somatic cells can be isolated from any patient to be reprogrammed into hiPSCs using pluripotency markers (i.e. Oct4, Sox2, Klf4, c-Myc). Induction of differentiation generates genetically matched specialized tissues which could be useful in cell-based therapy. hiPSCs can model disease of interest to study molecular mechanism of aberrant phenotypes and possibly be applied in screening of drug targets, related pathways and discovery of novel compounds. Drug testing (i.e. screening and toxicological assessment) can be analysed 'in a tube' before approval in clinical trials (Bellin et al., 2012).

Based on the literature, it is clear that a number of common and rare diseases can be modelled using iPSCs derived from somatic cells of patients. Generation of autologous cells upon *in vitro* differentiation to specific lineages is relatively achievable particularly in easy-to-induce cell types like neurons as compared to endodermal lineages. To date, however, several endodermal lineages were successfully differentiated such as pancreatic-hormone expressing endocrine cells (D'Amour, 2006), anterior foregut (Green et al., 2011), hepatocytes (Song et al., 2009) and intestinal cells (Spence et al., 2011). In fact, Pagliuca et al (2014) have generated hundreds of functional insulin-producing β cells from hPSCs which are characterized by expression of mature β cell markers, insulin packaging into vesicles, Ca^{2+} flux after glucose exposure and secretion of insulin *in vitro*. Interestingly, after transplantation in mice, these hPSCs secrete insulin into the serum in a glucose-regulated pattern and reduce hyperglycaemic in insulin deficient mice. Apart from that, several mesodermal lineages particularly kidney progenitor cells has also been developed to model disease by specifying target cell types.

In previous four years, several attempts have been made to model human genetic kidney diseases. For instance, mutations in cystic genes such as PKD1, PKD2 and PKHD1 have shown to induce cystogenesis in organoid culture (Freedman et al., 2015). Mutant PODXL lines displayed disrupted glomerular epithelial (Kim et al., 2017) whereby IFT140 mutation modelled nephronophthisis by formation of dysmorphic tubules with shorter primary cilia and disrupted apicobasal polarity (Forbes et al., 2018). Mutation of OCRL1 caused Lowe syndrome that diminished primary cilia functions and protein transport from Golgi complex (Hsieh et al., 2018). The attempts to model kidney diseases using organoids derived from hPSCs is an attractive approach to study human inherited kidney diseases thereby develop novel drug candidates. However, the protocols for differentiation, genetic background and transferability needed to be considered before translating any of these approaches into the clinics.

Table 1.7 Methods to induce kidney organoids

Protocol	Duration of time in culture until formation of NPCs	Pre-CHIR step	Duration of CHIR step	Duration between CHIR step and formation of NPCs	Cell types in the organoids				Disease modelling or knockout
					Glomerulus and/or renal tubule	Stroma	Endothelial cell	Ureteric bud	
Taguchi (2014)[22]	13–14 days	+ Activin low	6 days	2 steps	+	n.d.	n.d.	–	*NPHS1* (nephrin) and *PAX2*
Morizane (2015)[26]	9 days	–	4 days (noggin+/–)	2 steps	+	+	+	–	n.d.
Freedman (2015)[27]	n.d.	+	1.5 days	n.d.	+	+	+	–	*PODXL* and *PKD1/PKD2* (PC1/PC2)
Takasato (2015)[25]	10 days	–	4 days	1 step	+	+	+	+/–	*NPHS1* (nephrin) and *IFT140*
Taguchi (2017)[32]	12.5 days[a]	+ Activin high plus BMP	1.5 days	5 steps[b]	–	n.d.	n.d.	+	*PAX2*

+, – and +/–, indicated presence or absence of steps/ structures. NPCs, nephron progenitor cells, CHIR, CHIR99021, BMP, bone morphogenetic protein, PC, polycystin, n.d., not determined, PODXL, podocalyxin, PAX2, paired box gene 2. a) Time in culture until UB formation. b) Time between CHIR step and UB formation. Adapted from (Nishinakamura, 2019).

1.10 Kidney organoids model early-onset cystic kidney diseases

The utilisation of kidney organoids allowed screening of new therapeutic drugs which is not possible in animal models due to limited number of samples and species variation (Morizane and Bonventre, 2017b). Ethical concern has limited the investigation of early human kidney development. There are approximately 160 reported inherited kidney diseases (Devuyst et al., 2014) of which predominantly affect children and adults with ESRD. Polycystic kidney diseases (PKDs) especially ADPKD, that constituted almost 10% of all patients that underwent kidney replacement therapy, has been the main focus (Ong et al., 2015). Interestingly, clinical data revealed that ADPKD is a late-onset disease that affects people above 30 years. Organoid models however did not reveal convincing results due to absence of cyst formation (Van and Frank, 1995). For instance, complete knock-out of PKD1 and PKD2 genes in H9 hESC lines via CRISPR/Cas9 approach revealed only 6% cyst formations in mutant and rarely seen in unaffected lines (Freedman et al., 2015). In fact, ADPKD is heterozygous at the somatic level with presumption that the second allele is cyst-causing. Thus, development of *in vitro* organoids model that can model the second hit mechanism (Tan et al., 2018) and represent late stage of ADPKD phenotypes remain to be established (Nahm et al., 2002).

HNF1B functions in early kidney development by regulating cell-cell contact within UB region and ureteric tip domain to control cellular organisation and formation of CD. It has been reported that homozygous mutation of HNF1B (exon 2) disrupted proximal tubule and TAL segments formation (Przepiorski et al., 2018). Also, heterozygous mutation has led to defective epithelial arrangements, changes in cellular polarity and morphology of primary cilia (Desgrange et al., 2017) although

the cilia number retained. Further assessment to unravel mechanism that leads to spectrum of HNF1B phenotypes need to be carried out. Another cystic kidney disease that has been modelled was nephronophthisis, a phenotypically and genetically heterogenous disease caused by disrupted function and morphology of primary cilia (Braun and Hildebrandt, 2017). Because primary cilia can localise in many cells, the clinical manifestations may also include non-kidney organs such as eyes, liver or brain (Little and Quinlan, 2019). Creation of homozygous mutation in IFT140 gene by CRISPR edit led to formation of organoids with shortened and clubbed cilia (Forbes et al., 2018). Correction of point mutation using CRISPR has created isogenic lines that can be compared with patient lines. Utilisation of organoid model to recapitulate cystogenesis has increased in recent years with the hope to increase understanding regarding underlying pathogenesis in cystic formation.

1.11 Role cAMP-dependent calcium signaling in cyst-associated kidney disease

Cystic diseases affect both adults and children. It was reported that 73% of patient that harbour heterozygous *HNF1B* mutation developed cystic diseases (Heidet et al., 2010). The cysts were reported to develop in the renal cortex, with small but bright appearances and does not increase in amount over time (Faguer et al., 2011; Ulinski et al., 2006b). Multicystic dysplastic kidney (MCDK) was reported to be associated with mutation in exon 2 of PAX2 gene (Fletcher et al., 2005). PKD, on the other hand, is regarded as the primary cause of ESRD across the globe implicated in altered fluid secretion, diminished proliferation of cells, ECM abnormalities, macrophage activation, reduced tubular diameters and ultimately leads to formation of cysts. It was reported that disrupted cAMP signaling altered normal regulation of intracellular calcium thus mediating cystogenesis (Torres and Harris, 2014). It is known that mutation in either *PKD1* (encoding polycystin 1) or *PKD2* (encoding polycystin 2) has contributed to ADPKD whereas *PKHD1* (encoding fibrocystin) mutations lead to ARPKD that affected most children and infants (Morizane and Bonventre, 2017b). Collectively, these mutations have implicated in wide range of cystic phenotypes.

It was reported that *HNF1B* mutation significantly altered organoid morphologies and formation of differentiating structures. However, none of these organ cultures showed cystic features even though culture is being extended for additional 1 week. It was noted that the genetic factor alone was not sufficient to phenotypically generate cyst possibly due to maturation issues that can be improved using latest established protocols. Thus, the current approach would be to interrogate organoid's culture to adverse environments (elevated cAMP) that can potentially alter physiological homeostasis of kidney structures thus affecting cAMP signaling.

It was reported that polycystin 1 (PC1) and polycystin 2 (PC2) proteins were colocalised in the primary cilia of kidney epithelia that function as mechanosensors and can transduce calcium signals due to changes in tubular fluid flow. Defects in any of these proteins caused ciliary bending that may diminish normal sensing of mechanical stimuli and eventually affected cell's morphology and polarity thereby stimulating cystogenesis (Köttgen et al., 2008; Mekahli et al., 2012; Santoso et al., 2011). The fluid shear stress can trigger calcium signaling in primary cilia via PC2-dependent calcium release. This is however restricted to cilioplasm but in the presence of ryanodine receptor, the calcium signals can trigger cytosolic calcium response initiating calcium uptake from intracellular compartments (Morel et al., 2009). Another aspect is that PC2 can interact with transient potential receptor channels such as TRPC1 or TRPV4. TRPC1 and PC2 can interact to form heteromultimeric channel (in the absence of PC1) that can be activated by G-protein-coupled receptor (GPCR) stimulation thus showing single-channel conductance pattern, unlike the individual TRPC1 and PC2 channels. Activation of PC2/TRPC1 complexes either via bending of cilia or plasma membrane GPCR activation, can alter the mechanotransduction of calcium signals in cilia (Qian et al., 2003).

It was reported that PC2 can interact with TRPV4 and form heteromeric channel complexes that can act as mechanosensor and facilitate flow-induced calcium influx which can be diminished if TRPV4 channel in kidney epithelial cell is depleting (Tsiokas et al., 1999). Furthermore, polycystins can also interact with other cilia-associated proteins such as kinesin-II, inversin, cystin and polaris by which disrupted protein synthesis can cause cyst formations (Köttgen et al., 2008; Yamaguchi et al., 2006). It was reported that fluid flow has promoted cilia bending that in turn activated PC1/PC2, PC2/TRPV4 and PC2/TRPC1 complexes that regulate calcium signaling. Nonetheless, depletion of TRPV4 and TRPC1 alone has been shown to alter calcium signals but not associated with cyst formations. Thus, defects in cilia-dependent calcium signals alone are insufficient to promote cystogenesis. Instead, TRPV4/TRPC1 was reported to regulate polycystin functions as described in recent findings that reduction of cilia in cells with lower PC1 and PC2 proteins showed fewer cysts indicating that cilia depletion lead to milder cyst progression than the one seen in ADPKD cells (Geng et al., 2008). In addition, cilia-dependent cystic growth does not activate either MAP kinase, mTOR or cAMP pathways (Geng et al., 2008). Thus, it can be concluded that the polycystins mediate ciliary signaling via unknown mechanism while maintaining normal phenotype of kidney epithelial cell. In ADPKD, inhibition of polycystins rendered cilia-dependent signals thus promoted cyst formations.

1.12 Mechanism of cAMP activation and ECM regulation in kidney cells

Several animal models that suffered from PKD has shown increased intracellular cAMPs in kidneys (Gattone Ii et al., 2003; Smith et al., 2006; Yamaguchi et al., 1997) and other cells such as smooth muscle cells (Kip et al., 2005), cholangiocytes (Masyuk et al., 2007) and choroid plexus (Banizs et al., 2007). cAMP levels in tissues determined by complex membrane-bound activities such as G protein-coupled receptors (GPCR), extracellular ligands, adenylyl cyclase (AC) and phosphodiesterases (PDE). The elevated cAMP levels could be due to several reasons. Firstly, low calcium levels induce activation of calcium-inhibitable AC6, inhibit calcium/calmodulin-dependent PDE1 and cGMP-inhibitable PDE3 (Gattone Ii et al., 2003; Wang et al., 2010).

Secondly, disruption of ciliary protein complexes (PC2, A-kinase anchoring protein 150, PKA, PDE4C, AC5/6) whereby PC2-mediated calcium entry was blocked AC5/6 and activated PDE4C (Choi et al., 2011). Thirdly, depleted calcium stores in ER cause oligomerisation and translocation of stromal interaction molecule 1 to the plasma membrane where recruitment and activation of AC6 occurred (Pisitkun et al., 2004; Spirli et al., 2012). Finally, disruption of PC1 binding to heterotrimeric G proteins, increased vasopressin levels and accumulation of ATP, AC agonists, forskolin and lisophosphatidic acid in the cystic fluids contributed to the elevated cAMPs (Hovater et al., 2008; Putnam et al., 2007).

It was reported that canonical Wnt/β-catenin signaling is required in early stage of epithelial tubulogenesis whereas non-canonical Wnt/planar cell polarity (PCP) are essential at later stages (Carroll and Das, 2011). In this regard, primary cilia that are present on every almost mammalian cell types, act as the key modulator of Wnt signaling by sensing and transducing signals from microenvironments (Oh and Katsanis, 2012; Zaghloul and Brugmann, 2011; Radford et al., 2012). In renal fibrogenesis, damage of primary cilia may cause overactivation of canonical Wnt signaling and reduction of non-canonical Wnt signaling activity (Saito et al., 2015). Others reported that the continued canonical Wnt signalling (Qian et al., 2005; Saadi-Kheddouci et al., 2001), followed by reduced non-canonical/PCP signalling (Saburi et al., 2008), can diminish cilia synthesis and ciliary proteins (inversin) thus contributing to cystic disease.

In addition, it was found that increased cAMP and PKA signals have altered tubulogenesis. Wnt/ β-catenin signaling cascade was enhanced by PKA via phosphorylation of GSK 3β (to stabilise β-catenin)(Li et al., 2000) and via phosphorylation of β-catenin (to initiate transcription)(Taurin et al., 2006). Furthermore, it was reported that continued PKA-dependent canonical Wnt signaling

prevented epithelialisation of metanephric mesenchyme induced with spinal cord, leading to formation of irregular epithelial components and large dilations (Gallegos et al., 2012). Thus, hyperactivity of cAMP-PKA cues can alter tubular diameter in PKDs. However, these changes was not observed in the *HNF1B* mutant organoids at day 7+18 and thought to be stage-specific and predicted to affect tubules on longer culture.

1.13 Research aims

Several studies has reported different strategies to differentiate hPSCs to kidney lineage that comprise nephrons and vasculo-interstitial elements (Ciampi et al., 2016; Lam et al., 2014; Morizane et al., 2015; Narayanan et al., 2013; Song et al., 2012; Taguchi et al., 2014; Takasato et al., 2014a; Takasato et al., 2015a). The kidney cortex constituted up to 90% of nephron that function to hydrostatically filter blood and permit reabsorption of solutes via glomeruli and multi-segmented tubules, respectively. Reduced number of nephrons in people with CKD can eventually cause ESRD that rely upon replacement therapies (hemodialysis) or kidney transplant to restore kidney function. It is therefore an urgent need to create a new human kidney that can mimic morphological and physiological functions as seen *in vivo*. Generation of 3D kidney organoids from hPSCs *in vitro* have path the way to finding new therapies.

Human-derived iPSCs had promised greater advantage over hESCs (i.e immunocompatibility and personalised intervention) and could potentially be used in the transplantation therapy despite reported obstacles (i.e reprogramming inefficiency and economical aspects). Generation of cell lineage and tissues that genetically resemble human tissue *in vivo* is of utmost important in species-specific toxicology evaluation, drug screening and pathophysiology. However, it remains to be answered whether human iPSCs could reconstitute tissue-specific phenotypes seen in kidney disease. A study on kidney disease has reported differentiation of hPSCs into segmented, nephron-like structures, podocytes, proximal tubule and endothelium. Functional study on deletion of polycystic kidney disease gene using CRISPR/Cas9, the *PKD1* and *PKD2*, kidney tubules undergo cystogenesis alongside normal tubular organoids (Freedman et al., 2015).

Heterozygous mutation of *HNF1B* impairs early renal development in human particularly causing renal cysts and patients most commonly exhibited diabetes (RCAD) with associated extra-renal manifestations, especially in children, making them the best candidates to study mutation of genes involved in renal development. This study will utilise the advent of iPSC technology to create a genetically defined RTM model in a dish with emphasis on gene regulation during differentiation of hPSCs

to early kidney lineages. Although various barriers are yet to be solved, the promising results of iPSCs so far have sparked motivation among scientific communities to find the possible drug target and develop personalised medicine in near future.

1.14 Hypothesis

I hypothesise that human pluripotent stem cells carrying *HNF1B* mutation can be differentiated towards kidney progenitors *in vitro* expressing key transcriptional genes. These progenitors are expected to differentiate into a more complex 3D structure containing multiple cellular constructs that can self-organise and recapitulate some aspect of the kidney developmental phenotypes seen in the cystic kidney disease.

1.15 Aim and objectives

The research aims to develop kidney progenitor cells from human pluripotent stem cells as a model of renal tract malformations. To address the hypothesis, I aimed to perform the following experiments:

Aim 1: Investigate the differentiation potential of hPSCs towards kidney lineage

- To culture and differentiate hESCs to self-organizing structures of intermediate mesodermal kidney lineages.
- To generate hiPSCs from patient blood cells and their appropriate available controls (e.g. sibling or parents) using established reprogramming protocols.
- To characterise hPSCs by immunostaining, qPCR and embryoid body formations.

Aim 2: Investigate the phenotypic differences between organoids derived from healthy and HNF1B-affected lines

- To simultaneously culture and differentiate both healthy and HNF1B-affected hiPSCs into self-organised 3D kidney structures
- To evaluate morphological differentiation and gene expression profiles using qPCR at different organoid developmental stages
- To compare morphological characteristics, regionalisation and gene expression patterns of differentiating and differentiated hPSCs by immunohistochemical analysis.

Aim 3: Investigate the role of exogenous cAMP in tubular compartments of kidney organoids

- To identify and compare cyst formation in cAMP-treated organoids
- To determine transcript profiles of HNF1B targets before and after cystogenesis induction
- To perform functional OAT assay on differentiating tubular organoids

Chapter 2: Material and Methods

2.1 hESCs culture and differentiation

2.1.1 Coating plates with vitronectin

Truncated recombinant human vitronectin (VTN-N) (A14700, Thermo Fisher Scientific) was thawed at room room temperature (RT) and 60 µl aliquots were prepared in polypropylene tubes at a stock concentration of 500 µg/ml. Final coating concentration of 0.5 µg/cm^2 were used to coat the culture dishes. The aliquots were frozen down at -80°C or used immediately. For coating, VTN-N was taken from -80°C storage and thawed at RT. A total of 60 µL aliquots were added to 6 ml Dulbecco's phosphate-buffered saline (DPBS) without Ca^{2+} and Mg^{2+} (14190, Gibco) at RT. Diluted VTN-N was resuspended by pipetting up and down to get a working concentration of 5 µg/mL (1:100). Then, 1 ml of diluted VTN-N was added to each well of a 6-well plate. Coated plates were left at RT for 1 h or stored at 2-8°C up to 2 weeks. The coated plates should not be left dry. Prior to use, plates were pre-warmed at RT for 1 h and VTN-N solution was aspirated and discarded. Cells were passaged directly onto VTN-N-coated plates.

2.1.2 Thawing of human pluripotent stem cells

VTN-N-coated plates were pre-warmed at RT for 1 h before use. Excess VTN-N solution was aspirated and 1 ml of TeSR™-E8™ medium (#05990, STEMCELL Technologies) plus 10 µl RevitaCell™ Supplement (100X) (A2644501, Thermo Fisher) were added. hPSCs were removed from liquid nitrogen and thawed in a 37°C water bath. The cell suspension was transferred to a 15 ml falcon tube containing 2 ml of TeSR™-E8™ medium in a dropwise manner to the wall of the tube to avoid osmotic shock. Cells were centrifuged at 1200 rpm for 3 min (1-14 Microfuge, Sigma). After aspirating the supernatant, cells were suspended in 1 ml of TeSR™-E8™ medium and seeded over the surface of VTN-N-coated wells. Cells were kept in a 5% CO_2 incubator at 37°C. For counting, 10 µl of cells suspension were taken out and counted using a heamocytometer.

2.1.3 hESCs monolayer culture

Prior to thawing, cells were cultured in 6 well plates coated with feeder free substrate, VTN-N at density of 300,000 cells/cm^2. Cells were grown in TeSR™2 medium supplemented with 250X and 5X Supplements (05861, STEMCELL Technologies) with the addition of Rho-kinases (ROCK) inhibitors Y-27632 for the first 24 hours (1254, Tocris Bioscience). Medium was changed every other day till cells reached confluence of approximately 70-80% before commencing the differentiation protocol.

2.1.4 Cryopreservation of hPSCs

Confluent hPSCs in a well of a 6-well plate were washed twice with 1X PBS and 1 ml of 0.5 mM EDTA was added. Plates were left at RT for 7 min to dislodge cells. Excess EDTA was aspirated and 1 ml of PSC Cryopreservation medium (A2644601, Thermo Fisher) was gently added by tilting the plate at 45° to detach the colonies. Cells were transferred to cryovials (E3110-6122, Starlab) and kept at -80°C for overnight. Cryovials were transferred to liquid nitrogen the next day.

2.2 Pluripotency test

2.2.1 Immunocytochemistry of pluripotency markers

Near confluent cells (70-80%) in 24 well plates were washed with 1x PBS, fixed with 4% PFA for 20 min, blocked and permeabilised with 3% bovine serum albumin (BSA) (A1470, Sigma) in 0.3% Triton X/PBS for 1 h at RT. Primary antibodies at specific dilutions were prepared using 3% BSA in PBS. Plates containing cells were incubated overnight at 4°C and washed. Secondary antibodies were prepared at specific dilutions with 3% BSA in PBS. Cells were incubated protected from light at RT for 1 h and washed. Cells were stained with DAPI (1:5000) for 5 min on a rocker. For each washing step, cells were washed three times with 0.1% Triton-X (X100, Sigma) in PBS while rocking the plate for 3 min in each interval. Cells were washed 3 times and left in 300 µl PBS before storing at 4°C. Antibodies and dilutions are listed in Table 2.6.

2.2.2 Flow cytometry

A total of 0.5-1 million cells were centrifuged for 3 min at 600xg. Then cells were fixed by resuspending the pellet in 1 ml 4% PFA. Cells were pipetted up and down to mix before incubating for 7 min at RT in the dark. Then cells were centrifuged for 3 min at 600xg. Cells were blocked in 1 ml PBS with 5% FBS before being incubated for 30 min at RT. For cell surface staining, cells were divided into 5 portions, 200 µl each in Eppendorf tubes and centrifuged for 3 min at 600xg. Then the cell pellets were resuspended in 100 µl PBS-5% FBS before addition of fluorochrome-labeled antibodies to cell surface antigens. Cells were then incubated for 30 min at RT and washed with 1 ml PBS and centrifuged for 3 min at 600xg. To permeabilise, 1 ml of ice cold 70% methanol in PBS was added and mixed by pipetting before being incubated for 7 min at 4°C. Cells were then centrifuged for 3 min at 600xg. For intracellular staining, pellets were resuspended in 100 µl PBS-5% FBS, followed by addition of antibodies against cell surface antigens and isotype controls, as indicated in Table 2.6. Cells were incubated for 30 min at RT and washed in 1 ml PBS. Cells were centrifuged for 3 min at 600xg and resuspended in 400 µl PBS then left on ice.

For analysis, antibodies combinations were indicated as follow: 1_unstained, 2_mix1 (TRA181-PE; Nanog-AF488; Sox2-AF647), 3_mix2 (SSEA3-PE), 4_Ig ctrl1 (mPE; mAF488; mAF647) and 5_Ig ctrl2 (rat IgM-PE). Antibodies were summarised in the Table 2.6.

2.2.3 Embryoid body formation

2.2.3.1 Manual method

Cells at 80% confluent on 1 well of 6 well plate were used for stem cell potency characterisations. Colonies were cut into a grid pattern at slightly larger colony than for normal daily passaging using a glass pipette under the inverted phase microscope in a Class II biosafety cabinette. Few pieces of colonies at 80% confluency were transferred into embryoid body (EB) medium in suspension in a low adherence 10 cm petri dish. Colonies were incubated in 37°C incubator supplied with 5% CO_2 with medium change every 3 days for 10 days and morphologies were repeatedly recorded. After 10 days, EBs with fully formed and well-developed cavities were plated down onto 24 well plates pre-coated with 0.25 ml of 10% FBS at 37°C for 1 h. Serum was aspirated and 0.5 ml of EB medium was added into each well (each well can accommodate 3 EBs). EBs were incubated and fed for another 10 days while observing cell outgrowth by phase contrast using inverted light microscope (Leica Microsystems, USA). EBs were fixed with 4% PFA for 15 min at RT before being immunostained. List of antibodies for EB staining were indicated in Table 2.6 .

2.2.3.2 EDTA method

Cells at 80% confluency were washed with 1X PBS (without Ca^{2+} and Mg^{2+}). A total of 1 ml EDTA were added and incubated at RT for 7 min. EDTA solution were aspirated and 1 ml of EB medium was added. Larger clump of cells were collected, transferred into low adherence 10 cm non-coated petri dish, cultured and processed as in section 2.2.3.1.

2.2.3.3 Immunostaining of embryoid bodies

EB outgrowths in 24 well plates were blocked with 100 µl of 10% serum diluted in 0.1% Triton-X/PBS for 30 min at RT. A total of 100 µl primary antibodies were added (diluted with 1% serum in 0.1% Triton-X/PBS) and incubated for 2 h at RT or overnight at 4ºC. Cell outgrowths were washed 3 times with PBS and left in the third wash for 10 min for secondary antibodies preparation. A total of 100 µl of the appropriate secondary antibody was added (diluted with 1% serum in 0.1% Triton-X/PBS) and incubated in the dark at RT for 1 h. Then, cells were washed 3 times with PBS and left in the third wash for 10 min before stained with 100 µl of DAPI (300 nM

in PBS) for 5 min. Stained cells were washed 3 times with PBS and left in 0.5 ml of the last wash before imaged. Differentiation potential of cell lines was determined by staining for at least 2 markers of the 3 differentiation germ layer lineages (endoderm, mesoderm and ectoderm) as shown in Table 2.6 . To interpret the staining, any positive fluorescence detected (respective to each antibody) will indicate presence of differentiation and need to occupy at least 10% of the total stained area before classifying them as positive stem cell lines.

2.3 Derivation of human induced pluripotent stem cells (hiPSCs)

2.3.1 Blood donor

Patients with HNF1B associated disease and their families were assessed at Professor Woolf's Paediatric and Adult Renal Genetics clinics, held in the Royal Manchester Children's Hospital, and St Mary's Hospital, Manchester University NHS Foundation Trust, Manchester Academic Health Science Centre, Manchester, UK. Venous blood samples for generation of hPSCs were obtained after individual informed consent for taking part in the Manchester Gene Identification Consortium Study (REC 11/H1003/3; IRAS ID 64321).

2.3.2 Phlebotomy

A total of 4 ml of blood were withdrawn by Prof Woolf and transferred to BD Vacutainer™ Hemogard closure plastic K2-EDTA tubes (BD 367525, BD). Tubes were inverted 10 times to ensure blood and EDTA were well mixed and kept at RT until processing. The summary of the lines generated from patients' blood and its healthy related/non-related controls are summarised in Table 3.1 in Chapter 3.

2.3.3 PBMC isolation

For isolating peripheral blood mononuclear cells (PBMCs), 4ml of blood were diluted with 4 ml PBS (1:1 ratio). An equal amount of Ficoll® Paque Plus (GE17-1440-02, Sigma) was added in a 15 ml Falcon tube and the blood/PBS mix was carefully layered over the Ficoll reagent and centrifuged at 400xg for 40 min, RT. A total of 1 ml PBMCs was isolated using a sterile Pasteur pipette and transferred into a new 15 ml Falcon tube containing 9 ml of PBS. Diluted PBMCs were centrifuged at 200xg for 10 min. The supernatant was discarded and the pellet was washed with 10 ml of PBS. Centrifugation was repeated at RT and the supernatant were discarded. PBMCs were resuspended in 2ml (or 0.5 ml medium per ml of starting blood) of Erythroid expansion medium: StemSpan™ SFEM II (#09605, STEMCELL Technologies) and StemSpan™ Erythroid Expansion Supplement (100X) (#02692, STEMCELL

Technologies). Cells were counted using Trypan blue method (Louis and Siegel, 2011) and expected to contain $1x10^6$ PBMCs per ml of starting blood.

2.3.4 Expansion of erythroid progenitors

At day 0, $0.5x10^6$ PBMC were plated in one well of a 6-well plate (uncoated) containing 2 ml of erythroid expansion medium and incubated overnight. On day 1, all non-adherent cells (in the same 2 ml complete erythroid expansion medium) were transferred to a new plate. Adherent cells and the old plate were discarded. Cells were incubated in the CO_2 incubator overnight. On day 2, cells were fed by carefully removing 1.5 ml of used erythroid expansion medium and replaced with fresh medium. Feeding steps were repeated every 2 days up to day 7.

2.3.5 Transduction of erythroid progenitor cells

At day 8, $5x10^4$ cells per patient at 50-70% confluency were transduced with CytoTune™-iPS 2.0 Sendai Reprogramming Kit (A16517, Thermo Fisher) at an multiplicity of infection (MOI) of 5:5:3 (5 for hKOS, 5 for hc-Myc and 3 for hKlf4 vectors) using centrifugation to improve efficiency. Approval for using SeV in our building was obtained from the Health and Safety Executive (HSE). The volume of medium containing $5x10^4$ cells was calculated. Cells were transferred to a 15 ml Falcon tube and centrifuged at 300xg for 5 min at RT. A total of 250 µl transduction medium was prepared for each $5x10^4$ cells. For 4 patients, each $5x10^4$ cells were transfected with 10 µl hKOS, 12 µl c-Myc and 6 µl hKlf4 in 1 ml of complete erythroid expansion medium. Supernatant was discarded in virkon-containing waste bottle and cells were resuspended in 250 µl of made up SeV. Cells with SeV were centrifuged at 300xg for 35 min, RT. A total of 150 µl of expansion medium were added to tubes containing 250 µl SeV giving a total of 400 µl. A total of 200 µl of mixture were seeded onto 2 wells of non-coated 24-well plate.

The volume of each virus needed to reach the target MOI were calculated using the formula as below:

$$Volume\ of\ virus\ (\mu l) = \frac{MOI\left(\frac{CIU}{cell}\right) x\ number\ of\ cells}{titer\ of\ virus\ \left(\frac{CIU}{ml}\right) x\ 10^{-3}\ (ml/\mu l)}$$

MOIs were optimised for the desired application. The titer of each CytoTune™ 2.0 reprogramming vector is lot-dependent and was checked on thermofisher.com/cytotune. Re-freezing and thawing of reprogramming vectors was avoided since viral titres can decrease dramatically in each freeze/thaw cycle.

2.3.6 Reprogramming of erythroid progenitor cells

Cells were cultured in expansion medium (Section 2.3.4). At day 9 of culture, 200 µl expansion medium were added to each well to make up a total of 400 µl per well. At day 11, another 200 µl were added to make up to total 600 µl per well. At day 12, after counting, 600 µl of suspension cells were transferred onto VTN-N-coated 6-well plate containing 0.5 ml of ReproTeSR™ medium (#05921, STEMCELL Technologies). At day 14, 1 ml of ReproTeSR™ medium were added to give a total of 2.1 ml per well. By day 15-30, cells started to adhere to VTN-N. The medium was replaced with 1.5 ml ReproTeSR™ every 2 days and cellular morphologies were recorded. At about day 16, emerging iPSC colonies were detected.

2.3.7 Identification and isolation of iPS cell colonies

iPSCs colonies have distinct features and attached colonies detected before day 26 were avoided as these are likely to be only partially reprogrammed cells. A total of 1.5 ml TeSR™-E8™ were added to a VTN-N-coated well of 6-well plate. Using a pulled glass pipette, colonies were scored into a grid pattern. Using P200 pipette, pieces of cut colonies were carefully dislodge and transferred onto coated plates. One colony was deposited in each well and was regarded as an incipient clonal line and classed as passage 1 (P1). Colonies were incubated and fed daily for 4-6 days. Any good size colonies were passaged by using either manual or EDTA passaging method. Cells were passaged up to P20. A summary time course of derivation of iPSCs is illustrated in Figure 2.1.

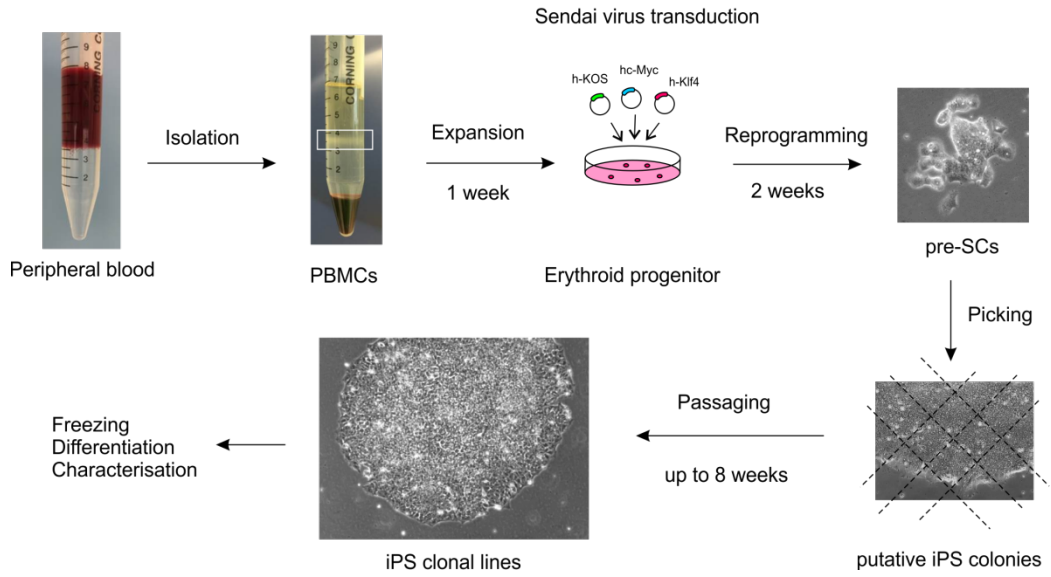

Figure 2.1 Schematic time course for iPSC generation. Isolation of PBMCs from venous blood were performed by addition of Ficoll's reagent. Thick middle cloudy layer were collected and expanded in expansion media for about 7 days. Prior to transfection, Sendai virus containing reprogramming factors were added. After 2 weeks, approximately 70% suspension cells adhered to the bottom forming pre-stem cell-like clusters. These cells were cultured, maintained and passaged to create a stable, integration-free iPS clonal lines. Established lines can be utilised for characterisations, differentiation and freezing. PMBC, peripheral blood mononuclear cells, h-KOS, human polycistronic Klf4–Oct3/4–Sox2, pre-SC, pre stem cells, iPS, induced pluripotent stem.

2.3.8 Passaging of human iPSCs by manual cutting

Newly reprogrammed iPSC colonies will stick to the bottom of the plate. For passaging, VTN-N-coated plates containing 1 ml TeSR™-E8™ medium was prepared and put aside in the cutting hood. Glass pipette were split into two using a Bunsen burner to taper them. Desired colonies were selected under the microscope and cut into a grid pattern to create smaller colonies. These colonies were picked and transferred to the new wells using a P200 pipette. Medium was changed every day. Medium from old plates was removed and the day of picking were noted as the beginning of first passage number.

2.3.9 Passaging of human iPSCs by EDTA method

Cells were passaged after reaching ~80% confluency. Confluent cells in 6-well plates (Corning) were washed with DBPS and 1 ml of 0.1% UltraPure™ 0.5M EDTA, pH 8.0 15575020, Thermo Fisher) was added to dissociate cells. Plates were incubated for 7 min and the edges of the colonies were monitored under the microscopes to visualise detachments. Once holes started to appear at the centre of the colony, the EDTA solution was gently aspirated. Then 1 ml of TeSR™-E8™ basal medium supplemented with 25X Supplement was added to the wall of the plate by tilting to allow cells to detach. These clumps of cells were then transferred onto new VTN-N-coated plates containing 1 ml of TeSR™-E8™ medium. Cells are plated at a seeding density of 1:5 to 1:10 (cells from 1 well were split into 5 to 10 wells) depending on

the passage number. Medium was changed every day. Cells were tested for Mycoplasma contamination by Mycoplasma detection kit (LT07-418, Lonza) and maintained at passage below 30.

2.4 Verification of a vector-free cell preparation

2.4.1 RNA isolation

Sendai virus clearance was performed using reprogrammed cells at passage 10. RNA isolation was carried out based on Rneasy Mini Kit (74104, Qiagen) following manufacturer's instructions. Medium was removed and cells were washed with PBS without Ca^{2+}/Mg^{2+} before addition of 350 µl cold RLT buffer RW1. Cells were transferred to Rneasy column and centrifuged for 15 sec at ≥8,000xg (≥10,000 rpm). Flow through was discarded and 10 µl of Dnase I stock solution were added to 70 µl Buffer RDD before gently mixing by inverting the tube. The Column was then briefly centrifuged. Dnase I incubation mix (80 µl) was added directly to the Rneasy column membrane, and placed on the benchtop (20–30°C) for 15 min. A total of 350 µl Buffer RW1 was added to the Rneasy column and centrifuged for 15 sec at ≥8,000xg. Flow through was discarded and RNA clean-up step continued by addition of 500 µl Buffer RPE to the Rneasy spin column. Column was centrifuged for 15 sec at ≥8,000xg to wash the membrane. Flow through was discarded. Then 500 µl Buffer RPE was added to the Rneasy spin column. Column lid was closed and centrifuged for 2 min at ≥8,000xg to wash the membrane. The Rneasy spin column was placed in a new 1.5 ml collection tube and 30–50 µl Rnase-free water was added directly to the spin column membrane. The column was centrifuged for 1 min at ≥8,000xg to elute the RNA. If the expected RNA yield was >30 µg, steps were repeated using another 30–50 µl of Rnase-free water. Alternatively, the eluate was used if high RNA concentration was required. RNA can be stored at -80°C or the A260/A280 nm ratio measured for RNA purity/concentration using NanoDrop™ 2000/2000c Spectrophotometers.

2.4.2 Dnase treatment

Cells were transferred to a0.5 ml Eppendorf tube and the volume was noted. A total of 8 µl RNA diluted to 125 ng/µl (1 µg total RNA) were mixed with 1 µl RQ1 Dnase buffer and 1 µl RQ1 Dnase (M690A, Promega). This 10 µl total Dnase reaction was incubated at 37°C for 30 min. Then 1 µl RQ1 Dnase stop solution was added and reaction was incubated at 65°C for 10 min to inactivate.

2.4.3 cDNA preparation

In-house cDNAs were prepared by reverse transcription. A total of 1 µl of 0.5 µg/ul of random primers (0.5 µg primer/µg RNA)(C118A, Promega) were added to 11 µl Dnase treated RNA (1 µg) and incubated at 70°C for 5 min. Tubes were immediately placed on ice and briefly spun. Then 5 µl M-MLV-RT reaction buffer, 1.25 µl 10mM dNTP mix, 1 µl 20U/µl Rnase inhibitor (20U), 1 µl 200U/µl M-MLV-RT (200U) and 3.75 µl nuclease-free water were added to 12 µl primer annealed RNA. The reactions were mixed by flicking and incubated at 37°C for 1 h.

2.4.4 RT-PCR of Sendai viral vectors

Detection of SeV genome and transgenes were carried out using RT-PCR. Reverse transcription is required for detecting the presence of the SeV genome in reprogrammed cells because the vectors are based on SeV, which is an RNA virus. PCR was carried out using 2 µl of cDNA from the reverse transcription reaction which is summarised in Table 2.1. The parameters for PCR reactions and primer sequences are tabulated in Table 2.2 and 2.3, respectively. PCR products were analysed using 2% agarose gel electrophoresis (1613100, Bio-Rad).

Table 2.1 Reaction components

Components	Amount (µl)
GoTaq® Green Master Mix	5
Forward primer	1
Reverse primer	1
cDNA	2
Nuclease-free water	1

Table 2.2 RT-PCR parameters

Step	Temperature	Time (sec)	Cycles
Denaturation	95°C	120	1
Denaturation	95°C	30	30-35
Annealing	55°C	30	
Elongation	72°C	30	
Elongation	72°C	300	1

Table 2.3 RT-PCR primer sets and product size

Target	Primer sets (5'-3')	Product size
SeV	Forward: GGA TCA CTA GGT GAT ATC GAG C* Reverse: ACC AGA CAA GAG TTT AAG AGA TAT	181 bp
KOS	Forward: ATG CAC CGC TAC GAC GTG AGC GC Reverse: ACC TTG ACA ATC CTG ATG TGG	528 bp
Klf4	Forward: TTC CTG CAT GCC AGA GGA GCC C Reverse: AAT GTA TCG AAG GTG CTC AA*	410 bp
c-Myc	Forward: TAA CTG ACT AGC AGG CTT GTC G* Reverse: TCC ACA TAC AGT CCT GGA TGA TGA TG	532 bp
GAPDH	Forward: AGC CAC ATC GCT CAG ACAC Reverse: GCC CAA TAC GAC CAA ATCC	

2.5 hESC differentiation into kidney lineages (2D monolayer)

Human embryonic stem cells, MAN11 and MAN13 lines (Ye et al., 2017) were routinely cultured on feeder free substrate, VTN-N at 0.5 µg/cm^2 or 5 µg/ml in TeSR™2 medium supplemented with TeSR™2 5X Supplement and TeSR™2 250X Supplement (05861, STEMCELL Technologies). Both lines at passage number 28 and 30, respectively have been used and cells were fed every two days and replated on VTN-N with addition of 10 µM ROCK inhibitors Y-27632 (1254, Tocris) prior to confluence. Differentiation protocols were adapted from Takasato et al. (2014a) with slight modifications. The day before commencing the differentiation, cells were plated at 30,000 – 35,000 cells/cm^2 on VTN-N coated 24 well plates and incubated overnight. Cells were treated with 8 µM of CHIR99021 (4423, Tocris) in serum-free STEMdiff™ APEL™ Medium (05210, STEMCELL Technologies) for 3 days, then exposed to 200 ng/ml FGF9 (100-23, PeproTech Inc.) and 1 µg/ml Heparin (H3149, Sigma-Aldrich) for 10 days. Cells continued to differentiate up to day 30 maintained in STEMdiff™ APEL™ basal medium with daily medium change.

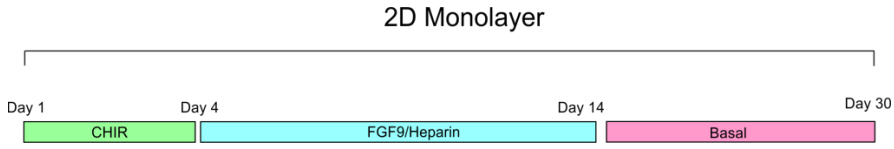

Figure 2.2 Differentiation protocol of monolayer culture. The depicted schematic summarizes protocols that have been used to differentiate hPSCs to kidney lineages for 30 days (Takasato et al., 2014a). CHIR, CHIR99021, FGF9, Fibroblast growth factor 9.

2.6 Differentiation of hPSCs to 3D kidney organoids

Differentiation of 3D kidney organoids utilised both monolayer and 3D platforms following protocols described by Takasato et al. (2016) with minimal modifications. iPSCs starting cell density of 18,000 cm^2 were plated on 24-well plates coated with 5 µg/ml recombinant human VTN-N (A14700, Life Technologies). Cells were differentiated in APEL2™ medium supplemented with 2% PFHM-II protein-free hybridoma medium. iPSCs were treated with 8 µM CHIR for the first 4 days followed by FGF9 (200 ng/mL, PeproTech) and heparin (1 µg/mL, Sigma-Aldrich) for another 3 days. At day 7, cells were dissociated with TrypLE and 200,000 cells were collected in Eppendorf tubes. Cells were centrifuged twice at 400 x g in 2 different directions, 2 min each. The pellets were subsequently cultured on a medium-air interface by transfer onto a 0.4 µm pore size MilliCell cell culture insert (#PICM03050, Millipore) in wells of 6-well plates. This inserts were made of low protein binding polytetrafluoroethylene (PTFE). In some occasions, Corning® Transwell® polyester membrane cell culture inserts (CLS3470, Sigma-Aldrich) will be used to replace MilliCell inserts. Cells were exposed to APEL2™ medium containing pre-warmed 5 µM CHIR for 1 h, before reverting back to APEL2™ containing FGF9/heparin for an

additional 5 days. Finally, the 3D cultures were maintained in basal APEL2™ medium for another 13-20 days (D7+18-25) with basal medium changed every other day. Schematic differentiation to 3D kidney organoids is illustrated in Figure 2.3 below.

Table 2.4 Media and reagents used in 3D kidney organoids differentiation.

Components	Stock conc.	Working conc.	Cat no	Company
STEMdiff™ APEL™2 Medium	n/a	n/a	05270	STEMCELL Technologies
CHIR 99021	20 mM	8 µM or 5 µM (pulse)	4423	Tocris
FGF9	1 µg/ml	200 ng/ml	100-23	PeproTech
Heparin	10 mg/ml	1 µg/ml	H3149	Sigma-Aldrich
PFHM II	100%	2%	12040077	Thermo Fisher

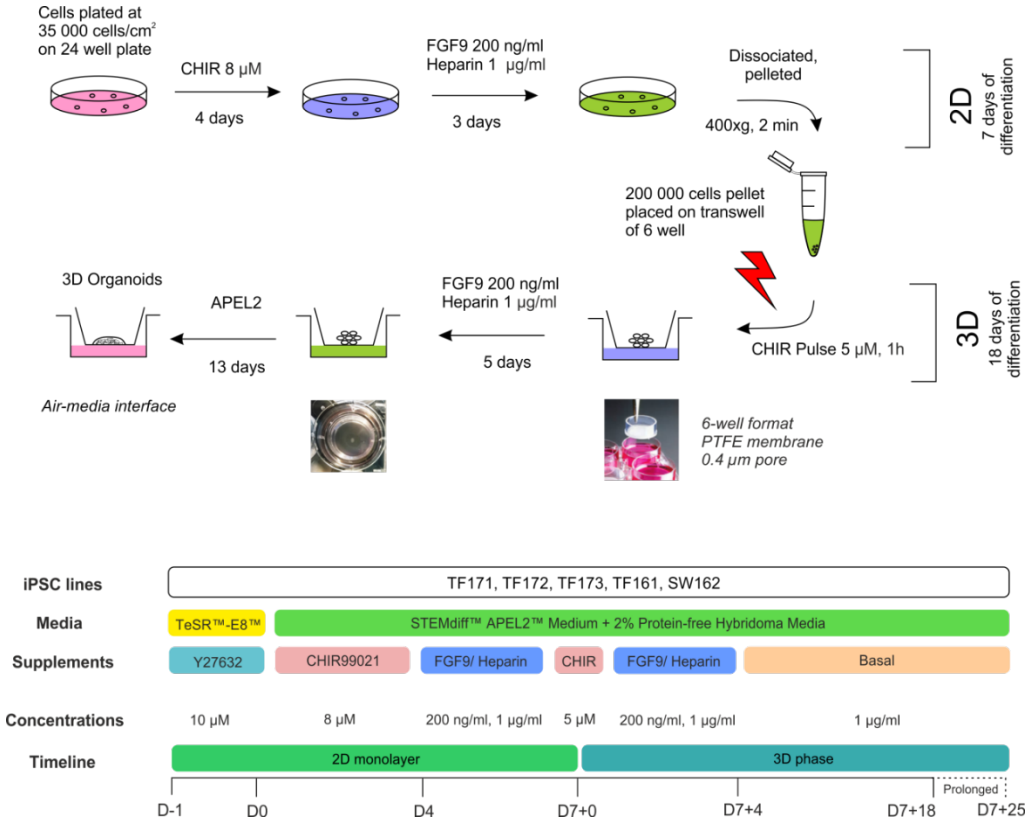

Figure 2.3 Kidney organoids differentiation scheme. hPSCs were differentiated as monolayer culture for the first 7 days (2D) before dissociated and pelleted at 200,000 cells per pellet. Pellets were maintained on 3D platform at air-liquid interphase for 18 days before characterisations. In some occasions, culture was prolonged up to day 7+25. Each transwell can accommodate 3-5 pellets at a time. The hPSC lines, media, supplements and concentrations were summarised in the colored boxes. CHIR, CHIR99021, FGF9, Fibroblast growth factor 9, Y27632, p160ROCK inhibitor.

2.7 PFHM-II titration

Optimal concentration of protein-free hybridoma medium (PFHM) for 3D kidney organoids differentiation were investigated by supplementing STEMdiff™ APEL™2 Medium either with 0, 1, 2, 3.5 or 5% PFHM-II. Both hESCs and hiPSCs were tested using these concentrations in the in 3D platform. Any morphological changes during differentiation were documented. Histological sections were paraffin-embedded and stained with Alcian Blue (pH 2.5) to indicate presence of acidic sulphated glycosaminoglycans (Scott and Dorling, 1965).

2.8 Cyst formation

Induction of cyst formation was adapted from Anders et al. (2014) with slight modifications. Basal media that includes STEMdiff™ APEL™2 Medium, 2% protein-free hybridoma (PFHM) medium and 1 µg/ml heparin were supplemented with 8-Bromoadenosine 3',5'-cyclic monophosphate sodium salt (8-Br-cAMP) (B7880, Sigma) and referred to as cystic medium. At D7+7 of culture, organoids were supplemented with 1.2 ml of cystic medium containing 50, 100 or 200 µM cAMP alongside vehicle (PBS only) and negative control. Cysts were identified by their translucent appearances and large bright structures under the inverted phase microscope. Tubules that appeared dilated were not regarded as cysts. Wells were imaged using Leica inverted phase light microscope. Medium were replaced every 2 days and culture was terminated at D7+25. Quantification of cyst count was analysed using ImageJ cell counter (http://imagej.net/Fiji) and expression level of cyst-related genes were quantified using qPCR.

2.9 OAT assay

Live organoids at d7+18 of culture were incubated in kidney differentiation medium (section 2.5) supplemented with 20 µg/ml rhodamine-conjugated peanut aggulutinin (RL-1072, Vector Laboratories) and 1 µM 6-carboxyfluorescein (6CF) (C-1360, Invitrogen) for 1 h at 37°C. Organoids were treated either with 2.5 mM probenecid that inhibit organic anion transporter (P36400, Life Technologies) or without (control). Both groups were washed with 1X PBS and incubated with 10 mM probenecid for 15 min at 37°C to trap intracellular fluorophore. Organoids were imaged using Leica SP8 inverted confocal microscope.

2.10 Efflux of anions (retention) assays

Organoids were preloaded with 1 µM 6CF in kidney differentiation medium for 1 h at 37°C. Organoids were washed in 1X PBS and wells were imaged to confirm uptake. Plates containing organoids were further incubated with/without 10 mM probenecid for 1 h at 37°C to block anion efflux. Organoids were washed in 1X PBS and imaged.

2.11 Characterisations of hPSCs-derived kidney cells

2.11.1 Karyotyping

For fixation, mitotically active hPSCs (70% confluence) were supplemented with 25 µl/ml BrdU/Colcemid stock (B5002, Sigma; 15210, Invitrogen) in mTeSR1 (#85851, STEMCELL Technologies) or TeSR™-E8™ (#05990, STEMCELL Technologies) medium and left to proliferate overnight. Cells were harvested the next day by removal of medium and washed with 2 ml PBS. Then 1 ml TrypLE™ Express Enzyme (1X) (12604013, Gibco) was added to each well and incubated for 2 min at 37°C. When cells were completely detached, 5 ml of post-harvest medium was added to each well to inactivate TrypLE before transferred to 50 ml falcon tube. Cells were centrifuged at 400xg for 5 min. Supernatant was removed and pellet were resuspended by flicking and 5 ml of warm freshly prepared hypotonic solution (tri-sodium citrate and potassium chloride) was added in a steady stream down the side of the tube. Tubes were incubated for 10 min at 37°C before centrifuged at 400xg to for 5 min get the cell pellet. Centrifugation was repeated if no visible pellet. Cell pellet were gently resuspended by flicking. Whilst constantly agitating the tube, 5 ml of freshly made ice cold fix were added. The first 1 ml fix was added slowly in a drop-wise manner while agitating the tube. The remaining fix continued ran down the side of the tube. Slides containing cells can be immediately stained after fixation or stored at -20°C for future slide making.

For slide making, cells were centrifuged at 400xg for 5 min. The supernatant was removed and the pellet resuspended in 200 µl-1 ml of fix, dependent on pellet size. Clean positively-charged glass microscope slides were humidified with breath and immediately 13 µl of resuspended cells were dropped on the slides at an acute angle, causing the droplet to spread along the slide. The slides were gently washed with 2 or more drops of fix, making sure it covered the whole slide. The slides were arranged upside down at an acute angle to dry. Once dried, slides were incubated for 45 min at 90°C in the lab oven. For staining, slides were placed in Coplin jars containing Hanks' Balanced Salt solution (H4641, Sigma) for 45 sec and briefly washed in 0.85% saline (NaCl) in water. Then slides were trypsinised with 5% trypsin in saline for 30 sec using 2.5% Trypsin (10X) (15090-046, Gibco) then briefly washed twice in Buffer

solutions, pH 6.8 and stained with Leishman's stain (L6254, Sigma) for 2.5 min before washed with water. Slides were left to dry before applying a cover-slip with Entellan mountant (107960, Merck Millipore) and viewed under immersion oil at 100x objectives. One test slide was first put through to calibrate incubation times for staining of subsequent slides.

2.11.2 hPSC genetic analysis

Analysis of karyotypic abnormalities was performed according to manufacturer's instructions. hPSC genetic analysis kit (#07550, STEMCELL Technologies) contain 9 primer-probe mixes that can estimate karyotypic abnormalities in stem cell lines. This qPCR-based method allowed screening multiple stem cell lines on a single assay with robust accuracy due to utilisation of double-quenched probe tagged with 5-carboxyfluorescein (5-FAM) dye. The genomic DNA control provided with the kit was validated as a diploid control, 2n. To begin with, concentration of harvested DNA was measured using NanoDrop™ spectrophotometer. At least two samples are needed to determine the copy number. In a 0.65 ml tube, 1.5 µl of control genomic DNA were added to 56.5 µl of nuclease-free water to obtain final concentration of 5 ng/µl. The tube was vortexed on high speed for 3-5 sec and placed on ice. A total of 290 ng of genomic DNA transferred to a separate 0.65 ml tube and the final volume adjusted to 58 µl with nuclease-free water to obtain final concentration of 5 ng/µl. Tubes were placed on ice. Master mix was vortexed on high for 5 sec and 145 µl was added to each genomic DNA samples as well as control DNA. Mixture were pipetted up and down 2-3 times before placed on ice and protected from light.

Primer-probe stock solutions were prepared by centrifugation at 750xg for 10 sec. Then, 33 µl of TE Buffer were added to each tube and pipetted up and down at the sides of tube to completely mix. Tubes were centrifuged at 750xg for 10 sec. The number of reactions required for each primer-probe was calculated using following equation:

$$Number\ of\ reactions\ per\ primer\ probe = (Number\ of\ genomic\ DNA\ (inc.control) x\ 3) + n$$

The primer-probe mix was prepared by combining each stock solution with nuclease-free water in individual 0.65 ml tube. Each tube was vortexed on high for 5 sec, placed on ice and protected from light. The mix were subjected to PCR reaction according to PCR cycling condition as shown in Table 2.5 below and data were analysed using the application available at www.stemcell.com/geneticanalysisapp. The copy number was calculated as, Copy number = ($2^{-\Delta\Delta Ct}$) x 2 and copy number <1.8 or >2.2 with a p-value <0.05 may suggest the presence of an abnormality within the culture.

Table 2.5 PCR cycling conditions for hPSC genetic analysis.

Stage	Cycles	Temperature (°C)	Cycling time (fast)
Polymerase activation	1	95.0	03:00
Amplification: - Denature - Anneal/extend	40	 95.0 60.0	 0:05 0:30

2.11.3 Viability/toxicity Assay

Cell viability, cytotoxicity and apoptosis were performed based on ApoTox-Glo™ Triplex Assay (G6320, Promega) according to the manufacturer's instructions. MAN13 cells were seeded at 35,000 cells per well in 24 well plate at day -1. Four time points after differentiations were assessed: day 0, 3, 7 and 19. Eight wells were used (for each non-transfected and lentiviral transfected cells). A total of 250 µl mTeSR1 were added to feed the cells. At day 0, all wells (n=8) of 24 well plate format that contain 200 µl of fresh mTeSR1 medium was added with 40 µl viability/cytotoxicity (VC) reagents and made up to 240 µl in total. Reagents were mixed by orbital shaking (300-500 rpm) using GlomaX multi detection system for 30 sec. Then plates were incubated for 1 h at 37°C in CO_2 incubator. Fluorescence is measured at 400/505-AFC Filter (Viability) and 485/520-Blue Filter (cytotoxicity). For apoptosis, a total of 200 µl of caspase reagent were added to all wells (n=8) mixed by orbital shaking (300-500 rpm) using GlomaX multi detection system for 30 sec and plate were incubated for 1 h at RT. A total of 100 µl cell lysate (of 24-well plate) were transferred to 96-well format (solid white plate) avoiding light exposure. Luminescence was measured and caspase activation indicated apoptosis. Methods were repeated at day 3, 7 and 19 of culture.

2.11.4 Whole mount 3D organoids immunofluorescence staining

Organoids at day 7+9, 7+12, 7+18 and 7+25 were selected for whole mount staining. Transwells were transferred to a new 6 well plate containing 1.2 ml PBS and anadditional 1 ml PBS was added on top of the membrane. After 2 washing steps, an equal amount of 4% PFA was added to the bottom and top of the transwell and incubated in 4°C for 20 min. Organoids were then washed and left in PBS until stained. For staining, organoids were transferred to 24-well plates (one organoid per well), blocked and permeabilised in 3% BSA/0.3% Triton-X in PBS. A total of 250 µl blocking solution was added in each well and incubated at RT for 30 min. Primary antibodies were prepared in 3% BSA/PBS and added to organoids before overnight incubation at 4°C. Organoids were then washed three times with 0.1% Triton-X/PBS and 250 µl of AlexaFluor™-488- or Alexa-Fluor™-594-labelled, species-specific secondary antibodies (diluted in 3% BSA/PBS) were added before incubated at RT for 1 h. Stained organoids were protected from light using aluminium foil. Organoids

were then washed three times with 0.1% Triton-X/PBS and incubated with 250 µl of 5 µg/ml (1:5000) 4',6-diamidino-2-phenylindole (DAPI) for 5 min. Organoids were washed twice with 1X PBS and transferred to a glass-bottom FluoroDish™ (FD3510, World Precision Instrument) (one organoid per dish). Excess PBS on organoids was removed by pipetting and a drop of ProLong™ Gold antifade Mountant with DAPI (P36935, Invitrogen) was added on top of the organoids. Immunofluorescence images were recorded using confocal microscope (Leica SP5 and SP8) and analysed using Leica LAS X software. Deconvolution was performed using Huygens Remote Manager (Scientific Volume Imaging) and the 3D reconstructions were executed using Imaris software. Antibodies used were summarised in Table 2.6.

2.11.5 Whole mount 3D organoids paraffin-embedded immunohistochemical staining

Kidney organoids at selected timepoints (d7+6,+9,+12,+18 and +25) were fixed in 4% paraformaldehyde, dehydrated though a graded series of alcohols and embedded in paraffin (B1002490, Thermo Fisher). Serial sections were cut on a Leica RM2255 microtome at 5 µm thick and subjected to H & E, Periodic Acid-Schiff (PAS), Alcian blue and/or immunohistochemical staining. The histological sections were selected based on strict rules that applied on both mutant and unaffected organoids. Top section refers to sequential sections cut from top that commenced from 2nd section onwards. The first top section is ignored. The same rule was applied for sections started from bottom region of organoids. Middle sections however are defined by the midpoint of total sections and one section on either side is selected for staining.

For staining, organoid sections were dewaxed in 2 changes of xylene, 5 min each at 37°C. Then sections were rehydrated in an alcohol 100%, 100%, 90%, 70%, 50% for 2 mins in each. ImmEdge hydrophobic barrier PAP Pen (H-4000, Vector Laboratories) was used to draw around the sections. For antigen retrieval, citrate buffer pH 6.0 at 1 mM concentration (unmasking solution) was used to boil the sections using an 800W microwave. Sections were boiled to 100% power for 3 min followed by 40% power for 10 min before cooling down at RT. Sections were then washed in PBS three times for 10 min each. Then sections were treated with 1% hydrogen peroxide (H1009, Sigma) in PBS for 10 min to block endogenous peroxidase activity before briefly washing in distilled water. Triton-X100 at 0.2% was added for 10 min before 3 washes with PBS, 10 min each. Sections were blocked with 10% normal serum (from the species in which the secondary antibody was raised) in 1% BSA (0.5 g in 50 ml PBS) for 60 min. Primary antibodies were prepared in 1% BSA/PBS, added and incubated at 4°C overnight. For control, PBS was used to replace primary antibody. The next day, sections were washed in PBS 3 times, 10 min each.

Then biotinylated secondary antibodies (diluted in 1% BSA/PBS) were added and incubated at RT for 2 h. Sections were washed 3 times in PBS, 10 min each and were incubated in avidin-biotin enzyme complex (ABC) VECTASTAIN® ABC reagents (PK-6100, Vector Laboratories) for 1 h then washed in PBS 3 times, 10 min each. To detect peroxidase activity, sections were developed in *SIGMAFAST*™ 3,3'-Diaminobenzidine (D4293, Sigma) for 2.5 min before washed in distilled water for 10 min. Sections were counterstained with hematoxylin for 20 sec and washed in running tap water until blue. Sections were dehydrated in series of alcohols (50%, 70%, 90%, 100%, 100%) for 2 min each and cleared in xylene I and xylene II (2 min each) before mounting in DPX mountant (06522, Sigma). Images were captured using Pannoramic 250 Flash III Digital Slide Scanners (3D HISTECH) using x20 objective (Zeiss) and analysed with Pannoramic Case Viewer software.

Table 2.6 List of antibodies and lectins used in immunological stainings.

Antibody	Host	Source	Catalogue no	Dilution
Primary antibodies				
Nanog (D73G4)	rabbit	Cell Signaling	#4903	1:200
Sox2 (D6D9)	rabbit	Cell Signaling	#3579	1:200
Oct-3/4	mouse	BD Biosciences	611203	1:100
SSEA4	mouse	Abcam	ab16287	1:200
TRA-1-81	mouse	Stemgent	09-0069	1:200
TRA-1-60	mouse	Thermo Fisher	MA1-023	1:200
HNF-1β	rabbit	Santa Cruz	sc-22840	1:200
HNF-1α	rabbit	Santa Cruz	sc-10791	1:200
collagen IV	rabbit	Abcam	ab6586	1:500
alpha 3 (IV)	rat	Chondrex Inc.	707	1:200
CD31	mouse	Cell Signaling	89C2	1:300
SLC22A6	rabbit	Abcam	ab131087	1:200
THP	rabbit	Santa Cruz	sc20631	1:300
UMOD	mouse	Abcam	ab167678	1:500
PKHD1 (Polyductin)	rat	Abcam	ab204951	1:200
PKD1 (Polycystin 1)	mouse	Abcam	ab74115	1:200
PKD2 (Polycystin 2)	rabbit	Proteintech	19126-1-AP	1:200
active Caspase 3	rabbit	Abcam	ab2302	1:200
Ki-67	rabbit	Abcam	ab15580	1:500
PCNA	mouse	Abcam	ab29	1:500
SYNPO	rabbit	Santa Cruz	sc-50459	1:200
PODXL	mouse	R&D Systems	MAB1658	1:300
NPHS1	rabbit	Abcam	ab136894	1:200
NPHS2	rabbit	Sigma	P0372	1:200
Nephrin	sheep	R&D Systems	AF4269	1:200
OSR1	mouse	Abnova	H00130497-M04	1:100
SIX2	rabbit	Proteintech	11562-1-AP	1:200
PAX2	rabbit	Life Technologies	71-6000	1:200
WT1	rabbit	Santa Cruz	sc-192	1:100
LHX1	goat	Santa Cruz	sc-19341	1:75
GATA3	goat	R&D Systems	AF2605	1:300
E-Cadherin	mouse	Abcam	ab76055	1:200
SALL4	mouse	Abnova	H00057167-M03	1:20
AQP1	rabbit	EMD Millipore	AB3272	1:200
AQP2	rabbit	EMD Millipore	AB3274	1:200
Acetylated tubulin	mouse	Sigma-Aldrich	T7451	1:1000
CUBN	goat	Santa Cruz	sc-20607	1:200
CALB1	rabbit	Abcam	ab25085	1:400
MEIS ½/3	mouse	Active Motif	39795	1:500
FOXD1	rabbit	Thermo Fisher Scientific	PA5-35145	1:50

TRPV4	rabbit	Alomone labs	ACC-034	1:500
TRPV5	rabbit	Abcam	ab137028	1:100
Flow cytometry antibodies				
TRA-1-81-PE	mouse	BD Pharmingen	560885	5:100
Nanog-AF488	mouse	BD Pharmingen	560791	11:100
Sox2-AF647	mouse	BD Pharmingen	562139	1.3:100
SSEA3-PE	rat	BD Pharmingen	560879	5:100
Embryoid body antibodies				
AFP	mouse	R&D	MAB1368	1:200
GATA6	mouse	R&D	MAB1700	1:1600
SOX17	goat	R&D	AF1924	1:200
FOXA2	rabbit	Cell signaling	8186	1:400
α-SMA	mouse	R&D	MAB1420	1:100
Brachyury	goat	R&D	AF2085	1:20
Vimentin	goat	R&D	AF2105	1:50
B-tubulin III	mouse	R&D	MAB1195	1:200
Neurofilament-L	rabbit	Cell signaling	2837	1:100
GFAP	mouse	R&D	MAB2594	1:100
Isotype controls				
IgM	mouse	Santa Cruz	sc-3881	1:200
IgG	mouse	Santa Cruz	sc-2025	1:200
IgG	rabbit	Santa Cruz	sc-2027	1:200
IgG	mouse	Cell signaling	5415S	1:200
IgG	rabbit	Cell signaling	3900S	1:400
IgG-AF488	mouse	BD Pharmingen	557782	1:100
IgG-AF647	mouse	BD Pharmingen	557783	0.3:100
IgG-PE	mouse	BD Pharmingen	550617	1.3:100
IgM-PE	rat	BD Pharmingen	553943	0.3:100
Secondary antibodies for ICCs				
anti-Rabbit IgG AF488	goat	Thermo Fisher Scientific	A-11008	1:400
anti-Goat IgG AF594	donkey	Thermo Fisher Scientific	A-11058	1:400
anti-Mouse IgG AF647	goat	Thermo Fisher Scientific	A-21235	1:400
anti-Rabbit IgG AF594	goat	Thermo Fisher Scientific	A-11037	1:400
Secondary antibodies for IHCs				
Biotinylated anti-Rabbit IgG	goat	Vector Laboratories	BA-1000	1:400
Biotinylated anti-Mouse IgG	horse	Vector Laboratories	BA-2000	1:400
Biotinylated anti-Goat IgG	horse	Vector Laboratories	BA-9500	1:400
Biotinylated anti-Rat IgG	goat	Vector Laboratories	BA-9400	1:400
Lectins				
Fluorescein labelled Lotus Tetragonolobus Lectin (LTL)		Vector Laboratories	FL-1321	1:500
Rhodamine labelled Peanut Agglutinin (PNA)		Vector Laboratories	RL-1072	20 µg/ml

2.11.6 Alcian Blue staining

Slides were deparaffinised by clearing in xylene I and xylene II for 3 min each, followed by hydration with decreasing concentration of alcohol (100%, 90% 70% and water) for 2 min each. Slides were incubated in 3% glacial acetic acid (537020, Sigma-Aldrich) for 3 min followed by Alcian blue 8GX (A5268, Sigma-Aldrich) for 30-45 min. Sections were washed in running tap water for 2 min. Nuclear fast red solution (N3020, Sigma-Aldrich) was added for 3-5 min and washing continued with running water for 1 min. Sections were rinsed in distilled water for 2 min followed by dehydration at increasing alcohol concentrations (70%, 95% and 100%), 2 min each. Slides were cleared in xylene I and xylene II twice, 3 min each and mounted with DPX mountant. Strongly acidic Glycosaminoglycans will be stained blue, nuclei range from pink to red and cytoplasm appears pale pink.

2.12 RNA analysis

2.12.1 RNA extraction

RNA were extracted based on *mir*Vana™ miRNA Isolation Kit (AM1560, Invitrogen) following manufacturer's instructions. Cells in 24-well plate were detached using 250 µl TrypLE and incubated for 1 min in the incubator. An equal amount of culture medium was added to inactivate TrypLE. Cells were centrifuged for 1 min at 12,000 rpm and washed in 1 ml PBS. A total of 300 µL lysis/binding solutions were added. Cells were vortex and pipetted rigorously to completely lyse the cells and to obtain homogenous lysate. Then 30 µl of miRNA homogenate additive were added to the lysate and mixed by vortexing. The mixture was left for 10 min on ice. RNA was isolated from lysates using phenol extraction method by adding 300 µl acid-phenol:chloroform and vortexed for 30 sec to mix. The mixture was centrifuged for 5 min at maximum speed 10,000xg, RT to separate the aqueous and organic phases. The interphase should be compacted, if not then centrifugation was repeated. The aqueous (upper) phase was transferred into fresh tube without disturbing lower phase. The volume collected was noted. Then 375 µl of 100% ethanol (RT) were added to the aqueous phase and pipetted to mix. The mixture were transferred onto supplied collection tube and centrifuged for 15 sec at 10,000xg to pass through the filter. Flow-through was discarded and 700 µl of miRNA Wash Solution 1 were added to the filter cartridge and centrifuged for 30 sec. Flow-through was discarded and the filter was washed twice with 500 µl Wash Solution 2/3. After removal of the flow-through from the last wash, the filter cartridge in the same collection tube was replaced and the assembly were spun for 1 min at 10,000xg to remove residual fluid from the filter. The filter cartridge was transferred into a fresh collection tube and 100 µl of pre-heated (95°C) nuclease-free water were applied at the centre of the filter and the cap was closed. To recover RNA, the tube was spun for 1 min at maximum speed (12,000 rpm). The eluate was collected and stored at -80°C.

2.12.2 DNase Treatment

Contaminating DNA, DNase and divalent cations were removed from extracted RNA using DNA-free™ DNA Removal Kit (AM1906, Invitrogen). For a total 100 µl of extracted RNA, 0.1 volume (10 µl) of 10X DNase I Buffer and 1µl rDNase I were added to the RNA and mixed gently followed by incubation for 30 min at 37°C. A total of 5 µl resuspended DNase Inactivation Reagent was added and mixed well. The mixture was incubated for 2 min at RT and occasionally flicked and mixed further. Then it was centrifuged at 10,000xg for 1 min. The supernatant (RNA) was transferred to a fresh tube before measuring the RNA concentration.

2.12.3 RNA quantification

Absorbance was measured using NanoDrop™ 2000/2000c Spectrophotometers (Thermo Scientific). RNA absorbs at 260 nm thus will contribute to the total absorbance of the sample. The ratio of absorbance at 260 nm and 280 nm was used to assess purity of RNA samples. A 260/280 ratio of ~2.0 is accepted as pure for RNA. A lower ratio indicated presence of contaminants such as protein or phenols that absorbs strongly at 280 nm.

2.12.4 Primers design

Primers were designed using free, open-source graphical user interface (GUI) application PerlPrimer (http://perlprimer.sourceforge.net/) and used to amplify the target sequence. The optimal primer length was set to 20-25 bases. The GC content was kept in the 30-80% range. T_m was maintained between 59-61°C with 1°C difference between primers. Identical nucleotides runs were avoided. If repeats could not be avoided, it was assured that there were fewer than 4 consecutive G bases. The last 5 nucleotides at 3' end were checked to contain no more than two G and/or C bases. If no acceptable primer sequences were available, another amplicon site was selected.

2.12.5 Quantitative qRT-PCR for kidney-related genes

Power SYBR® Green RNA-to-CT™ 1-Step Kit (4389986, Applied Biosystems™) performed one-step RT-PCR with SYBR® Green reagents for quantitation experiments on a real-time PCR system. Reverse transcription and PCR were both carried out in one reaction tube. AmpliTaq Gold® DNA Polymerase UP (Ultra-Pure) is a highly purified DNA polymerase that allows efficient hot start PCR by only being activated at high temperature when DNA is fully denatured. The quantification of the RNA template was calculated using formula as below.

$$Concentration\ of\ single\ stranded\ RNA = A_{260}\ x\ 40\ \mu g/ml$$

Ramp speed was set to 'Standard' mode with a total 10 µl reaction volume. Melt (dissociation) curve was performed to detect non-specific amplification after the RT-PCR cycles. Thermal cycling conditions and reaction components were summarised as in Table 2.7 below. GAPDH were used for data normalization and primer sequences used in this study are listed in Table 2.9.

Table 2.7 qRT-PCR reaction parameters for 40 cycles

Stage	Step	Temp	Time
Holding	Reverse transcription	48°C	30 min
Holding	Activation of AmpliTaq Gold® DNA Polymerase, UP (Ultra-Pure)	95°C	10 min
Cycling	Denature	95°C	15 sec
	Anneal/extend	60°C	1 min
Melt curve	Denature	95°C	15 sec
	Anneal	60°C	15 sec
	Denature	95°C	15 sec

Table 2.8 RT-PCR components

Component	Volume for 1 reaction
Power SYBR® Green RT-PCR Mix (2X)	5.0 µl
Forward primer (100 to 200 nM final)	0.5 µl
Reverse primer (100 to 200 nM final)	0.5 µl
RT Enzyme Mix (125X)	0.08 µl
RNase-free H_2O	0.42 µl
RNA template (up to 100 ng)	3.5 µl
Total Volume	**10 µl**

Pipetting error (or excess volume) was multiplied by 1.2 of total reaction volume

Table 2.9 qPCR primer sequences for kidney cells characterisation

No	Gene	Forward Primer	Reverse Primer
1	*T*	AGGTACCCAACCCTGAGGA	GCAGGTGAGTTGTCAGAATAGGT
2	*OSR1*	CTCCTCGAGATCCGGATTGAG	GTTCACTGCCTGAAGGAAGG
3	*SIX2*	CGCCCATGTGGGTCAGTGGG	AGCCGGGAGCGCTGTAGTCA
4	*PAX2*	GCAACCCCGCCTTACTAAT	AACTAGTGGCGGTCATAGGC
5	*WT1*	GGCAGCACAGTGTGTGAACT	CCAGGCACACCTGGTAGTTT
6	*HNF1B*	AACCACCGAAGAGGAAGCAA	TCGCATCAGTTTGTTCGATGA
7	*HNF1A*	AACACCTCAACAAGGGCACTC	CATCACCTGTGGGCTCTTCAA
8	*AQP1*	ATTAACCCTGCTCGGTCCTT	ACCCTGGAGTTGATGTCGTC
9	*AQP2*	GTGCGCCGAAAATTTCCA	CCTCGACTTCTCCTTGAAGCA
10	*HOXB7*	GCCTACAAATCATCCGGCCA	GGTTGGAAGCAAACGCACAA
11	*LHX1*	ATGCAACCTGACCGAGAAGT	CAGGTCGCTAGGGGAGATG
12	*SALL1*	AGCGAAGCCTCAACATTTCCAATCC	AATTCAAAGAACTCGGCACAGCACC
13	*CITED1*	GCTGGCTAGTATGCACCTGC	CATTGGCTCGGTCCAACCC
14	*CITED2*	CACCAATGGGCTGCACCATCAC	GCCGCTCGTGGCATTCATGTTG
15	*SALL4*	CAGATCCACGAGCGGACTCA	CCCCGTGTGTCATGTAGTGA
16	*FOXD1*	GACTCTGCACCAAGGGACTG	CCTCGAGCGCGCTAACATAG
17	*GATA3*	GCCCCTCATTAAGCCCAAG	TTGTGGTGGTCTGACAGTTCG
18	*KDR (Flk1)*	CATAATAGAAGGTGCCCAGGA	GATGATGACAAGAAGTAGCCAG
19	*UMOD*	AACATCACTGATATCTCCCTCCT	TTGTCTCTGTCATTGAAGCCC
20	*PDGFRB*	GCCGTCAAGATGCTTAAATCC	TATAGATGGGTCCTCCTTTGGT
21	*HOXD11*	GCCAGTGTGCTGTCGTTCCC	CTTCCTACAGACCCCGCCGT
22	*TBX6*	CATCCACGAGAATTGTACCCG	AGCAATCCAGTTTAGGGGTGT
23	*MIXL1*	GGTACCCCGACATCCACTT	GCCTGTTCTGGAACCATACCT
24	*SOX17*	ACGCCGAGTTGAGCAAGA	TCTGCCTCCTCCACGAAG
25	*GSC*	GAGGAGAAAGTGGAGGTCTGGTT	CTCTGATGAGGACCGCTTCTG
26	*EYA1*	GGACAGGCACCATACAGCTACC	ATGTGCTGGATACGGTGAGCTG
27	*RET*	TATCCTGGGATTCCTCCTGA	TCTCCAGGTCTTTGCTGATG
28	*FOXF1*	GCGGCTTCCGAAGGAAATG	CAAGTGGCCGTTCATCATGC
29	*SOX9*	CCGAAAGCGGAGCTCGAAAC	AGTTTCCGGGGTTGAAACTGG
30	*SF1*	GTGTACCAAGTGTGGAGGGG	AGGTGCTTCACCCAGTTCAG
31	*GATA6*	CATGACTCCAACTTCCACCT	ACTTGAGCTCGCTGTTCTCG
32	*SOX1*	CACAACCGAGATCAGCAA	GGTACTTGTAATCCGGGTGC
33	*PAX6*	GTCCATCTTTGCTTGGGAAA	TAGCCAGGTTGCGAAGAACT
34	*FOXA2*	GGAGCGGTGAAGATGGAA	TACGGTCATGCCGTTCAT
35	*GAPDH*	AGCCACATCGCTCAGACAC	GCCCAATACGACCAAATCC
36	*PARAXIS*	GCGGGCAGTGCCAAGGGCG	CCCTCACCTTCAAGCAGCTGC
37	*LIM1*	TCATGCAGGTGAAGCAGTTC	TCCAGGGAAGGCAAACTCTA
38	*NANOG*	GGCTCTGTTTTGCTATATCCCCTAA	CATTACGATGCAGCAAATACAAGA
39	*OCT4*	AGACCATCTGCCGCTTTGAG	GCAAGGGCCGCAGCTT
40	*PKD1*	ATTCTAAGAGTCTGGTGTGCTG	CAGATTGCTACCCACAATGGA

41	*PKD2*	ATACCGTGGATGACATTTCAGAG	GTATGGCCCTTCCCTTTGAG
42	*PKHD1*	CTTCAACGCAGGTACATTTAGAG	CGCTATCAAGAATTAGGACCAC
43	*NPHP1*	GAACCTACCTAGAGCCTTATAGTG	CATCTGCTGTTTCATCCACC
44	*IFT88*	CAGAAGACCTCCATCCAAGAC	CTAGTAACTCCATCCTGAATAGCC
45	*SYNPO*	GGACTGGGATGTAGTGAAGG	CTTCTTTCAGATCCTTCTCCGT
46	*PODOCALYXIN*	TCATCATCACCATCGTCTGC	CCACCTTCTTCTCCTGCATC
47	*NPHS1*	AGTGTGGCTAAGGGATTACCC	TCACCGTGAATGTTCTGTTCC
48	*NPHS2*	CAAAGTGCGGATGATTGCTG	GTGTGGAGGTATCGAAGCTG
49	*PECAM (CD31)*	AACAGTGTTGACATGAAGAGCC	TGTAAAACAGCACGTCATCCTT
50	*CDH1*	CAATACATCTCCCTTCACAGCA	AATGATAGATTCTTGGGTTGGGTC
51	*LRP2*	AAATTGAGCACAGCACCTTTGA	TCTGCTTTCCTGACTCGAATAATG
52	*CALB1*	TCCAGGGAATCAAAATGTGTGG	GCACAGATCCTTCAGTAAAGCA
53	*HNF4A*	CGAAGGTCAAGCTATGAGGACA	ATCTGCGATGCTGGCAATCT
54	*SLC12A1*	AGTGCCCAGTAATACCAATCGC	GCCTAAAGCTGATTCTGAGTCTT
55	*SLC22A6 (OAT1)*	TTCGGCTACCTTGCAGACAG	GAATGGGCATCCACTCCACA
56	*SLC22A8 (OAT3)*	ACTCGGGTACTGCTACACCT	CAGGTCACTTGCGGTGTACT
57	*SLC22A11 (OAT4)*	AGGTTCGTGCTCAGATGGTG	CCATGGCCTGGAATCTGTGT
58	*SLC22A2 (OCT2)*	CATCGTCACCGAGTTTAACCT	GTAGCCGATACTCATAGAGCC
59	*SLC22A1 (OCT1)*	CATCGTCACTGAGTTCAACCT	AAAGTAGCCAACACCGAGAG
60	*IRX1*	GCTCTTCGGCAGCGACAC	GCTCTGGGGCCTCCTTTG
61	*IRX2*	CAGCAATGCAAATCTCTGCG	GCCTCCTTGATATGTACTTAAATGC
62	*IRX3*	CGGAACAGATCGCTGTAGTG	GGGTTTAACTGTAGGGTGGG
63	*WNT4*	ACCTGGAAGTCATGGACTCG	TCAGAGCATCCTGACCACTG
64	*WNT9B*	AGTACAGCACCAAGTTTCTGAG	ACTCTTCACAGCCTTGATGC
65	*LFNG*	AAGGAGATGACGTTCATCTTCAC	CTCGATGAAGCGGTCATACTC
66	*GDNF*	GAGCAGTGACTCAAATATGCC	CTGCCATTTGTTTATCTGGTGAC
67	*CUBN*	AGTCATTCTCCTCAACTTCACTG	CTGCTACCAATCTCAACATAATCTG

2.13 Genomic DNA dosage assay

Extraction of genomic DNA was performed based on Wizard® Genomic DNA Purification Kit (A1120, Promega) following manufacturer instructions. Primers were designed using PerlPrimer software. Optimal primer length ranged from 18-23 bases and the amplicon size was set to 80-120 bp. Reactions were designed to bind at 4 different locations on Exon 9 (n-terminal, middle and c-terminal) together with a control pair that binds Exon 2. Gene dosage was analysed based on amplification of a target gene (mutant *HNF1B*) and control gene (unaffected lines) in a SYBR green reaction, followed by comparison between the ratio of *HNF1B* patient (mutant) and unaffected control (unaffected) melting curve peaks. DNA concentration was quantified using NanoDrop™ 2000/2000c Spectrophotometer (Thermo Fisher) and DNA samples were diluted to 100 ng/µl. Before the start of qPCR assay, DNA samples again were diluted to final concentration of 10 ng/µl, from which 10 µl was used for each reaction (20 ng DNA).

Table 2.10 Primer sets for genomic DNA dosage assay

No	Gene	Location	Forward Primers	Reverse Primers
1	*HNF1B* (control)	Exon 2	CCTCCGACAATTCAACCAGAC	CATGGCTCTGTTGACTGAACTC
2	*HNF1B n-terminal (5′ binds deletion site)*	Intron 8-Exon9	GTGTCCTCTACAAGCCTGGT	CAGAGGGTGATGGTGTGGA
3	*HNF1B n-terminal (3′ binds deletion site)*	Intron 8-Exon9	GTTGAGTTGGGCATCATCTCC	ATCACCAGGCTTGTAGAGGAC
4	*HNF1B mid*	Exon9	GAAGCAAGAAAGCCGTACTG	CTCAGTTCAATAGCACATGTCC
5	*HNF1B c-term*	Exon9	GACAGCATACCTTGGACTGAC	AAGCTGGCATGTTACTCTGAC

2.14 DNA Sequencing

2.14.1 Primers design

Forward and reverse primers were designed to cover 200 bp of DNA length. The optimal primer length was set to 18-23 bases. The GC content was kept in the 40-60% range and T_m was maintained between 55-60°C. The primers are designed 100 bases upstream of *HNF1B* gene. If no acceptable primer sequences were available, another amplicon site was selected.

Table 2.11 Primers set for PCR of genomic DNA and sequence analysis

Gene	Forward Primer (binds intron 8)	Reverse Primer (binds exon 9)
HNF1B	CTTCTTTCTTCTGAAGTGGC	GCATAGAAGGGAAACTGGG

2.14.2 Genomic DNA extraction

Genomic DNA of hPSCs were extracted based on Wizard® Genomic DNA Purification Kit (A1120, Promega) following manufacturer instructions. Cells were detached using TrypLE and centrifuged for 10 sec at maximum speed (13,000–16,000×g). Cell pellet were washed with PBS, vortexed and added with 600 µl of Nuclei Lysis Solution then mixed by pipetting. For lysis and protein precipitation, a total of 3 µl of RNase Solution were added to the cell lysate and mixed. Cell lysate was incubated for 15–30 min at 37°C and cooled to RT. Then 200 µl of Protein Precipitation Solution was added. Cells were vortexed and chilled on ice for 5 min before centrifuging for 4 min at maximum speed. For DNA precipitation and rehydration, supernatant was transferred to a fresh tube containing 600 µl of RT isopropanol and mixed by inversion. Cells were centrifuged for 1 min at maximum speed. Supernatant was removed and 600 µl of 70% ethanol were added then mixed. Cells were centrifuged for 1 min at maximum speed. The ethanol was aspirated and the pellet air-dried for 15 min. DNA was rehydrated in 100 µl of DNA Rehydration Solution for 1 h at 65°C or overnight at 4°C. Then the DNA was amplified by PCR reaction in a total of 10 µl reaction as described in Table 2.12 below.

Table 2.12 Reaction setup for amplification of genomic DNA by PCR

Reaction	Volume (for 10 µl reaction)	Volume (for 30 µl reaction)
Forward primer (20 µM)	0.5 µl	1.5 µl
Reverse primer (20 µM)	0.5 µl	1.5 µl
Genomic DNA	2 µl	6 µl
GoTaq® Green Master Mix	5 µl	15 µl
Nuclease-free water	2 µl	6 µl
Total	**10 µl**	**30 µl**

Table 2.13 PCR parameters

Step	Temperature	Time (sec)	Cycles
Denaturation	95°C	120	1
Denaturation	95°C	60	35
Annealing	60°C	60	
Elongation	72°C	60	
Elongation	72°C	300	1
Cooling	4°C	∞	-

A total of 10 µl PCR products from each line were run on the 2% agarose gel electrophoresis to check for visible bands. Another 10 µl PCR products were subjected to PCR Purification.

2.14.3 PCR products purification

DNA purification was performed using QIAquick PCR Purification Kit (28104, Qiagen) following manufacturer's instruction. A total of 5 volumes of Buffer PB were added to 1 volume of the PCR reaction and mixed. If the color of the mixture turned orange or violet, 10 µl 3 M sodium acetate, pH 5.0 were added. Subsequently the mixture will turn yellow. A QIAquick column was placed in a provided 2 ml collection tube. To bind DNA, samples were applied to the QIAquick column and centrifuged for 30–60 sec until all the samples have passed through the column. Flow-through was discarded and the QIAquick column was placed back in the same tube. To wash, 0.75 ml Buffer PE was added to the QIAquick column and centrifuged for 30–60 sec. Flow-through was discarded and the QIAquick column was placed back in the same tube. The QIAquick column was centrifuged once more in the provided 2 ml collection tube for 1 min to remove residual wash buffer. Each QIAquick column was placed in a clean 1.5 ml microcentrifuge tube. To elute DNA, 50 µl Buffer EB (10 mM Tris·Cl, pH 8.5) or water (pH 7.0– 8.5) were added to the center of the QIAquick membrane and the column was centrifuged for 1 min. For increased DNA concentration, 30 µl elution buffer was added to the center of the QIAquick membrane, the column left to stand for 1 min, and then centrifuged. If the purified DNA was to be analyzed on a gel, 1 volume of Loading Dye was added to 5 volumes of purified DNA. The solution was mixed by pipetting up and down before loading onto the 2% agarose gel. For sequencing, the total 10 µl reactions were prepared as follows.

Table 2.14 Reaction components for Sanger sequencing

Components	Amount (µl)
Primer 5 µM (either forward or reverse)	5 µl
DNA	2 µl
Nuclease-free H_2O	3 µl
Total	10 µl

2.14.4 PCR and Sanger sequencing analysis

Sanger sequencing of *HNF1B* (NM_000458.4) was performed on PCR-amplified and purified fragments of all 3 newly generated lines (TF171, TF172, TF173). The analysis included intron-exon boundaries that begin from end of intron 8 into exon 9 (400-500 bp). These fragments were directly sequenced in either directions using ABI3730 Sequencer (Applied Biosystems, USA). The electropherogram were aligned to the reference sequence using SnapGene Viewer software. Experiments were repeated 3 times and data obtained from the sample containing only DNA from the unaffected control was used for normalisations.

2.14.5 DNA gel electrophoresis

A total of 2 g agarose (1613100, Bio-Rad) were added to 1X 100 ml of TBE buffer (15581044, Thermo Fisher) to make up 2% agarose. Agarose solution containing 6 µl of SYBR safe DNA gel stain (S33102, Thermo Fisher) was boiled. Gel was left solidified at 45°C for 20 min. A total of 10 µl PCR product was loaded alongside DNA HyperLadder™ 100bp (BIO-33056, Bioline) and the gel was run at 110 V for 1 h.

2.15 Western blotting

2.15.1 Protein extraction from E15 mouse embryonic kidneys

Twenty pieces of E15 mouse embryonic kidneys (at approximately 50 mg), were washed with 1X PBS, sliced and homogenized using a Dounce homogenizer in a microcentrifuge tube. A total of 700 µl of RIPA buffer (Thermo Fisher Scientific) that contains protease inhibitors (87786, Thermo Fisher) were added, to prevent proteolysis and maintain phosphorylations of proteins. The tubes were vortexed, resuspended and keep on a rotating wheel in the cold room for 1 h. The tubes were then centrifuged at 14,000 rpm for 10 min at 4°C. The protein supernatant was transferred into a pre-chilled microcentrifuge tube and kept on ice. The protein extracts are stored at -80°C until use.

2.15.2 Protein extraction from hPSCs

Cells were harvested, washed twice with PBS and total numbers of cells were counted. Cells were transferred to Eppendorf tubes and 350 µl of RIPA lysis buffer and protease inhibitors (1 capsule in 10 ml of RIPA) were added per 2 million cells. Tubes were kept at 4°C on a rotating wheel for 30 min. Cells were centrifuged at 13,000 rpm for 10 min, 4°C. The protein supernatant was transferred on ice-cold Eppendorf tubes.

2.15.3 Protein quantification

Quantification of proteins were carried out based on BCA™ Protein Assay Kit-Reducing Agent Compatible-Pierce (23250, Thermo Fisher). Assays were performed in 96-well plates. A total of 30 µl of water were added to well A1, A2 and A3 and another 20 µl were added to well A1-H1. A total of 10 µl pre-diluted BSA samples (protein concentration ranged from 125 - 2,000 µg/ml) were added to A1-H1 and 10 µl of mixture were transferred to column 2 and 3. The same steps were applied for the test samples. A working reagent solution 50:1, solution A: solution B (blue) was prepared and 200 µl were loaded into each well. The plate was incubated at 37°C for 30 min and the absorbances were recorded at 560 nm using Promega GloMax® Multi detection plate reader.

2.15.4 Protein sample preparation and loading

A total of 30 µg of protein extract was added to Pierce™ Lane Marker Reducing Sample Buffer (39000, Thermo Fisher) and brought up to 40 µl with water. The mixture was vortexed and kept at 96°C for 10 min. The samples then were loaded on the gel or kept at RT until ready to load. For loading, 20 ml of NuPAGE™ MES SDS Running Buffer (20X) (NP0002, Thermo Fisher) were added to 380 ml of deionised distilled water and poured into the running tank. NuPAGE™ 10% Bis-Tris Protein Gels, 1.0 mm, 10-well (NP0301BOX, Thermo Fisher) were briefly washed with water and inserted into the tank. Additional running buffer was added: enough to cover the wells and the rear part of tank. A total of 40 µl of samples were loaded alongside 10 µl of a protein ladder, Color Protein Standard, Broad Range (11–245 kDa) (P7712S, New England Biolabs). Gel were run at 60 V for 10 min and continued with 120 V for 1 h.

2.15.5 Gel transfer

Transfer of gel was performed following manufacturer's instruction using iBlot 2 Dry Blotting System (Life Technologies). The gel was first immersed on water. Spacer gel (top and bottom part) was removed using scalpel and transferred onto iBlot2 Transfer Stack. Gel and filter were rolled and the gold layer stack was left on top. Gel part was retained on the membrane and program 'P3' were chosen and left for 7 min for transferring 30-150 kDa proteins.

2.15.6 Blocking and antibody incubation

The membrane was incubated with blocking solution 5% Milk-PBS-T (2.5 g skimmed milk, 50 ml PBS in 0.1 % Tween 20) (PP9416, Sigma) for 1-3 h at RT or overnight at 4°C. Primary antibody was prepared in 5% Milk-PBS-T for overnight incubation at 4°C or 2-3 h at RT. The membrane wasre washed with PBS-T 3 times (10 min each). Then, secondary antibody (IRDye® 800CW, LI-COR) diluted in 5% Milk-PBS-T was added and left for 1 h at RT in a closed container to avoid dehydration. The membrane was washed with PBS-T for 3 times (10 min each) and protein band developed using Odyssey CLx Imaging system (LI-COR Biosciences, Germany). Antibodies used were summarised in Table 2.15 below.

Table 2.15 Antibodies used for protein detection in Western blotting

Antibodies	**Isotype**	**Reactivity**	**Stock concentration/ Unit/ Sizes**	**Dilution**	**Cat No.**	**Supplier/ Brand**
Primary						
HNF-1β Antibody (H-85)	Rabbit polyclonal IgG	mouse, rat, human	200 µg/ml	1:200	sc-22840	Santa Cruz Biotechnology
HNF-1α Antibody (H-140)	Rabbit polyclonal IgG	mouse, rat, human	200 µg/ml	1:200	sc-10791	Santa Cruz Biotechnology
GAPDH (D16H11) XP® Rabbit mAb	Rabbit monoclonal IgG	Human, mouse, rat, monkey	n/a	1:2000	#5174	Cell Signaling Technology®
Secondary						
IRDye® 800CW Goat-anti-Rabbit	Goat-anti-Rabbit IgG	Rabbit	1 mg/ml	1:15000	926-32211	LI-COR Biosciences

2.15.7 Removal of antibodies (Stripping)

The membrane was folded and inserted into a 50 ml falcon tube containing 20 ml of stripping buffer: 6.2 ml of TRIS-HCl (0.2 M, pH 6.7), 2 ml of 20% SDS, 11.8 ml of water and 140 µl of β-mercaptoethanol (100 mM). The tube was sealed with parafilm and left at 55°C for 1 h on rotator. The film was developed to confirm that membrane is clean.

2.16 Statistical Analysis

Experiments are not random and researchers were kept non-blinded to the HNF1B conditions. Differentiation of hiPSCs was performed in parallel (unaffected versus mutant) for all conditions except for hESCs. Statistical analysis was performed using two-tailed t-test for two samples with unequal variance (heteroscedastic). Data are represented as mean±S.E.M from technical replicates (n=3) and comparison between the groups was calculated using an unpaired t-test (two-tailed). A value of $p<0.05$ was considered to be statistically significant. All statistical analyses were carried out using GraphPad Prism 7 software.

Chapter 3: Can human pluripotent stem cells be used to model kidney development?

3.1 Aims and introduction

Kidney is a mesodermal organ that is derived from intermediate mesoderm (IM). The IM differentiates to give rise to both ureteric bud (UB) and metanephric mesenchyme (MM) that interacted reciprocally to generate kidney cell types. It is however known that human kidney completed before birth and no new nephrons being produced postnatally (Takasato et al., 2014a). Hence, there are no renal stem cells to replace any damage or loss of nephrons. From literature, it is known that hPSCs can be differentiated to kidney lineages expressing early progenitor markers (Morizane and Lam, 2015). Thus, in Kimber Lab, I have set up a 2D kidney differentiation protocol to generate kidney-specific cells. This *in vitro* model could then be used to test the hypothesis that human-derived PSCs can be utilised to identify molecular and cellular aberrations which will model morphological and biological aspects of RCAD. Towards answering this question, I have laid several aims that include:

1. To derive and characterise human induced pluripotent stem cell from *HNF1B* families and its related healthy controls.

2. To culture and differentiate hPSCs to self-organizing structures of intermediate mesodermal kidney lineages to establish an *in vitro* model for kidney development.

3. To characterise morphological differentiation also documenting expression of major kidney marker genes using qRT-PCR and immunofluorescence staining upon kidney differentiation for 30 days.

4. To investigate the temporal expression patterns of *HNF1B* during formation of kidney organoids and comparing this to *HNF1B* nuclear localisation in E14 mouse kidneys sections.

5. To simultaneously compare morphological characteristics, gene and protein expression pattern of differentiating and differentiated hPSCs.

In this section, I will report on the derivation, characterisation and directed differentiation of unaffected hPSCs (MAN13 and TF173 lines) towards kidney lineage under defined conditions by utilising growth factors involved in normal embryogenesis. Precise control of gene expression is critical for appropriate differentiation of kidney precursor thus I adapted a previously described protocol (Takasato et al., 2014b) with slight modifications. The current differentiation strategy has successfully enabled generation of both UB/MM derivatives with evidence of key nephron progenitors. This chapter describes a complete characterisation of kidney

precursors on monolayer culture (2D) together with expression levels throughout the differentiation. However, the *HNF1B* mutant hiPSCs (TF172 and TF171 lines) were not tested in 2D culture system and will be discussed in the following 3D organoid differentiation chapter.

3.2 Results

3.2.1 Generation of *HNF1B*-derived iPSCs using Sendai reprogramming method

Upon receiving the blood samples, cells were immediately being isolated, counted and frozen down. PBMCs are the cloudy mid-layer portion of the separated total blood and a total of $3.0x10^5$ PBMCs were plated on each well of 6-well plate, for each line. These erythroid progenitors-containing PBMCs were expanded for a week in StemSpan™ Serum-Free Expansion Medium II (SFEM II). It is noted that the total number of suspension cells were increased in all hiPSC lines (TF171, TF172, TF173) by 43-, 27-, and 31-fold, respectively, by day 8 of expansion as compared to initial cell number at plating day (day 0)(Figure 3.2;e). After a week of expansion, these clustered erythroid progenitors were transduced with SeV containing human transcription factors (c-Myc, h-KOS, h-Klf4) with (MOI=5,5,3), respectively. After 24 hours of transfection, it is observed that small clump of cells began to adhere to culture plate with high proportion of cells remained floating in clusters. Low degree of colony overgrowth from these attached cell clusters were also being identified and regarded as putative iPS colonies.

After 2 weeks post-transduction, most suspension cells adhered to plastic and exhibited ESC-like small colonies. At this stage, colonies remained small, flattened with sharp-edge but exhibit high nuclear to cytoplasmic ratio. These colonies were then selected for further passaging and manually picked on the basis of size and morphology. These emerging colonies were checked to be free from substantial spontaneous differentiation before being transferred onto VTN-coated plate. These transferred cut colonies were regarded as passage 1 (Figure 3.2;f). A colony may take a week to form a decent size before ready for the next passage. Colonies at early, mid and terminal stage of splitting were frozen down as backup. Colonies that emerged before around day 26 were excluded as these are likely to be only partially reprogrammed. The timeline and experimental processes for reprogramming blood samples were presented in Figure 3.1. At day 37 of culture, I have successfully yielded 6 colonies for TF171 and 8 colonies each, for TF172 and TF173 (Figure 3.3). Two colonies of TF171 line however were infected and could not proceed to the next passaging. The 3 newly-established hiPSCs showed distinct colony and cellular morphologies that can be distinguished from non-reprogrammed control cells of the

same culture. Details of the mutations and donor characteristics are presented in Table 3.1.

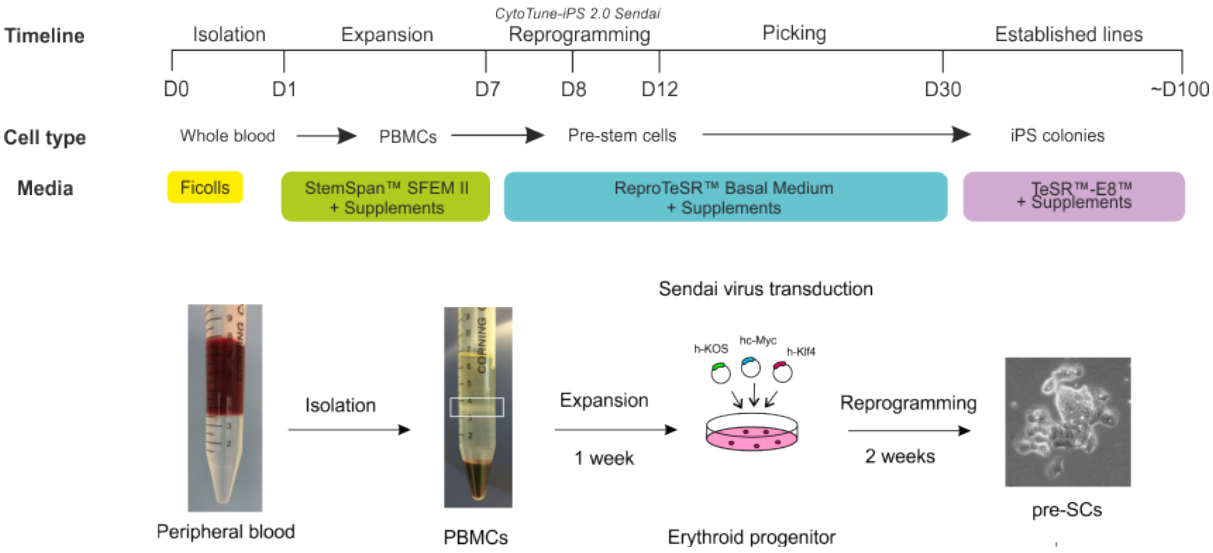

Figure 3.1 Timeline of reprogramming processes. Derivation of iPSCs began with the isolation of PBMCs from venous blood samples using density centrifugation method (Ficoll-Paque). At day 1, these suspension cells were expanded for a week before transduced with SeV carrying reprogramming factors. After 2 weeks, these suspension cells were found to show clustering activity and adhere to the bottom of the VTN-coated plate. These putative iPSC colonies we passaged up to 20 passages before start of differentiation.

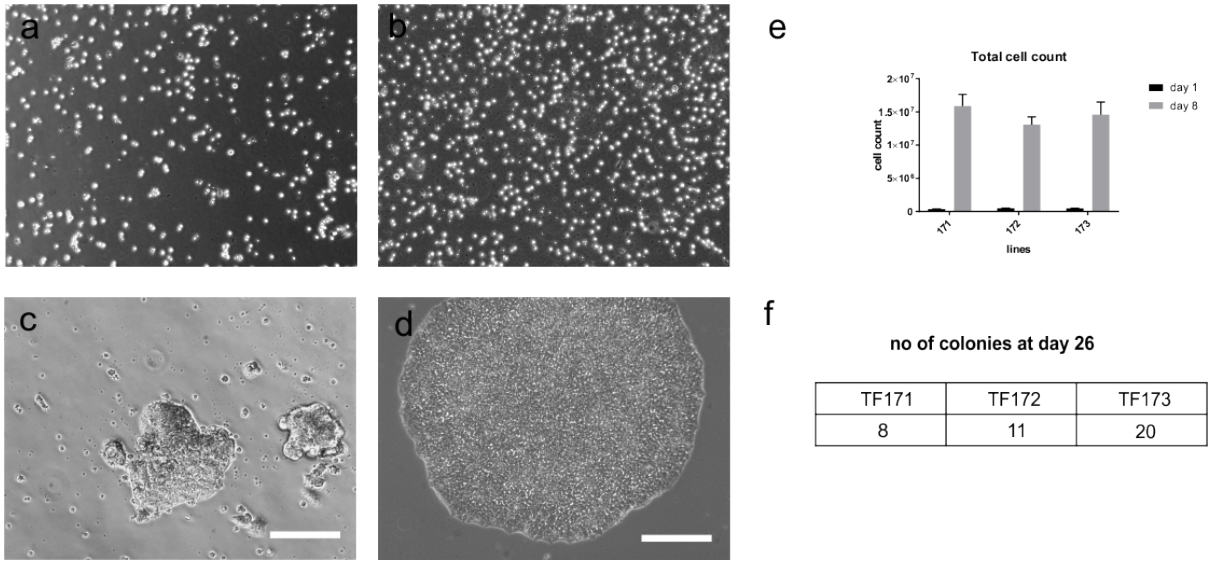

TF171	TF172	TF173
8	11	20

Figure 3.2 Morphological changes during reprogramming of PBMCs (a) day 1 prior isolation, blood cells well seeded onto 24-well plate (b) after a week of expansion, PBMC increases total viable cell count and began to form small clusters (c) in 2 weeks post-Sendai transfection, cell suspension started to attach to plastic and exhibit epithelial-like morphology (d) putative iPS colony emerged after approximately 4 weeks of culture. (e) total cell count before and after expansion phase (f) number of putative iPSC colonies generated after 2 weeks of transfection. Scale bar, 50 μm (a,b,d), 20 μm (c).

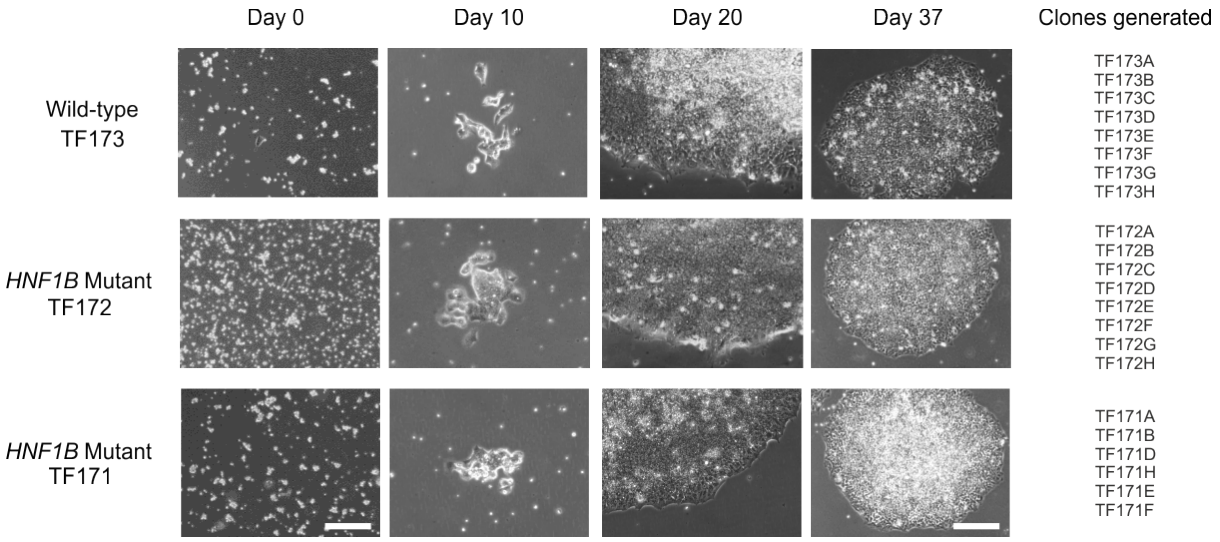

Figure 3.3 Morphological changes of PBMCs during generation of *HNF1B*-derived iPS lines. Isolated PBMCs were plated at 300,000 cells per well. At day 10 of culture, PBMCs formed cluster of cells and attached to the bottom of plate. After 2 weeks of SeV transduction, putative iPS colonies began to emerge and exhibited characteristics of pluripotent cells. Colonies with high nuclear to cytoplasm ratio were identified, picked and transferred to a new plate and marked with respective passage number. Right most column showing number of clones generated for each line. Scale bar day 0 and day 37, 200 µm, day 10, 50 µm, day 20, 100 µm.

Table 3.1 Venous blood donor characteristics and iPSC lines derivations

No	Lines	Sample (with/-out mutation)	Cell source	Clinical manifestations	Relationship		No. of Clones generated
1	TF171	HNF1B Mutation: c.1654-?_1674+?del which causes a deletion of exon 9.	PBMCs	Cystic dysplastic kidney detected antenatally	Family of 3	Affected son	6
2	TF172	HNF1B Mutation: c.1654-?_1674+?del which causes a deletion of exon 9.	PBMCs	Cystic dysplastic kidney detected antenatally		Affected son	8
3	TF173	No mutation	PBMCs	Healthy		Healthy mum	8
4	SW162	No mutation	PBMCs	Healthy	Unrelated healthy male		4

From this derivation experiment, I have successfully generated 3 hiPSC lines (namely TF171, TF172 and TF173) with 22 total iPSC clones. These lines were derived from a family of 3. The other unrelated healthy controls (SW162) were reprogrammed by Steven Woods (Kimber Lab) from healthy adult with no mutation and served as unrelated unaffected control. Here, I demonstrated that iPSCs grown on VTN-coated plate can support prolonged iPSCs culture and retain pluripotent features. At passage 15 and above, all of these newly generated iPS colonies were characterised for its pluripotency and considered as established lines.

3.2.2 Characterisation of hiPSCs generated from *HNF1B* family

3.2.2.1 Establishment of integration-free iPSCs

Seven different iPSC lines at passage number 14-16 were selected for Sendai vector evaluation. These colonies were harvested, RNA-extracted and evaluated for presence of SeV and its related transgenes by DNA gel electrophoresis. In this experiment, one clone of each (TF171, SW162) and 2 clones of TF172 and TF173 were tested. The RT-PCR products revealed that all iPSC lines were free from exogenous SeV except TF173BP14 (Lane 5) with a lower existing copies of Sendai vector, approximately 200 bp (Figure 3.4;a). Interestingly, amplicons were negative against transcription factors KOS, Klf4 and c-Myc when compared to human dermal fibroblast (HDF), which indicated high copies of reprogramming factors (Figure 3.4; b,c,d). It is evident that the persistent and lowly replicated Sendai vector was completely removed from newly established iPSC lines beginning from passage 15 but not passage 14 and below. Thus, I can conclude that the Sendai vector infection has led to the effective generation of reproducible 'footprint-free' iPSCs. Only colonies at passage 15 and above were considered free from genetic modifications and were selected for further characterisations.

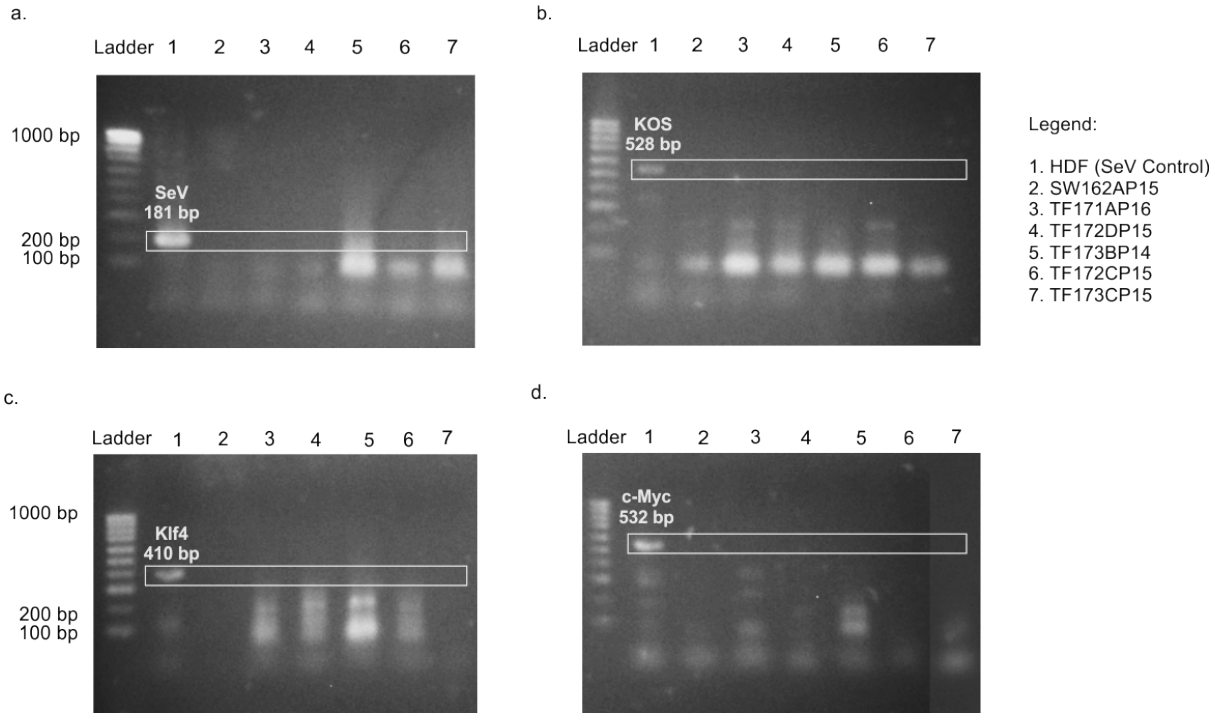

Figure 3.4 DNA gel electrophoresis of newly reprogrammed iPSCs. (a) Gel showing no expression of SeV except lane 5 (TF173BP14) and control lines, HDF. (B) Gel marked KOS-free in all tested 7 lines except HDF that contain 528 bp band. (c,d) Both bottom gels showing iPSC lines free from Klf4 and c-Myc transcription factors, 410 bp and 532 bp, respectively. The primers tested contain SeV genome sequences which allow detection of transgenes included in the CytoTune® 2.0 Sendai reprogramming factors.

3.2.2.2 Normal karyotype of newly generated hiPSCs are maintained in defined culture conditions

All 4 tested lines showing properties of pluripotency and self-renewal. hPSCs genetic analysis have been designed to report on commonly affected chromosomes. The analysis revealed that hiPSCs at passage 20 showing normal karyotype for TF173 and SW162 lines. *HNF1B*-mutant lines (TF171 and TF172) however suggested karyotypic abnormalities on Chromosome 8q and 12p. These abnormalities (n copies>3) indicated amplification in these lines and need repeats. This could be due to primer-probes specificities. Karyotype of X chromosome revealed consistent gender of all derived lines (XX=TF173, XY=TF171, TF172, SW162). Although the data is not suggestive of the real chromosomes stabilities and status, G-banding assessment still needs to be done to confirm these findings.

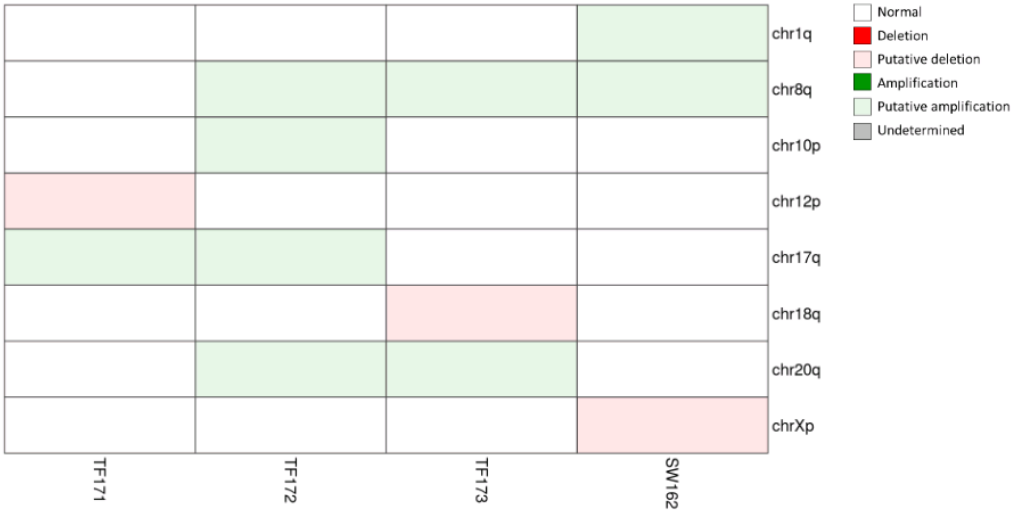

Figure 3.5 Predicted genetic analysis for 4 hiPSC lines. Pink shade indicated putative deletions that are observed in Chr12p, Chr18q and ChrXp of TF171, TF173 and SW162, respectively. Green shade indicated putative amplification that occurs in various locations on chromosomes. White boxes indicated normal copy number. None of the samples are showing deletion or amplification (bright red or bright green, respectively).

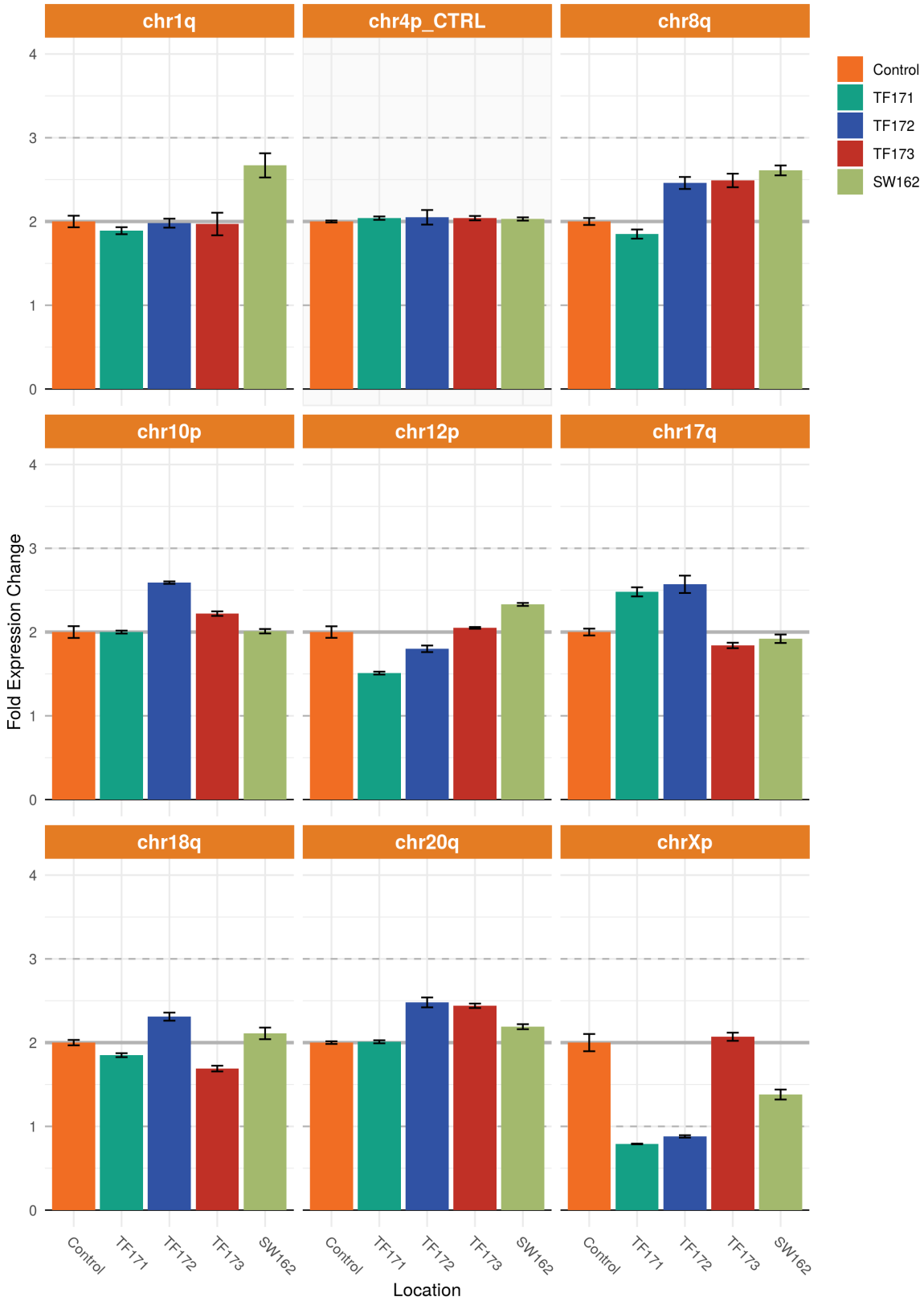

Figure 3.6 hPSCs genetic analysis for 4 hiPSC lines. All lines were PCR-amplified for 8 most commonly reported chromosomes, with Chr4p as internal control. All chromosomes showing normal copy number in all lines except variations in term of fold expression change. Fold expression change equals to 2 indicate normal copy number in all lines. A copy number < 1.8 or > 2.2 with a p-value*< 0.05 may indicate the presence of an abnormality within the culture.

This assay utilised nine primer-probe mixes to detect any karyotypic abnormalities in human PSCs. From the analysis, I found that all chromosomes were predicted normal for TF171 line except putative deletion and amplifications detected in Chr12p and Chr17q, respectively. TF171 has a possible deletion in a minimal critical region of Chr12p with a calculated copy number of 1.51. Chr12p abnormalities are typically amplifications, but while rare, deletions have been identified in hPSC cultures. Typically they involve a small deleted region on the p-arm. Chr17q has a possible amplification in a minimal critical region with a calculated copy number of 2.48. Amplification of Chr17q is a common abnormality seen in hPSC cultures most likely involves complete chromosome duplication, but duplications of all or part of the q-arm have also been reported. It is noted that only one copy of ChrXp is detected which suggested TF171 lines were derived from male donor.

As for TF172 line, putative amplifications have been detected in 4 locations (Chr8q, Chr10p, Chr17q and Chr20q. Chr8q has a possible amplification in a minimal critical region with a calculated copy number of 2.46. Amplification of Chr8q is commonly observed in cultures. They are duplications that involved the whole chromosome, but smaller amplifications seen in the q-arm have also been reported. Chr10p has a possible amplification in a minimal critical region with a calculated copy number of 2.59. Although rare, amplification of Chr10p typically involved whole chromosome duplication. Chr17q has a possible amplification in a minimal critical region with a calculated copy number of 2.57. This abnormality routinely involves complete chromosome duplication, but duplications of all or part of the q-arm have also been reported. Chr20q has a possible amplification in a minimal critical region with a calculated copy number of 2.48. This routinely involves a minimal amplification at a centrometic region of the q-arm. Notably, classical G-band karyotyping often does not have the resolution to accurately detect this abnormality. Whole chromosome duplications have also been observed for Chr20. However, Chr1p, Chr12p and Chr18q were reported a normal copy number, ranging from 1.8-2.2. For sex chromosomes, only one copy of ChrXp was detected which suggested a male samples.

In TF173 lines, 4 regions were predicted to have normal copy number (Chr1q, Chr10p, Chr12p and Chr17q). Chr8q however has a possible amplification in a minimal critical region with a calculated copy number of 2.49. Amplification of chr8q is common in hPSC cultures and often showing duplications that involved the whole chromosome. Smaller amplifications in the q-arm have also been reported. Chr18q has a possible deletion in a minimal critical region with a calculated copy number of 1.69. The q-arm of chr18 is commonly deleted in hPSC cultures. This abnormality ranges in size from the whole q-arm to a telomeric minimal region. Chr20q has a possible amplification in a minimal critical region with a calculated copy number of

2.44. This routinely involves a minimal amplification at a centrometic region of the q-arm. No deletion observed in the ChrXp that suggested a female donor.

In the unaffected SW162 controls, all chromosomes were detected as normal except Chr1q and Chr8q. Chr1q has a possible amplification in a minimal critical region with a calculated copy number of 2.67. This abnormality ranged from a whole chromosome polyploidy to smaller regions of amplification, almost exclusively involving the q-arm. Chr8q suggested a possible amplification in a minimal critical region with a calculated copy number of 2.61. Amplification of chr8q is often duplications involving the whole chromosome, but smaller amplifications seen in the q-arm have also been reported. ChrXp has a possible deletion in a minimal critical region with a calculated copy number of 1.38. This suggested a male line.

3.2.2.3 Genotyping of *HNF1B*-derived iPSCs and genomic DNA dosage assays

All newly derived iPSCs were DNA-extracted, PCR-amplified and purified before Sanger sequencing analysis. PCR reaction of target genes using designed primers yielded 100-200 bp amplicons. Primers were designed to span intron-exon boundaries that cover approximately 400-500 bp of DNA length. Electropherogram of intron 8 spanning exon 9 revealed no differences between peaks in all 3 lines (TF171, TF172 and TF173). Deletion of exon 9 could not be detected from this assay suggesting the occurrence of mutation in the other allele (heterozygous). Hence, to investigate the affected allele, I carried out a gene dosage assay to measure the dose of affected *HNF1B* gene.

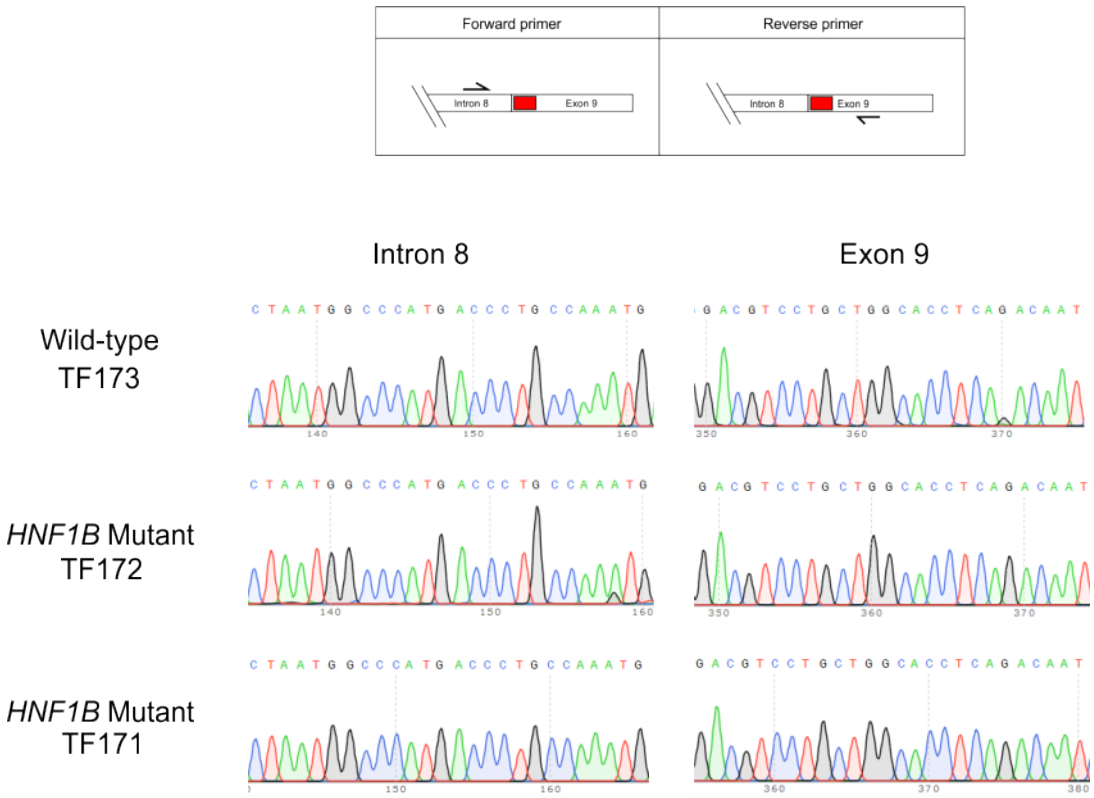

Figure 3.7 Sanger sequencing of newly generated *HNF1B*- iPSC lines. Chromatogram of intron 8 and exon 9 (400-500 bp) showing no differences between peaks generated suggesting affected region could occur on the other allele. Experiments were performed in triplicate for each line.

Because *HNF1B* patients commonly characterised by loss of function mutations present only in one allele, this has led to me to hypothesise that the deletion could exist in the second allele. To test this, I collected genomic DNA from heterozygous *HNF1B* samples (TF171 and TF172) and ran qPCR to effectively assess the dose of affected *HNF1B* gene. The primers were designed in a way that it will bind upstream (denoted as 5'), middle or downstream (3') region of exon 9. These data were normalised to unaffected controls (TF173 and SW162 lines). The qPCR data revealed that when using both primer pair 1 (forward primer binds deletion site) and pair 2 (reverse primer binds deletion site), the amount of DNA in *HNF1B* samples were reduced by approximately half of that unaffected TF173 controls. Interestingly, these data were equally replicated when normalised to unrelated SW162 controls suggesting consistent gene dosage effects of *HNF1B* samples.

To further verify deletion of exon 9, I designed primer sets that bind further downstream of exon 9. The qPCR reaction of middle region showed a similar pattern for both affected TF171 and TF172 lines, with 68% and 79% reduction, respectively. When compared to TF172, it is observed that TF171 samples showed slightly lower degree of reduction suggesting its patient-specific identity. From 3' region of exon 9 qPCR data, TF172 samples showed 58% loss in the amount of amplified *HNF1B* genomic DNA when compared to unaffected TF173 control (no reduction). TF171

samples however are less affected with only 30% reductions, reflecting its middle region dosage effect. Notably, primer pair that binds exon 2 showed comparable DNA dosage pattern. Amplification of exon 2 in both TF171 and TF172 lines were affected by the exon 9 deletion (42% and 59% reduction, respectively) but not in the TF173 and SW162 samples.

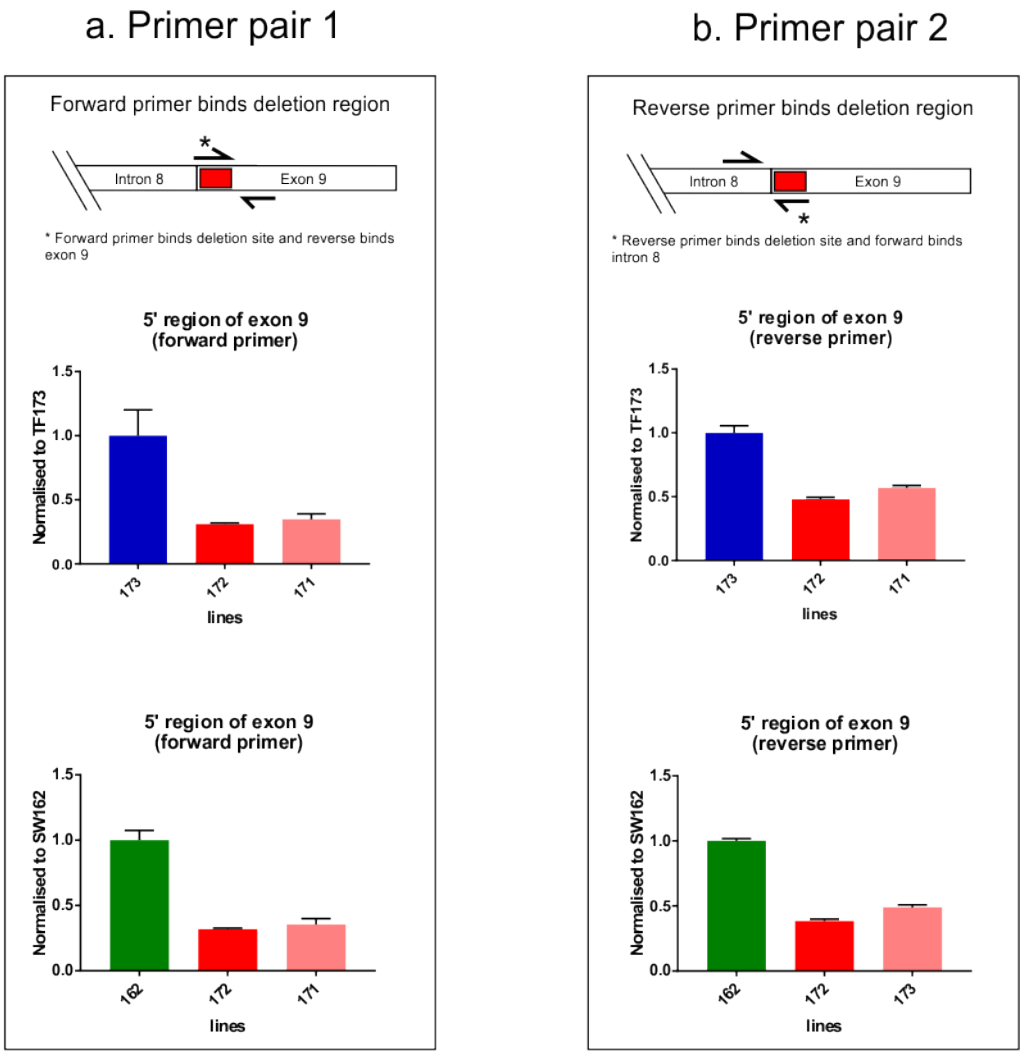

Figure 3.8 Gene dosage assay of *HNF1B*-derived iPSCs. (a) Top bar graph: forward primer binds predicted deletion site at n-terminal region of exon 9 and reverse primer binds further downstream. qPCR revealed more than half reductions in *HNF1B* samples, TF171 and TF172 when normalised to TF173 control. Bottom: Similar decreasing pattern in *HNF1B* samples when normalised to SW162 unrelated control. (b) Top bar graph: reverse primer binds predicted deletion site whereas the forward primer binds terminal region of intron 8. Both *HNF1B* samples (TF171 and TF172) showing reduction by half but to a lesser degree when compared to primer pair 1. Bottom: *HNF1B* samples were normalised to unrelated control (SW162). Data are represented as Mean±S.E.M from technical replicates (n=3).

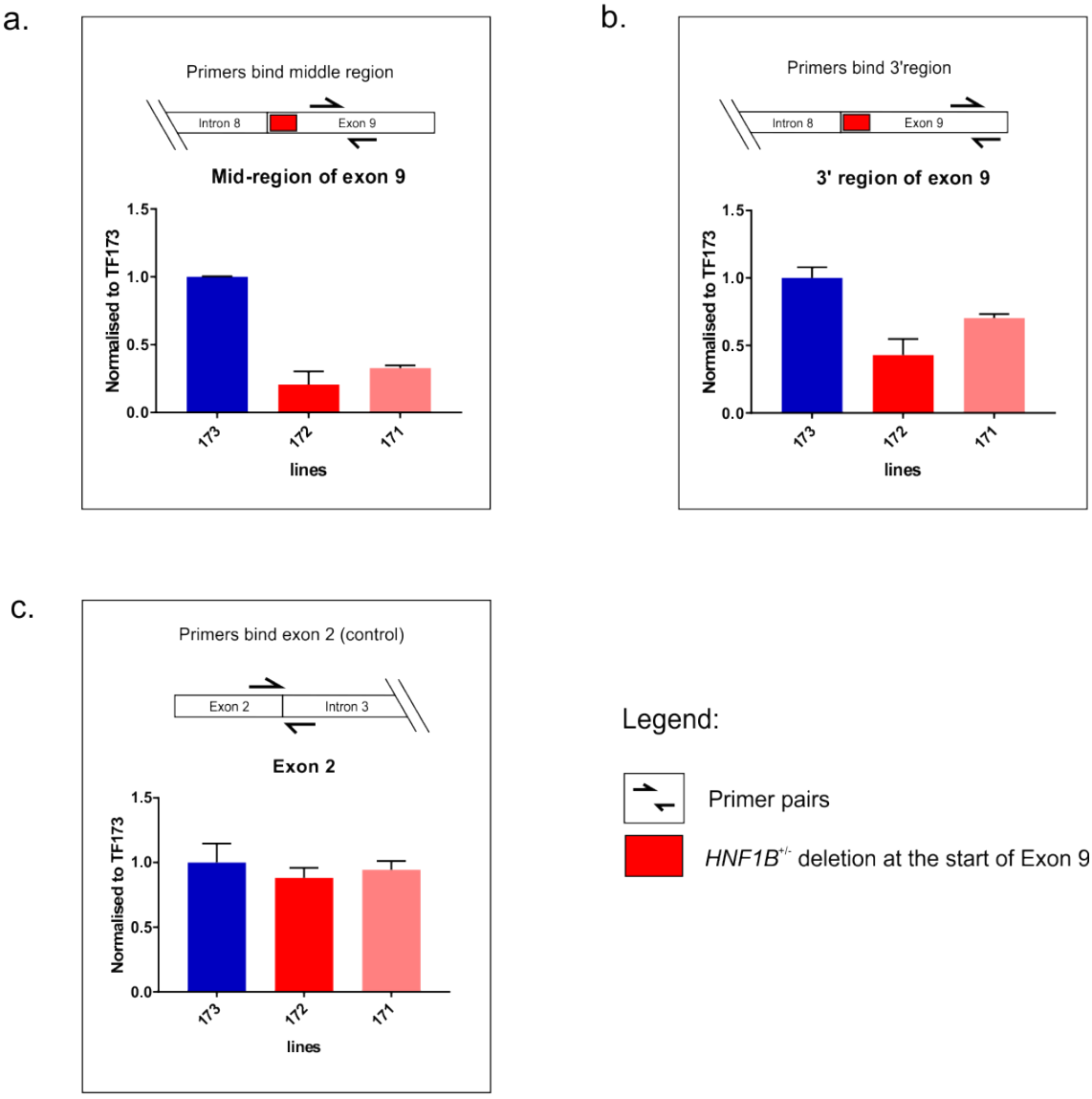

Figure 3.9 Gene dosage effects of *HNF1B*-derived iPSCs. (a) Amplification of mid-region of exon 9 showed more than half reduction in *HNF1B* samples (TF171 and TF172) when normalised to TF173 control. (b) Primer pair that amplify c-terminal region of exon 9 showing a reduced DNA products in the mutant samples (TF171=30%, TF172=58%). (c) Exon 2 region in *HNF1B* samples were affected by the exon 9 deletion (TF171=42%, TF172=59%) when compared to TF173 control. Data are represented as Mean±S.E.M from technical replicates (n=3).

3.2.2.4 Differentiation potential of hiPSCs by formation of three germ layers in embryoid body culture

The established hiPSCs showed characteristics of human ESC-like morphologies. I assessed the 3 newly-established hiPSCs to verify whether they are different in term of EB formations and differentiation potential. I found that EBs generated from TF171, TF172 and TF173 lines were smooth, rounded, transparent and had an intact boundaries with observable internal cavities (Figure 3.10;a). In the first week of culture, all 3 hiPSC lines were able to form EB structures in suspension culture despite variation in size and morphologies. At day 12 of culture, these EBs were easily broke due to mechanical movements during feedings. Hence, only intact and rounded EBs

were harvested and transferred to serum-coated plates for differentiation assessments.

After 3 days of culture, floating EBs began to attach to the plate and formed EB core with epithelial-like overgrowth extending from the inner structure. These mixtures of differentiated cells were fed up to additional day 14.

From the immunostaining, I found that the ectoderm marker, β-tubulin III and neurofilament-L were positive in all 3 hiPSC lines and there were no morphological differences observed between these lines. The staining of ectodermal cells against β-Tubulin III and neurofilament-L antibodies revealed positive green microtubules stainings and emergence of filament proteins on the outer cell membrane, respectively (Figure 3.10; b). Nuclear staining of endoderm marker (GATA6, FOXA2 and SOX17) indicated that almost equal amount of endoderm-positive cells (green) and DAPI-positive signal (blue) in all lines. Furthermore, staining for mesodermal markers (α-SMA and vimentin) revealed positive signal in all tested lines. These actin filaments and filamentous proteins were found to be highly expressed in cytoplasm that surrounds the nuclei core, respectively. It was evident from the stainings that most cell strongly expressed GATA6 (endoderm) and α-SMA (mesoderm) that suggested co-expressions of these two markers during formation of germ layers. All of 3 lines showed negative staining for anti-OCT4 antibodies suggesting loss of pluripotency at this stage (data not shown). These results suggested that the *HNF1B*-derived hiPSCs and its related control are capable of differentiating into several cell types *in vitro*.

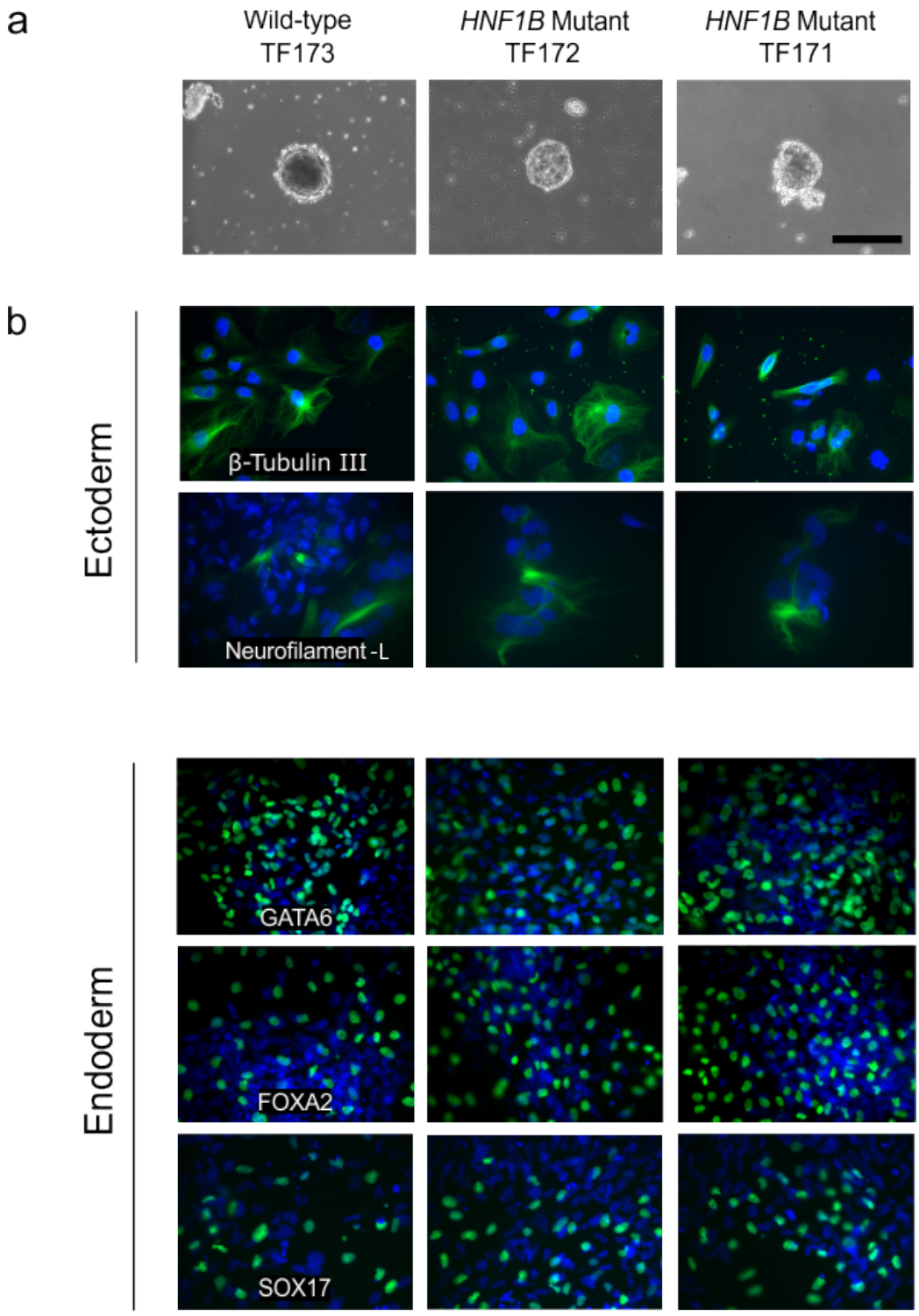
a
Wild-type
TF173
HNF1B Mutant
TF172
HNF1B Mutant
TF171
b
Ectoderm
β-Tubulin III
Neurofilament -L
Endoderm
GATA6
FOXA2
SOX17

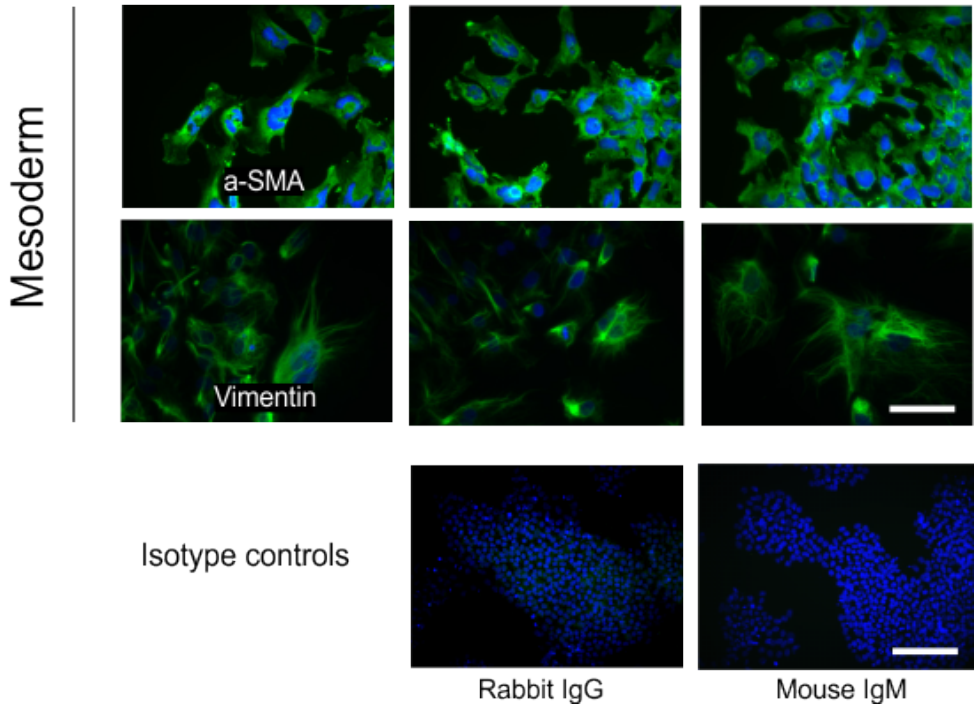

Figure 3.10 Embryoid body (EB) formation using feeder-free system (a) Phase contrast images of EB formed at day 12 before plated onto serum-coated wells for 3 individuals (b) EB-mediated differentiation of 3 hiPSC lines (TF171,TF172,TF173) assessed by immunostaining of attached EBs post 2 weeks of culture. Each line was analysed by immunocytochemistry for markers of each germ cell layer (green) with DAPI (blue) as a counterstain. Ectoderm markers: β-tubulin III and neurofilament-L; mesoderm markers alpha-smooth muscle actin (alpha-SMA) and vimentin; endoderm markers: GATA6, FOXA2 and SOX17. Scale bar, 100 μm.

3.2.3 Pluripotent state of hPSCs determines robust differentiation strategies

For each newly derived hPSC line, it is essential to perform an exhaustive characterisation to unequivocally define their cellular populations and to determine the pluripotent capacities. Here, the pluripotent state of hPSCs was determined by immunostaining and quantified by flow cytometry. The hPSCs expressed pluripotency markers that include nuclear transcription factors (Nanog, Oct4, and Sox2), glycolipid antigens (SSEA3 and SSEA4) and keratan sulfate antigens (Tra-160 and Tra-181). SSEA1, a negative marker in human pluripotent cells has been widely used as a control for early differentiation. Thus, in order to characterise pluripotency, stem cell line should express all pluripotency markers and able to differentiate to all three germ layers both *in vitro* and *in vivo.*

In order to examine the pluripotency and self-renewal capacities of hPSC lines, I performed a series of parallel immunochemical staining before initiating differentiation. Also, key functional characteristics of undifferentiated hPSCs have been evaluated. In over 20 serial passages, the cells remain in the pluripotent states, evident by expression of pluripotency markers such as Nanog and Sox2, self-renewal marker, the Oct4, and surface markers such as SSEA-4, TRA1-61 and TRA1-80. The stem cell differentiation marker, SSEA-1 was negative in the pluripotent state. It

would be upregulated as the cells differentiate. Isotype controls, mouse IgG, IgM and rabbit IgG revealed lack of non-specific antibody binding to the antigenic determinants.

Another rapid assessment of pluripotency can be performed by flow cytometry analysis. In this experiment, quantification of the pluripotency score (%) on directly conjugated antibodies (Nanog and Sox2) were performed by double staining and data were reported as percentage of pluripotent score (%). It was found that all tested lines showed double positive for transcription factors (NANOG, SOX2) with a total score that indicated the sum of these two antibodies signals. MAN13 and LV-MAN13 lines were highly pluripotent, scored as 99.2% (59.4%:Nanog, 39.8%:Sox2) and 99.7% (34.7%:Nanog, 65.0%:Sox2), respectively. OCT4 however was not tested in this analysis. Futhermore, flow cytometry analysis of hiPSCs showed a consistent signal for pluripotency markers such as NANOG, TRA1-81, SOX2, OCT4 and SSEA3 (Figure 3.11). The newly generated hiPSCs (TF171,TF172 and TF173 lines) were highly pluripotent, scored 98.0%, 98.9% and 99.6%, respectively. These accounted for NANOG, TRA1-81 and SOX2 antibodies altogether (Figure 3.12). Staining for OCT4 and SSEA3 showed 94.8%, 94.9% and 93.9% pluripotency score for TF171, TF172 and TF173, respectively (Figure 3.13 and 3.14).

The LV-MAN13 line has initially been used in the study to evaluate the efficiency of differentiation. It was found that the integration of lentivirus does not affect the initial or terminal outcomes of differentiation, either morphologically or at transcript levels. I have proposed that this stable line can further be propagated to investigate the identity of kidney precursors in lineage tracing studies. However, this chapter will limit their utilisation only for *in vitro* characterisation and 2D differentiation in comparison with two healthy PSC lines, MAN13 and TF173. This is to prove that hPSCs can be used as an indefinite source of pluripotent cells to recapitulate kidney development. In fact, the transfected line has been used and described in our paper demonstrating that differentiating LV-MAN13 does not compromise pluripotent potential of hPSCs when subcutaneously implanted in the backs of SCID/beige mice (Bantounas et al., 2018). From the current results, it was evident that all tested hPSC lines are pluripotent, remain in an undifferentiated state and capable to self-renewal thereby suggesting its applicability for directing differentiation towards several germline, particularly kidney lineages.

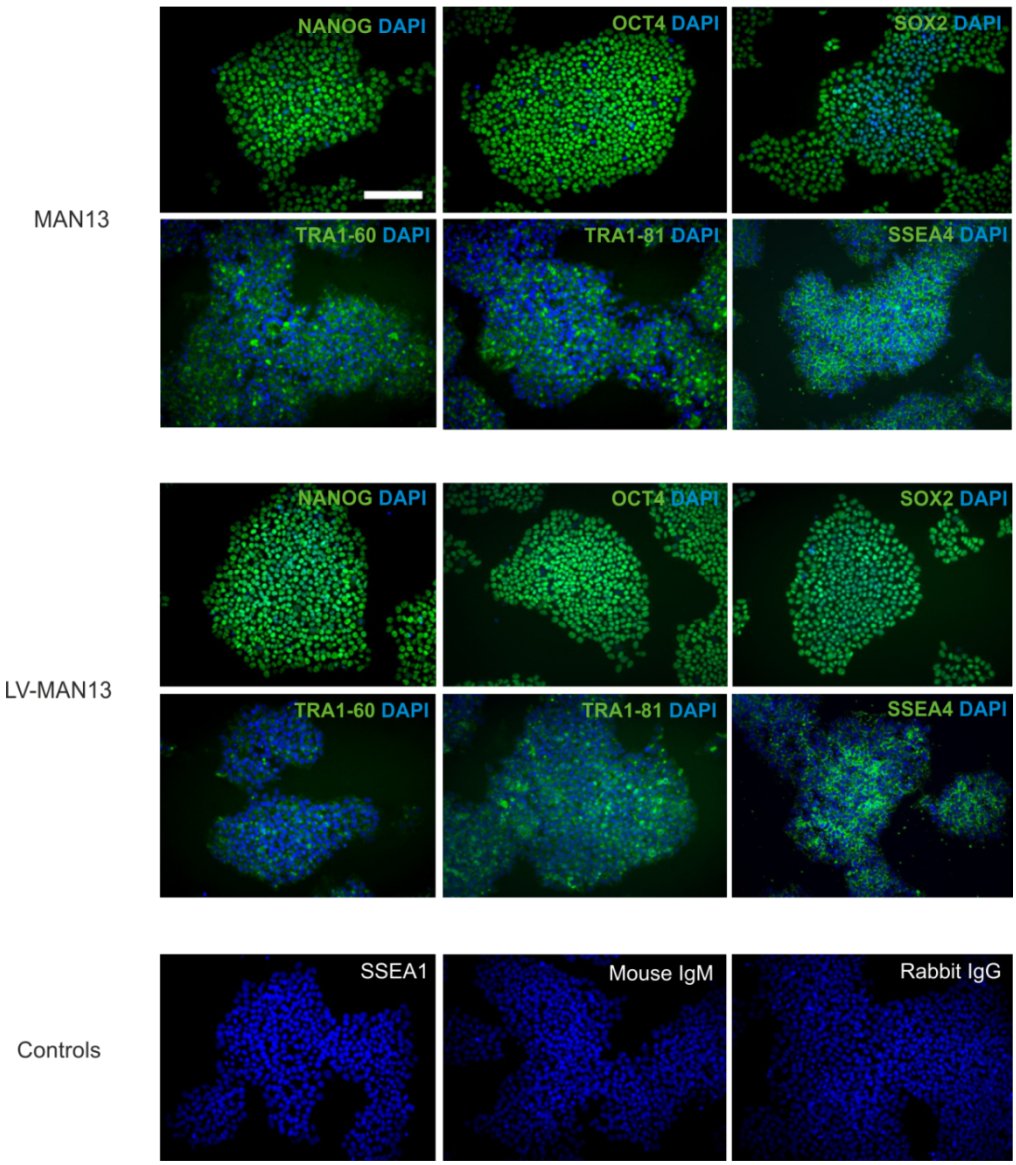

Figure 3.11 Assessment of pluripotency–associated markers on three hESC-lines, Man13 with and without LV-iRFP/Luc construct (a) Staining of MAN13 lines showing pluripotency-associated marker proteins, Nanog, Sox2, Oct4, SSEA4, TRA1-60 and TRA1-81. To identify individual cells, nuclei were counterstained with 4',6-diamidino-2-phenylindole, DAPI (blue) (b) Lentiviral-transfected (LV-iRFP/Luc) MAN13 counterparts differentiated in-parallel, showing comparable pluripotent stage. (c) TF173 pluripotent cells. All merged images were using combination of Alexa488 secondary antibody (green) and DAPI (blue). Mouse IgM and Rabbit IgG were used as isotype controls and negative (SSEA1) staining used to indicate lack of differentiation. Nuclear staining is observed in the negative controls. Scale bars, 50 μm.

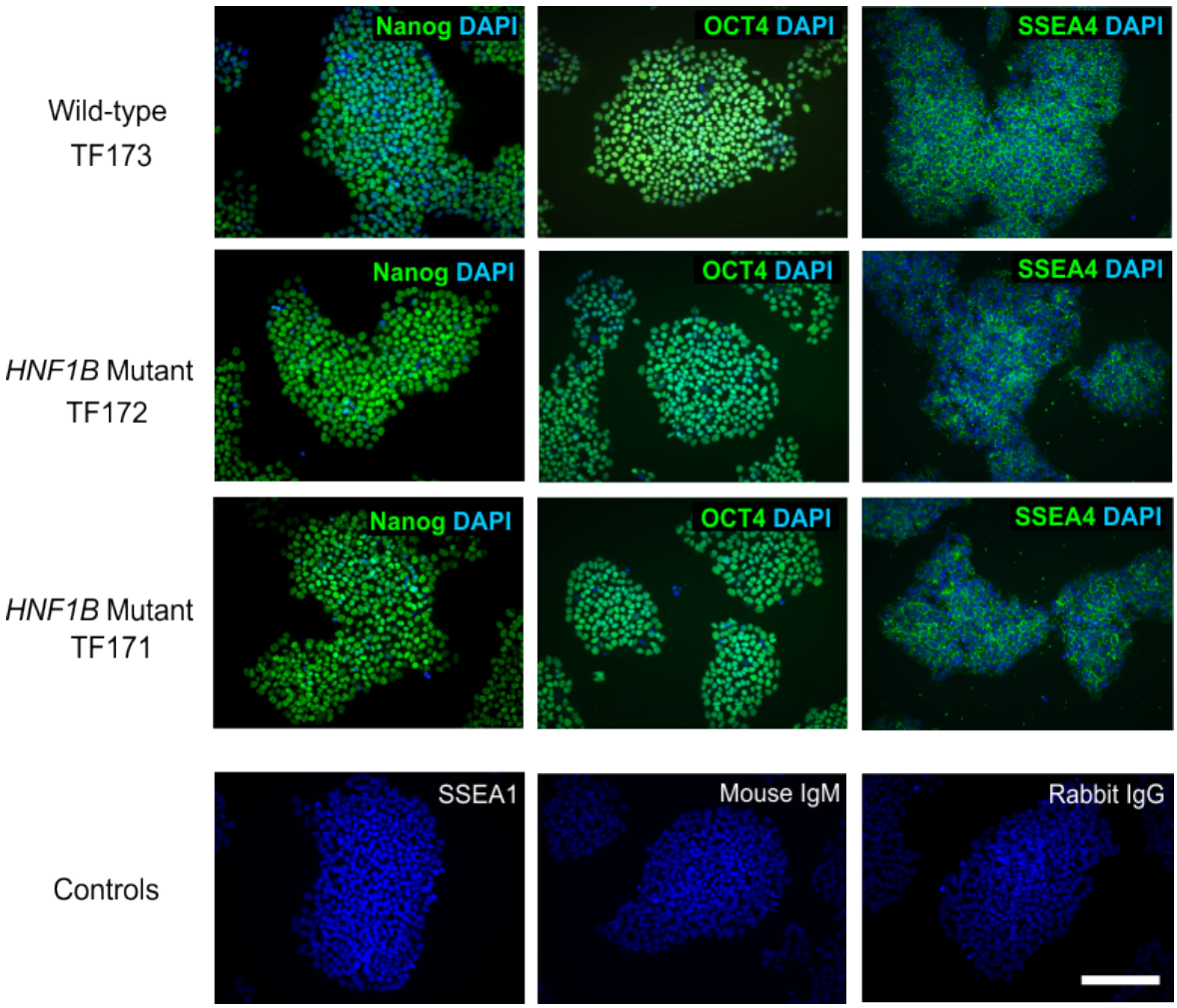

Figure 3.12 Assessment of pluripotency–associated markers on three hiPSC-lines, TF171, TF172 and TF173. (a) Staining of hiPSC lines showing pluripotency-associated marker proteins, Nanog, Oct4 and SSEA4. To identify individual cells, nuclei were counterstained with 4',6-diamidino-2-phenylindole, DAPI (blue). All lines were cultured in-parallel, showing comparable pluripotent stage. All merged images were using combination of Alexa488 secondary antibody (green) and DAPI (blue). Mouse IgM and Rabbit IgG were used as isotype controls and negative (SSEA1) staining used to indicate lack of differentiation. Nuclear staining is observed in the negative controls. Scale bars, 50 μm.

a

MAN13

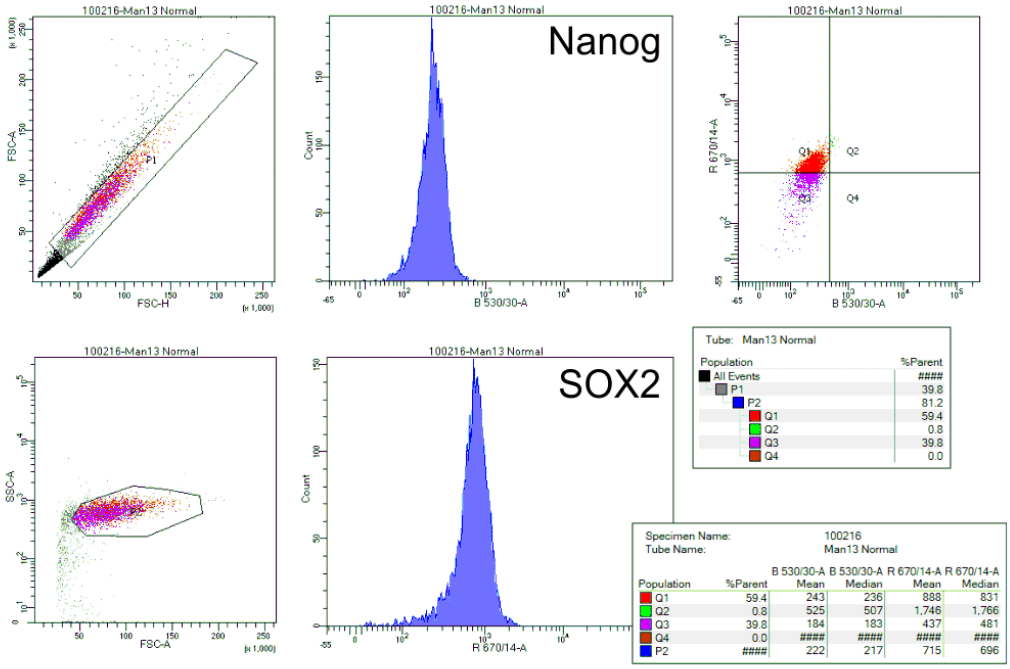

Isotype controls

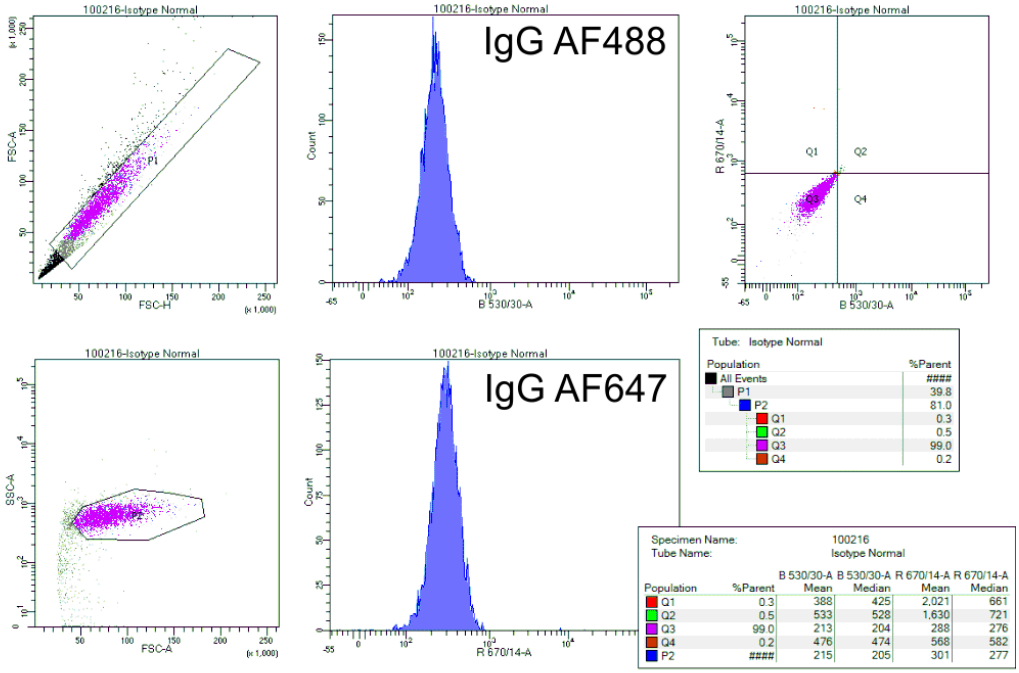

b

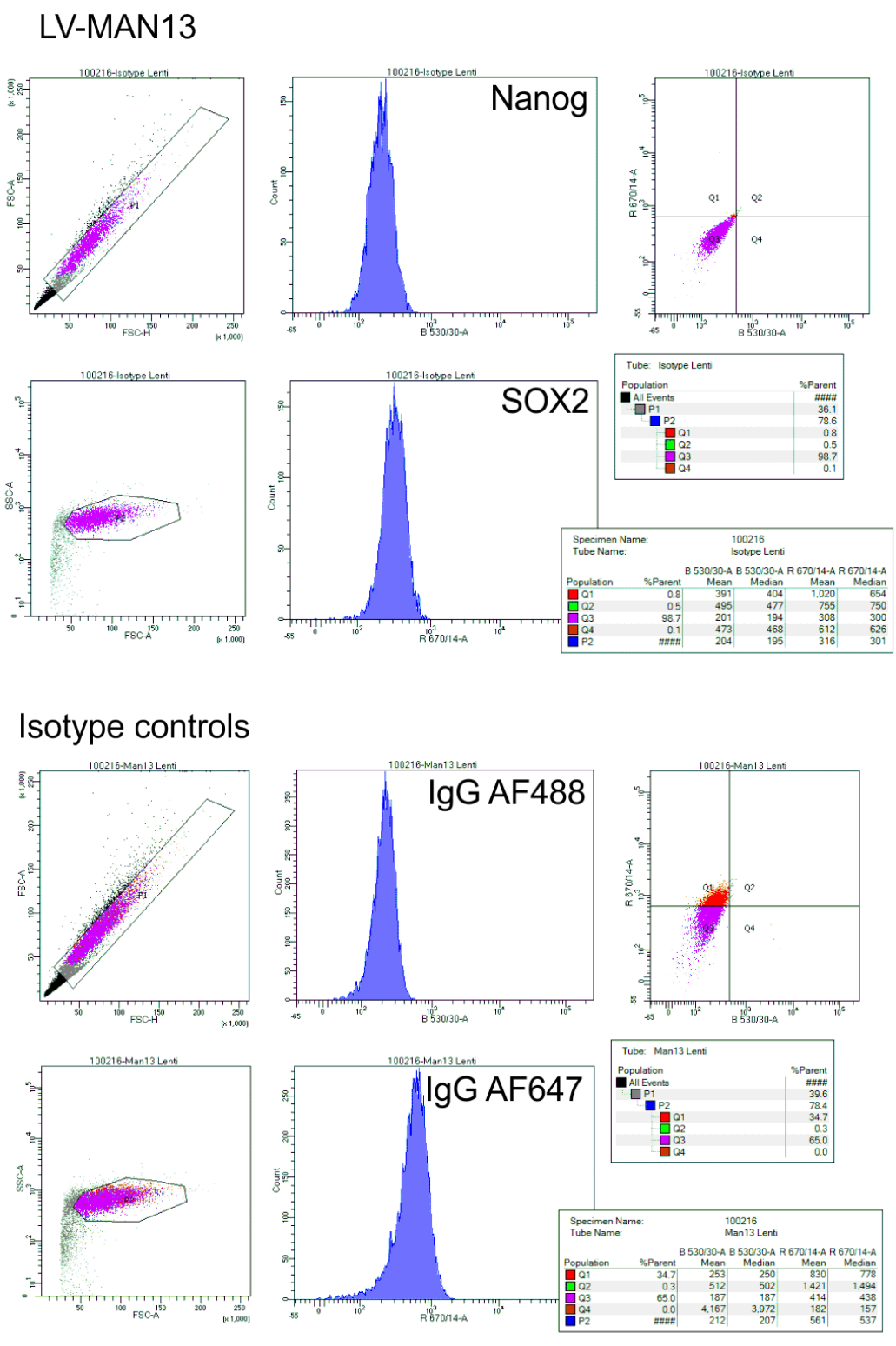

Figure 3.13 Flow cytometry analysis of pluripotency markers of hESCs. (a) Representative histograms showing profile of Nanog (top panel) and Sox2 (bottom panel) reactivities with MAN13 and TF173. (b) LV-MAN13 generates equivalent pluripotent score of Nanog and Sox2 when compared to that of MAN13. The two MAN13 lines were harvested at passage 30. For each analysis, a minimum of 10,000 events were recorded. All experiments were carried out at the same time (n=3 experiments).

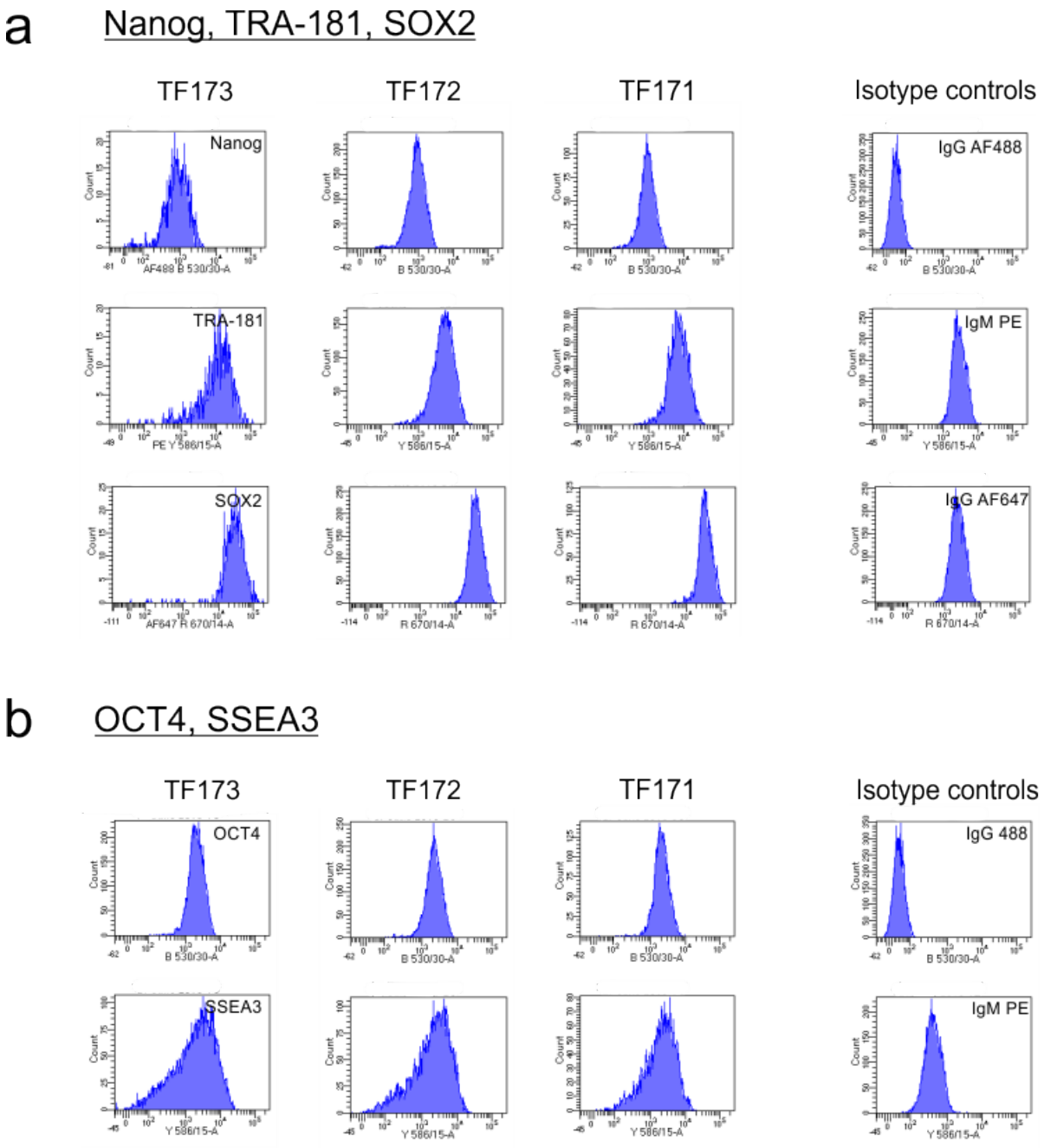

Figure 3.14 Flow cytometry analysis of pluripotency markers of hiPSCs. (a) Representative histograms showing profile of Nanog (top panel), TRA1-81 (middle) and SOX2 (bottom) reactivities with TF171, TF172 and TF173, respectively. (b) All lines generated approximately equivalent pluripotent score of OCT4 and SSEA3 when compared to that of isotype controls. The hiPSC lines were harvested at passage 20 and above. For each analysis, a minimum of 10,000 events were recorded. All experiments were carried out at the same time (n=3 experiments).

3.2.4 Directed differentiation of hPSC lines generate mini kidney organoids in monolayer culture

hPSCs have been directed to 2D kidney differentiation either with or without integrating LV-iRFP/Luc. This vector carries a bicistronic cassette (expressing a near infrared fluorescent protein, iRFP, and firefly luciferase under the control of the EF1α promoter) and has been shown to generate a robust expression of the fluorescent protein. It is reported that transduction has no effect on cell viability and appeared to be non-toxic in both MAN11 and MAN13 lines (Bantounas et al., 2018). The LV-MAN13 containing reporter gene was shown to positively emit iRFP signal at 720 nm suggesting a stable integration in hPSCs genome. These lines were previously used to assess pluripotent potential of hPSCs *in vivo* (Teratoma Assay).

After preliminary evaluation of different protocols in the literature (Ioannis Bantounas personal communication), I chose to evaluate kidney differentiation from both hESCs (MAN13, LV-MAN13) and willd-type hiPSCs (TF173) using a 2D protocol adapted from Takasato et al. (2014). However, none of the 2D differentiation of mutant hiPSCs (TF171 and TF172) will be discussed in this section. On splitting day, pluripotent stem cell colonies were dissociated into single cell suspensions and sparsely plated on vitronectin-coated 24-well plate ($3.5x10^4$ cells per well). At day 0, all tested lines exhibited pluripotent characteristics, showing flat, discoid-shape colonies with defined borders. Colonies displayed a high nucleo-cytoplasmic (NC) ratio with at least five nuclei per cell. The colonies were interspersed across the well with minimal cell death. No sign of differentiation was observed at this stage in either of these lines and colonies remain attached as monolayer culture.

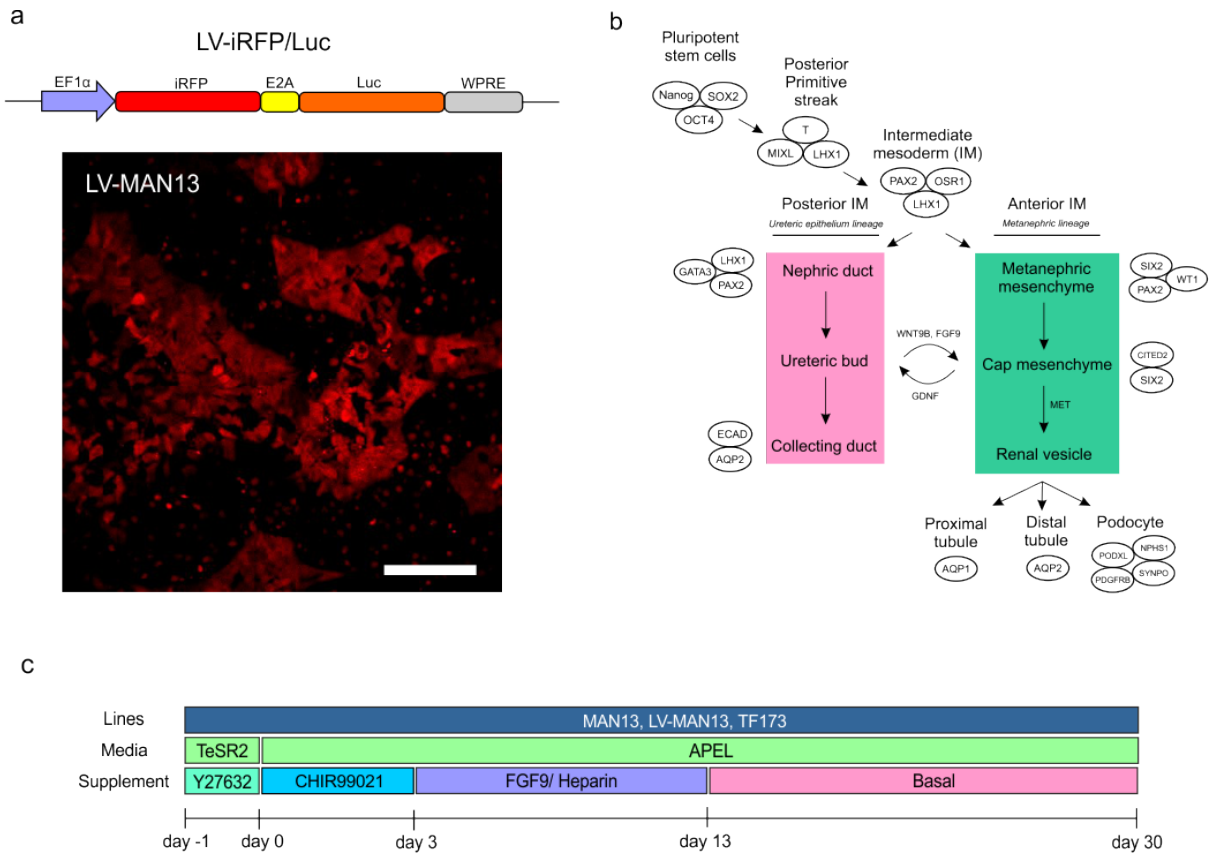

Figure 3.15 (a) Diagram of expression cassette showing the reporter cassette. iRFP fluorescence after transduction of MAN13 hESCs with the lentiviral vector expressing a bicistronic iRFP-E2A-luciferase cassette is indicated in red (Bantounas et al., 2018)(b) Schematic representation of stepwise temporal induction of ureteric and metanephric progenitors from hESCs. Genes associated at specific stages refers to key kidney markers. (c) Schematic differentiation protocol adapted from Takasato *et al* (2014) showing switching of growth factors and inducers to generate renal cell types at specified time points over 30-days differentiation course *in vitro* on a cell culture dish. Scale bar, 50 μm.

Prior differentiation, hPSCs were initially exposed to 8 μM CHIR99021 for 3 days following 10 days of 200 ng/ml FGF9, 1 μg/ml heparin treatment before switching to APEL 2 basal media alone until day 30, all on a cell culture plate (Takasato et al., 2014b). At day 3, colonies began to lose pluripotency and were individually rearranged into a loose cell-cell network. This morphology persisted up to day 7, at which the cells began to proliferate and reached confluency. At day 10, group of cells elicited minimal condensation on near-confluent monolayers. Approaching day 19, bright-round clusters began to emerge and self-organised into different assemblies and structures. These different cell types progressively increase in size, orientate in variable direction and elongates towards the termination of culture (day 30). LV-MAN13 generated similar renal precursor structures as in the non-transfected cells and with roughly the same time course. For each line, differentiation protocol was repeated in three separate experiments and there were little variation observed between lines or differentiation run. This monolayer rudimentary morphogenesis has been further evaluated by immunostaining (Figure 3.19 and 3.20) and transcript profiles analysis (Figure 3.18).

Notably, phase contrast images of differentiating MAN13 and TF173 cultures were observed to be morphologically comparable at designated timepoints. For example, directed differentiation of MAN13 cells displayed cell-cell connection and formed a cellular network as early as day 3. These morphologies were changed at day 10 whereby the cells form a confluent layer with few areas showing signs of condensation. Furthermore, these arrangements were shifted to well-defined structures, with various cell shapes organised in the form of condensated cell clusters. Interestingly, a more prominent of early kidney entities emerged at day 30 where it is observed that cells began to show features of involution, elongation and extension. This could be presumptive of comma- and S-shaped body formation as seen in embryonic kidney development. However, these organoids resembling embryonic structures need further characterisation by staining with kidney-specific progenitors to represent early kidney development. Also, quantitative assessment on the mRNA will correlate and support these claims.

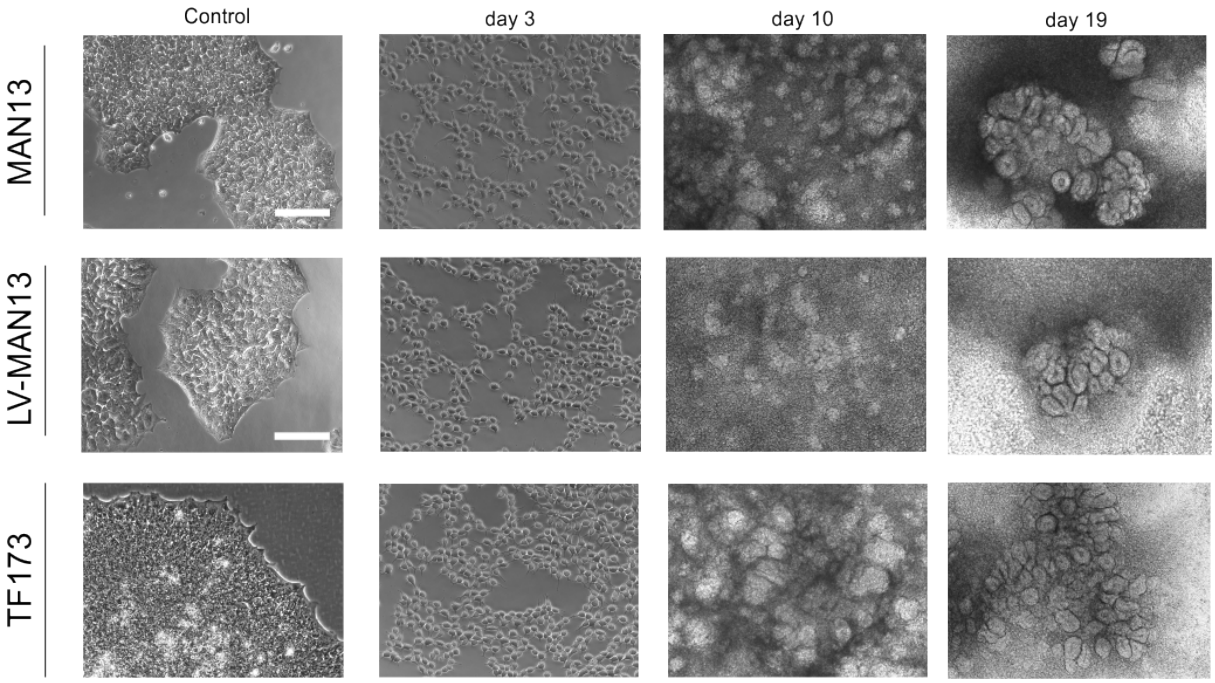

Figure 3.16 Phase contrast images of hESCs differentiation to renal lineages. MAN11 (top panel), LV-Man 11 (middle) and TF173 (bottom) showing differential morphologies on monolayer system. Days of differentiation are indicated above images. All lines underwent mesenchymal-to-epithelial transition (MET) generating complex kidney cell types within 19 days. Differentiation of MAN13, LV-MAN13 and TF173 were extended over 30 days and forms elongated tubular structures. Consecutive days are shown, with day 1 indicating the time point immediately after differentiation stimulation as compared to control at day 0. Experiments were performed in parallel, with medium changed every day. Magnification, 20X. Scale bars, 50 µm.

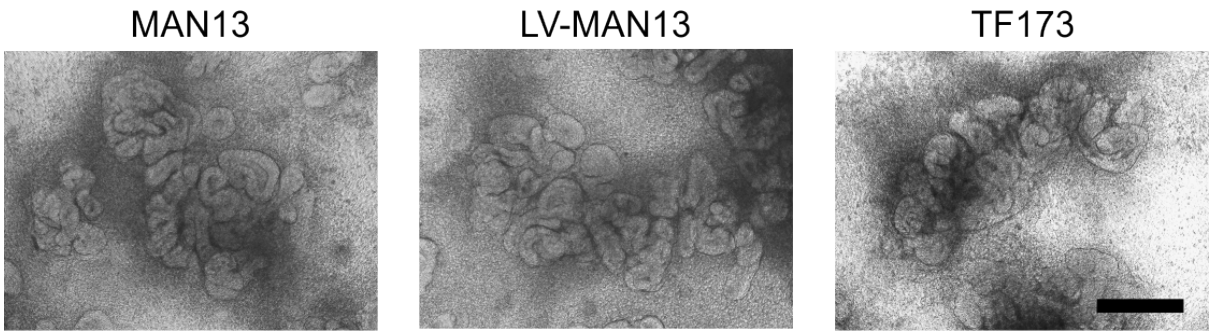

Figure 3.17 Phase contrast images of day 30 differentiation. Mixed populations of kidney cell types showing spatiotemporal segmentations and patterning. Magnification, 20X. Scale bars, 50 μm.

3.2.5 Gene expression profiles in hESCs induced to form kidney-specific cell types

To further characterise cellular identity during specification of mesoderm, IM, MM, nephron segments and UB/collecting duct structures, I measured mRNA expression levels of 21 selected key transcripts using qPCR. RNA samples were collected at 11 time points along the differentiation programme with three separate experimental runs. Generally, it was found that the differentiating cells were induced to both collecting duct and kidney mesenchymal lineage which is evident from mRNA transcript analysis. Pluripotency markers, NANOG and OCT4 were greatly downregulated at start of differentiation and remained low-to-absence as the cells differentiate in all tested lines. Stimulation of differentiation with Wnt agonist, the CHIR99021 was found to highly upregulate T (Brachyury), the posterior PS marker, which decreases towards day 5. A similar pattern was found in MIXL1 (mesoderm/mesendodermal transcription factor) where expressions peaked at day 1 but decreased soon after IM markers appeared. Induction of IM from PS is marked by variable OSR1 and PAX2 expression. Both transcripts were maintained throughout the protocol with a slight reduction in LV-MAN13 approaching day 30. It was previously reported that PAX2 was differentially expressed in both UB and MM lineage whereas OSR1 was evident only in MM (Bantounas et al., 2018).

Expression levels of SIX2, WT1, LHX1, SALL1 and HOXD11 for the first 10 days were markedly upregulated, with a prominent early rise in HOXD11 and SALL1, and sustained subsequent WT1 and SIX2 expression. UB lineage marker (HOXB7, SALL4) were stably activated in the first week and peaked at day 7 in both lines. Following differentiation, there were progressive rise in the AQP1 (that encodes proximal tubule water channel) transcript levels with variable PODXL expression between day 10 and 20. CITED2 showed a sharp rise in the first week but remain constant towards the end with a slightly lower expression in MAN13 lines. AQP2 (that codes for collecting duct water channels) increased gradually and remain constant until day 30 whereas UMOD (a gene expressed in the ascending loop of Henle) was minimally detected

across differentiation. PDGF chain B (PDGF-BB) signaling through fibroblast PDGF receptor-β (PDGFRβ) contributes to interstitial-epithelial cell communication and facilitates regenerative functions in several organs. PDGFRB, which is expressed in endothelial progenitors and lymphatics, has been shown to facilitate interstitial-epithelial cell communication and supporting renal tubular regeneration (Schiessl, 2018). PDGFRB expressions that persisted up to day 19 in all lines are reflective of late-stage kidney development. FOXD1, a stromal progenitor marker increased only after day 10 and KDR expression (a VEGF cell surface receptor for vascular development) remained at low level but consistent from the start till the end of the protocol.

Simultaneous induction of ureteric epithelium and mesenchymal progenitors occurred in three separate experiments in both lines giving rise to comparable expression patterns despite minor variation in transcript levels. Moreover, Bantounas et al (2018) has reported that MAN11 and HUES-1 lines displayed analogous morphogenesis and expressions. Hence, it can be concluded that MAN13, its lentiviral versions and TF173 lines do not differ in mRNA profiles and were highly congruent. This reflects the reproducibility of MAN13, LV-MAN13 and TF173 lines as source of hPSCs regardless genome-modified or not. All of the lines showed pluripotent state and able to be differentiated without compromising progenitor's identity. Monolayer differentiation has showed consistency of organoids generation with minimum variations. Lentivirus does not affect differentiation potential of these lines. This data is essential as a determining factor to further define specificity of mesodermal origins.

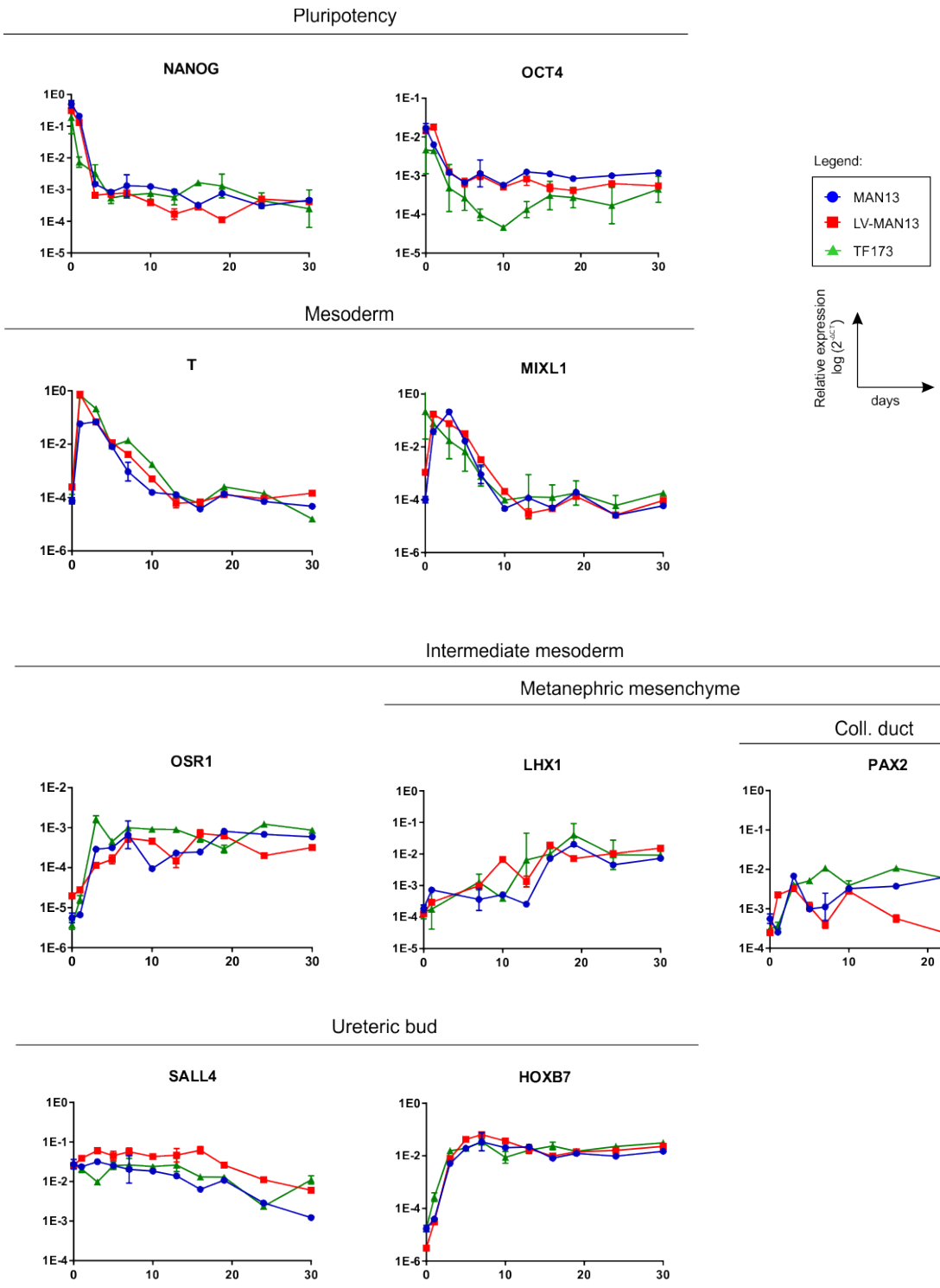
Pluripotency
NANOG
OCT4
Mesoderm
T
MIXL1
Intermediate mesoderm
Metanephric mesenchyme
Coll. duct
OSR1
LHX1
PAX2
Ureteric bud
SALL4
HOXB7
Legend:
MAN13
LV-MAN13
TF173
Relative expression
log (2-ΔCt)
days

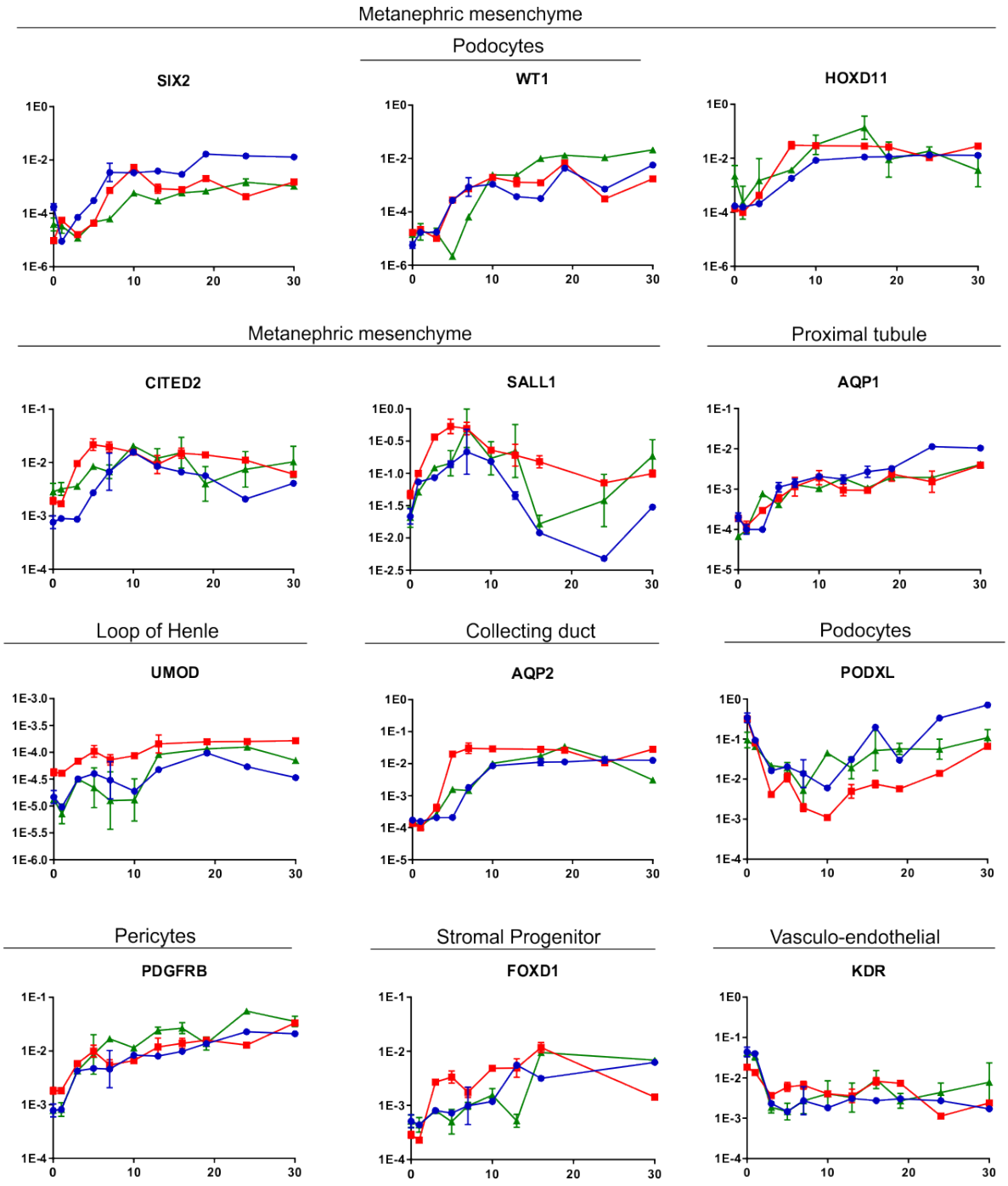

Figure 3.18 Time course of relative expression levels of 30 days MAN13, LV-MAN13 and TF173 specification. differentiation of developing kidney was assessed by qRT-PCR representing key regulator genes that include pluripotency markers (NANOG, OCT4), primitive streak (T, MIXL1, LHX1), IM (OSR1, LHX1, PAX2), MM (SIX2, WT1, OSR1, HOXD11, CITED2, SALL1), UB lineage (HOXB7, SALL4, PAX2), podocytes (PODXL), proximal tubule (AQP1), loop of Henle (UMOD), collecting duct (AQP2), tubular (PDGFRB), stromal (FOXD1) and vasculoendothelial (KDR). Graph showing similar expression profiles of all lines (each line represents three independent experiments, n=3), depicting level of target transcripts normalised to GAPDH expression. Mean±SEM.

3.2.6 Assemblies of renal-specific cell types across differentiation suggest early specification and patterning of intermediate mesoderm

To evaluate renal-specific cell types that were generated across time-course differentiation, I performed double immunofluorescence staining against SIX2, WT1 and CDH1 marker proteins expressed in the differentiating cells at day 7, 13 and 19. On day 13 of the 2D differentiation protocol, cultures began to occupy whole surface and become confluent with some area exhibited condensed populations. These presumptive of kidney progenitors were immunostained for transcription factors (WT1, PAX2, SIX2) expressed by nephrogenic MM and UB/collecting duct lineages (GATA3, PAX2). Most epithelial tissues are marked by cadherin 1 (CDH1).

SIX2+ condensed early mesenchymal cells were prominent at d7 in all lines MAN13, LV-MAN13 and TF173 lines (Figure 3.19). At d19, the WT1+ cell clusters, a prominent nascent nephron precursor, was found to co-localised with CDH1+ populations. SIX2+ cells are prominent at d13 where they assembled around early tubules and detected in loose populations that surround CDH1+ structures although both CDH1+/SIX2+ populations likely indicative of initial epithelialisation in MM and nephron derivatives. Also, PAX2+ cells were observed some of which containing CDH1+ cores. Expression of both SIX2 and WT1 proteins marked the MM/nephron precursor populations. Induced mesenchyme and glomerular podocytes was reported to express WT1 *in vivo*. However, staining for podocyte marker (NPHS1) and distal convoluted tubules (TRPV5) on 2D organoids appear negative (Bantounas et al., 2018).

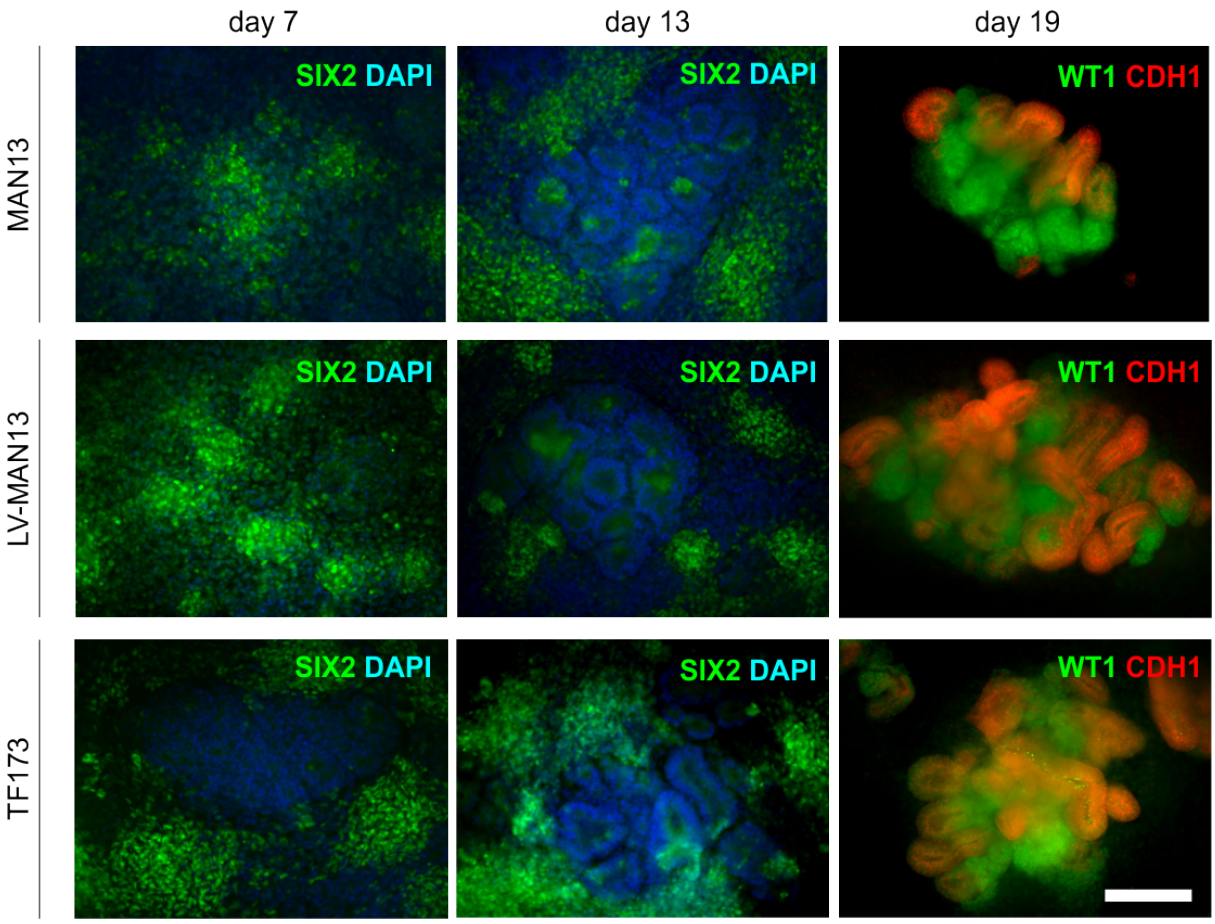

Figure 3.19 Assemblies of renal-specific cell types in differentiating cells for MAN13 (top panel), LV-MAN13 (middle) and TF173 (bottom). Time-course immunofluorescence at d7, d13 and d19 showing formation of several mesenchyme lineage markers, SIX2 (green), and co-expression of WT1 (green) and E-cadherin (red) proteins. Days of differentiation indicated above figures. To identify individual cells, nuclei were counterstained with 4',6-diamidino-2-phenylindole, DAPI (blue). Magnification, 20x. Scale bars, 50 μm.

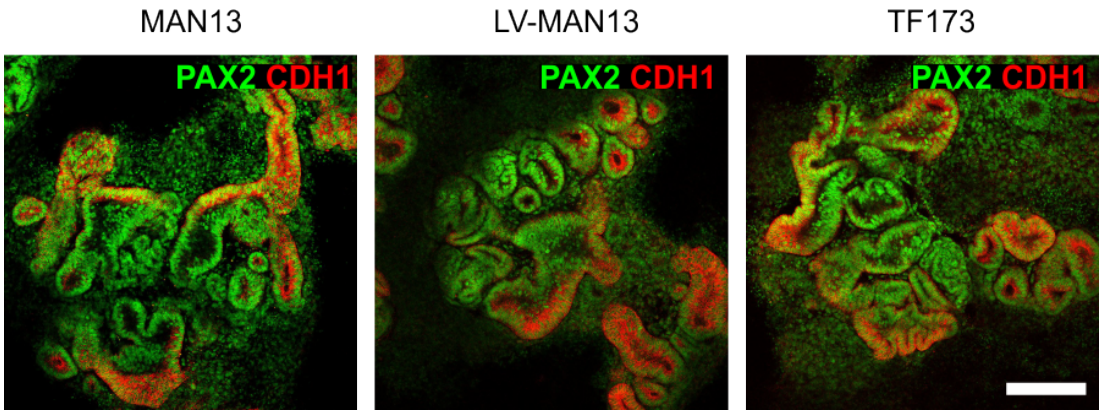

Figure 3.20 Co-localisation of PAX2 (green) and CDH1 (red) in differentiating cells at day 19. Immunofluorescence staining of MAN13, LV-MAN13 and TF173 showed generation of mesenchymal identities with elongated tubular structures. Magnification, 20x. Scale bars, 50 μm.

When hESCs were initially induced with CHIR99021 followed by FGF9, there is evidence of UE formations marked by condensed PAX2+ MM which is suggestive of nephrogenic progenitors potential. It has been reported that prolonged induction with FGF9 (10 days) sequentially induces PS, IM and UE/MM with enhanced marker

stimulation and prolonged expression of SIX2 (Takasato et al., 2014a). Another UE marker, GATA3, although not specifically marks collecting duct, has been found to co-expressed in the PAX+ MM cells. However, no condensation around UE tips was observed (a feature of developing kidney). At day 30, more complex kidney architecture has been observed where the clusters form mini organs (organoids). Interestingly, SIX2+ clusters stably being expressed that suggest the suitability for pushing nephrogenesis further thus creating advance organoids (Kobayashi et al., 2008).

3.2.7 HNF1B factors are highly expressed in ureteric bud differentiating into collecting duct.

To elucidate the function of HNF1B in early kidney development, I quantified *HNF1B* transcript expression together with its paralogue, *HNF1A* and measured localisation of HNF1B in differentiating organoids. Similar expression pattern was observed in all lines (MAN13, LV-MAN13 and TF173) for both genes. During differentiation, *HNF1B* expression began at day 7 and persisted towards the end of differentiation which reflected an increased structural complexity, evident by HNF1B+ cells as the cells differentiated. HNF1A expression however was only minimally detected at day 19 but demonstrated a gradual increase over time which suggested its functions during organoids maturation. Apart from that, both differentiating lines were stained against HNF1B transcription factors at day 19. HNF1B+ cells were exclusively distinguished from ECAD+ cells which suggest the tubular precursors that will give rise to collecting duct. An increasing complexity and tubular elongation were observed as the organoids mature. To compare HNF1B expression of renal precursors generated from differentiating cells, an immunohistochemical assessment was performed on E14 mouse embryonic kidney tissue that recapitulates week 5 of gestation in human. Positive stain for the protein was observed in the medullary collecting duct (brown) with lower expression in tubular components near the nephrogenic zone and cortex (Figure 3.22). This is similar to what has been reported from *in situ* hybridization of 90th day of gestation human fetal kidney where HNF1B signal was prominent in medullary collecting duct but weaker in immature glomeruli (Kolatsi-Joannou et al., 2001).

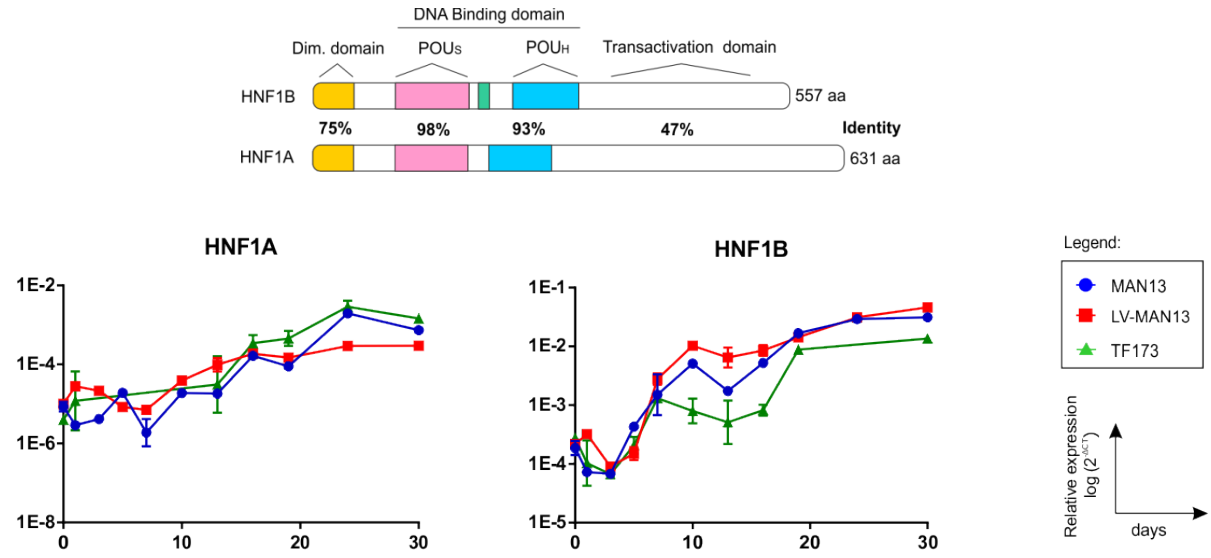

Figure 3.21 Localisation of HNF1B during early embryonic kidney development. (a) Time course quantitative PCR of *HNF1A* and *HNF1B* for 30 days indicated higher *HNF1B* expression in all MAN13, LV-MAN13 and TF173 as compared to *HNF1A* which progressively increased but at lower amount.

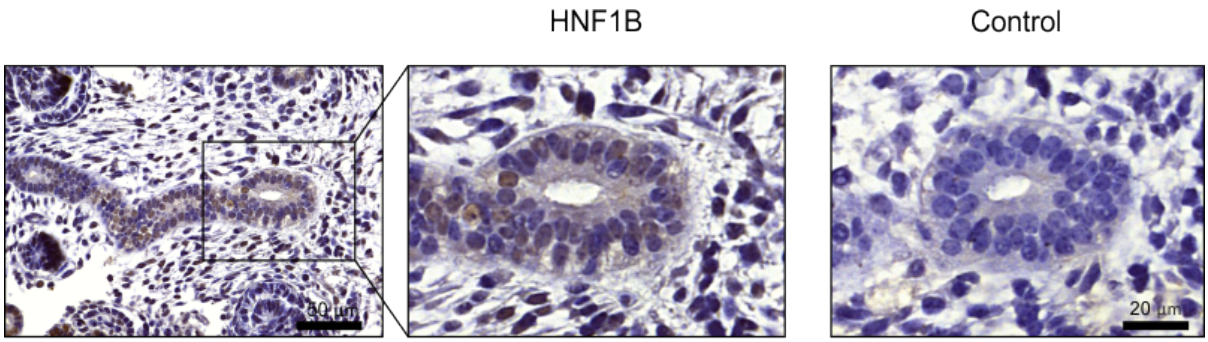

Figure 3.22 Immunodetection of HNF1B in E14 mouse fetal embryonic kidney by immunohistochemistry. Paraffin-embedded kidney sections revealed highly expressed HNF1B+ cells (brown) at collecting duct (CD). Negative controls were stained with hematoxylin and relatively different from antibody-treated sections. Tissues were sectioned at 4 µm. Scale bar, 50 µm.

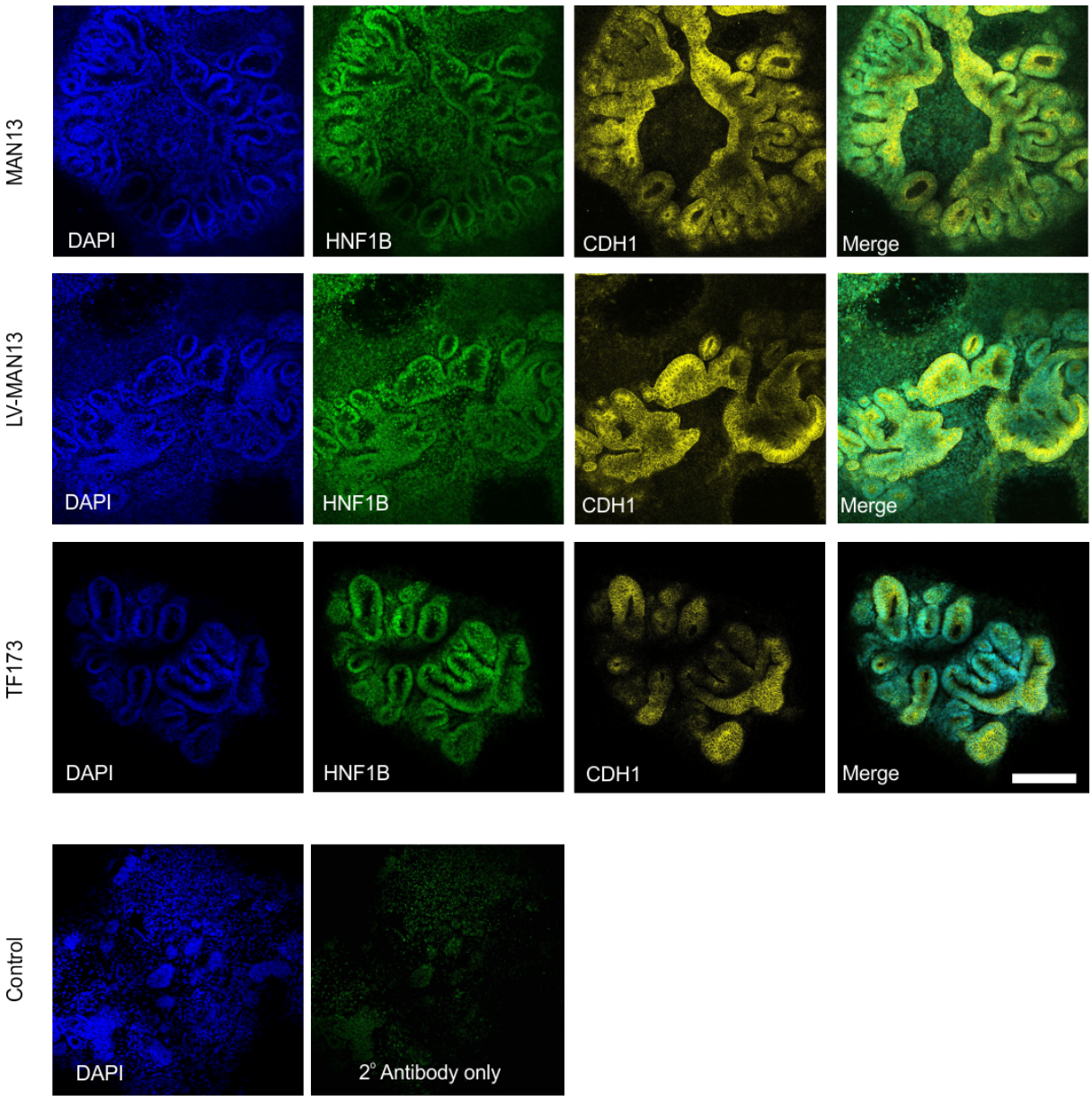

Figure 3.23 Representative confocal images showing nuclear localisation of HNF1B in hPSC lines at day 19. HNF1B+ cells show highly intricate collecting duct identity which surrounded by CDH1+ adherens proteins and branching characteristics. Tissues were sectioned at 4 µm. Scale bar, 50 µm.

3.2.8 MAN13 mini 3D kidney organoids expressing HNF1B at day 19 of differentiation

To verify presence of HNF1B proteins in differentiating and differentiated cells, the protein size has been measured at day 7 and 19 together with E15 mouse kidney. Early in differentiation of both lines, at day 7, they did not express HNF1B protein which supports the qPCR expression profiles. However, western blotting of cell lysate at day 19 MAN13 yield a 65 kDa protein which was absent from the LV-MAN13 protein lysate. E15 mouse kidney on the other hand produces a double protein band at 72 and 61 kDa, respectively. This is possibly due to inter-species variation, splice variants, protein phosphorylation, dimer formation, highly glycosylated proteins or shared epitopes. The E15 mouse tissue used is highly congruent to 6th week in

human kidney development. Undifferentiated embryonic stem (ES) cell control does not express any protein. GAPDH were found to ubiquitously express in all cell types. TF173 lines however was not tested for protein level at any stages.

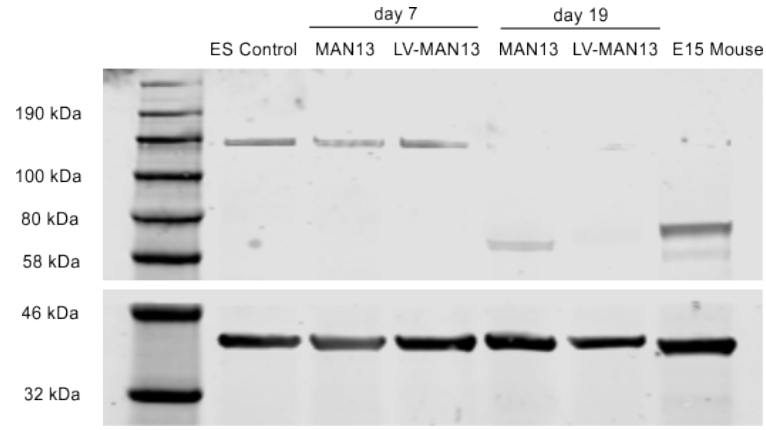

Figure 3.24 HNF1B protein detection in differentiating MAN13 lines. Day 7 of differentiation revealed absence of HNF1B proteins whereas day 19 MAN13 lines showed 61 kDa protein presumptive of HNF1B proteins. No band was detected in LV-MAN13. E15 mouse embryonic kidney showed double band ranged from 72-58 kDa proteins. ES control is undifferentiated MAN13 lines. ES, embryonic stem cell, LV, lentiviral, E15, embryonic stage.

3.3 Discussion

3.3.1 Vector-free iPSC lines determines safety for *in vitro* applications

Integrating viral vectors into biological systems has raised safety concerns due insertional mutagenesis, tumor generation caused by reactivation of reprogramming factors (Carey, 2011; Okita, 2007) and perturbed differentiation program by residual expression of transcription factors (Sommer, 2010; Seiler, 2011). There are multiple strategies to generate hiPSCs either from peripheral blood cells or fibroblasts. These include chemical, lentiviral or retroviral-mediated gene transfections. DNA-based vectors such as adeno-associated virus, plasmid and adenovirus are widely used to express reprogramming genes (OCT4, SOX2, KLF4, and C-MYC). Although these vectors do not require integration, there still possibilities of integration within host chromosomes. One alternative approach to avoid these consequences is by using the integration-free system such as SeV, synthetic mRNA, transposons, artificial chromosome vector, minicircle DNA vector, piggyBac system, oriP/EBNA1-based episomal vectors and recombinant proteins (Fusaki et al., 2009).

CytoTune™-iPS 2.0 reprogramming system that are based on modified and non-transmissible virus can be safely and effectively delivered to reprogram somatic cells to iPSCs. This non-integrating SeV that do not alters or integrate within the host genome and remains in the cytoplasm (footprint-free). This is due to its identity as a negative-sense RNA virus that has a limited DNA stage during its life cycle (Bitzer, 2003). SeV however can infect various cell types that include CD34+ cells, fibroblasts

and T-cells (Wakao, 2013; Ban, 2011). It has been shown that the current SeV system has effectively increase transfection efficiency, lower cytotoxicity and yield faster SeV clearance. In this study, I have successfully delivered Sendai particles containing three vector preparations that include polycistronic Klf4–Oct3/4–Sox2, Klf4 and cMyc for efficient iPSC generation from blood cells. This has replaced the multiple days of transduction using mRNA-mediated reprogramming. In addition, serum-free medium did not reduce SeV transduction efficiency.

From the DNA gel electrophoresis, it was evident that all newly generated iPSC lines were free from SeV and its related transgenes. However, the unaffected iPSC lines from healthy control (TF173BP14) showed minimum SeV expressions, approximately 200 bp. This could be due to low copies of the Sendai vectors that persist up to 14 passages. This is however not an uncommon phenomenon because even though SeV does not integrate into the host genome and vector copies diminishes in every passage, small amount of vectors may retain. In order to clear SeV from hiPSCs, the vectors have been modified via introduction of point mutation in the P and L genes making them effectively sensitised to temperature shift (Ban, 2011). Thus, any vector that persists after 5-10 passages can be possibly removed by incubating iPSCs at 38–39°C for 5 days. This method will enhance hc-Myc vector that remained longer in cells to be reduced to undetectable level due to its temperature sensitive mutation. In this study, any lines at passage 14 and lower were excluded from characterisations.

3.3.2 Genomic stabilities is essential for robust differentiation

It is well-known that hPSCs are easily sensitised to physiological or mechanical stress. These factors contributed to recurrent genetic aberrations especially during extensive culturing. The abnormal karyotype can halt how the iPSCs behave thus can affect the end point purposes either disease modelling, therapeutics or pharmacological screening. The hPSC genetic analysis was performed due to its reliability using nine primer-probes which can detect over 70% of the most common karyotypic abnormalities reported in hPSC cultures. This qPCR–based kit has enabled screening of multiple hPSC lines in a rapid, cost-effective manner. This assay utilised a double-quenched probes (with 5-carboxyfluorescein), which give superior performance over single-quenched probes. This allows detection of copy number at the minimal critical regions of commonly mutated genetic loci with high specificity and sensitivity thus maintaining stem cell culture quality.

If a qPCR experiment was good with very low replicate variability and all other regions were close to 2 copies (1.9 - 2.1) this is a higher cause for concern than if replicate values were more variable and the copy number of other regions contained a wider

spread (1.5 - 2.5). The latter scenario may indicate a pipetting error. Similarly, it is less likely to be a true result if there were multiple "abnormal" or "possibly abnormal" regions per sample (2-4 regions). If a clear abnormality an "abnormal" or "possibly abnormal" result is found then it would be recommended to re-extract gDNA at the same passage or a slightly later passage, perform qPCR and analyse again to confirm. If the sample reconfirms as "abnormal" it is recommended that the this cell line sent for G-banding or whole genome sequencing (e.g. SNP array).

However, it is important to address the sources of variability when interpreting this data. Properly calibrated pipette can avoid errors while loading of genomic DNA samples and can yield more robust interpretation. Incomplete vortexing of the reagents may affect reproducibility between batches. Low quality of DNA should be prevented by making sure the concentrations are accurate and comparable. Genomic DNA samples should have absorbance ratios in the range of A260/280 ~1.8-2.0 and A260/230 ~1.9-2.2. Furthermore, if using Nanodrop for DNA concentration measurement, they should be properly calibrated and that the pedestal was clean to avoid miscalculation. High variability between technical replicates will significantly impact downstream analysis. This is particularly important in any genetic assay within the control sample and also for the Chr 4p genetic assay within test samples, as this data is used for normalisation.

To date, the most frequently used techniques to detect gene copy number alterations include array comparative genomic hybridization (aCGH), Multiplex Ligation-dependent Probe Amplification (MLPA), which depends on the availability of the gene of interest; and quantification using real-time PCR, which can be performed with intercalating dyes (such as SYBR® Green) or TaqMan® assays. Regular SYBR® Green qPCR can be performed either in a single tube with an internal control fragment (competitive PCR) or using separate reactions for the target and control genes (differential PCR). However, competitive qPCR is a time-consuming process that is limited to sets of primers available from one supplier (Mocellin, 2003) and the reproducibility of differential qPCR is inevitably compromised by the variable efficiency of the PCR itself because small variations in reaction components can greatly influence the final yield of the amplified product (Ruiz-Ponte, 2006).

3.3.3 hPSCs commitment towards IM and nephron lineage

In this chapter, I have discussed the utilisation of hESCs and hiPSCs as an ideal cell source to direct differentiation towards kidney precursors via PS or IM under chemically defined monolayer culture condition. The idea of using hPSCs is made more attractive by their ability to differentiate into the three embryonic germ layers that can generate tissues of the developing foetus, and their self-renewal capacity

that allows indefinite maintenance of the undifferentiated state *in vitro*. Thus, the utilization of these MAN13, LV-MAN13 and TF173 lines, which are derived in the lab, will help us to understand some developmental aspects of genetic kidney disease.

To test applicability of this cell source, all lines have been cultured and maintained on functionally defined feeder-free substrates, the recombinant vitronectin which functions to support a sustained self-renewal and pluripotency of hESC apart from Matrigel and fibronectin matrices (Braam et al., 2008). Directed differentiation was based on protocol adapted from Takasato et al. (2014) with minimal changes and the cells were characterized in detail. Upon differentiation, all lines resulted in synchronous induction of UB and MM that form self-organizing structure similar to collecting duct and nascent nephron percursors. Early treatment with an optimal concentration of 8 μM CHIR99021, the Wnt agonist (or selective GSKβ inhibitor) has stimulated the canonical Wnt signaling pathway which is reported as an inducer for primitive streak in mouse and human ESCs (Gadue et al., 2006; Sumi et al., 2008). Three days of CHIR99021 treatment is optimal for posterior PS induction, evidenced by increased expression of T (Brachyury) in both lines which immediately reduced after day 3 (Takasato et al., 2015b).

The second stage of differentiation involved the differentiation of definitive mesoderm to IM, lateral plate (LPM) and paraxial mesoderm (PM). These cells were continuously fed with FGF9 and heparin for a period of 10 days to direct differentiation of primitive streak to intermediate mesoderm. OSR1, a robust marker of IM and MM formation were found to be differentially expressed during this stage together with more definitive IM markers, PAX2 and LHX1. FGF signaling was utilized to direct this stage and it was found that FGF9 and FGF2, but not FGF8, efficiently specify IM after the primitive streak stage and maintain MM survival *in vitro* (Takasato et al., 2014b). FGF9 expression was also found in the PM (Colvin et al., 1999b; Crossley and Martin, 1995). In the presence of FGF9, OSR1, PAX2 and LHX1 were found to be co-expressed, which suggests induction of IM. However, FGF9 is dose-dependent (optimally 200 ng/ml) causing suppression of FOXF1, the LPM marker, as well as OSR1. Treatment of FGF9 alone is sufficient to sustain induction of IM markers, PAX2 and LHX1 (Takasato et al., 2014a).

Further differentiation into metanephros largely depend on reciprocal stimulation between UB and MM. MM drives ureteric epithelium outgrowth/branching via GDNF whereas UB in turn promote MM survival via FGF9 and WNT9B signaling as seen in mouse nephron progenitors *in vitro* (Barak et al., 2012). Specifically, WNT9B controls the MET transition in this differentiation. Moreover, simultaneous induction of nephric duct/ureteric epithelium genes (CRET and HOXB7) was also reported. Our immunofluorescence data demonstrated that the WT1+ cells condense tightly around

ECAD+ epithelium at day 13, suggestive of simultaneous proliferation and differentiation of two distinct renal lineages which are expected to give rise to nephrons and collecting duct, respectively, and this corresponds with our qPCR data. As the cells differentiate, early mesenchymal lineages were positively stained for SIX2 and WT1 proteins which appear to surround ECAD+ collecting ducts that peaks at day 19. Differentiation to WT1+ or SIX2+ cells continued to increase up to day 30 possibly reflecting upregulation of these proteins in developing nephron progenitors. However, evidence of lumen formation connecting ureteric epithelium and renal vesicle was observed which suggest the need for a more advanced microenvironment to induce nephrogenesis.

The transcript analysis revealed structural development and differential expression of renal-specific cell components over 30 days of differentiation. This includes primitive streak (T, MIXL1, LHX1), IM (OSR1, LHX1, PAX2), MM (SIX2, WT1, OSR1, HOXD11, CITED2, SALL1), UB lineage (HOXB7, SALL4, PAX2), podocytes (PODXL), proximal tubule (AQP1), loop of Henle (UMOD), collecting duct (AQP2), tubular (PDGFRB), stromal (FOXD1) and vasculoendothelial (KDR). Another criteria would be the inclusion of PAX6 and SOX17 in the mRNA transcripts analysis to confirm that there were no ectodermal and endodermal commitment, respectively, and differentiation are mesoderm-specific (Takasato et al., 2014b). Although morphological development was apparent, it was observed that the temporal pattern and amount of gene expression slightly differs. This is possibly due to the number of differentiating or mature organoids formed over time, the cell density-dependent nature of initial culture and variation in genetic background that suggest differences in receptor density. Seeding density of $3.5x10^4$ has reported to be an optimum initial culture (Takasato et al., 2015b). However, keeping cells at constant number, homogenous cell dispersion across wells and complete dissociation into single cell remain as challenges that should be overcome.

When comparing MAN13 lines with the transfected and TF173 lines, there are no structural differences detected at any time point. However, transcription profiles of LV-MAN13 seem to differ slightly from the non-LV counterparts, suggesting alteration in transcriptional regulation possibly due to the amount of differentiating cell components and differentiated organoids formed at specified time points. This is evidenced by the low protein expression in LV-MAN13 at day 19, but not in MAN13 line. Further experiment should be focused on optimising initial plating cell density, gentle media loading to avoid early cell detachment and driving differentiation of LV-MAN13 to increase the number of developing organoids for a higher protein yield.

3.3.4 Conclusion

In this chapter, I have successfully demonstrated generation of hiPSCs from peripheral blood and maintained them in undifferentiated state up to passage 20 in a defined serum-free medium. These hPSCs retained properties of self-renewal and pluripotency over prolonged culture. I found that the both hESCs and hiPSCs were able to differentiate to kidney lineage under defined conditions and signals. The monolayer (2D) culture system has allowed me to elucidate the cellular responses to small molecules and growth factors. This will serve as the basis of molecular mechanism and reliable as an *in vitro* model to recapitulate early events in kidney development. Thus, based on the data gathered, I can summarise that we have showed the possibilities of hPSCs as a source of pluripotent cells for the generation of 2D-derived kidney tissues but presented limitations such as lack of maturity, absence of vascularisations and incapable to mimic physiological kidney conditions. Despite these limitations, I aimed to further investigate the potential of these hPSCs to forms more mature and intricate kidney structures. Taking this forwards, these hPSCs has been differentiated to a 3D environment to better mimic real tissue organisations.

Differentiation to kidney lineages is inevitably very complex due to the presence of more than 20 cell types and spatio-temporal demarcation between intricate structures. Coordinated cell induction from various key cellular populations demonstrates the need for interacting niches to create complex morphogenetic structures. From the current results, it can be summarized that I have successfully documented hPSC differentiation in monolayer culture *in vitro* over 30 days. This generates a reciprocal induction of early kidney progenitor populations which are able to self-organize, reflecting suitability for generating renal tissue from unaffected and disease affected pluripotent cell sources. The current data have given some insights regarding synchronous cellular responses to CHIR99021 and FGF9.

Equilibrium in differentiation of nephron progenitors and self-renewal should also be carefully monitored. Takasato et al. (2014) has reported development of multiple renal vesicles but significant loss of nephrons with time, suggesting premature nephron differentiation and indicative of cells that cannot be sustained to differentiate any further. Changing growth factors, extracellular matrix and oxygen tension will improve this condition. The idea of a staged shift to organoid culture in bioreactors will facilitate a more 3D environment.

In this chapter, I have successfully demonstrated that different hPSC lines can be differentiated to generate kidney precursors *in vitro*. MAN13 lines (together with respective LV-transfected lines) and hiPSCs (TF173) documented consistent

differentiation outcomes, analysed by transcript profiles and immunostainings, although derived from different genetic backgrounds. The LV-transduced hESCs (containing reporter genes for lineage tracing studies) have been shown to be stably integrated into the genome without compromising the differentiation potential (Bantounas et al., 2018). Although differentiation and maturation efficiency can be further optimised, I have established proof-of-principle that hPSCs can be induced to form kidney precursors *in vitro*. This work has advances our understanding on early kidney morphogenesis and can be further optimised towards using stem cells as tools for kidney repair and modeling genetic kidney diseases.

It was reported that using the standard adhesion culture, the 2D monolayers able to spontaneously generate multilayers and 3D structures (Morizane and Lam, 2015). However, the unfavourable environment may not promote morphogenesis, self-organisation or advance maturations thus making 2D culture best suited for live cell tracking and immunocytochemistry due to tissues organisations which are relatively thinner as compared to 3D platforms. To further investigate the spatiotemporal regulation and specifications, induced kidney cells at day 7 of 2D phase were dissociated, pelleted and cultured at an air-media interphase. Early segmentation, patterning and nephron formation were characterised in details which will be discussed in the next chapter. However, special attention needs to be focused on a balanced control of progenitor self-renewal and differentiation to nephrons, apart from UE/MM balance. Improving differentiation protocol will remain as a key challenge as normal kidney development easily halted by altering growth factors, extracellular matrix and oxygen tension (Barak et al., 2012; Linton et al., 2007; Uchiyama et al., 2010). Bioreactors would be interesting alternatives to mimic 3D environments.

Chapter 4 Generation of hPSC-derived 3D kidney organoids and their phenotypic comparison

4.1 Aims and introduction

Most of the published kidney differentiation protocols have based on animal models and 2D culture systems. Even though animal models can suitably recapitulate systemic nephrotoxicity *in vivo*, it is however noted that the differences between species, time and cost issues have limited its applicability in pharmaceutical research. Cell culture models using mammalian cells have been established to serve as an alternative to model biological, physiological and mechanical aspects of human tissues. However, monolayer culture lacks robustness to mimic human biological conditions, particularly kidney filtration systems. For example, primary proximal tubule cells grown in 2D systems lost their function after hours of isolations (Weber et al., 2016). Alternatively, research has focused on generation of immortalised human proximal tubules to better model nephrotoxicity. Yet, some kidney cells treated with nephrotoxicants are unable to upregulate kidney injury biomarkers and some other cells failed to transport cations and anions due to insufficient transporters which further halt drug metabolisms (Jenkinson et al., 2012). Moreover, a newly generated human proximal tubule epithelial cell with a wide range of functional transporters that is capable of responding to carcinogens and antivirals, still could not represent tissues due to lack of structural accuracy (Aschauer et al., 2015; Nieskens et al., 2016; Simon-Friedt et al., 2015). Further, 2D culture platforms provide less interaction of single cells and the surrounding environments, and reduced structural complexity.

There has been huge interest in using 3D printing technology for printing biological samples that can generate a layer-by-layer tissue thus resemble complex tissue architecture. However, viability issues had limited its applications. Current attempt can only print proximal tubule structures (Homan et al., 2016). Furthermore, decellularised kidneys can also be repopulated with embryonic stem cells in a way that can induce spatial influences on differentiation and migration (Batchelder et al., 2015). Nonetheless, this method was found to be less efficient in generating normally occurring kidney cell types (Mckee and Wingert, 2016). Modeling a kidney disease *in vitro* inevitably requires understanding of its increasing complexity of anatomical organisation and interactions with surrounding environments. The intricate interplay between specialised cells in 3D structure will govern its physiological function. Formation of the correct cell types at the right location in sufficient amount can potentially sustain kidney development. Thus, generation of self-organised 3D kidney organoids was proposed, to recapitulate embryonic kidney in term of structure and functions.

It is however important to emphasise that 3D reconstruction of a given organ should ideally lead to an identical replica of the normal healthy organ. Though this poses a significant challenge, it is also very important to distinguish possible alterations that may derive from the pathogenic mechanism of a given disease rather than from alterations due to sub-optimal culture conditions. Several methods to generate replica of human kidney from hPSCs has been reported and this has speeded up the rate of disease diagnosis and development of new therapeutics to treat genetic kidney diseases (Morizane and Bonventre, 2017b). This showed the possibilities of growing patient-specific hPSCs and creating an *in vitro* model of human kidney. To achieve this aim, I combined monolayer culture and a 3D organoid protocol based on a slight modification of a previously described protocol (Takasato et al., 2016). Here, generation of kidney progenitors in monolayer culture via directed differentiation of hPSCs followed by 3D culture has advanced kidney structure formation and will be discussed in details.

It is known that understanding of specific signalling cues between interacting cells and ECM are essential to study kidney organogenesis both in its developmental aspect and regenerative potential. HNF1B, which is expressed during early kidney development, is essential in regulating cell-cell contact within UB tip for appropriate epithelial rearrangements and differentiation of CD (Desgrange et al., 2017). Mutation in *HNF1B* has led to variety of kidney phenotypes such as cystic kidney disease including MODY and pancreatic hypoplasia. Thus, in this chapter, I will describe the generation of kidney 3D organoids by directing differentiation of *HNF1B*-mutant hiPSCs as well as a closely related healthy control. This 2 phase differentiation protocol (2D and 3D) can be used to test the hypothesis that 3D kidney organoids can model human genetic kidney malformations caused by *HNF1B* mutation as seen in RCAD patients. Towards answering this question, I have several aims that include:

1. To culture and differentiate hESC (MAN13 lines) and *HNF1B*-mutant hiPSCs together with its related control as self-organising 3D kidney organoids.

2. To investigate the effect of varying initial cell number on organoid structure at terminal day of differentiation.

3. To study the effect of prolonged culture on differentiating organoids by documenting transcript expression profiles.

4. To characterise morphological differentiation and expression of major kidney marker genes that include *HNF1B* downstream targets using qRT-PCR and immunostaining upon kidney differentiation for 25 days.

5. To simultaneously compare morphological characteristics, regionalisation and gene expression patterns of differentiating and differentiated hPSCs by immunohistochemical analysis.

In this section, I will report on the differentiation and characterisation of 3D kidney organoids derived from hPSCs (MAN13, TF171, TF172, TF173 and SW162 lines) under defined conditions by utilising growth factors involved in normal embryogenesis. The current differentiation strategy has successfully enabled generation of 3D kidney organoids containing both UB and MM derivatives with evidence of key nephron progenitors. This chapter describes a complete characterisation of 3D kidney structures together with expression levels throughout the differentiation. As for the terminologies, monolayer culture (2D) will refer to day 1 to day 7 and days on 3D phase from now will be indicated as day '7+' onwards.

4.2 Results

4.2.1 Differentiation of hPSCs into self-organised 3D kidney organoids resemble embryonic stage of kidney tissues

To test the robustness of the adapted protocol (Takasato et al., 2016), I began the differentiation using wild type hPSCs (MAN13 lines). This involved directed differentiation for 7 days on 2D platform continued with 18 days in 3D phase. A total of 35,000 cells were plated at day 0 and were treated with 8 μM CHIR99021 (Wnt agnonist) for 4 days followed by 200 ng/ml FGF9, 1 μg/ml heparin for additional 3 days before pelleted at day 7 of culture. Monolayer culture at this stage were dissociated and plated at 200,000 cells/pellet. Organoids were fed with FGF9/heparin for another 4 days before switching to basal medium. Medium was change every 2 days up to day 7+25. Organoids were harvested at specified timepoints for gene expression and histochemical analysis. Figure 4.1 summarised the differentiation protocol.

At day 1 of culture, cells were sparsely interspersed on VTN-coated plate. At this stage, single cells were more prominent and began to interact with surrounding cells approaching day 4. At day 5, single cells tend to group with nearby populations and reach approximately 70% confluency. It is observed that at day 7 of culture, cells were 90% confluent with multiple visible spherical clusters (20-50 μm in diameter) suggesting the beginning of formation of kidney progenitors. These confluent cells were dissociated and counted before plated on transwell at an air-media interface. Organoids showed loose aggregates with some area detached from the main core structure. However, after 1 hour of CHIR99021 treatment, individual cells began to interact with surrounding cells concentrating central region with higher number of

cells making the whole organoids slightly reduced in whole organoid's diameter as compared to measurement on initial plating.

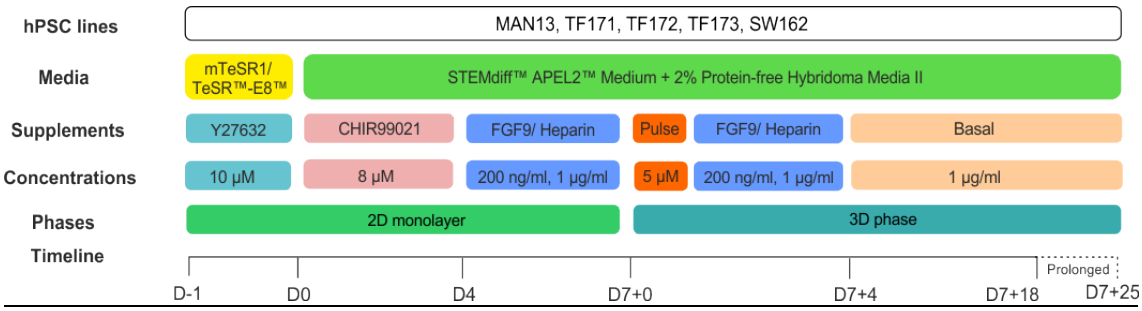

Figure 4.1 Differentiation protocol for generation of kidney organoids. hPSCs were differentiated as monolayer culture in the first 7 days and switched to 3D platform on day 8 onwards. Confluent layer at day 7 were dissociated and pelleted at 200,000 cells per well for pellet formation. Organoids were grown on transwell at air-medium interface and medium was changed every 2 days. Timeline depicts the duration of culture up to day 7+25. CHIR99021 pulse was added for 1 hour continued by FGF9/hep-containing media.

After CHIR pulse, organoid were exposed to FGF9/heparin medium for an additional 4 days. The phase contrast image captured at single plane complicated whole organoids visualisations. At day 7+4, organoids increased in size with opaque blackish middle portion and small rounded structure filling up the edge area. This phenomenon could be due to different level of cell layer/organisations. As the cells progressing towards day 7+11, organoids showed to generate multiple cell types. Some are rounded, oval while other showed few elongated identities. At this stage, cell types at the middle area appeared smaller in diameter as compared to the peripheral cell populations. At day 7+18 of culture, all organoids revealed a dome-shaped structures comprise of elongated tubular at the edge and relatively rounded structure at the centre. The images were taken at the same time every day to detect any morphological differences.

It was noted that each transwell can accommodate 3-10 organoids at a time. However, increasing total number of organoids per transwell necessitate frequent media changes and this study revealed that n=5 organoids would be the optimal number per transwell with organoids fed every 2 days. Figure 4.2 showed serial phases contrast images that showed increased depth with middle area nearly out of focus whereas the rounded cell types that surrounded the organoids were clearly visible. The transition of pellet from day 7+0 to day 7+4 was rapid (from flat organoids surface to emerging distinct colonies). However, beginning at day 7+7, organoids appeared to expand at slower pace but advanced more vertically, evidenced by increased in organoids thickness. As the organoids progressing through differentiation protocol, different cell types were seen to appear with some elongated and extend in both vertical and horizontal directions. When visualised at higher magnification, these organoids indicated presumptive kidney cells acquiring

glomeruli, UB branching tip and comma-shaped body characteristics (Figure 4.3). However, the identities were confirmed by immunostainings which were described in the next section.

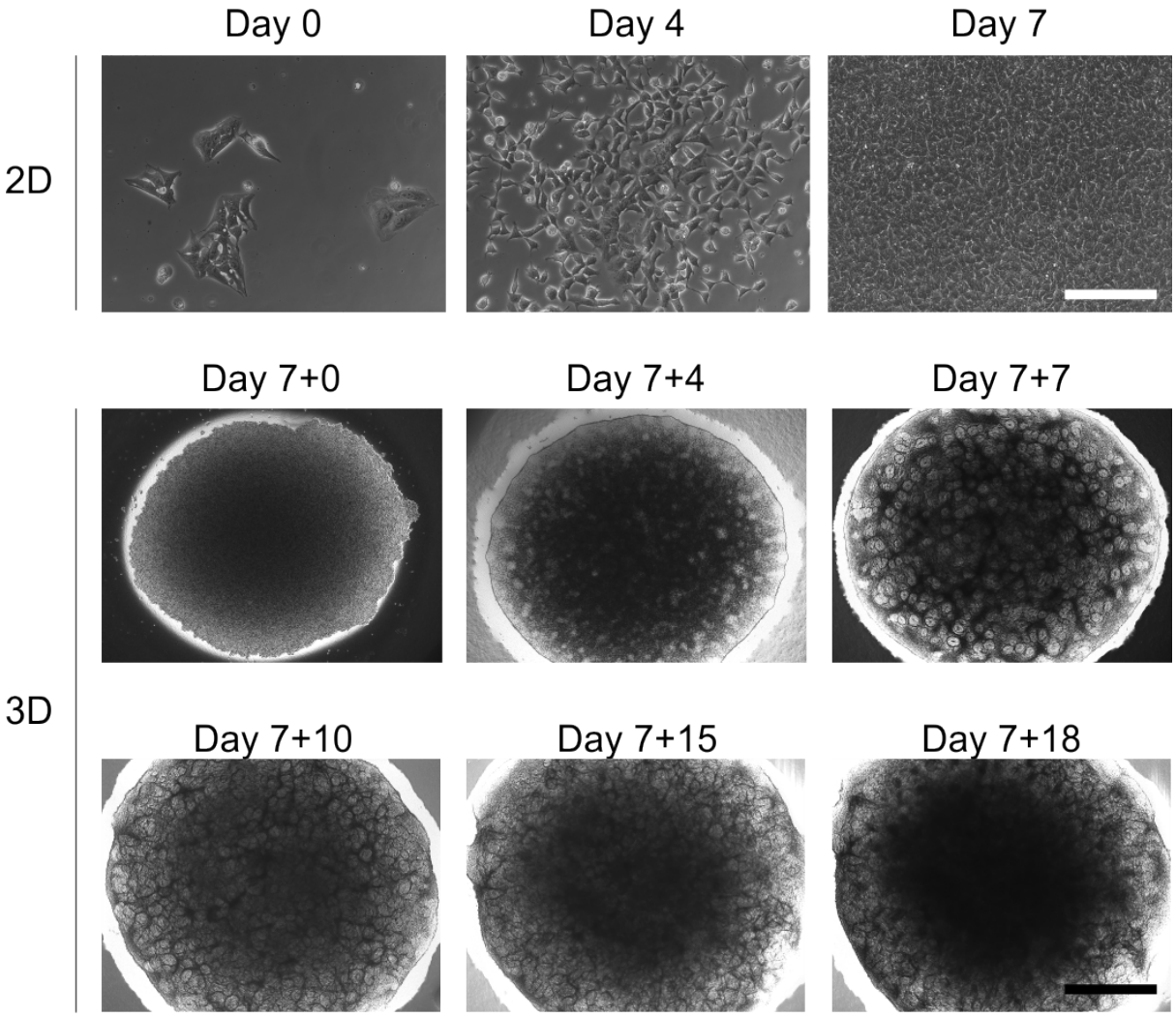

Figure 4.2 Morphological changes during differentiation of MAN13 lines to 3D kidney organoids. (*First row*) Serial phase contrast images of monolayer culture. After 4 days post-CHIR treatment, single cells began to differentiate into elongated cell that forms clusters. At the end of monolayer culture (day 7), cells are 90% confluent and ready to be dissociated to pellet-size cluster of cells. (*Second and third row*) Organoid phase contrast images indicated 3D culture. At day 7+7, rounded cells began to form that progressively built the whole structures. Towards the end, more advanced structure formed with the middle area not clearly visible suggesting multiple level of cellular organisation. Scale bar, 50 μm.

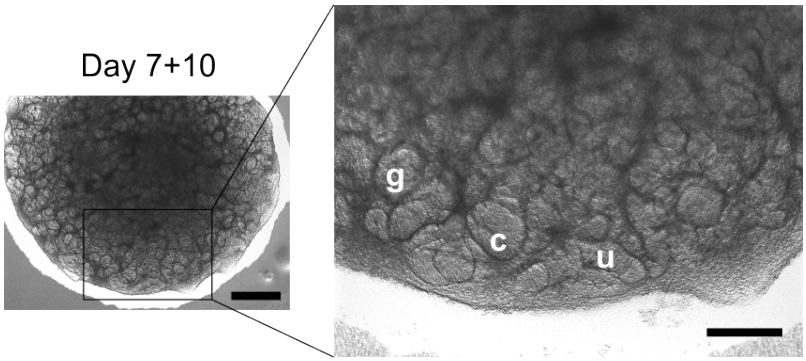

Figure 4.3 Representative of differentiating hESC 3D culture at day 7+10. MAN13 were subjected to the kidney differentiation protocol, harvested at day 7, pelleted and transferred to organ culture on a membrane at the medium-air interface. By day 10 post-transfer, the organoid acquires complex morphology. Higher magnification of the resultant mini-kidneys showed formation of early structures as seen in the developing kidney *in vivo* (Marked in white: g, glomerulus, c, comma-shaped body, u, ureteric bud branch tip). Scale bars: 50 μm (left); 20 μm (right).

From immunohistochemical staining (Figure 4.4), sections of MAN13-derived organoid has confirmed the generation of UB and MM lineages. When displayed at high magnification, it was found that the organoid section were positively stained for WT1, LAMB2 (glomerular basement membrane), COL4A3 (alpha 3 chain of glomerular basement) and NPHS2 (podocin). Staining for the vasculature (PECAM+ staining) showed minimal invasion of capillary network into the glomerular tuft. This is a manifestation of a pre-mature state of the filtration unit. On the other hand, it was observed that UB lineages comprised of tubular elements that were nuclear-stained by HNF1A (proximal tubules) and HNF1B (distal tubule/CD) transcription factors. Staining with UMOD antibodies indicated positive staining on the inner surface of tubules that suggested thick ascending limb (TAL) of LOH. GATA3+ cells that colocalised with CDH1+ epithelial tissues signified distal tubule/CD identities.

a. Metanephric mesenchyme derivatives

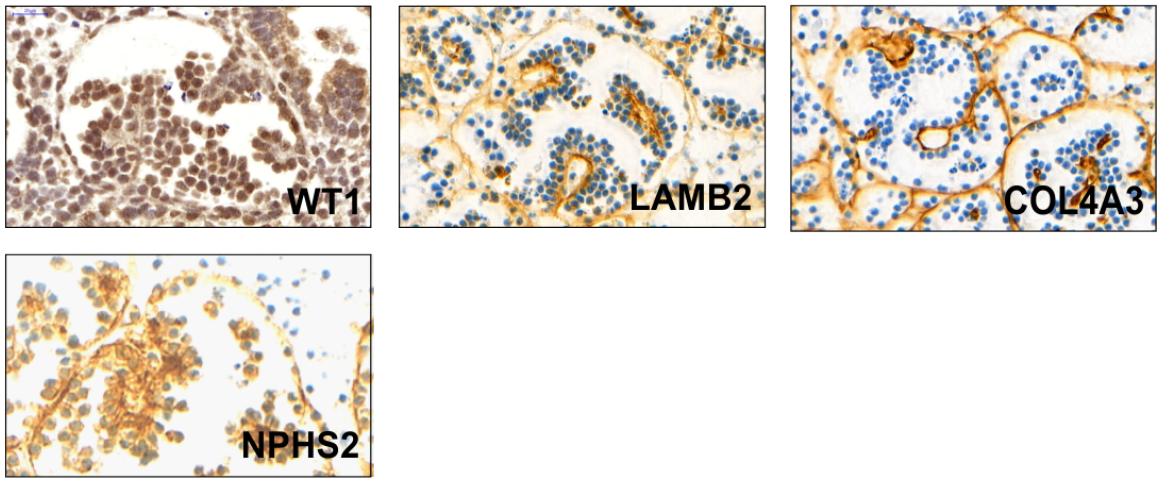

b. Ureteric bud lineage

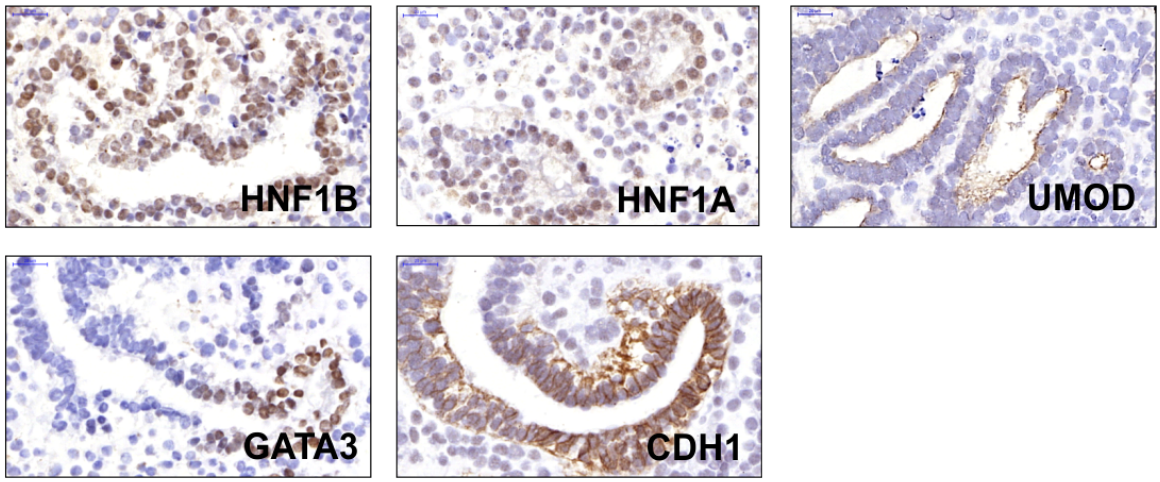

c. Insterstitial and endothelial cells

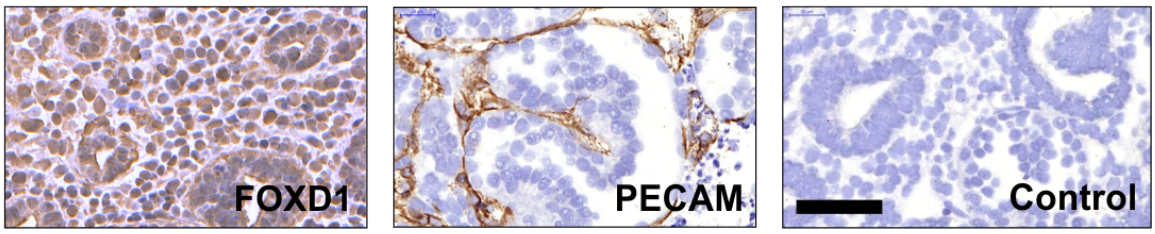

Figure 4.4 Immunohistochemical staining of UB/MM elements in MAN13-derived organoids at day 7+18. Organoids were stained positive for all key kidney markers for both derivatives (MM and UB). Glomerular podocytes were present indicated by NPHS2/podocin and WT1 staining. Minimal vascularisations were observed (PECAM+) whereas tubular identities marked by HNF1A, UMOD, GATA3 and HNF1B were specific. Epithelial marker, CDH1 was observed to localise on the outer surface of tubules.

4.2.2 Varying the number of starting cells does not affect an organoid's final structure

To test whether varying initial cell density during pelleting affected final kidney structure formation, I utilised unaffected MAN13 line to begin with. Two sets of MAN13 cells at same passage number were thawed and differentiated in-parallel. Cells were maintained using similar condition for the first 7 days and harvested (Takasato et al., 2016). During dissociation, cells were prepared at 2 different cell number, 100,000 (or 100K) (n=4) and 200,000 (or 200K) (n=6) cells per pellet. These organoids were maintained in 3D phase for 18 days before characterisations. Figure 4.5 showed that the 100K generated slightly smaller diameter organoids as compared to 200K. However, no other morphological differences were detected. Moreover, when these organoids were histologically sectioned and stained, it was revealed that the number of tubules and glomeruli on each middle section of organoids were only slightly differ and not significant ($p>0.05$) suggesting starting cell number, at least during pelleting, does not affect generation of kidney structures both in early and terminal culture (day 7+18). Thus, subsequent differentiations will utilise 200K for pellet formations.

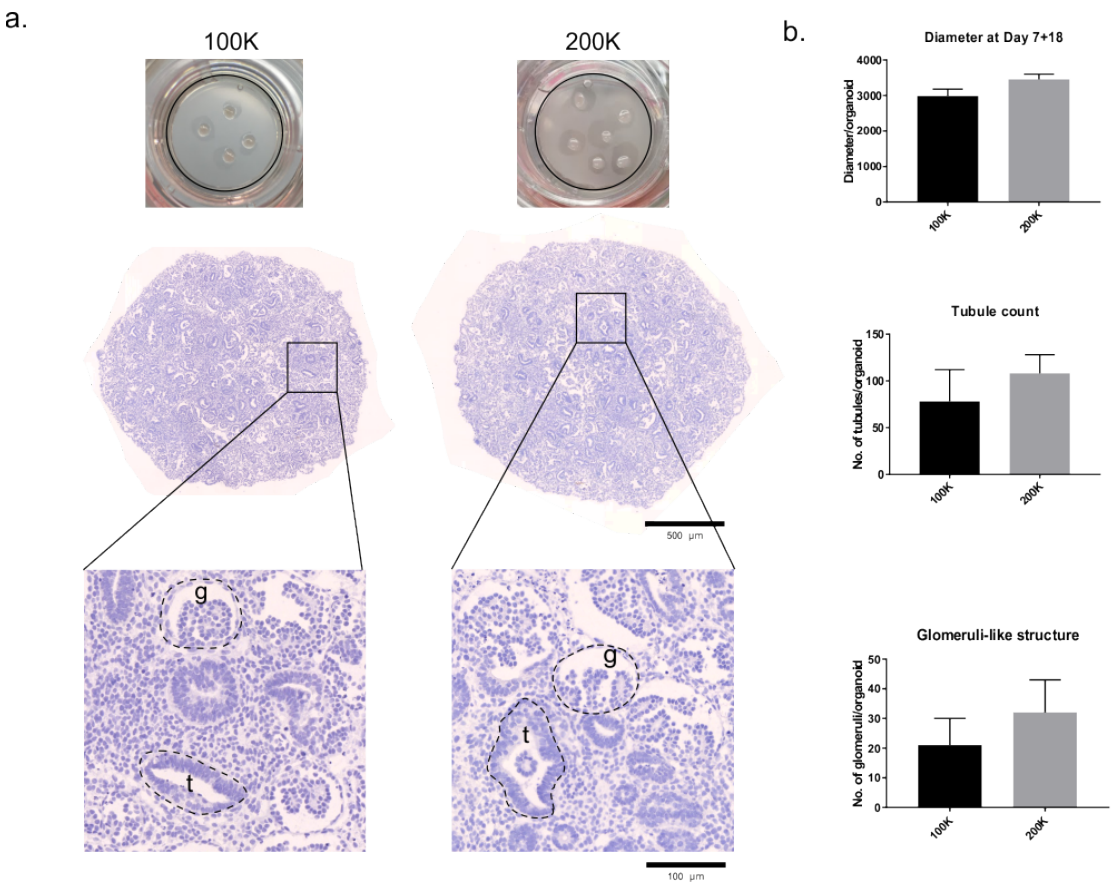

Figure 4.5 Effect of starting cell on organoid's morphologies. (a) Pellets were prepared either at 100K or 200K cells and plated on transwell. At the terminal differentiation day (7+18), 100K organoids were slightly smaller in diameter as compared to 200K ($p>0.05$). (b) Quantification of diameter differences and the number of tubules or glomeruli-like structures based on middle sections through the organoids. t, tubules, g, glomeruli-like. Scale bar whole mount, 500 µm, high magnification, 100 µm.

4.2.3 Different type of transwell affects differentiating 3D organoids morphologies

In order to investigate whether the type of transwell is important for successful organoid formation, I cultured MAN13 cells at similar passage number and directed them to differentiate towards kidney lineage as shown in Figure 4.1. These cells were differentiated as monolayer for the first 7 days and harvested at 200,000 cells per pellet before plating on Millipore or Corning transwells. Figure 4.6 showed that for the first 4 days of 3D culture no morphological differences were detected. However, as the organoids progressed from day 7+10 onwards, distinct morphologies were detected in both conditions. At day 7+13, the organoids plated on the Millipore inserts were filled up with a group of cells that were abundant at the periphery and started to fill the middle area evidenced by the emergence of tiny rounded clumps of cells in each organoid. Conversely, organoids adapted on the Corning transwells tend to spread over transwell surfaces and implicated in separation of thick/compact core from thin/less dense outer populations surrounding the whole organoids. The inner core showed intact structures filled with mixed cell populations. The structures formed at the edge however were observed to be less complex but contained minimal

elongated structures. Unlike Millipore-adapted structures, these presumptive early-stage organoids appeared sticky and could not easily be detached from the transwell thus complicated further characterisations. However, both inserts generated dark opaque middle structures that suggested a compact and multi-layered cellular organisation.

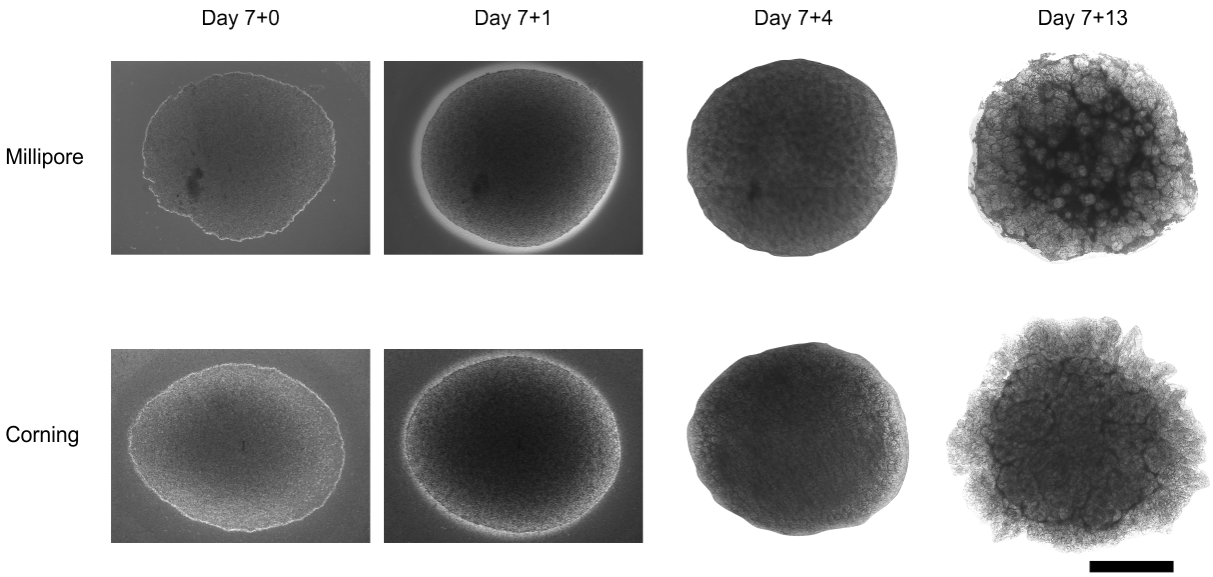

Figure 4.6 Effect of transwell type on organoid's differentiation. (*Top row*) Differentiating organoids using Millipore transwell showed intricate kidney structures by 7+ 13 days (*Bottom row*) Corning inserts generated two major structures with distinct middle cell characteristics and elongated transparent cell types at the edge. Morphologies of both culture groups relatively are similar up to day 7+4 but differ significantly commencing day 7+13 onwards. Scale bar wholemount, 500 µm.

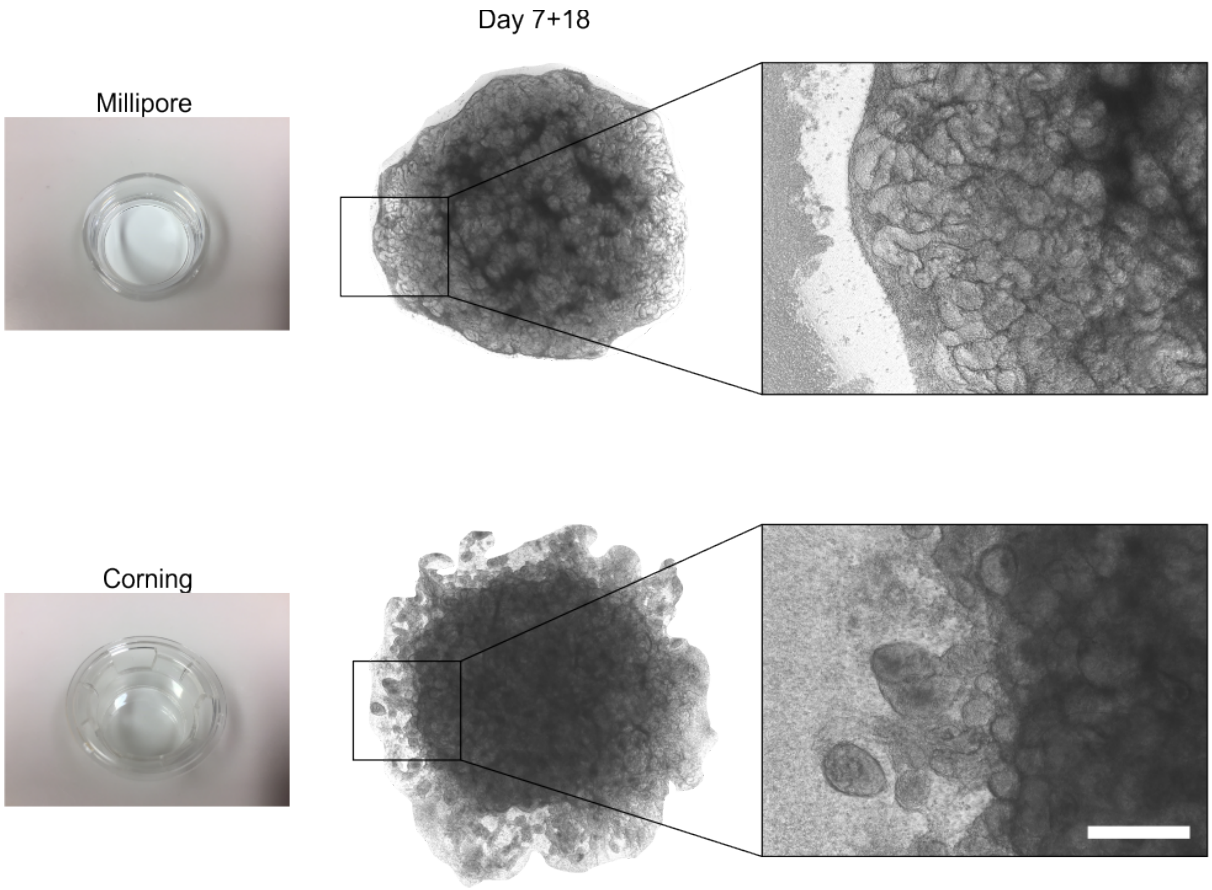

Figure 4.7 High magnification of organoid's morphologies maintained in different transwells. (*Top*) Organoids plated on Millipore inserts made up of hydrophilic, low protein binding PTFE polymer membrane with 0.4 μm pore size. (*Bottom*) Corning polyester membrane transwell with 10 μm thick and 0.4 μm pore size. Millipore version generated more intact organoids whereas the Cornings developed spherical cell population that escaped from the main core. Scale bar wholemount, 100 μm.

At day 7+18, it was observed that the Millipore-adapted organoids formed a visible and intricate kidney structures. The higher magnification phase contrast images (Figure 4.7) showed elongated tubular entities at the edges and a mixture of rounded tissues at the center. Conversely, the Corning transwells failed to maintain a spherical organoid structure but the organoids segregated into two major cell components comprising inner core filled with thicker cellular entities and translucent outer tissues. A focused image showed a ball-like entities filled by dark spots. However, when these Corning-mediated differentiations were prolonged up to day 7+25, the whole structures degenerated and shrunk inward making them unsuitable for analysis. Millipore inserts on the other hand exhibited lesser degree of degeneration prior termination of culture. To summarise, organoids at day 7+18 was chosen as the optimal timepoint and Millipore inserts were utilised in the subsequent differentiations.

4.2.4 MAN13-derived kidney organoids contain both CD and mesenchymal progenitors that able to form nephrons

It is known that both nephron progenitor and CDs are derived from IM origins. However, these derivatives are temporospatially distinct. In this study, it was observed that the directed differentiation of MAN13 lines to kidney organoids for over 25 days had synchronously induced formation of both nephron and CD lineages. From the immunostaining analysis, it was found that SIX2+ cells sparsely surrounded CDH1+ population at day 7+9. These SIX2+ progenitor cells were reported to be expressed as a subset of MM where the expression was maintained throughout kidney development (Self et al., 2006). Also, WT1, an early podocyte marker, was found to invade around the tip of CDH1+ cell clusters as shown in Figure 4.8. Interestingly, PAX2+ cells were also present exhibiting a more stretched/elongated structure and often colocalised with CDH1 populations. This was an early indication of progenitor formations that will give rise to distal/CD elements. Furthermore, prolonged differentiation up to day 7+18, although very rarely, has generated more advance entities such as capillary network (CD31) that surrounded glomerular podocytes (NPHS1). Of note, staining of tubular element with HNF1B and GATA3 antibodies have indicated positive staining presumptive of distal tubule/CD lineages. These immunofluorescence stainings have supported the existence of MM/UE lineage specification during organoids differentiation.

These immunostainings data have collectively supported the existence of reciprocal interaction between UB/MM signals and confirmed the inclusion of vascularisations during kidney development. However, the current visualisation techniques failed to provide clear indication of interacting structure and multi-layered cell organisations as a result of patterning and segmentations. In order to quantify and serially visualise organoids at multiple planes, I analysed each wholemount organoid using confocal microscopy system. This system was able to detect multiple fluorescence probe and separate individual channel as well as providing series of optical sections (z-stack). This has helped to better visualise each component and provided quantitative measurements regarding staining efficiency.

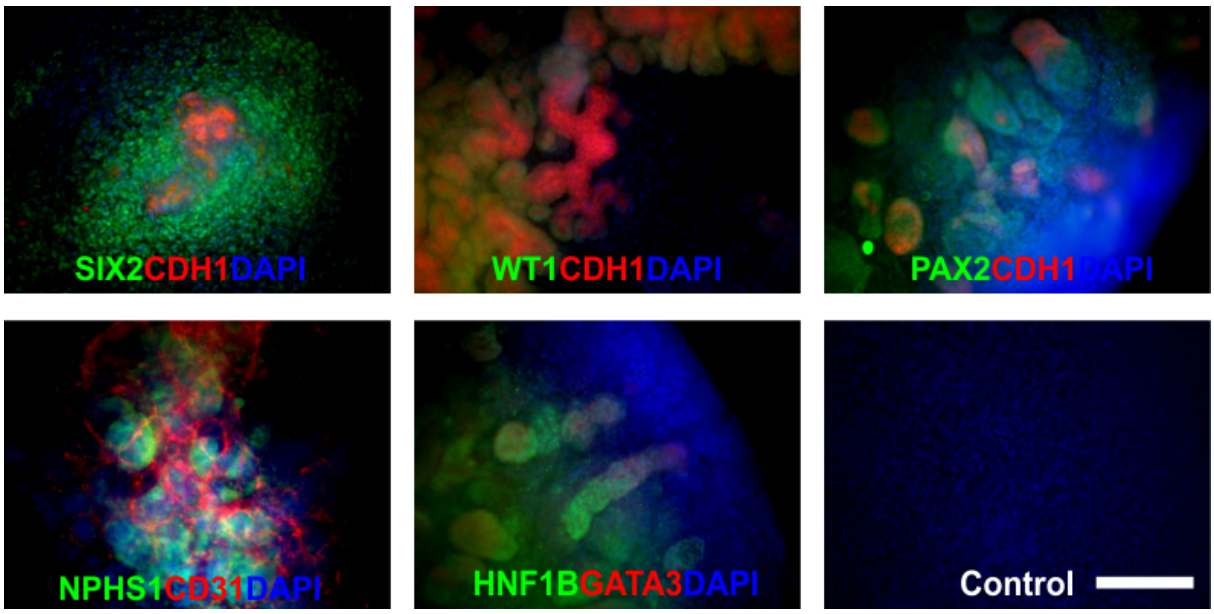

Figure 4.8 Immunostaining of differentiating 3D organoids. (*Top row*) Kidney progenitor cells were visible day 7+9 of culture stained with PAX2, SIX2 and WT1. CDH1 was found to co-localise with these nephron progenitors. (*Bottom row*) At day 7+18, organoids showed more advanced cell types stained for both distal/CD (marked by HNF1B and GATA3) and glomerular elements. Glomerular podocyte (marked by NPHS1) are surrounded by CD31+ endothelial networks. However, invasion into glomerular tuft rarely seen. Scale bar, 50 μm.

To analyse the pattern of expressions, I quantified expression level of the selected kidney genes at 9 timepoints along differentiation course and analysed the mRNA transcripts by qPCR. Figure 4.9 reported expression of 6 selected kidney markers (SIX2, PAX2, WT1, HNF1B, AQP2 and NPHS2) that were highly consistent with immunostainings. SIX2 expression progressively increased up to day 7+3 before reach plateau at later stage. PAX2 on the other hand peaked at day 5 on monolayer culture and reached equivalent expression level to that of SIX2 after day 7+3. WT1 was found to gradually increase commencing day 5 towards the end of the differentiation. To simplify, more advance structure was transcriptionally found to be generated at later stage of differentiation. There were tremendous upregulation of distal tubules/CD identity (AQP2) commenced from day 5 onwards. Glomerular podocytes (NPHS2) were increased towards the end except a slight reduction at day 7+11. Interestingly, pan marker of tubules/CD, HNF1B was found to retain lower level in the first phase of 3D culture which then peaked at day 7+18. These expression levels have supported the use of current optimised protocol that has the propensity to develop near-complete kidney elements.

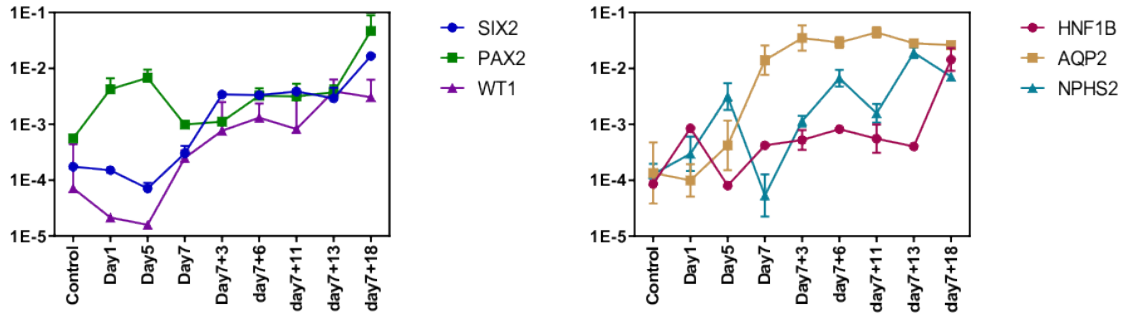

Figure 4.9 qPCR analysis of differentiating kidney organoids. (*Left*) Expression levels of kidney progenitors (SIX2, PAX2, WT1) that responsible for generation of both MM and UE cells. (*Right*) Expression of definitive kidney genes forming tubular and glomerular elements marked by HNF1B/AQP2 (distal tubule/CD) and glomerular podocytes (NPHS2).

Based on these transcript profiles, it was clear that NPHS2 progressively increases alongside HNF1B+ tubules that appeared to also increase slightly later. To put this into context, I quantified the number of glomeruli and tubular elements in differentiating organoids at day 7+18, by selecting 6 different middle section of MAN13 histology slides and stained with SYNPO and HNF1B to mark the glomeruli and tubular identities, respectively. On average, it was found that there were 49±7 glomeruli and 38±4 tubular units in each organoid. Moreover, Figure 4.10 revealed that 28.7% of stained area showed SYNPO+ cells and 17.8% were positive for HNF1B that correlated the transcript profiles indicating an increase in differentiating podocytes (NPHS2) followed by HNF1B expressing tubules. Although these findings have presented consistent efficiency between each run of 3D organoids differentiation, the selected middle sections were inadequate to draw any conclusion regarding the complete organoid's topology. To address this issue, I collected sequentially sectioned 3D organoids and stained with SYNPO/HNF1B including top and bottom sections to designate regionalisation. This was verified by confocal microscopy images that indicated self-organisation and distinct regional distribution of structures.

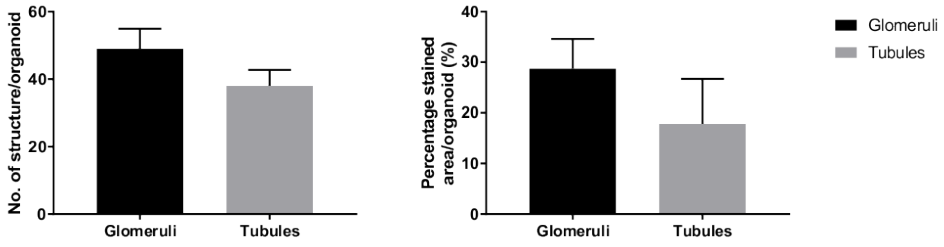

Figure 4.10 Quantification of total number of glomeruli and tubular elements together with the percentage (%) of stained area in MAN13-derived kidney organoids. These sections were stained with SYNPO and HNF1B to demarcate UB/MM origins. The experiment utilised only middle sections, n=6.

4.2.5 Kidney organoids revealed regionalisation of glomerular and tubular elements.

To further examine the positioning of each glomerular and tubular element, I stained the wholemount organoids with SYNPO and HNF1B antibodies, and visualised the structures in z-stack order (from bottom to top) at 5 μm intervals. The staining revealed presence of both SYNPO+ and HNF1B+ populations at various optical sections. Based on immunostaining analysis, it was found that the glomeruli accommodated most of mid-top regions (SYNPO+) whereas tubules can be found in all regions (HNF1B+). This regionalisation showed that the organoids structures can self-organise and relocated into a defined location within 3D niche. These complex morphogenetic patterning with presumptive of CD originated at the bottom, mixed proximal and distal tubules at the middle and glomeruli occupying the top region seemed to resemble mammalian kidney anatomy where the CD branched out from the middle region and glomeruli dominating the renal cortex. However, the relative amount of CD versus glomeruli in each organoid may vary between runs.

In order to quantify the amount of HNF1B+ and SYNPO+ cells beginning from the first optical section to the last, I quantified the amount of fluorescence intensity of selected top, bottom and middle region of 6 organoids for each marker. It was found that the top sections were highly stained for SYNPO+ glomeruli ($p<0.05$) but not the HNF1B+ tubules (Figure 4.11). This quantification correlated with the immunostaining that showed abundance of glomeruli structures at the top region. However, analysis of the middle sections revealed that HNF1B+ and SYNPO+ cells accommodated the middle region. There were no differences observed between the mean fluorescence intensities between these two markers ($p>0.05$). Further analysis on the bottom regions indicated lower amount of SYNPO+ cells but twice the amount in the case of HNF1B+ cells. This has led to conclusion that the CD/distal tubules were enriched at the base of organoids and elongated/orientated either vertically or horizontally to support glomeruli development at the top regions.

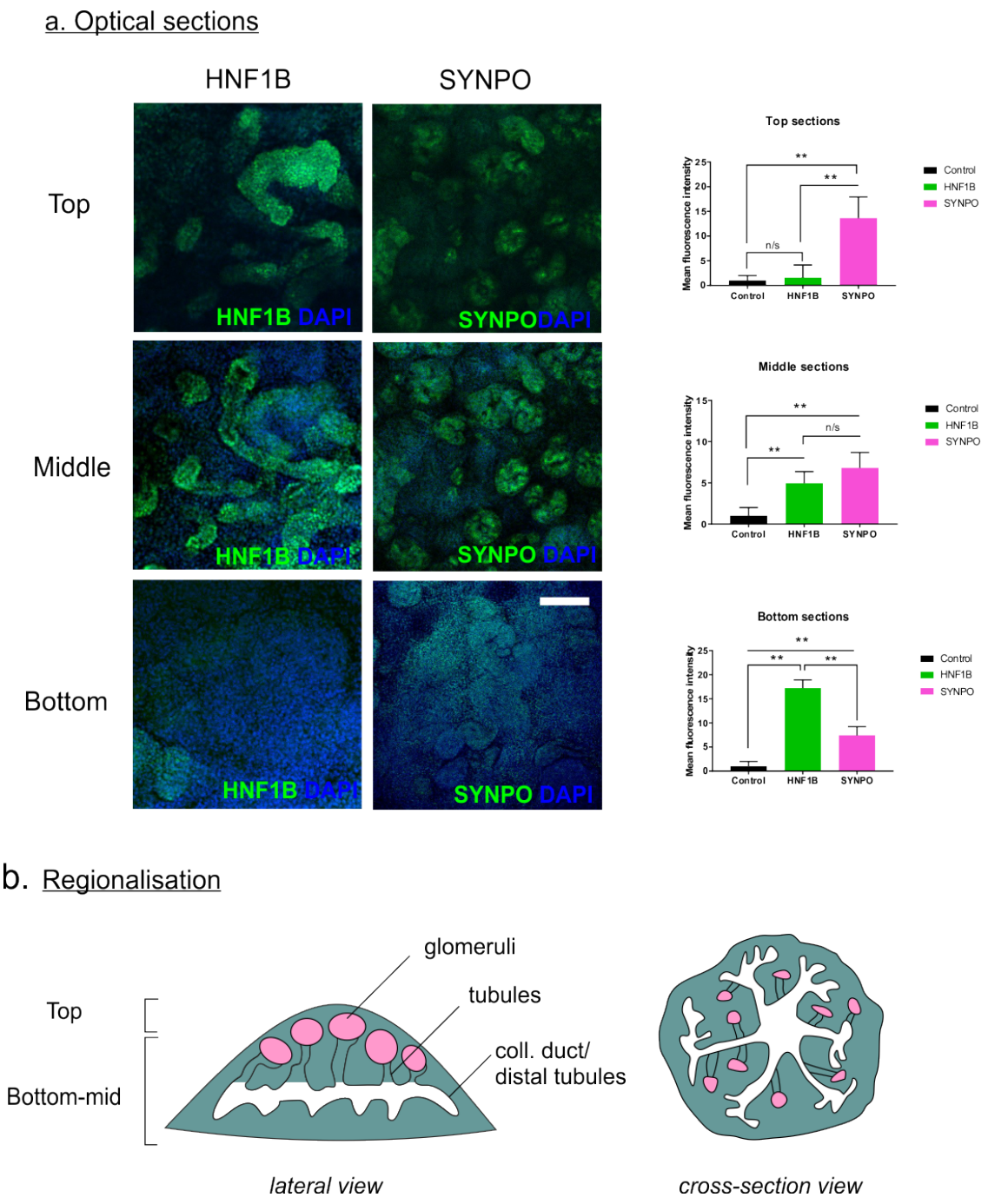

Figure 4.11 Representative image of organoids regionalisation visualised with confocal microscopy. (a) Top sections revealed abundance of SYNPO+ cells and considerable HNF1B+ tubular elements. Middle sections showed presence of nuclear-stained HNF1B+ elongated tubules. SYNPO+ cells were found to distribute sparsely throughout middle region. Bar chart on the right indicated mean fluorescence intensity for top, middle and bottom sections plotted against immunological control. Data are represented as mean±S.E.M from technical replicates (n=3 organoids). Statistical analysis was performed using one-way ANOVA, **p < 0.05, ***p < 0.001, n/s, not significant. Bottom section revealed HNF1B+ nuclear-stain but not SYNPO+ elements. (b) Schematic representation of unaffected 3D kidney organoids from cross-section and dorsal view. Scale bar, 100 μm.

4.2.6 Prolonged organoid culture indicated degeneration and apoptotic events

To investigate whether prolonging the duration of culture may improve or advance the tissue formation, I extended the culture for another week up to day 7+25 and performed RNA analysis. From the phase contrast images, it was observed that the organoids maintained an intact structure on day 7+6 with few rounded cell clusters occupying the periphery (Figure 4.12). The middle core region showed lesser developing structures at relatively smaller size. As the organoid reached day 7+18, mixed ball-like (presumptive glomeruli) and elongated structures were present. The middle areas were not clearly visible possibly due to different organoid's layer of organisation and limited magnification using light microscopy. Interestingly, day 7+25 organoids appeared to shrink, reduced in diameter and started to lose border integrity. Close up images at day 7+25 showed tubular element at reduced length while other region exhibited signs of degeneration and necrosis. Thus, to examine the extent of degeneration, I stained day 7+25 organoids with proliferation marker, Ki-67, apoptosis marker, Caspase-3 and alpha smooth muscle actin (α-SMA) to detect non-renal cell origins. In addition, quantification of diameter changes from day 7+6 to day 7+18 and 7+25 revealed 8% and 15% size reduction, respectively.

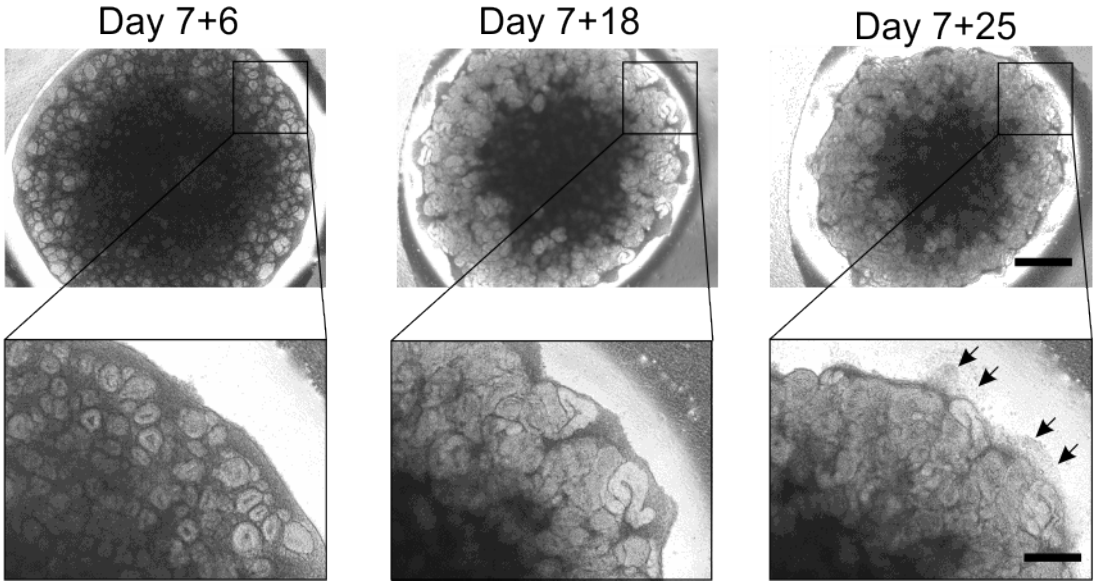

Figure 4.12 Representative organoids at various timepoints showing progressive degeneration at extended culture. (*Left column*) Day 7+6 organoids showed differentiating vesicle-like elements surrounded by rigid cell border. (*Middle column*) Organoid at day 7+18 optimally generated stretched and elongated tubules at the edges with the inner core showing rounded cell characteristics (*Right column*). Degenerating organoid at day 7+25 indicated loss of cellularity and observable necrotic debris (indicated by black arrow). Scale bars, top, 200 μm, bottom, 20 μm.

From immunohistological analysis (Figure 4.13), it was observed that day 7+25 organoids showed positive Ki-67 nuclear staining in tubular structure but present at lower degree. None of the Ki-67 staining found in the glomeruli structures (not shown). Interestingly, staining for activated caspase-3 has revealed interspersed localisation in the stromal region with low level in tubules but not glomeruli. The middle core appeared to degenerate and lose cellularity beginning day 7+18. This could be due to increased organoids size and suboptimal oxygen diffusion. Staining against α-SMA revealed a patch of smooth muscle in few areas suggesting generation of off-target cells in extended culture. To confirm degeneration of organoids at prolonged timepoint, I measure the transcript profiles for day 7+6, 7+18 and 7+25 (Figure 4.14). It was observed that glomeruli marker (NPHS1, PODXL) were minimally expressed at day 7+6, peaked at day 7+18 and continued by downregulation at day 7+25. The similar expression pattern was observed at day 7+6 and day 7+18 in HNF1B and HNF4A transcripts that marked the tubular elements. However, there were only slight downregulation approaching day 7+25. Moreover, CDH1 expression was found to be upregulated at day 7+18 but not at day 7+25 that suggested reduced epithelialisation. The failure of these organoids to sustain intact morphology appeared to have indirectly reduced expression of circulating vasculoendothelial network (CD31) in the extended period (day 7+25).

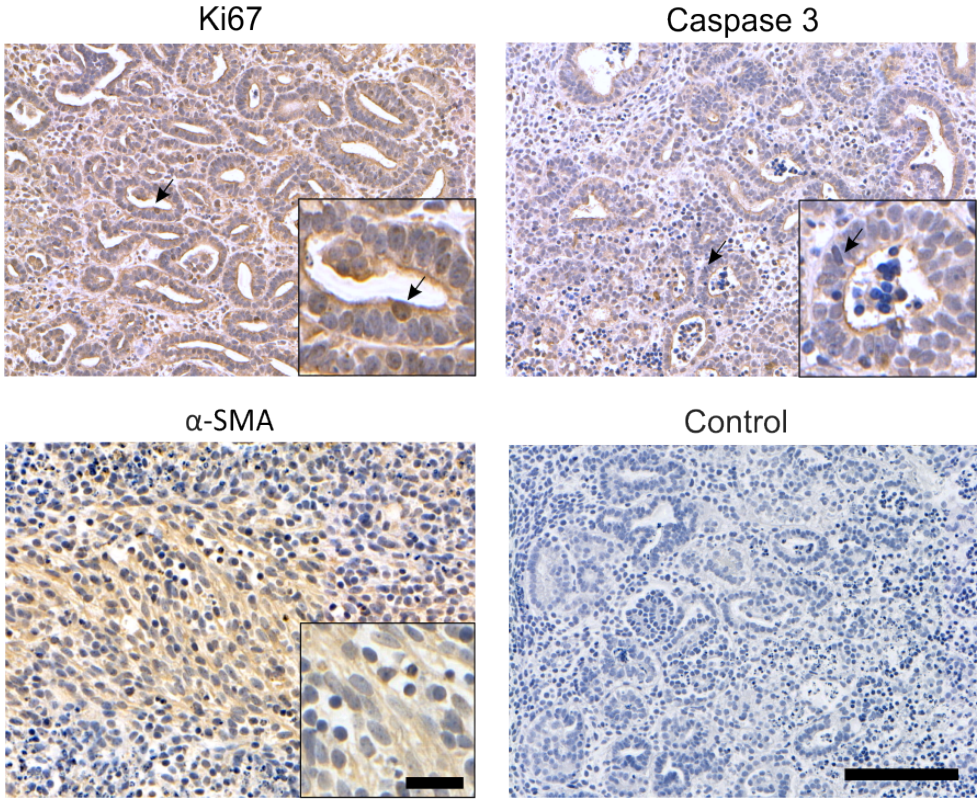

Figure 4.13 Immunohistochemical staining of organoids at day 7+25. Proliferative capacity of organoids was reduced evidenced by low level of Ki-67 staining in tubules. Apoptotic cells were detected by positive Casp-3 staining in stromal and tubule structures. Staining of smooth muscle actin (α-SMA+) suggested loss of kidney identities and progression of fibrotic lesions. Scale bar, low power, 100 μm, high power, 20 μm.

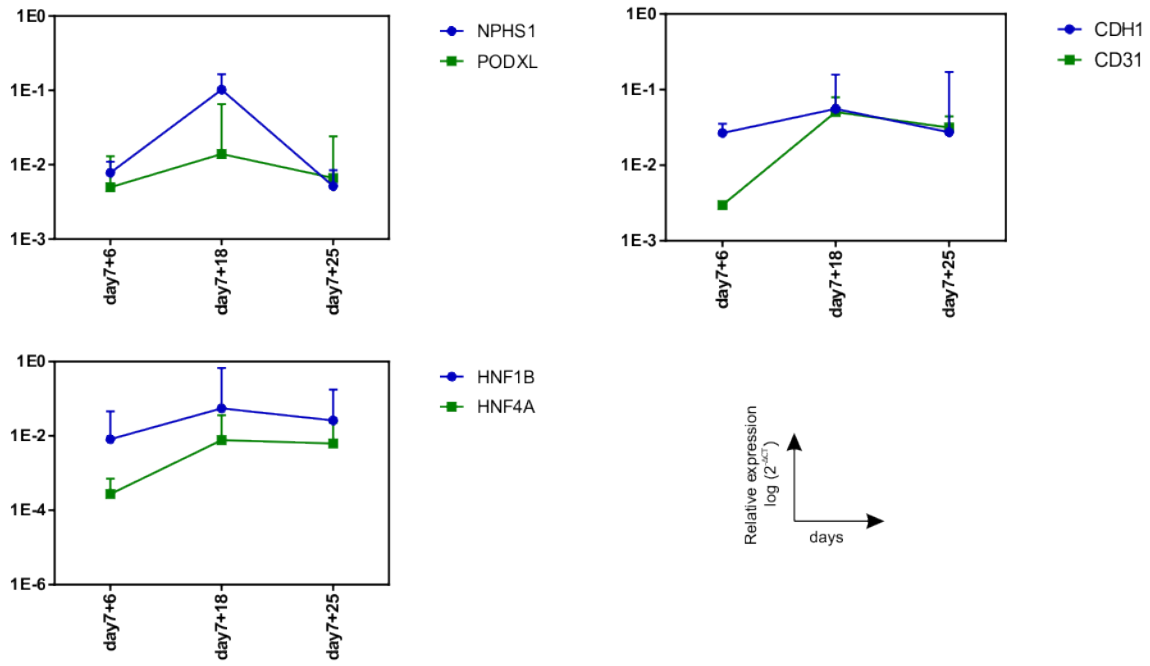

Figure 4.14 qPCR analysis during early, midterm and extended culture. Glomerular podocytes (NPHS1, PODXL) were upregulated at day 7+18 and reduced as organoids degenerated. Tubular elements (HNF1B, HNF4A) are less affected by the prolonged culture and expected to sustain tubular integrity. CDH1 minimally expressed at day 7+25 indicated reduced epithelialisation as compared to day 7+18. Expression level of CD31+ endothelial network decreased approaching day 7+25 that compromised tissue's maturation. Data are represented as mean±S.E.M from technical replicates (n=3 organoids).

4.2.7 Absence of protein-free hybridoma extract addition leads to generation of cartilage

It was noted that change in the differentiation media provided by the supplier has affected the organoids morphologies. The formulation (APEL medium) that previously contained protein-free hybridoma medium (PFHM II) has been changed to a non-PFHM containing APEL2 medium which halted reproducibility of differentiation. Histological sections on organoids cultured in the new APEL2-medium showed domination of cartilage-like structures. The exclusion of PFHM II from the main APEL2 medium at that time remained undisclosed thus complicating subsequent differentiations. After disclosure regarding the excluded supplement (PFHM II), I obtained the supplement from a separate supplier. However, the exact concentration to use in kidney differentiation required optimisations.

To address this issue, I determined the optimal concentration of PFHM II by varying its concentration in a dose-dependent manner (0,1,3.5 and 5%). Organoids were differentiated up to day 7+18, sectioned and stained. From the Alcian blue staining, it was obvious that APEL2 differentiation medium without addition of PFHM II (0%) generated cartilage-like tissue (Figure 4.15) in approximately ~80% of the total area of organoids. Addition of 1% PFHM II however tremendously reduced the cartilage formation with few smaller structures positive for Alcian blue. These smaller cartilage cells however restricted to the periphery. Interestingly, when 3% PFHM II was added,

the resulting organoids at day 7+18 were free from any cartilage-like elements with normal glomeruli and tubular cell types. However, increasing PFHM II concentration to 5% resulted in a shift of tubules and glomeruli populations towards the centre leaving peripheral region with presumptive stromal cells. free from any kidney cells. Thus, from this experiment, it can be concluded that a PFHM II concentration of 2-3.5% would be the best concentration for kidney organoids formation. In the next section, I decided to supplement this newly formulated APEL2 differentiation medium with 2% PFHM II and this was used in the all subsequent differentiation unless otherwise mentioned.

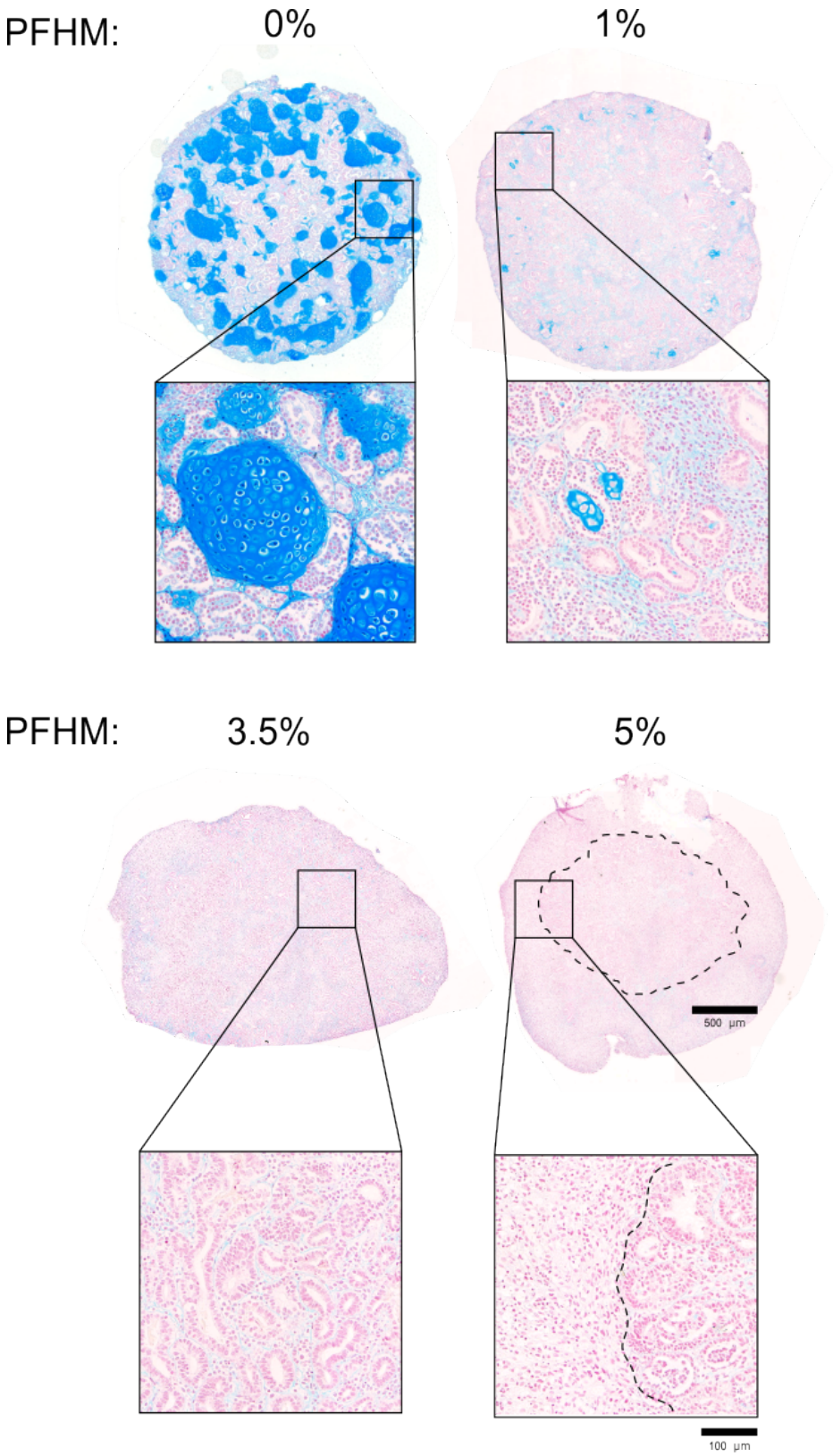

Figure 4.15 Optimisation of kidney differentiation protocol by varying PFHM II concentration. Without any addition of PFHM II media (0%), cartilage-like structures emerged and occupied organoid's surface. Organoid supplemented with 1% PFHM reduced most of cartilaginous tissues with some cells remained at border surrounding organoids. Addition of 3.5% PFHM completely removed formation of cartilage-like structures while preserving tubules and glomerular structures. 5% PFHM could not sustain a well-formed organoid although successfully abolished cartilage cells. Blue staining indicated Alcian blue stain for sulphated GAGs.

4.2.8 *HNF1B*-derived kidney organoids are double the size of unaffected healthy controls

The previous section has described 3D kidney organoid's development, regionalisation and proportion of differentiating structures using hESC-derived MAN13 lines. In order to determine whether iPSC-derived kidney organoids could be able to replicate these conditions, as well as in the lines that harbour HNF1B mutation, I derived 2 mutant (TF171 and TF172) lines and an unaffected (TF173, parental control) line. These iPSCs together with SW162,an unrelated control line donated by Steven Woods (Kimber Lab) were differentiated to 3D kidney organoids. Experiments were conducted in parallel, involved pairing of one mutant and one unaffected line, respectively (TF172/TF173 and TF171/SW162). The phenotypic differences were evaluated based on immunostaining and transcript profiles. From Figure 4.16, it was observed that commencing day 0 of differentiation, all 4 lines displayed comparable stem cell colony morphologies with defined borders. Any colony that showed signs of spontaneous differentiation before the beginning of the protocol were excluded from subsequent differentiation. Prior to seeding, colonies that reached 70-80% confluency were dissociated into single cell and sparsely plated. At day 1, these individual cells appeared to form cluster with neighbouring cells. Interestingly, during day 3 of CHIR exposure, these clusters of cells became elongated and again dissociated into individual cells. When these cells were treated with FGF9/heparin on day 5 onwards, the cells began to form a confluent monolayers and were harvested at day 7 for pellet formation.

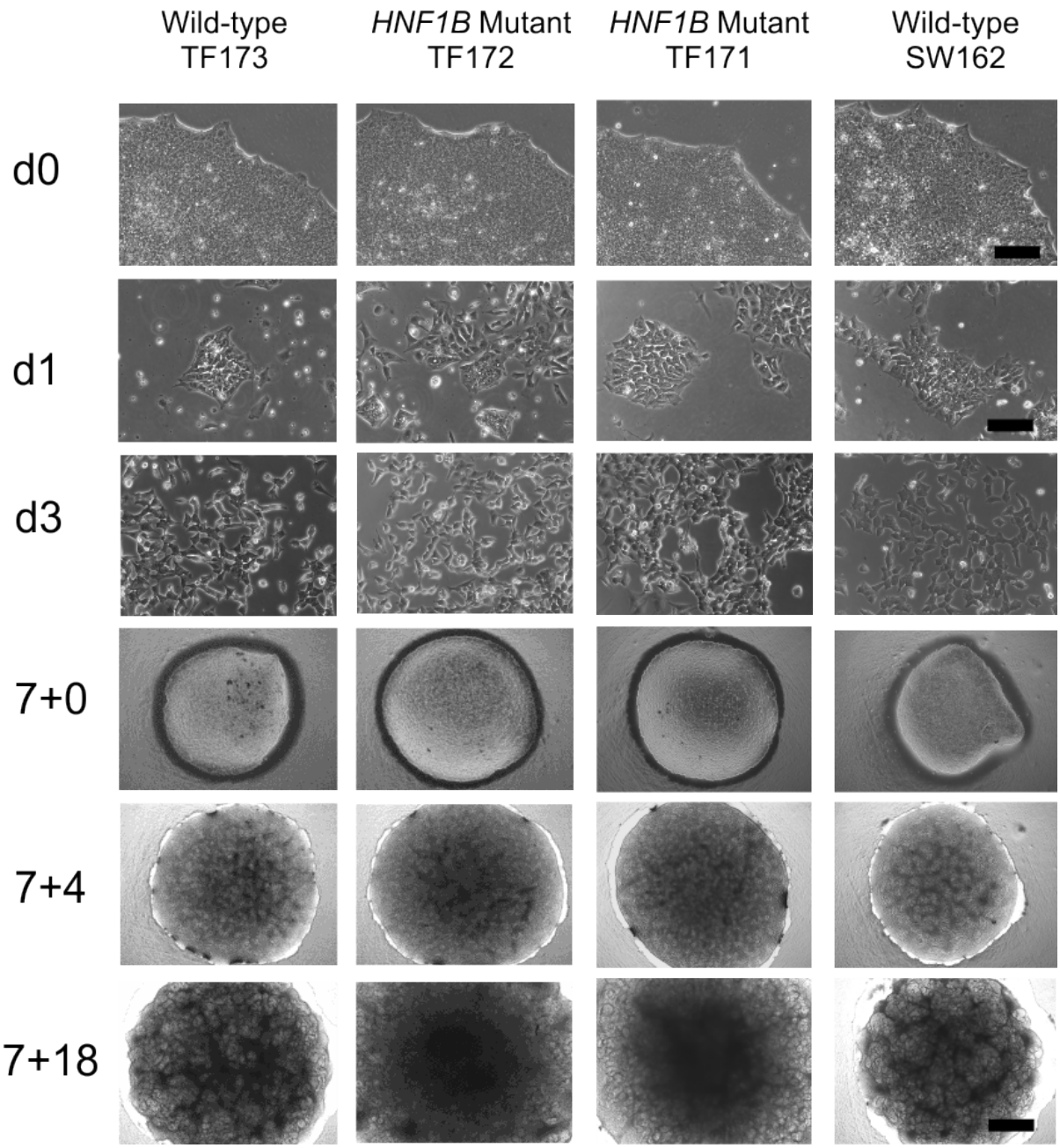

Figure 4.16 Phase contrast images of differentiating kidney organoids for four different lines. Directed differentiation of 3D kidney organoids involved 2 culture phases. The first 7 days involved standard adhesion culture (2D monolayer) followed by additional 18 days on transmembrane that were cultured at air-media interphase. The two middle columns (TF171 and TF172 mutants) showed increased in total organoid's size observed at day 7+18. Scale bar, day 0, 100 µm, day 1, 50 µm, day 7+10 to 7+25, 500 µm.

A total of 200,000 cells were harvested together and pelleted on transwell at an air-media interface. At day 7+0, these organoids showed no morphological differences either unaffected or mutant-derived. However, organoids at day 7+4 revealed slight differences in organoids diameter. It was found that both mutant lines (TF171 and TF172) generated increased organoid's size in comparison with the healthy lines (TF173 and SW162) probably due to increased individual cell size (hypertrophic) which remained to be investigated. Yet, there were no differences observed within

mutant lines. At day 7+18 of differentiation, remarkable phenotypic differences were detected between these groups. The mutant lines showed formation of structures at the edges with a hollow middle region. Conversely, unaffected organoids revealed visible formation of intact structures both at the periphery and middle area although the total diameter appeared smaller than the mutant organoids. The same morphology was observed in previously described MAN13-derived organoids. The expanded images of each organoid (Figure 4.17) showed formation of elongated tubular elements in both unaffected organoids. In contrast, a lower degree of tubule formation were observed in the mutants with a gap between the edges and the tubule containing region.

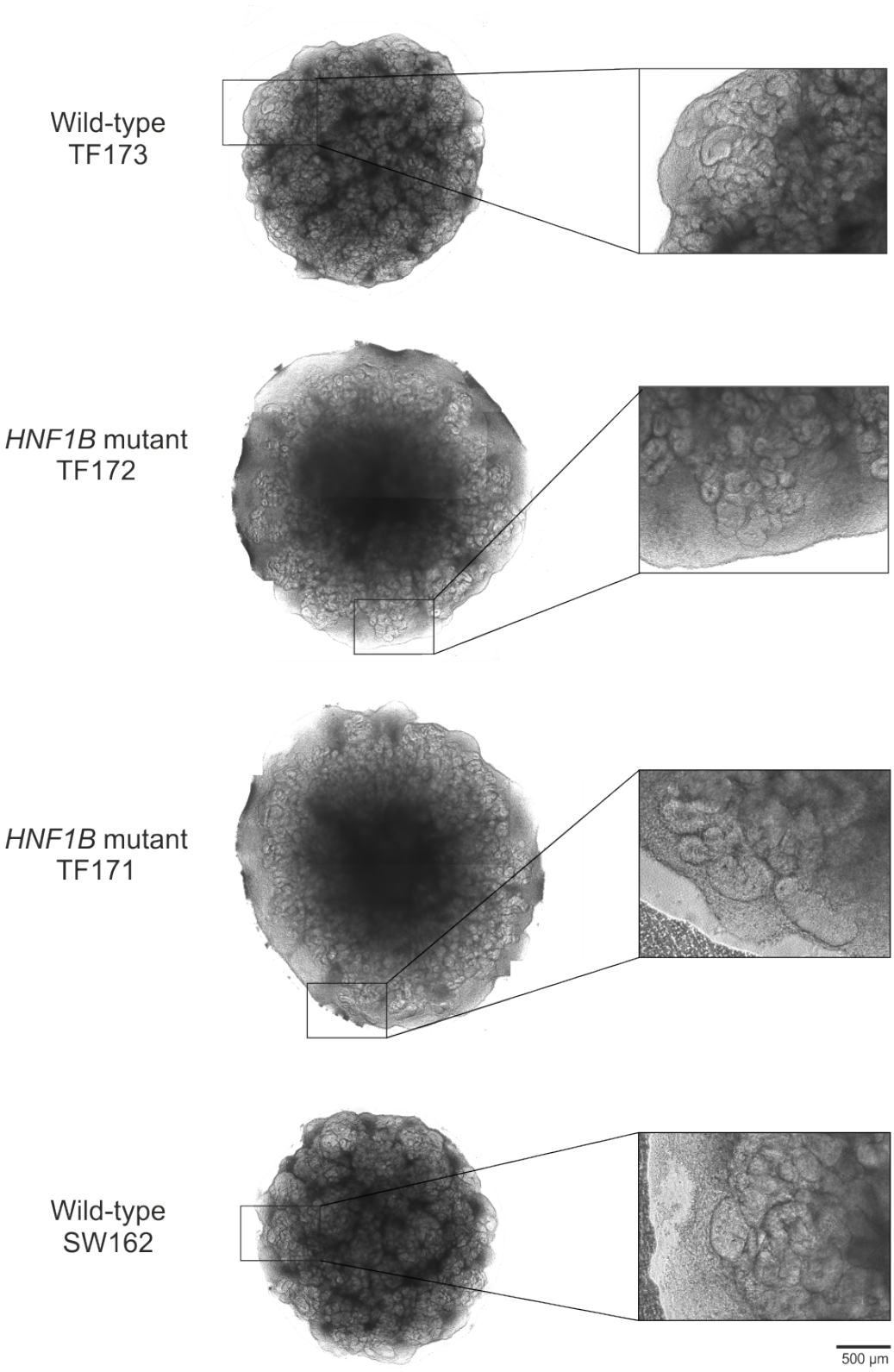

Figure 4.17 Expanded phase contrast images of kidney organoids at day 7+18. Unaffected organoids (TF173 and SW162) showed relatively smaller diameter but comprised of more visible structures whereas mutant organoids showed a shift from peripheral cell population towards the centre although exhibited approximately 2-fold diameter expansion. Scale bar, 500 µm.

4.2.9 *HNF1B*-derived mutant organoids generated fewer tubular elements at day 7+18

To further investigate tubulogenesis in each organoid, I quantified the amount of tubule/CD elements by staining the wholemount organoids with HNF1B and CDH1 markers. From Figure 4.18, it was found that both mutant organoids (TF171 and TF172) were minimally stained with HNF1B and this correlated with shorter tubule length and minimum degree of tubule extension or lumen expansion. However, unaffected organoids (TF173 and SW162) were found to occupy the organoid's edges, filled with elongated tubules and ball-like structures presumptive of glomeruli. Staining for epithelial marker, CDH1 revealed co-localisation at different intensities in both mutant and unaffected organoids.

To determine the abundance of HNF1B+ and CDH1+ cells, I measured the mean fluorescence intensity for each organoid. Although quantifying the number of fluorescent cells is desirable this is however not been performed due to limited number of stained organoids, fixation and photo bleaching issues. It was found that the unaffected organoids stained larger proportion of tubular elements marked by HNF1B and reported higher fluorescence intensity as compared to mutant. This is consistent with previously described MAN13-derived unaffected organoid culture. Distal/CD epithelial structures marked by CDH1 however showed variation in staining intensities between lines. It was evident that SW162 (healthy) lines were highly stained with CDH1+ clusters with longer tubules elements whereas TF173 (healthy) and TF172 (mutant) revealed comparable CDH1+ intensities. CDH1+ structures in TF172 tend to sparsely distribute across the organoid's surface with smaller developing tubules but CDH1+ cells in TF173 are restricted to the peripheral region. TF171-derived mutant tubules however indicated minimal generation of epithelial cells.

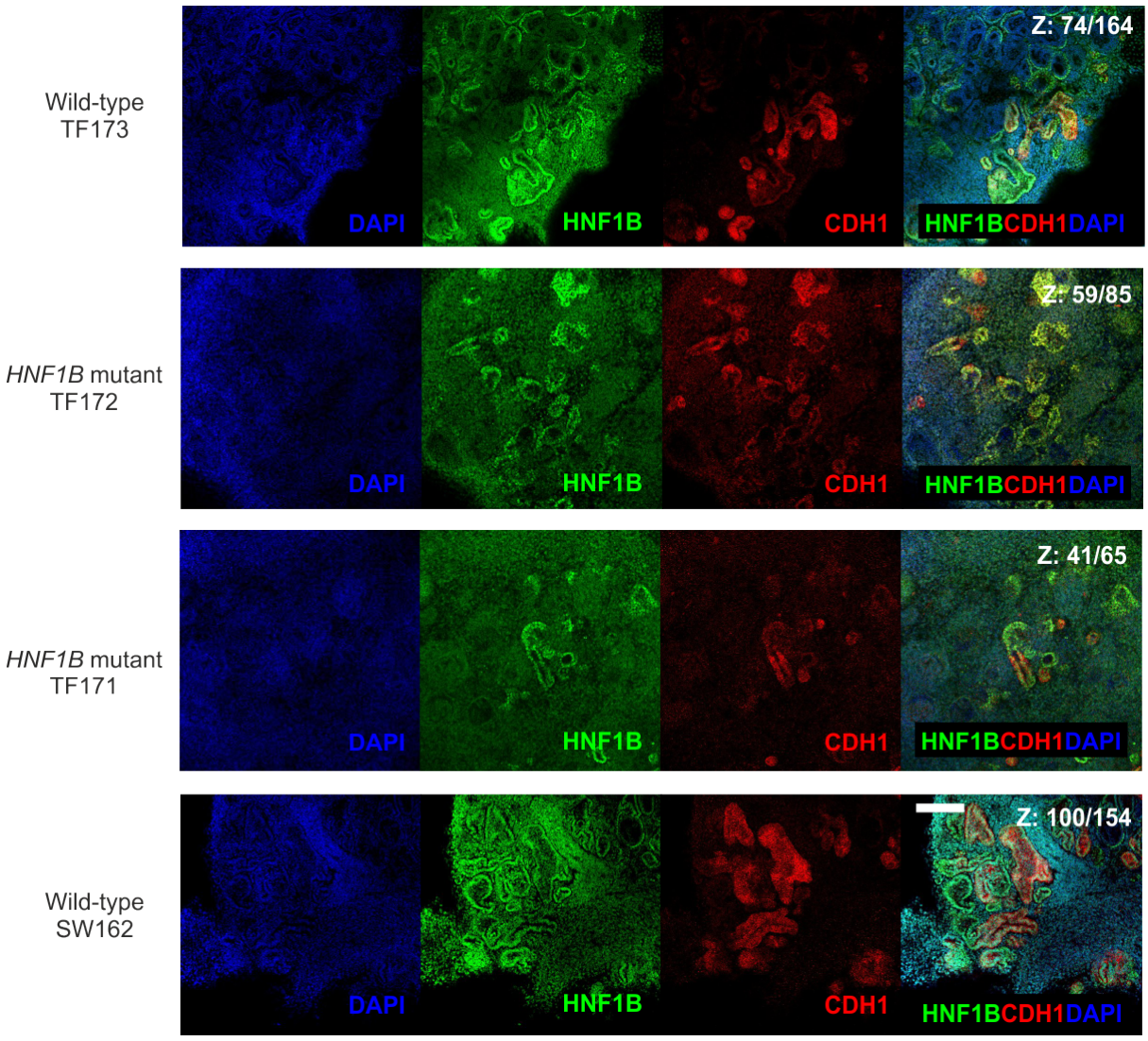

Figure 4.18 Immunofluorescence stainings of four whole mount organoids at middle region. Organoids at day 7+18 displayed variable density and distribution of nephron segments. Mutant organoids (TF172, TF171) showed lesser number of differentiating tubular structures (HNF1B, in green) and reduced epithelialisations (CDH1, in red). Number in white on merged images indicated optical section of each section plane of z-stack. Images were captured using Leica SP8 inverted microscope. Scale bar, 20 μm.

It was noted that both mutant and unaffected organoids were visualised at the middle region through the whole mount organoids (optical sections). In most of the cases, the mutant organoids were found to be flatter and almost half of unaffected organoid's thickness (Figure 4.19). This has led to the assumption that these mutant organoids failed to self-organise or generate complex morphogenesis thus turning them into flatter cellular structures which contributed to a larger diameter. However, this confocal imaging data were restricted to middle sections and is insufficient to draw any conclusion regarding distribution of each structure. Thus, to determine whether the structure able to be distributed and regionalised to specific region as the organoid developed, I hypothesised that these organoids can generate different amount of tubular and glomerular elements that can regionalise at different

distribution throughout the organoids. Towards achieving this aim, I selected bottom, middle and top organoids section and quantified proportions of nephron segments at day 7+18 which will be discussed in the next section.

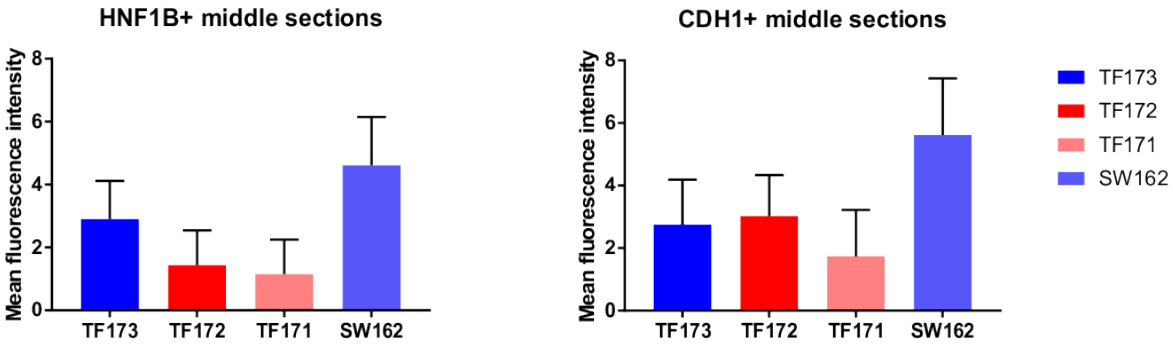

Figure 4.19 Mean fluorescence intensity of tubular and epithelial elements. (*Left*) Middle sections revealed highest intensity of HNF1B+ structures in SW162 followed by TF173, TF172 and TF171. (*Right*) CDH1+ epithelial cells remained highest in SW162 and approximately half in TF172, TF173 and TF171. Mutant organoids (TF171 and TF172) indicated reduced kidney components in all runs. Data are represented as mean±S.E.M from technical replicates (n=3 organoids).

4.2.10 *HNF1B*-derived mutant organoids can regionalise across differentiation but display disorganised structural distribution

To investigate whether each organoid can self-organise and position cell types at specific location, I collected day 7+18 organoids and sequentially sectioned from bottom to top. These organoids were then histologically stained with HNF1B, SYNPO and CDH1 marker to demonstrate tubular, glomerular and epithelial identities, respectively. When these 4 different organoids were stained for HNF1B in the middle region (Figure 4.20), it was found that the TF173 organoids showed uniform distribution of tubular elements that radiate from the centre to the edges. The similar pattern was also observed in TF172 and TF171 mutant organoids but at greater amount due to larger surface area. SW162 organoids revealed brighter HNF1B staining that distributed evenly across middle sections. Interestingly, staining for SYNPO (Figure 4.21) showed distribution of 'ring-like' bright staining that accommodated the edges of unaffected organoids (TF173 and SW162) with lesser SYNPO+ cells in SW162 organoids.

In contrast, mutant organoids (TF171 and TF172) revealed disorganised SYNPO+ distribution across middle sections with few clusters exhibited higher proportions than the other. Figure 4.22 showed CDH1 staining of the middle sections that displayed intense brown staining in both TF171 and TF172 mutant organoids with elongated structures mostly occupied organoid's edges. TF173 unaffected organoids however showed minimal CDH1 across the whole section whereas SW162 displayed similar distribution but at greater intensities. From the morphometric quantifications (Figure

4.23), it was noted that the bottom sections were positively stained for HNF1B and CDH1 in both lines (TF172 and TF173) with greater percentage of positive staining in mutant organoids. This higher proportions in mutant could be due to accumulation of tubular and distal components at the bottom section that failed to vertically organised. This is evident when mutant organoids revealed a reduced positive staining in respective middle and top sections. SYNPO+ cells however were minimally stained in both lines (TF172 and TF173) in these bottom regions. No bottom sections were measured for TF171 and SW162 organoids due to time limitations.

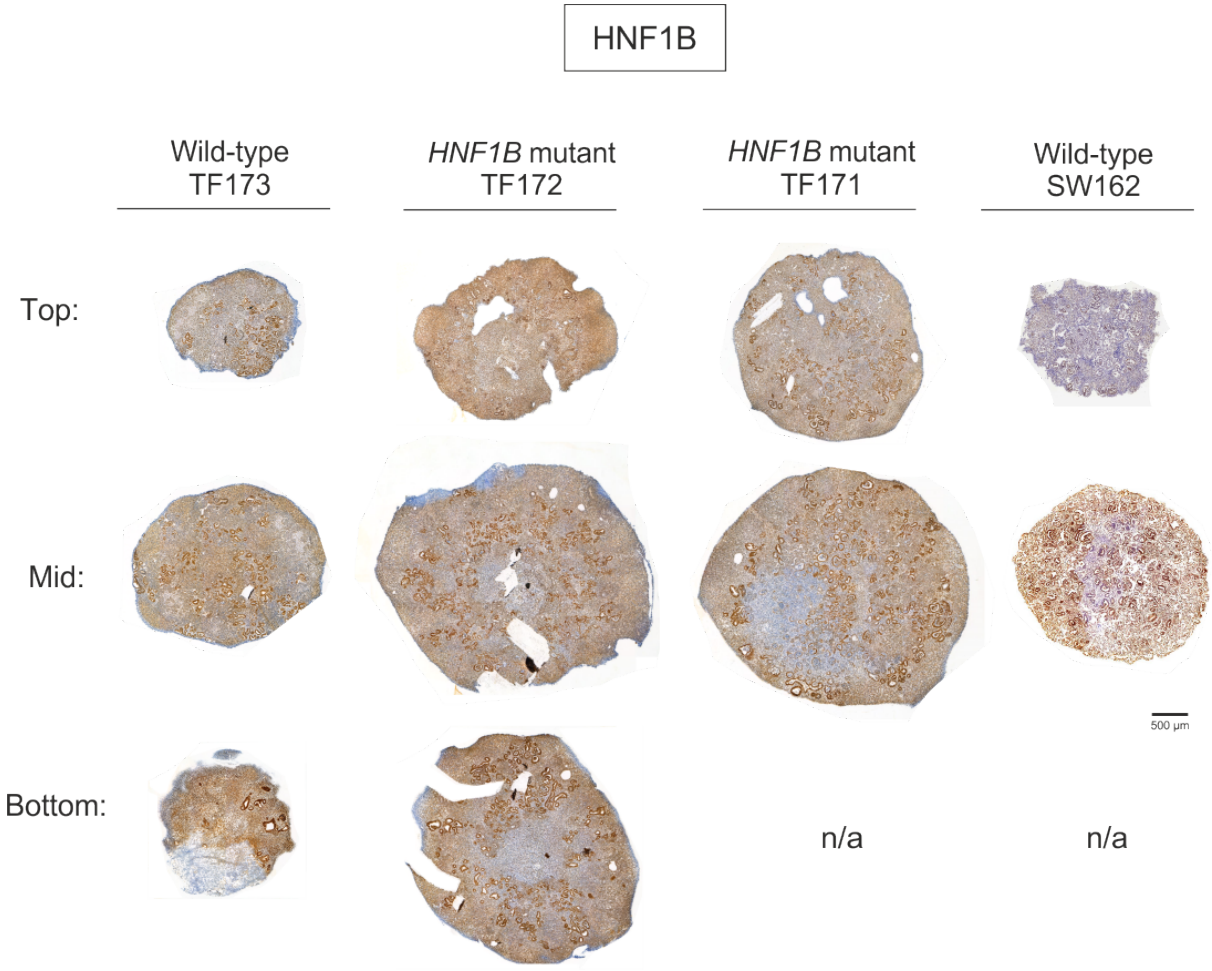

Figure 4.20 Representative of histological sections at day 7+18 stained with HNF1B marker at top, middle and bottom regions of hiPSC-derived kidney organoids. Mutant organoids (TF171 and TF172) show morphological alterations with greater surface area and diameter as compared to unaffected organoids (TF173 and SW162). HNF1B staining of top sections was positive in TF173: 25%, TF172: 12%, TF171: 15% and SW162: 35%. HNF1B at middle regions positively stained in TF173: 15%, TF172: 12%, TF171: 15% and SW162: 15%. Bottom region showed positive HNF1B staining in TF173: 4% and TF172: 13%. No staining of bottom sections performed on TF171 and SW162 due to time constraints. Organoids were counterstained with hematoxylin. Scale bar, 500 µm.

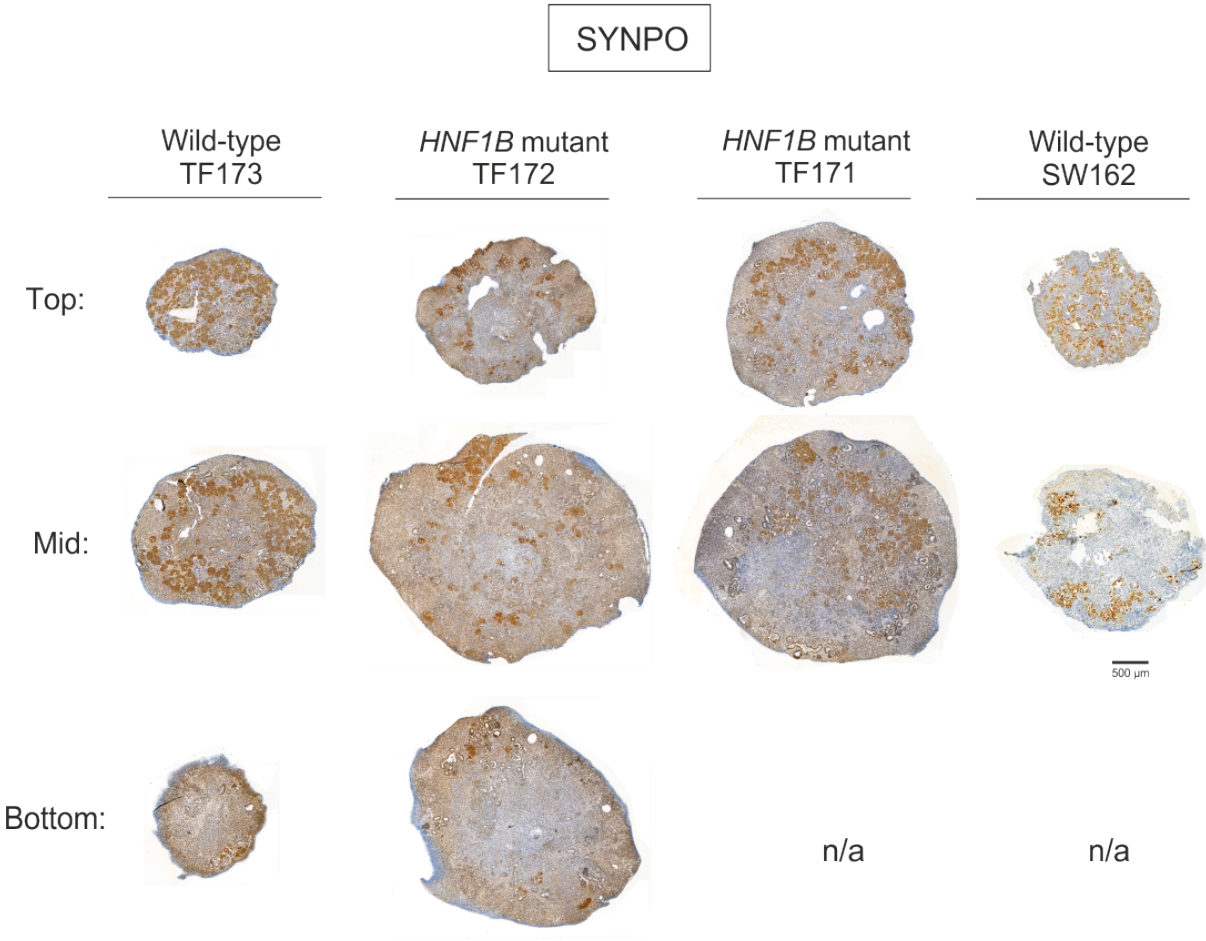

Figure 4.21 Representative of histological sections of day 7+18 stained with SYNPO marker at top, middle and bottom regions of hiPSC-derived kidney organoids. Mutant organoids (TF171 and TF172) implicated in morphological alterations with greater surface area and diameter as compared to unaffected organoids (TF173 and SW162). SYNPO staining of top sections were found positive in TF173: 45%, TF172: 13%, TF171: 20% and SW162: 40%. SYNPO at middle regions positively stained in TF173: 17%, TF172: 7%, TF171: 12% and SW162: 21%. Bottom region showed positive SYNPO staining in TF173: 2.7% and TF172: 5%. No staining of bottom sections performed on TF171 and SW162 due to time constraint. Organoids were counterstained with hematoxylin. Scale bar, 500 µm.

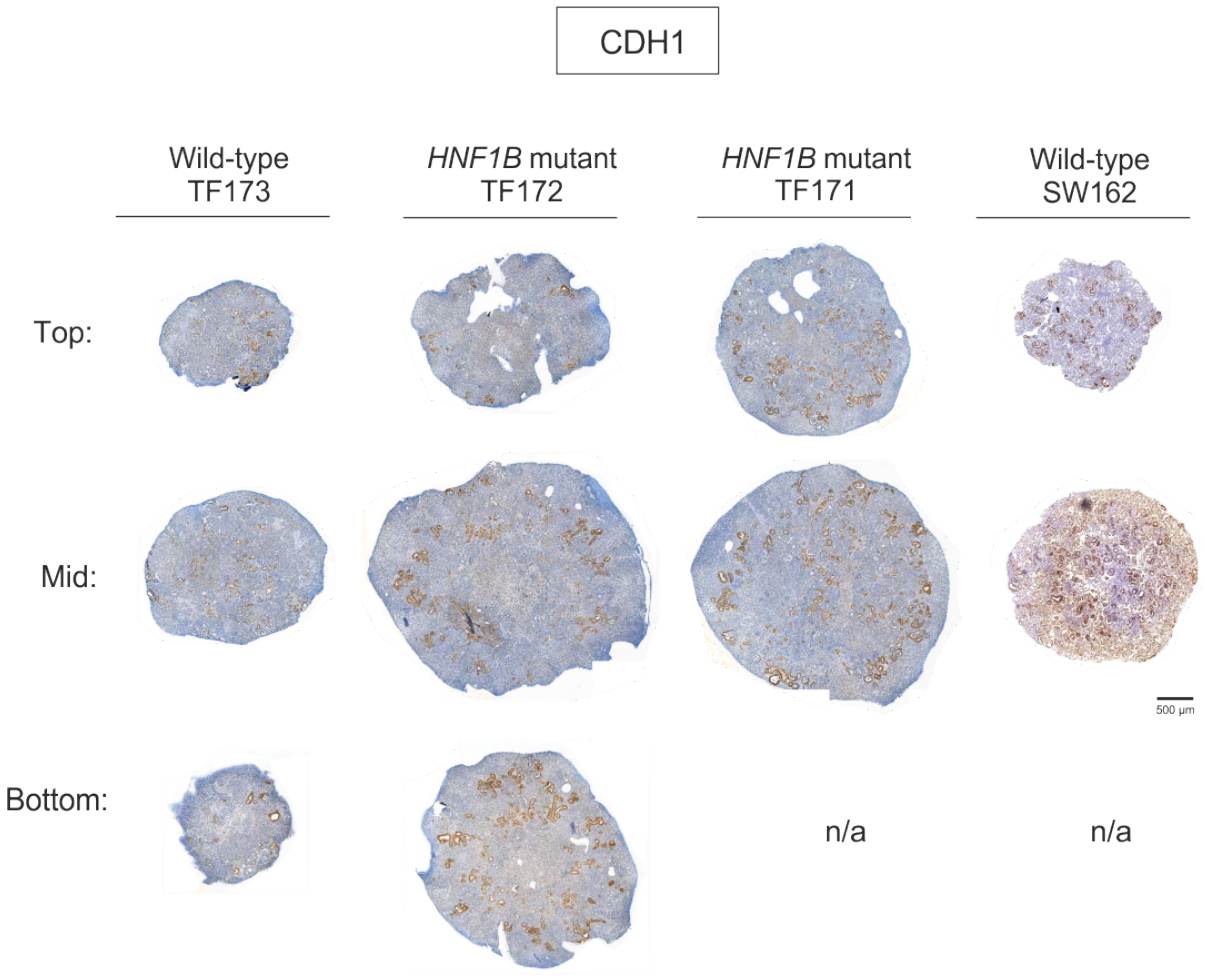

Figure 4.22 Representative of histological sections of day 7+18 stained with CDH1 marker at top, middle and bottom regions of hiPSC-derived kidney organoids. Mutant organoids (TF171 and TF172) implicated in morphological alterations with greater surface area and diameter as compared to unaffected organoids (TF173 and SW162). CDH1 staining of top sections were found positive in TF173: 18%, TF172: 10%, TF171: 12% and SW162: 32%. CDH1 at middle regions positively stained in TF173: 12%, TF172: 11%, TF171: 15% and SW162: 18%. Bottom region showed positive CDH1 staining in TF173: 3% and TF172: 15%. No staining of bottom sections performed on TF171 and SW162 due to time constraint. Organoids were counterstained with hematoxylin. Scale bar, 500 µm.

Staining of top sections exhibited higher percentage of HNF1B staining in the unaffected organoids when compared to both mutant organoids. However, the staining was not entirely restricted to any particular area in all of the organoids. Interestingly, unlike SYNPO staining of the middle, the top SYNPO section of unaffected organoids (TF173 and SW162) exhibited evenly distributed glomerular podocytes. In contrast, these SYNPO+ cells were not found to invade the central region in mutant organoids (TF171 and TF172) and were present at various location throughout with lower total percentage of SYNPO+ cells per organoid. Staining of CDH1 in the top regions varied from TF172 that showed the lowest amount to SW162 with greatest CDH1 staining. Interestingly, TF173 and TF171 organoids showed almost similar CDH1 staining distributions.

Morphometric assessments of each organoid's diameter revealed hypertrophic conditions in mutant organoids (TF171 and TF171) but not in the unaffected (Figure 4.23). Diameter of mutant organoids ranged from 3-4 mm and appeared to be approximately twice larger than the unaffected (TF173 and SW162). It was observed that the bottom sections of TF172 organoids comprised higher proportions of HNF1B, SYNPO and CDH1 stained structures per organoid with 13%, 5% and 15%, respectively. TF173 organoids showed lower percentage of differentiating structures with 4% HNF1B, 2.7% SYNPO and 3% CDH1 cells. Interestingly, top sections showed remarkable amount of SYNPO+ cells in both TF173 and SW162 unaffected organoids (45% and 40%, respectively) as compared to mutant (13% in TF172 and 20% in TF171). Moreover, HNF1B+ and SYNPO+ cells were reported to be higher in the unaffected organoids. In all top section staining, TF172 organoids indicated lowest percentage of positively stained elements among other structure-containing organoids.

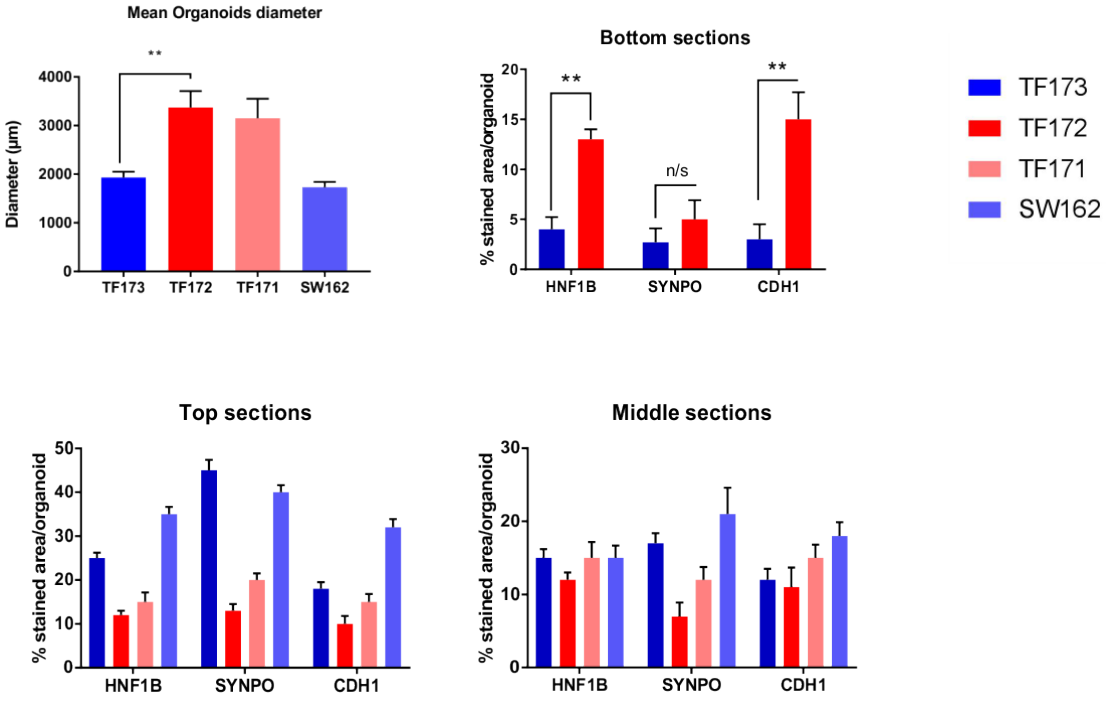

Figure 4.23 Morphometric assessments of organoids for top, middle and bottom sections of differentiated organoids at day 7+18 in hiPSC lines. The sections were stained for HNF1B, SYNPO and CDH1 as an indicator of kidney structure formation. Diameter of organoids revealed significant differences between unaffected (TF173, SW162) and mutant organoids (TF171, TF172). Top and middle sections of all hiPSCs were stained with all markers except bottom sections that are limited to TF173 and TF172 organoids. Data are represented as mean±S.E.M from technical replicates (n=3 organoids). Statistical analysis was performed using one-way ANOVA, **p < 0.05, ***p < 0.001, n/s, not significant.

Staining of the middle sections revealed comparable percentage of HNF1B staining for TF173, TF171 and SW162 with minimal amount in TF172 organoids. Interestingly, SYNPO+ cells in unaffected organoids (17% in TF173, 21% in SW162) were found to approximately double the number of differentiating glomeruli as compared to mutant (7% TF172 and 12% TF171). These staining and morphometric analysis have directed towards visualisation of each structure at higher magnification in order to detect any signs of abnormalities and to correlate with the change in total organoid's diameter. To achieve this, I documented morphological changes of tubules and glomeruli stained with HNF1B, SYNPO and CDH1 and compare between organoids, regardless mutant or unaffected organoids which will be discussed in the next section.

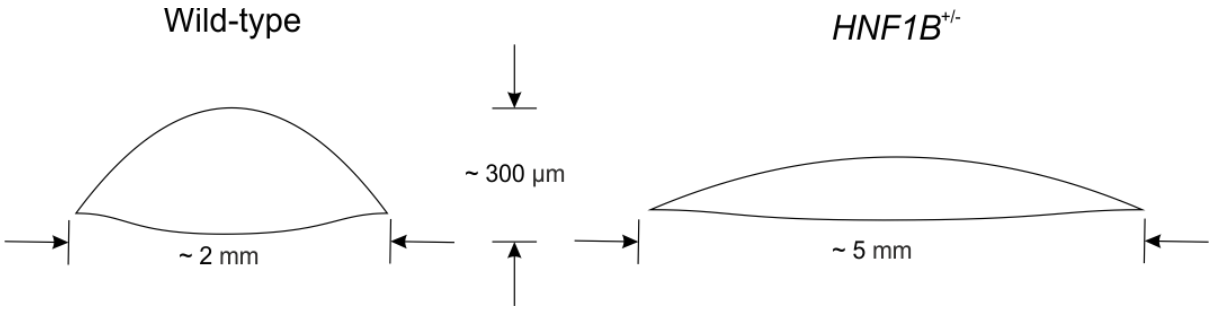

Figure 4.24 Schematic diagram showing morphological differences between mutant and unaffected organoids. The mutant approximately exhibited 2-fold diameter increase but appeared flatter and reduced structural thickness as compared to unaffected controls that displayed vertical growth expansion at smaller diameter.

4.2.11 *HNF1B* mutant organoids generated dysmorphic glomeruli and multi-layered tubules

To further evaluate the morphological differences, I examined each organoid stained for tubules and glomeruli marker and compare the phenotypes at day 7+18. Figure 4.24 showed that there were obvious differences in structures generated between mutant and unaffected organoids. When stained for HNF1B, all 4 organoids (TF173, TF172, TF171 and SW162) showed distinct and bright nuclear HNF1B staining. However, both mutant organoids (TF171 and TF172) revealed dilated, multi-layered, thicker tubules organisations and larger lumen size. Unaffected organoids (both TF173 and SW162) revealed single-layer, stretched and elongated tubules.

Interestingly, when these organoids were stained for glomerular podocyte marker, SYNPO, the mutant organoids exhibited dysmorphic glomeruli structures and only few small elements were stained positive. TF172 mutant organoids showed the presence of small immature glomeruli at the tip of tubules whereas TF171 glomeruli were enclosed in a capsule but failed to form complete glomeruli morphology. The TF173 organoids however showed increased and compact podocyte staining that

occupied Bowman's capsule. However, SW162 organoids revealed fewer and less compact podocytes with visible empty area within capsule. Notably, the SYNPO+ cells appeared smaller in size as compared to TF173 podocytes.

Unlike the unaffected, mutant organoids generally showed greater CDH1+ cells stained on the tubule surfaces. The TF172 organoids exhibited a large empty lumen but the TF171 lumen comprised of irregular structures. Yet, the unaffected organoids revealed lesser percentage CDH1+ cells on tubular cells. Furthermore, the diameter of each epithelial tubule appeared to be smaller than mutant organoids. To summarise, although the staining of CDH1+ cells appeared to be less abundant at higher magnifications, the total percentage of CDH1+ populations in unaffected organoids were greater than mutant with respect to the ratio of developing epithelial elements per organoid (Figure 4.23).

Based on these histological sections, it can be concluded that there was apparent variation between phenotypes of each organoid from different lines in term of complete glomeruli structure, diameter and length of tubules, size of lumen and tissue organisation. Whether these phenotypic changes are regarded as the main cause to the increased in organoid diameter however remained to be elucidated. To summarise, based on the generation of abnormal dysmorphic glomeruli and multi-layered tubular elements in mutant organoids, I hypothesise that there could be a slight delay in nephron specification and *HNF1B* mutation could be the cause leading to abnormal regulation of tubulogenesis. To address this, I monitored the expression of kidney developmental genes and HNF1B downstream targets by documenting transcript profiles at various stages through the differentiation which will be discussed in the next section. Figure 4.25 illustrated the morphological disparities between mutant and unaffected controls.

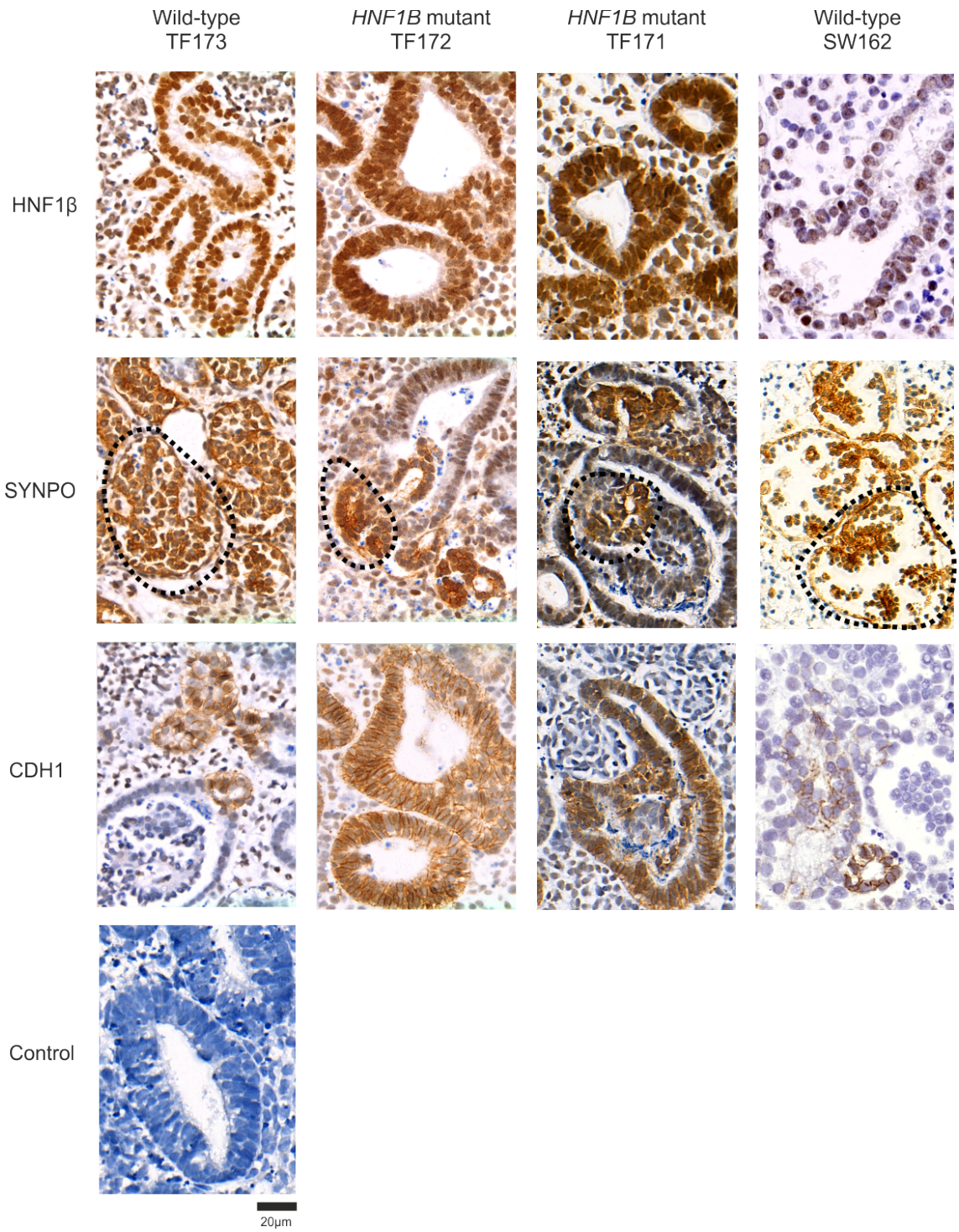

Figure 4.25 Phenotypic differences between mutant and unaffected organoids at day 7+18. Sections were obtained from all hiPSC-derived organoids (TF173, TF172, TF171, SW162) and were stained for HNF1B, SYNPO and CDH1 antibodies. Immunohistological staining displayed structures at high magnifications that indicated morphological changes in mutant versus unaffected organoids. HNF1B staining of both mutant organoids exhibited multilayer tubular components but normal single layer characteristics were observed in unaffected controls. Staining for SYNPO has revealed dysmorphic glomeruli in mutants with relatively fewer podocyte that co-existed within tubule-like entities. Glomeruli in TF173 were highly compacted with podocytes whereas SW162 exhibited lower number of differentiating podocytes within Bowman's capsule. Unlike the unaffected, mutant organoids showed greater CDH1+ cells stained on the tubule surfaces. TF172 organoids displayed large empty lumen but the TF171 comprised of lumen with irregular structures. TF173 and SW162 unaffected organoids revealed lesser CDH1+ cells surrounded the outer surface of tubule cells. Sections were counterstained with hematoxylin. Dotted lines in SYNPO stainings indicated glomeruli structures. Scale bar, 20 μm.

4.2.12 Transcript profiles of differentiating *HNF1B* mutant kidney organoids revealed delays in glomerular podocyte formation and disturbed normal tubulogenesis

Transcript profiles were executed on 4 hPSC-derived organoids for various timepoints across differentiation. I performed qPCR from organoids harvested at both monolayer and 3D phases of differentiation that includes day 1, 5, 7, 7+3, 7+6, 7+11, 7+13 and 7+18. From Figure 4.26, it was found that all lines transiently upregulated T (Brachyury) between day 1 to day 5 of monolayer culture and began to decreased thereafter. This is consistent with the early expression of T in the embryonic kidneys that suggests primitive streak identity. Similarly, OSR1 were found to increase up to day 5 in all lines except TF172 in which it was downregulated. These increments reached plateau towards the end of the culture. Moreover, PAX2 expression followed the similar trend as for OSR1 but at lower level with downregulation observed at day 7 but increased again at day 7+3 before reaching a plateau.

Podocyte marker, WT1 was found to be upregulated from the beginning of differentiation towards the end. Induced mesenchymes that were marked by SIX2 were found to peak at day 7 in unaffected controls but not in both TF171 and TF172 mutant lines. CUBN, that marked the proximal tubules were highly upregulated in both mutant lines at day 5 with reduced expression level in unaffected controls. These unaffected showed a sustained and increasing trend up to day 7+18. CUBN in mutant lines however were found to peak up to day 7+11 and constantly expressed towards the end. LRP2 or megalin expressions were only found in the 3D phases without detectable expressions in the monolayer culture. It was observed that all 4 hPSC lines upregulated LRP2 up to day 7+11. However, both mutant lines revealed a massive LRP2 reduction at day 7+13 that continued to rise on day 7+18. The unaffected controls showed lower expression level but at an increasing pattern throughout differentiation. Interestingly, HNF4A, a proximal tubule marker showed no differences in expression level of all differentiating lines.

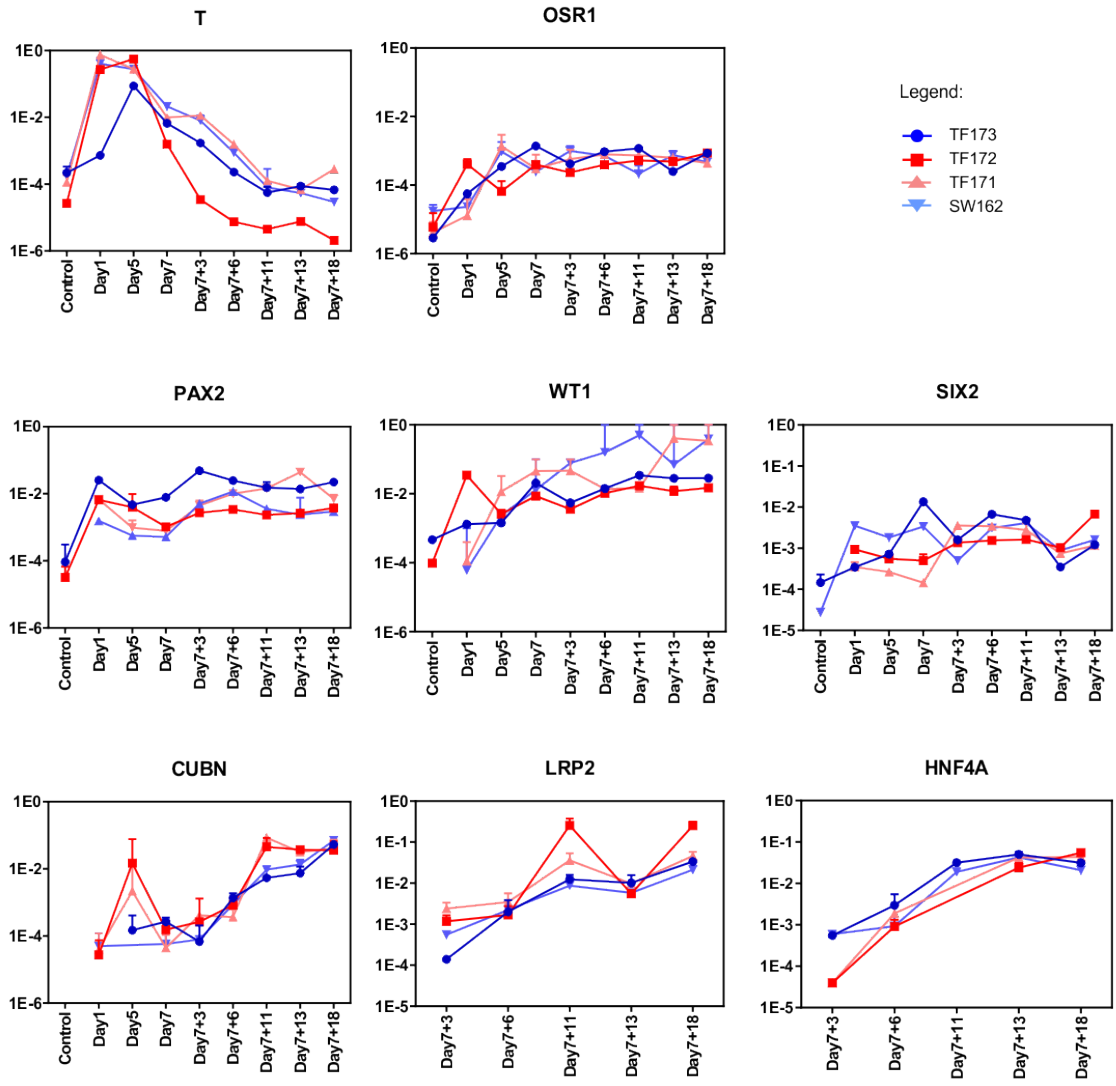

Figure 4.26 Time course of relative expression levels of four hiPSC lines specification. Differentiation of developing kidney was assessed by qRT-PCR representing key regulator genes that include primitive streak marker (T), IM (OSR1, PAX2), MM (SIX2, WT1), proximal tubule (CUBN, LRP2, HNF1A). Graph showing expression profiles of all lines. Data are represented as mean±S.E.M from technical replicates (n=3 organoids), depicting level of target transcripts normalised to GAPDH expression.

Another interesting aspect would be to answer whether the tubular cells contain transporters. It was reported that he organic anion transporters (OATs) of the solute carrier (SLC22) gene family can be found in the proximal tubules that functions in excretion of endogenous and exogenous compounds (Zeng et al., 2012). Figure 4.27 showed that OAT1 or SLC22A6 level in unaffected organoids was found to rise commencing day 7+3 and day 7+6 (SW162 and TF173, respectively) and peaked at day 7+11. However, these were reduced approaching day 7+18. Interestingly, mutant organoids revealed a constant low expression from start to end of culture with no significant differences between both lines (TF171 and TF172) at any timepoint. It was observed that WNT4, in both unaffected lines slightly upregulated at day 7+11 without observable increase in mutant lines at day 7+18. CITED1 were similarly expressed in all lines beginning day 1 to day 7+6. However, these increasing

trends were reduced progressively in unaffected controls. It was noted that both mutant lines upregulated CITED1 at day 7+11 and continued to reduce at day 7+18.

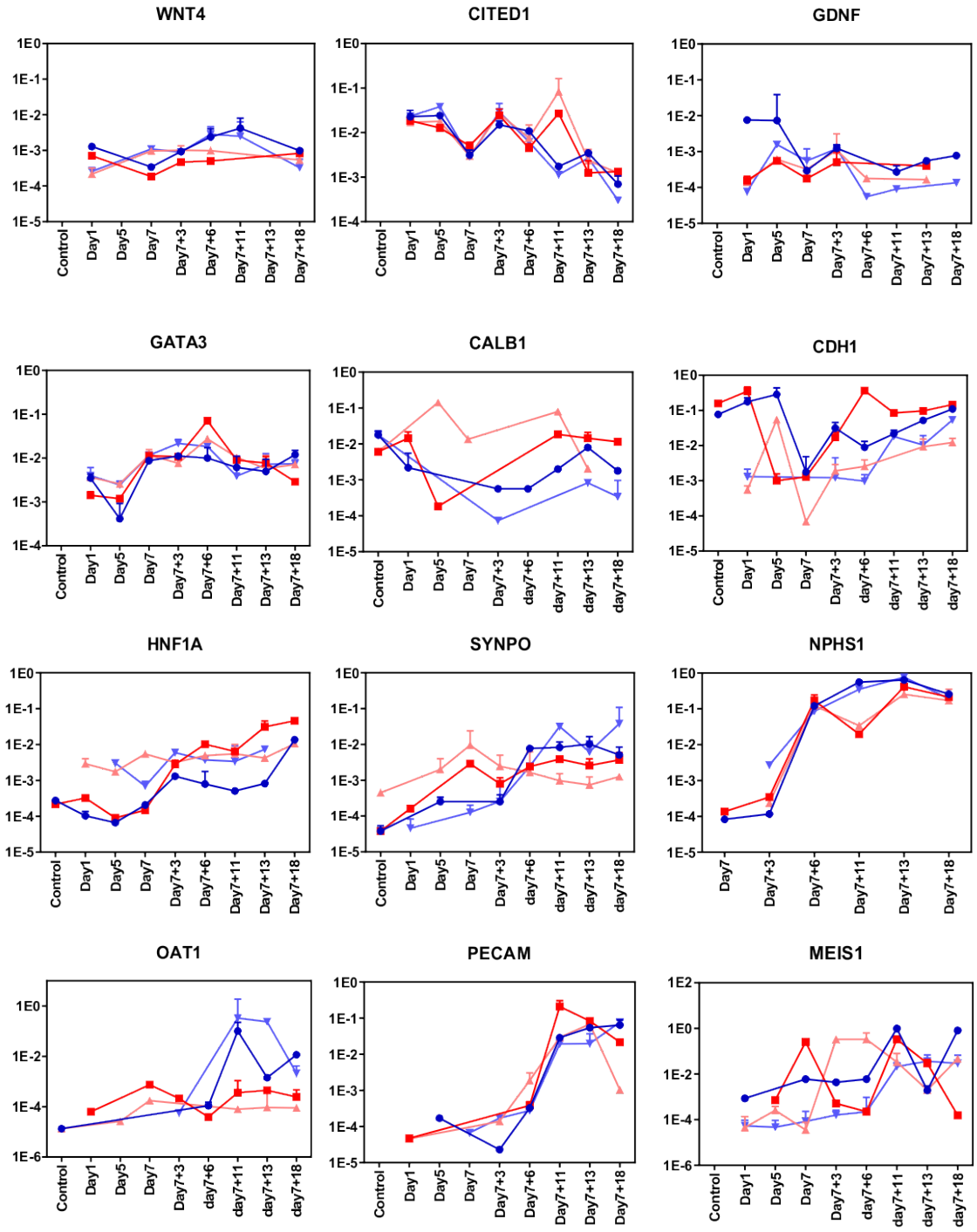

Figure 4.27 Time course of relative expression levels of four hiPSC lines specification. Differentiation of developing kidney was assessed by qRT-PCR representing key regulator genes that include comma/S-shaped nephron progenitors (WNT4), UB outgrowth and branching (GDNF), condensed MM (CITED1), tubular marker (OAT1,HNF1A), podocytes (SYNPO, NPHS1), collecting duct/distal (GATA3, CDH1, CALB1), vasculoendothelial (CD31) and stromal cells (MEIS1). Graph showing expression profiles of all lines. Data are represented as mean±S.E.M from technical replicates (n=3 organoids), depicting level of target transcripts normalised to GAPDH expression.

GDNF that marked UB branching was found to peak at day 5 of all lines except SW162 that maintained high expression from day 1 to 5. Approaching day 7, all lines reduced GDNF expression before continued to rise again at day 7+3. These levels were continuously expressed at later stages but at lower level. CALB1 that marked the kidney tubules were found to be reduced in the unaffected organoids from the start of differentiation up to day 7+3 but elevated again and peaked at day 7+13 before reduced at day 7+18. In contrast, both mutant lines upregulated CALB1 at day 7+11 that decreased towards end of culture. TF171 showed slightly delayed CALB1 expression but at higher transcript level as compared to TF172. GATA3 expression was found to peak at day 7+6 in both mutant lines. A constant expression was observed in the unaffected controls beginning day 7 of differentiation up to day 7+18. SYNPO were progressively expressed in the unaffected lines with higher expression level documented at later stage followed by temporal loss of early nephron progenitors. Mutant lines however peaked at day 7 and reduced at day 7+3 before stably expressed till the end. NPHS1 were found to be downregulated at day 7+11 in mutant lines but not in the unaffected that continued to rise up to day 7+18.

CDH1, epithelial marker was found to be variably expressed in all lines. All lines showed reduction of CDH1 expression on day 7 except SW162 line that remained at low level from the start to day 7+6 of culture. However, all lines gradually increased CDH1 at day 7+18. PECAM/CD31 endothelial marker revealed the highest expression at day 7+11 in the mutant lines that followed by downregulation approaching day 7+18. In contrast, unaffected continued to constantly rise from day 7 to end of differentiation. HNF1A that marked the proximal tubules was found to be slightly increased in TF173, TF172 and SW162 beginning day 7+11 onwards. However, TF171 line remained at constant level from day 1 to day 7+18 with only slight increase at day 7 of culture.

In order to investigate the function of HNF1B in the developing kidney organoids, I targeted the HNF1B transcription factor gene that is essential in tubule formations. I began with 2 set of primers that bind to Exon 2 and Exon 9 of HNF1B (which is missing in the mutant allele). From the qPCR data (Figure 4.28), it was found that HNF1B peaked at day 1 of culture but then reduced at day 5 both unaffected and mutant lines. These observations were similar for both Exon 2 and Exon 9. However, transcript levels of Exon 2 in all lines increased progressively up to the end of the culture. Interestingly, primers to the last exon of HNF1B (Exon 9) revealed remarkable differences between unaffected and mutant lines. It was found that the HNF1B transcript in mutant lines rise more slowly in midterm of differentiation and slightly delayed expression until day 7+13 before reaching comparable level as

unaffected at day 7+18. Unlike mutant, the unaffected showed parallel increased expression of HNF1B transcript using both primer sets.

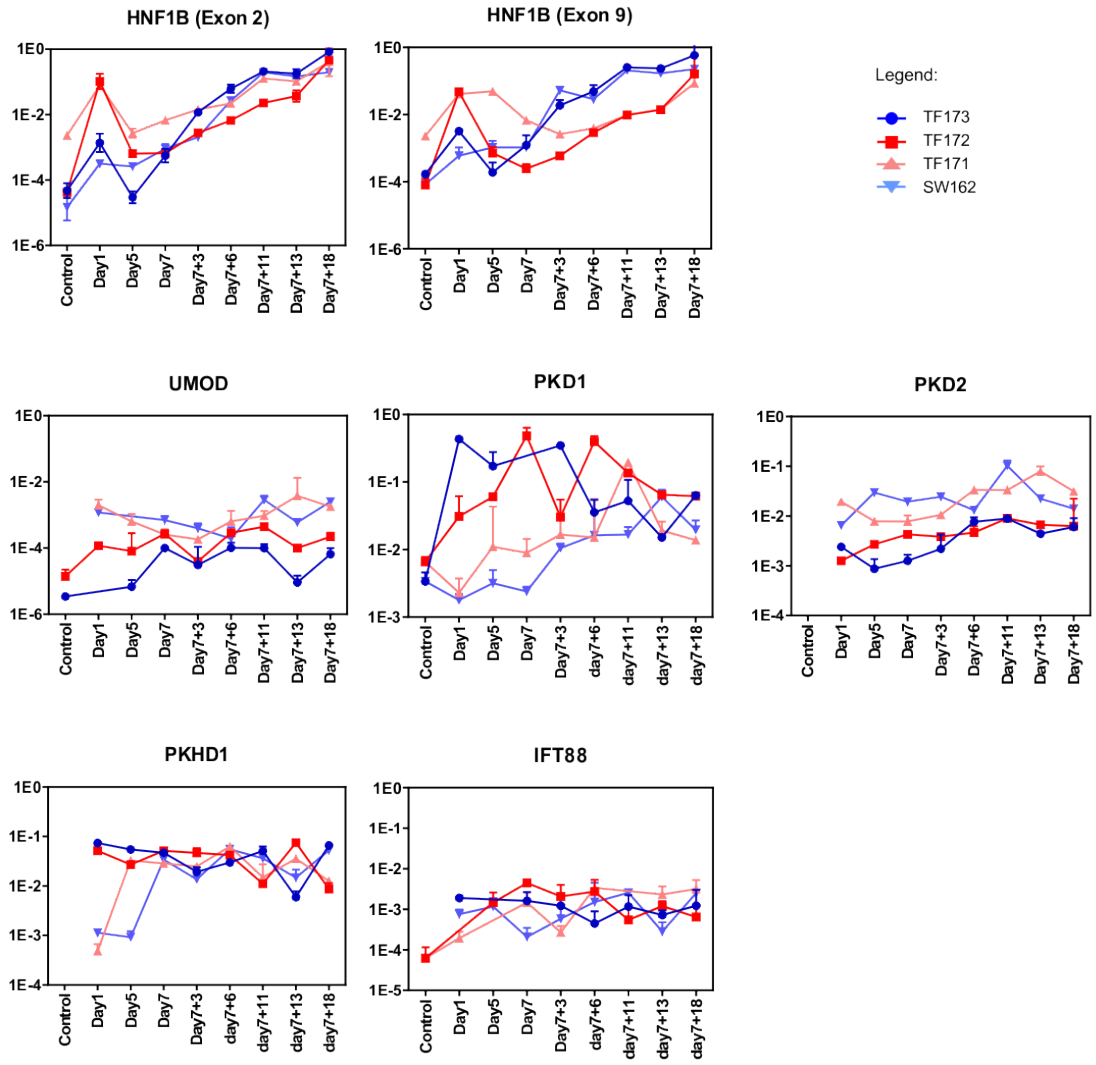

Figure 4.28 Time course of relative expression levels of HNF1B at exon 2 and exon 9 together with transcriptional targets. Expression of downstream targets (UMOD, PKD1, PKD2, PKHD1 and IFT88) were assessed by qRT-PCR. Graph showing expression profiles of all lines. Data are represented as mean±S.E.M from technical replicates (n=3 organoids), depicting level of target transcripts normalised to GAPDH expression.

To further evaluate HNF1B activity, I analysed the HNF1B downstream targets such as UMOD, PKD1, PKD2, PKHD1 and IFT88. It was found that UMOD that marked the thick ascending limb of Henle (LOH) was reduced at day 7+3 of culture in all lines. This expression continued to increase very gradually up to day 7+18 except a slight downregulation at day 7+13 in all but, TF171. PKD1 expressions were fluctuated and not consistent between mutant and unaffected lines. Each line revealed variation in expression pattern except a slight similarity between TF171 and SW162 lines. PKD2 expression showed an increase in the unaffected lines with the highest level at day 7+11. There were no significant differences observed between PKD2 transcripts between both unaffected and mutant lines. Mutant and unaffected lines showed

opposite changes in PKHD1 expression patterns beginning day 7+11 onwards. Accordingly, IFT88 showed a sharp increase in both mutant lines (TF171 and TF172) in the first 7 days of monolayer culture stating form a lower PSC base line than mutant. In the unaffected transcript levels remained at a constant level from day 1 except a minor reduction at day 7 and day 7+13 in SW162 line. Overall, no significant differences observed in HNF1B downstream targets between mutant and unaffected organoids.

Collectively, these qPCR data generated from 4 different hiPSC lines demonstrated specification of pluripotent stem cells into primitive streak after 4 days of CHIR treatment and subsequently induction of IM (OSR1). The generation of kidney derivatives along differentiation protocol showed heterogenous population that comprised of cells showing characteristics of condensed MM (WNT4), UB outgrowth and branching (GDNF) nephron progenitors (SIX2, PAX2, WT1), early podocyte structures (SYNPO, NPHS1), proximal tubule elements (CUBN, HNF1B, LRP2, HNF4A), distal/CD (GATA3, CALB1, AQP2) and interstitial marker (MEIS1). Mutant organoids maintained a constant but low level of glomerular podocytes expression towards end of differentiation whereas unaffected organoids showed a progressive earlier increase up to day 7+18. These findings reflected histological staining of podocytes showing reduced number of SYNPO+ glomeruli in mutant organoids. Interestingly, exon 9 HNF1B transcript profiles revealed reduced expression in mutant organoids but reaching comparable expression level as unaffected at d 7+18. In fact, exon 2 HNF1B transcripts remained consistent in all organoids. These data have indicated significant changes between important kidney transcripts in mutant and unaffected organoids throughout developments.

4.3 Discussion

4.3.1 Formation of complex multicellular kidney organoids from directed differentiation of hPSCs

In this study, I described the generation of human kidney organoids using hPSCs that involved establishment of kidney structures comprising specification of IM on monolayer culture, pelleting and maintenance of 3D organoid structures. The initial differentiation was conducted based on Takasato et al. (2015a) protocol slight modifications using unaffected MAN13 lines followed by iPSCs derived from patients with *HNF1B* mutation together with their related/unrelated healthy controls. The resulting organoids were maintained up to day 7+25 and revealed morphological differences at specified timepoints. The 7 days monolayer culture was able to direct hPSCs towards kidney lineage by generating nephron progenitor cells (PAX2+, WT1+ and SIX2+). The subsequent 3D phase has formed a complex kidney organoids expressing essential kidney marker genes that comprised of both MM and UB lineages

(Takasato et al., 2015a). These hPSC-derived organoids have revealed generation of 4 elements in an organised and continuous rearrangements after co-labelling staining which include early proximal tubules (CUBN/LRP2/HNF1A/HNF4A/CDH1), collecting duct (HNF1B/GATA3/CDH1), distal tubules (HNF1B/GATA3/AQP2/CDH1) and glomeruli (SYNPO, PODXL, NPHS1, NPHS2). AQP1 staining, that marked proximal tubules however less efficient possibly due to specificity and quality of antibodies.

Continued addition of FGF9 after CHIR pulse was reported to maintain nephrogenesis, suggesting exclusive role of FGF9 prior Wnt-activated nephron stimulation and to increase total nephron counts (Takasato et al., 2015a). Approaching the end-stage (day 7+5 onwards), FGF9 was withdrawn and the organoids were left at gas-medium interface to allow maturation and self-organisation. This could be due to production of FGFs by the differentiating organoids itself. This protocol has reproducibly proven to generate both UB/MM precursors thus better recapitulated kidney embryogenesis (as shown by Takasatao et al 2015). The resulting organoids also showed multiple structures that are similar to human fetal kidney. It is worth noting that extracellular matrix (ECM) also plays an essential role in early kidney differentiation especially in monolayer culture.

4.3.2 Extended culture suggest the need for further functional maturation

The prolonged 3D culture (up to day 7+25) is considered suboptimal and does not seem to improve structure maturation although the transcripts data revealed an increase in generation of complex kidney structures evidenced by upregulation of distal and proximal tubules, LOH, podocytes and interstitial markers. The essential kidney components were formed with some areas showed signs of degeneration. A similar observation was also reported with generation of various pattern of dysplastic tissues that include cystogenesis and expansion of mesenchyme upon differentiation from day 7+28 onwards (Kumar et al., 2019). This phenomenon was also described by researchers (Cruz et al., 2017; Czerniecki et al., 2018; Przepiorski et al., 2018). Variation in pathologies may include formation of fibrotic tissues, presence of mutation and technical issues during transfer of 3D organoids.

It was reported that day 7+41 proximal tubules showed reduced albumin uptake which indicated loss of functioning proximal tubules. Earlier stage such as day 7+14 proximal tubule was also reported to be suboptimal and less mature thus could not sufficiently uptake albumin (Kumar et al., 2019). qPCR analysis has verified these assumptions by reduction in gene expressions of markers of proximal tubule (HNF1B and HNF4A), podocytes (NPHS1 and PODXL), epithelialisation (CDH1) and vascularisation (CD31) at day 7+25. Apart from that, these degenerations lead to reduced Ki-67 staining which suggested loss of tubular elements, induction of

apoptosis (CASP3) in epithelial comparments and fibrosis evidenced by ECM deposition (α-SMA+). These extended organoids culture depleted tubule and glomeruli counts thus limited their utilisation at later stages.

It was also reported that stromal compartments were expanded and ECM accumulated at late stage of organoids culture. For instance, MEIS1 populations were reported to significantly differ between day 7+18 and day 7+25 of culture (Kumar et al., 2019). This may indicate that reduced proliferation capacity at extended culture contributed to gradual degeneration and constriction of whole organoids structure with some area positively stained for necrotic markers. Similarly, it was reported that PCNA+ cells were present in rare tubules at day 26 but not in nephrons or interstitial cells (Przepiorski et al., 2018). This could be due to limited nutrients and depleting oxygen diffusion as the organoids size increased (Hubert et al., 2016; Van Winkle et al., 2012). In fact, prolonged culture up to day 7+53 does not improve maturation of the kidney components except by enhancing the amount of epithelial tissue relative to stroma (Van Den Berg et al., 2018).

This is consistent with previous report that described the downregulation of vascular gene at day 7+11 and 7+18 (Takasato et al., 2015a). The possible reason behind insufficient vascularisation could be lack of VEGF synthesis by the podocytes. To relate, although VEGF transcript levels were not measured, the immunohistological staining revealed that CD31+ vasculoendothelial network rarely invade glomerular tufts suggesting formation of immature glomeruli that might stimulate capillary loop formation if the culture is prolonged (Van Den Berg et al., 2018). The immature state of kidney organoids may be due to limited time for segmentation, tubules elongation and end structure specifications. Eventually, these effects were expected to result in hypoxia and metabolic insufficiency. Although the current protocol is indispensable to recapitulate nephron development and patterning, prolonged culture is not the best option to show functional maturation of structures. Thus, it can be concluded that day 7+18 is the latest time point which can be relied on for generation representative nephron and tubular identities although the nephrons appeared to be less mature due to lack of vascularisations.

4.3.3 *HNF1B* mutation influenced phenotypic attributes of hPSC-derived kidney organoids

Heterozygous mutation of *HNF1B* has been shown to be implicated in severe pancreas hypoplasia and multicystic renal dysplasia (Haumaitre et al., 2006). Some suggested that kidney malformations occurred due to disruption of tubulogenesis (Heliot et al., 2013; Nakayama et al., 2010; Naylor et al., 2013). In this study, two *HNF1B*-derived mutant lines were differentiated in parallel at an equivalent efficiency towards kidney

organoids with two unaffected lines (one of which derived from the same family). Both mutant lines harbour exon 9 *HNF1B* mutation that was predicted to delete region starting from exon 9 (included 3' UTR). Immunohistochemistry results showed an increase in total diameter of HNF1B mutant organoids from both TF171 and TF172 lines. This amounted to about a 2-fold increase at day 7+18 compared to both unaffected controls (TF173 and SW162). Closer observation of tubules and glomeruli structures revealed phenotypic differences in structural organisation and number of developing nephrons in mutants. These observations reflected expression profiles evaluated by qPCR where mutant organoids showed lower level of podocyte markers (SYNPO and NPHS1). However, expression of tubule markers (CUBN, LRP2, HNF4A) showed only slight difference between mutant and unaffected organoids. It was thought that *HNF1B* mutation disrupt normal regulation of podocyte formation in the midpoints but found to compensate to relatively similar expression levels at later stage (day 7+18).

I propose that this may indicate that the mutant organoids have delayed developmental progression towards formation of kidney structures. This was evident when observed using confocal microscopy, HNF1B+ and CDH1+ populations in mutant organoids from both line appeared less elongated and reduced in total tubular structures as compared to unaffected controls. This could be due to dysregulation of genes that control tubular development. Immunohistochemistry reported that the mutant tubules comprised of a multi-layered epithelium along with bigger lumen size. In fact, these findings correlated with the level of tubule marker expressions (LRP2, CUBN, HN4A) with only slight difference observed between these mutant and unaffected organoids.

Based on the qPCR analysis, when all 4 lines were assessed for HNF1B gene expression using primers bound to exon 2, none of the lines showed any differences in expression level suggesting that the exon 2 could be a positive control. However, when exon 9 was evaluated, both mutant organoids (TF171 and TF172) indicated reduction in HNF1B transcript profiles approximately by half of unaffected line (TF173). Interestingly, this reduced expression kinetics seemed to be restored at day 7+18. This phenomenon suggested a delay in developmental program. The cells may compensate by upregulating transcription from the non-mutated allele or theoretically there could be a change transcript stability.

HNF1B transcriptional targets such as UMOD, PKD1, PKD2 and IFT88 were found to be comparably expressed and remained unchanged between mutant and unaffected controls. This would suggest that the HNF1B protein in mutant organoids was still be able to bind to appropriate promoter regions and regulate its downstream targets which is assumed to be via transcription of the non-mutated allele. Although the

morphological data has suggested an altered tubulogenesis that can mimic the pathological phenotypes in patients with HNF1B mutation, the minimal transcript differences between mutant and unaffected organoids suggested the need for testing other HNF1B targets that can regulate morphogenesis and control tubulogenesis in order to better explain the differences.

For example, the genome-wide analysis combined with CHIP-chip-mRNA microarray revealed that HNF1B binds to SOCS3 promoter region and inhibit its transcription, leading to overexpression of SOCS3 in renal epithelial cells. This overexpression inhibit tubulogenesis via reduction of Erk and STAT3 phosphorylations (Ma et al., 2007). Assessing the level of SOCS3 can be a useful marker to detect kidney malformations in organoids. In addition, SOCS3 was found to negatively regulate signaling of cytokines and growth factors that involved in tubulogenesis and nephrogenesis such as insulin-like growth factor-1, FGF, EGF, leukemia inhibitory factor and angiotensin-II (Sakurai et al., 1997; Plisov et al., 2001).

4.3.4 Kidney organoids as a disease model

One of the most attractive application of kidney organoids is to model diseases in order to search for new potential drugs. Using organoids, multiple number of chemicals can be screened without the need to consider ethical issues especially compred to large animal testing and to evaluate nephrotoxicants *in vitro* when drug-based clinical trials were conducted. For example, the use of cisplatin as anti-cancer drugs has been reported to cause kidney injury (Perazella and Moeckel, 2010). The uptake of cisplatin by organic cation transporters (OAT) in proximal tubules can determine maturation of nephrons, its function and extend of injury. Treatment of 5 μM cisplatin overnight was shown to upregulate kidney injury molecule-1 (KIM1) and γH2AX (marker for DNA damage) in LTL+ proximal tubules (Ludwig et al., 2004; Morizane and Bonventre, 2017a; Morizane et al., 2015). Also, cisplatin at higher than 50 μM was shown to cause a global damage of DNA.

In the study, it was found that *HNF1B*-derived mutant organoids delayed cell types formations and showed hypertrophic morphologies. This could be due to abnormal HNF1B function in controlling kidney morphogenesis and indicated the failure to direct normal tubulogenesis during development. However, although these mutant lines were derived from patients with cystic dysplastic kidney, none of the mutant organoids showed signs of cystic formation. This could be due to the immature state of the kidney organoids and lack of physiological conditions to mimic whole kidney environment. The formation of cyst could be due to the late onset mechanism as seen in patients with ADPKD (Freedman et al., 2015) and thus could not be seen in organoid models. However, early events that lead to cystic features can be detected

such as reduction of PKD1/PKD2 transcripts (binding target of HNF1B) that cause disruption of PKD1/PKD2 ciliary protein synthesis. In fact, these phenotypes can be detected early in the undifferentiated state of hiPSCs (Van and Frank, 1995).

Another study reported that when PKD1 and PKD2 gene were completely knocked out using CRISPR/Cas9 system, 6% of the organoids developed cyst formation whereas these phenotypes were rarely seen in the unaffected H9 hESCs. Also, organoids that lack PODXL were found to have disrupted junctional organisations (Freedman et al., 2015). However, this protocol needed further refinement due to limited cyst numbers and does not recapitulate heterozygous mutation as in most human kidney diseases. Nevertheless, the current study has the advantage of keeping the same genetic background with TF173 lines derived from healthy mum and the other two lines (TF171 and TF172) derived from both sons that harbour heterozygous *HNF1B* mutation. To put this into context, any phenotypic differences can be directly compared. Moreover, CRISPR/Cas9 can potentially create an isogenic line that contain heterozygous exon 9 deletion and resulting clone can be compared with the hiPSC-derived mutant lines as well as the healthy non-mutant parents, but not in the whole exon 9 knock out model. The utilisation of hPSCs may facilitate personalised medicine for kidney disease patients. However, the design should consider the genetic background, epigenetic variabilities, differentiation strategies, type of transmembrane, concentration of hybridoma extracts and quality of cell lines in order to analyse disease-phenotypes relationships.

4.3.5 Conclusion

In this study, I have demonstrated a detailed characterisation of heterozygous mutant *HNF1B*-derived iPSCs through a 2 step differentiation protocol. This data is essential for creating MM/UB kidney lineage that might be useful as a source of kidney disease model, pharmacological screening and ultimately regeneration of kidney tissue for transplantation. The optimised protocol has successfully generated kidney organoids with essential nephron segments however lacks advance nephron development with insufficient mature protein as those need in formation of mature glomerular basement membrane. This is required in blood ultrafiltration (Kimber and Woolf, 2018). However, when these hPSC-derived progenitors were subcutaneously transplanted in mouse, glomeruli were formed with capillary loops, with mature glomerular basement membrane between podocytes and endothelia (Bantounas et al., 2018) suggesting its potential regenerative capacity although still far from generating the whole kidney.

Although generation of kidney organoids had posed enormous benefits for regenerative medicine, some challenges still need to be addressed. The obvious

anatomy between organoid and native kidney remained as a major challenge. For instance, there were no formation of ureteric duct containing single urine path as seen in human kidney. Unlike human kidney that have nephrons arranged around a single collecting duct tree, organoids displayed interspersed, multiple disconnecting CD throughout organoids. The size differences made it impossible to reflect kidney anatomy at which organoids appeared to reach up to 8 mm in diameter comprising of less than 100 nephrons (Kimber and Woolf, 2018). This work also reported presence of vascularisations in organoid's glomeruli evident by staining of endothelial capillary network. However, these capillaries rarely invade glomerular tufts and lacked peritubular vasculature. Sorting different cell types from the organoid, and combining them in the right proportion to engineer a more organized structure could be a way to solve part of the problem.

Furthermore, post-renal failure, dialysis treatment provided renal function equivalent to 15% of glomerular function that suggested the need to generate more than 100,000 nephrons to replace this function. However, the scale-up version of organoids will not be as beneficial if they could not functionally reclaim amino acids, fluids, nutrients and electrolytes. Although still far from generating a whole functioning kidney, the current organoid model could be used as a tool for generating a functional replacement organ, nephrotoxicity screening and disease modelling. Nevertheless, detailed assessment on maturation of each generated cell types should be continued.

Although the current work provided significant advances in our understanding regarding development of kidney organoids, there were some limitations that need to be addressed. It was reported that 10-20% of organoids cells are from non-renal origins. The availability of these off-target cells such as neurons and muscle cells in resulting organoids could be minimised by inhibiting BDNF-NTRK2 signaling cues that was found to reduce up to 90% of off-target cell types (Wu et al., 2018). In this project, I found that organoids cultured over day 7+18 generated non-specific kidney cell types, evidenced by formation of α-SMA cells. Whether these rarely formed α-SMA+ cells are pericytes (or vascular smooth muscle cells) that failed to organise due to degeneration or signs of fibrosis are remain to be elucidated. However, my monolayer culture suggested that PDGFRB expression level that marked for pericytes are progressively increased as early as day 3 of culture. It is also important to determine the identity of these pericytes because capillary pericytes, for example, do not express α-SMA, but do express PDGFRB and NG2 (Yamazaki and Mukouyama, 2017). One possible test that can be done is by co-labelling NG2+ cells with CD31+ populations and quantify their expression levels.

Apart from that, characterisation of induced mesenchyme, stromal and surrounding interstitium could be performed to better reflect the proportion of presenting organoids and give information regarding state of maturation in each organoid. scRNA-seq from hPSC-derived kidney organoids can be used to investigate signalling pathways and molecular mechanism in a non-invasive way due to limitations obtaining samples from human. Despite large disparities between human kidneys and organoids, I have shown that differentiation of hPSCs to self-organising kidney organoids expressed essential kidney genes. This study demonstrated balanced anterior-posterior patterning of IM involving coordinated stimulation of starting cells differentiating into various cell types in order to create intricate multicellular morphogenetic structures comprised of segmented nephrons surrounded by endothelial and interstitium.

Furthermore, the complexity of tissue organisation and degree of phenotypic resemblance supported the use of these organoids for disease modeling or functional genomics. However, the absence of cysts in these organoids made it necessary for further intervention by interrogating the non-genomic factors. To address this issue, I tested these organoids for cyst formation by exogenously adding chemicals such as cyclic adenosine monophosphate (cAMP) that resulted in increased intracellular cAMP level (Low et al., 2019) which will be discussed in the next chapter.

Chapter 5: Possible effect of cAMP on differentiation of hPSCs towards renal end-points

5.1 Aims and introduction

The previous chapter has described phenotypic comparisons between mutant and unaffected hPSCs and revealed remarkable features of differentiating mutant organoids suggesting hypertrophic manifestation and decreased cellular development. However, none of these mutant organoids (TF171 and TF172) exhibited cyst formation as always seen in the patient harbouring *HNF1B* mutation (that leads to cystic dysplastic kidney). Most published cystogenesis experiments revealed that cyst were predominantly in CD compartments as seen in patient with cystic dysplastic kidney (Haumaitre et al., 2006). Some studies have reported that elevated intracellular cAMPs were associated with increased cell proliferation, cystic growth and stimulation of transepithelial fluid transport after stimulation with 8-Br-cAMP, arginine vasopressin, prostaglandin E1, forskolin and phosphodiesterase inhibitor 1-methyl-3-isobutylxanthine (IBMX) on primary culture of human kidney, established renal cells and human cystic cells (Calvet, 2015).

Although there are several mechanisms involved in elevating cAMP at various kidney segments, it should be noted that cAMP level remained normal at early stage of disease process. It was reported that cAMP alone is non-cystogenic in healthy animals (Wang et al., 2008) and there is insufficient evidence to claim that elevated cAMP can convert healthy cells to become cystic. Therefore, in this chapter, it should be clear that cAMP would only be regarded as a cyst-promoting agent and not referred as the sole factor that can generate cyst. From the previous chapter, it was shown that the mutant organoids do not generate cyst at any point of differentiation. Therefore, in order to test whether these organoids can respond to cAMP, I decided to exogenously induce cyst formation in organoids using cAMP analogue such as 8-Br-cAMP that can generate cystic conditions as seen unaffected mouse embryonic metanephroi (Anders et al., 2014).

In order to test whether these mutant organoids can recapitulate the human cystogenesis, I hypothesised that differentiating hPSC-derived kidney organoids, when exposed to cAMP, the growth and differentiation trajectories will deviate from unaffected forming cyst. The response of the mutant would be different from the healthy developing kidney tissue. If there were cyst formed, then these organoids will be characterised to determine if they were specific to any nephron segments. Thus, to reproduce phenotypes relevant to renal tract malformations as seen *in vivo*, I cultured mutant hiPSCs in parallel with unmodified isogenic control lines and

perturbed the normal differentiation protocol at day 7+7 by adding 8-Br-cAMP) at an increasing concentration.

Heterozygous *HNF1B* mutations leads to Renal Cysts and Diabetes (RCAD) characterised by renal malformations and early onset of diabetes (Heidet et al., 2010). Fetuses carrying this mutation displayed bilateral dysplastic kidney containing cysts that derived from CD and nephron compartments (Haumaitre et al., 2006). Also, conditional *Hnf1b* inactivation in tubules generated cysts postnatally (Hiesberger et al., 2005) suggesting a role for *HNF1B* in early kidney morphogenesis. However, the main challenge towards understanding function of HNF1B in early kidney formation was the lack of a human cellular model that can efficiently mimic cystogenesis. Thus, to address this issue, I have several aims that include:

1. To establish a cystogenesis differentiation protocol by determining a specific timepoint for ectopic induction of chemical inducer.
2. To differentiate hPSC-derived kidney organoids that can promote cysts formation by addition of 8-Br-cAMP
3. To evaluate the characteristics of cyst that include area of cyst per total organoid's area, cyst formation rate, size per mm organoid and number of cysts per tubular organoid.
4. To investigate expression profiles of organoids before and after induction of cystogenesis.
5. To study functional transport mechanism in tubular segments of kidney organoids by utilising fluorescent anion (6-CF) as a tracer molecule.

Here, the progression and characteristics of cyst were assessed in both mutant and unaffected organoids by utilising 8-Br-cAMP as a chemical inducer to recapitulate cystic kidney disease. The number of cysts and localisation were quantified and assessed to indicate severity and whether cysts are specific to glomeruli or any tubule segment. These findings have supported the idea that adverse fetal environment may induce organoid cystogenesis. Apart from that, I showed that the organic anion transporter was expressed in kidney organoids at day 7+18 and able to facilitate uptake of anions. Although this model does not function like a metanephric tubule, the organoid tubules have many of their characteristics and can possibly facilitate transepithelial transport of organic anions through apical and basolateral membrane.

5.2 Results

5.2.1 Proximal tubules express CUBN as early day 7+6 in unaffected organoids

In order to determine the suitable time point for induction of cystogenesis, I first determined the start of tubule formations in kidney organoids. I ran a differentiation protocol using MAN13 lines and fixed the organoids at selected timepoints (day 7+6 and 7+12). These fixed organoids were sectioned and immunohistochemically stained with proximal tubule marker such as CUBN. From the staining, it was found that the mutant organoids at day 7+6 was minimally stained with CUBN particularly on the basal region. Interestingly, healthy organoids were positively stained with CUBN in both apical and basal layer (Figure 5.1). At this stage, both mutant and unaffected organoids displayed an interspersed distribution of structure across organoids and were not restricted to any particular region. Further staining at day 7+12 showed that the tubules become more prominent in both lines (TF172 and TF173) with emergence of elongated tubular morphologies (Figure 5.2). These findings reflected the previously described CUBN transcripts and provided essential information to challenge tubular response in adverse environments.

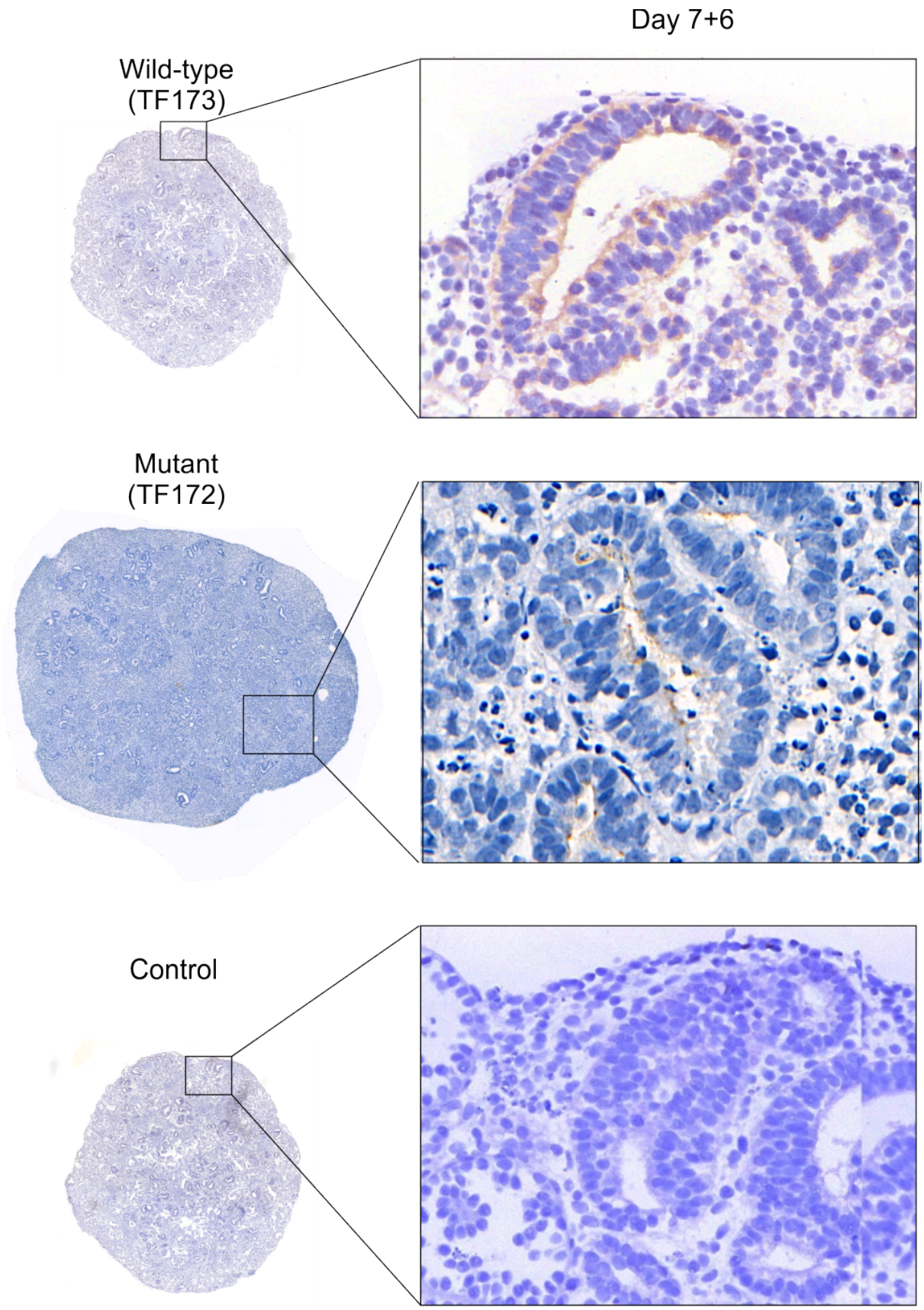

Figure 5.1 Staining for CUBN in unaffected and mutant organoids at day 7+6. (*Top*) Unaffected organoid showed formation of proximal tubule (brown staining) that was present throughout organoid's area. (*Middle*) Mutant organoid displayed minimal CUBN+ staining in the basal surfaces of tubules. (*Bottom*) Immunological control stained by hematoxylin. Scale bar, whole mount, 50 μm, magnified, 20 μm.

5.2.2 Establishment of cystogenesis protocol in MAN13-derived kidney organoids

Based on the CUBN staining of hiPSC-derived organoids at day 7+6 and respective expression profiles, it can be concluded that day 7+6 marked the initiation of proximal tubule generation in the unaffected (TF173) organoids but this appeared to be delayed in the mutants (TF172). To begin with, I utilised MAN13 line and differentiated into kidney organoids according to Takasato et al. (2016) protocol with slight modifications (Figure 5.2). Based on previous chapters, it was shown that MAN13 lines displayed comparable upregulation of AQP1 to the hiPSC-derived unaffected organoids (TF173) commencing day 7+6. These results have suggested that the tubules began to form as early as day 7+6 in unaffected thus I selected day 7+7 (the next day) as the proposed starting point of cystic induction. The chemical stimulation was performed using water soluble 8-Br-cAMP supplemented in the differentiation medium that was replaced every other day.

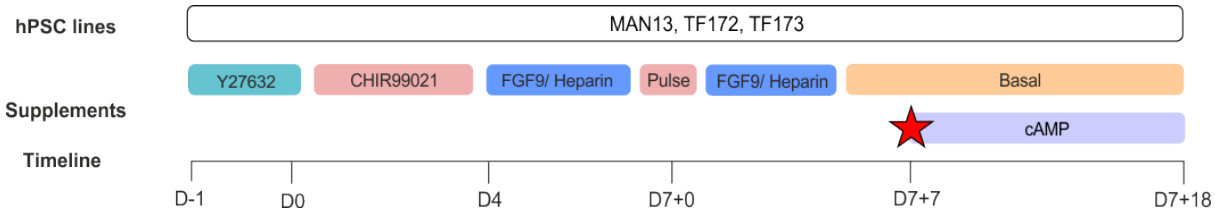

Figure 5.2 Protocol for cystogenesis induction. 8-Br-cAMP were added commencing day 7+7 and replaced every 2 days. Untreated controls were differentiated in-parallel and fed with basal medium only. Organoid cultures were terminated at day 7+18 before further characterisations. This protocol were modified as previously described in chapter 3 and 4.

Based on the results, it was shown that MAN13 lines can be differentiated into kidney organoids containing cysts. Figure 5.3 showed both 2D and 3D phase contrast images at specified timepoints. During the day of induction (day 7+7), addition of 8-Br-cAMP turned the smooth-edge organoid morphology into one with irregular edges, increased in size and development of structural complexities. However, at day 7+11, these organoids were separated by two distinct areas. The outer region was absent from any structures whereas the core was filled with smaller cell clusters. Although appeared smaller in size as compared to day 7+7, these cluster of cells were found to be connected with neighbouring cells. Interestingly, few bright tiny structures were detected in some area. The central region also exhibited darkened area suggesting different cell layers. After a week (day 7+18), these organoids began to form brighter and bigger white structures that indicated cyst-like formation. The kidney structures and cystic entities continuously expanded in terms of size and number. The total cyst-like structures were measured to examine effectiveness of 8-Br-cAMP concentrations. However, only single dose was utilised and almost no cysts were observed in the *HNF1B* mutation line (TF172). To further evaluate the effectiveness

of these cAMP treatments, I differentiated hiPSCs (both mutant and unaffected) and induced them with cAMP in a dose-dependent manner.

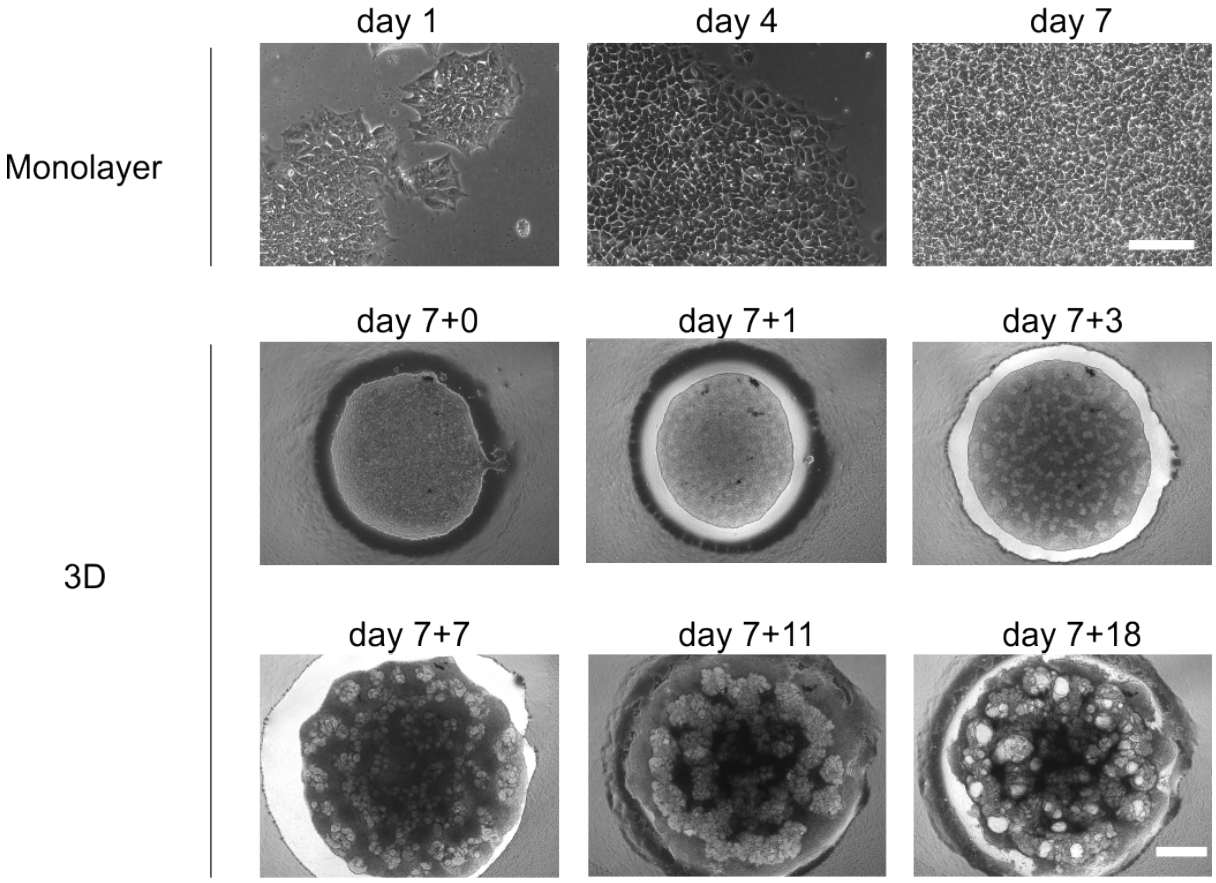

Figure 5.3 Phase contrast images depicting differentiation of MAN13 lines into cyst-containing organoids. Induction of 8-Br-cAMP began on day 7+7 of 3D culture and were replaced every 2 days. Morphological differences were documented at specific timepoints as the organoids developed up to day 7+18. Cystic features were first observed at day 7+11 (4 days after induction). Day 7+18 contained bigger and increased cysts numbers. Experiments were terminated at day 7+18 and no further assessments were carried out. Scale bar, 500 µm.

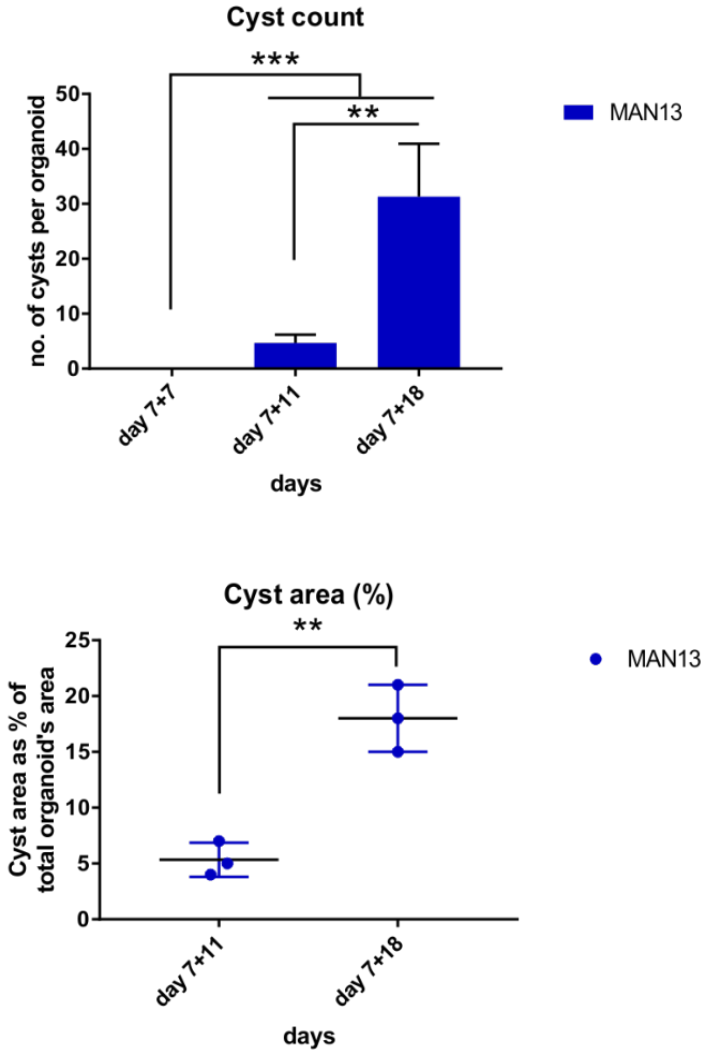

Figure 5.4 Quantification of cysts in MAN13-derived kidney organoids. (*Top*) Average of cyst count at day 7+7, 7+11 and 7+18 of cultures. No cyst formation was observed at day 7+7 but began to emerge at day 7+11. Day 7+18 displayed highest number of cysts. (*Bottom*) Percentage of cyst area in total organoid's area at day 7+11 and 7+18 of cultures. Cyst exhibited larger area approaching terminal day of culture (day 7+18). Data are presented as mean ± SEM (n = 3 independent experiments). Statistical analysis was performed using one-way ANOVA, **p < 0.05, ***p < 0.001.

5.2.3 Varying cAMP concentration does not modify organoid's cyst count

In order to determine whether increasing cAMP concentration can affect the extend of cyst formations, I gradually increased the dose of cAMP (50, 100 and 200 μM) at day 7+7 in both mutant and unaffected organoids that were differentiated in parallel. Cysts were detected based on its distinct features that appeared to be bright and shiny in culture. Based on the results, it was found that there were no differences found in term of cystic count and severity of organoids in unaffected organoids (TF173) treated with 50, 100 or 200 μM cAMP at day 7+18. However, the cyst count was slightly different at day 7+11. None of the organoids displayed cystic features at day 7+9. All cAMP-treated unaffected organoids responded similarly at day 7+18 by generating 20-100 μm cysts diameter and approximately 20-30 cysts. Interestingly, mutant organoids (TF172) treated with 50, 100 and 200 μM cAMP displayed absence

to low number of cysts at day 7+18 of culture (Figure 5.5, 5.6 and 5.7, respectively). Fewer ambiguous cyst-like structures were observed at the end of the protocol and no morphological differences were observed between the doses. However, it was observed that the total size of organoids was gradually decreased in 100 and 200 μM cAMP but not in 50 μM cAMP treatment.

When comparing unaffected to mutant organoids, it was evident that the unaffected hiPSC responded similarly to the MAN13 lines with the first emergence of cyst began at day 7+11 (4 days after induction) although unaffected hiPSCs (TF173) displayed relatively greater number and bigger cyst's size. Mutant organoids on the other hand only showed cysts at day 7+16 of culture (9 days after induction). Mutant organoids at day 7+9 were observed to be slightly bigger in total size as compared to unaffected. Although smaller, the number of developing structures in unaffected was found to be relatively higher and accommodated the whole organoids with increasing structural complexities towards day 7+18. The mutant, however, formed an empty middle region with no observable structures. At day 7+11, mutant organoids were found to respond minimally to any of the cAMP concentrations although increased in the number of intricate structures. It was observed that mutant organoids at day 7+11 treated with 200 μM cAMP generated bigger black middle areas compared to 50 and 100 μM cAMP treatments. From the results, it was evident that mutant organoids showed delayed cystic formations with the first cyst developed between day 7+14 to 7+16. To examine whether these cysts were capableof expanding and increasing, I extended the culture up to day 7+25 in both mutant and unaffected.

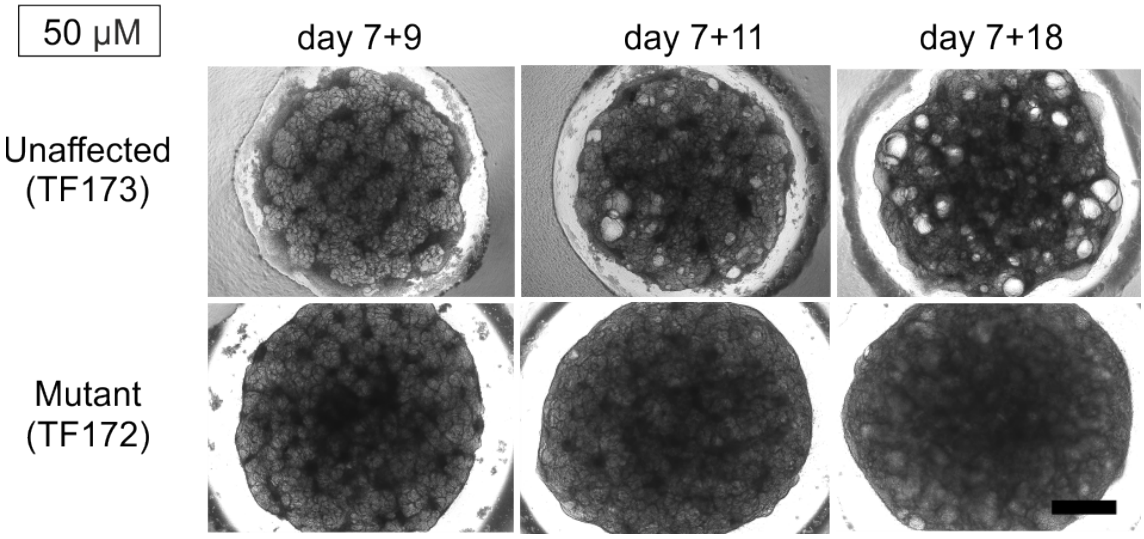

Figure 5.5 Differentiation of unaffected TF173 and mutant TF172 hiPSC lines into cyst-containing organoids using 50 μM cAMP. Induction of 8-Br-cAMP began on day 7+7 of 3D culture and was replaced every 2 days. Morphological differences were documented at specific timepoints as the organoids developed up to day 7+18. Cystic features were first observed at day 7+11 (4 days after induction) in unaffected organoids and found at day 7+16 in mutant (9 days after). Day 7+18 unaffected organoids contained bigger and higher cysts numbers as compared to mutants. Experiments were terminated at day 7+18 and images are representatives for each treatment groups, N=3. Scale bar, 500 μm.

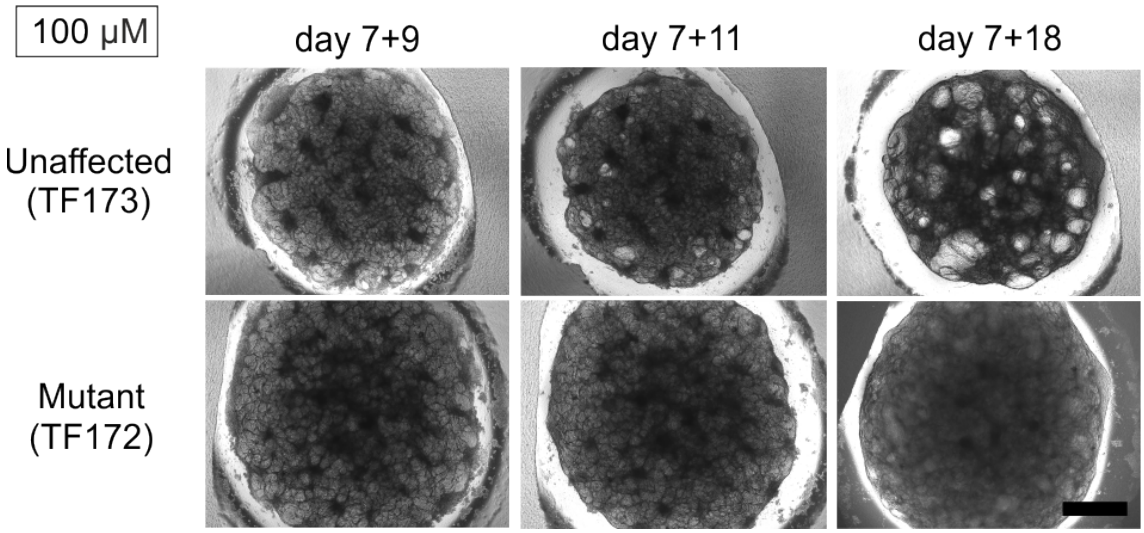

Figure 5.6 Differentiation of unaffected and mutant hiPSC lines into cyst-containing organoids (TF173 and TF172, respectively) using 100 µM cAMP. Induction of 8-Br-cAMP began on day 7+7 of 3D culture and was replaced every 2 days. Morphological differences were documented at specific timepoints as the organoids developed up to day 7+18. Cystic features were first observed at day 7+11 (4 days after induction) in unaffected organoids and found at day 7+16 in mutant (9 days after). Day 7+18 unaffected organoids contained bigger and higher cysts numbers as compared to mutants. Experiments were terminated at day 7+18 and images are representatives for each treatment groups, N=3. Scale bar, 500 µm.

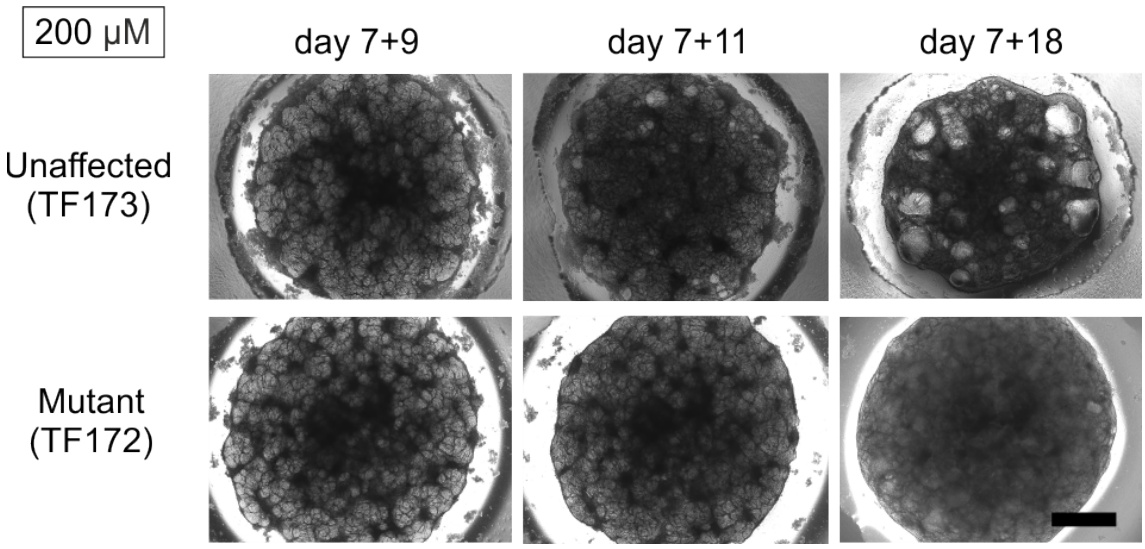

Figure 5.7 Differentiation of unaffected and mutant hiPSC lines into cyst-containing organoids (TF173 and TF172, respectively) using 200 µM cAMP. Induction of 8-Br-cAMP began on day 7+7 of 3D culture and was replaced every 2 days. Morphological differences were documented at specific timepoints as the organoids developed up to day 7+18. Cystic features were first observed at day 7+11 (4 days after induction) in unaffected organoids and found at day 7+16 in mutant (9 days after). Day 7+18 unaffected organoids contained bigger and higher cysts numbers as compared to mutants. Experiments were terminated at day 7+18 and images are representatives for each treatment groups, N=3. Scale bar, 500 µm.

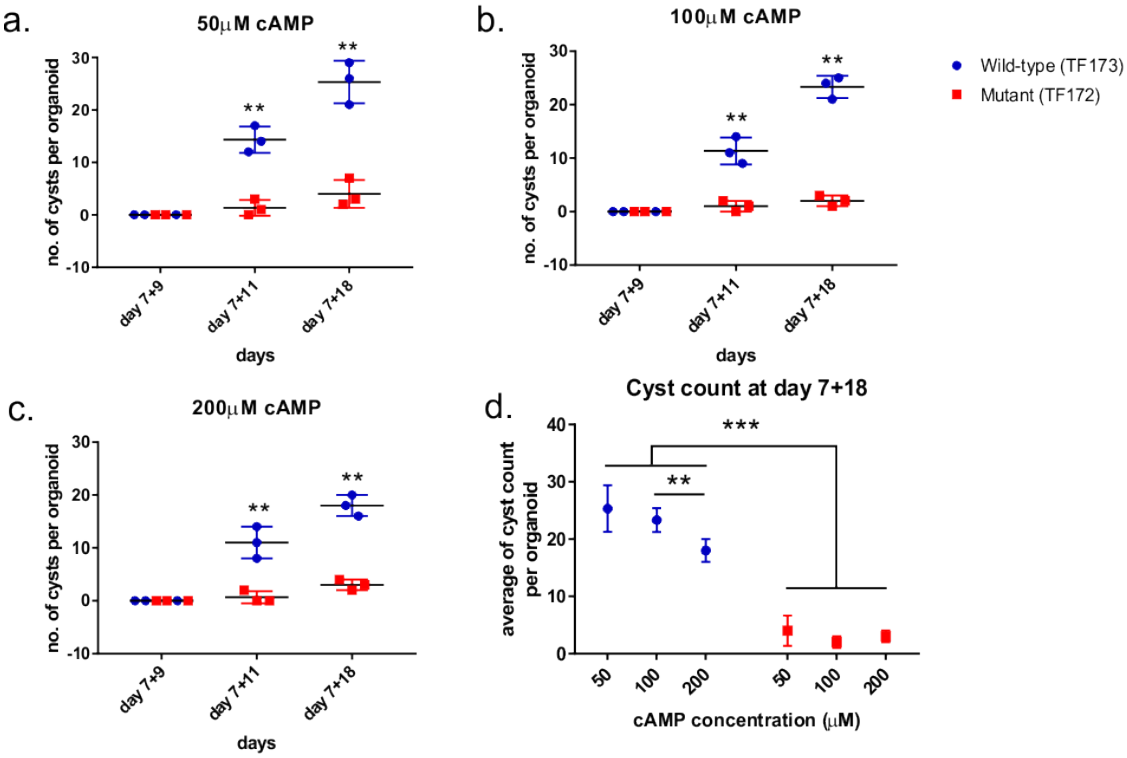

Figure 5.8 Effect of varying cAMP concentration on cyst counts. (a) number of cysts after induction with 50 μM cAMP. None of the groups (mutant or unaffected) showed any cyst formation at day 7+9. At day 7+11, unaffected organoids displayed small bright cyst-like appearances and there were more of these compared to mutant organoids. At day 7+18, both groups showed increased number of cyst structures. (b) and (c) Cyst counts in mutant and unaffected organoids treated with 100 and 200 cAMP, respectively. (d) Average number of cysts at day 7+18 of culture between mutant and unaffected organoids. Data are presented as mean ± SEM (n = 3 independent experiments). Statistical analysis was performed using one-way ANOVA, **p < 0.05, ***p < 0.001. Black horizontal bars demarcated means of cyst number.

5.2.4 *HNF1B*-derived mutant organoids generated lower cyst count and smaller diameter in extended culture

From this differentiation, it was found that the mutant organoids responded less efficiently to cAMP although the culture was extended up to day 7+25. Generally, all organoids (mutant, unaffected, vehicle and untreated controls) showed comparable morphologies (Figure 5.9) with emergence of early kidney structures that continued to develop commencing day 7+0 to day 7+7. At day 7+7, kidney organoids showed greater number and size of internal structures. Four days post cAMP induction (day 7+11), these organoids began to exhibit variable morphologies with unaffected organoids began to form cyst-like structures. However, no cysts were observed in other groups. Mutant organoids began to show dark middle regions suggesting different layer organisations. Also, it was observed that vehicle control groups showed a reduction in the total organoid diameter with internal structures clustered at the centre. Untreated control however retained normal organoid's morphologies.

At day 7+18, it was shown that the number of cysts in unaffected organoids was increased by half from day 7+11 organoids. The total organoid diameter however remained unchanged. Interestingly, mutant organoids began to form cyst but at

slower pace, less in number and restricted to edges (not at the middle area as seen in unaffected organoids). Vehicle controls (PBS only) showed reduced diameter but few globule-like appearances began to accommodate periphery. Untreated controls increased in complexity and were cyst-free. When these organoids were extended up to day 7+25 (Figure 5.10), cysts in unaffected organoids were less visible and become smaller with reduced cyst diameter. Similar changes were observed in the mutant groups and no changes in organoid diameter were detected. However, vehicle control groups revealed increased number of globules in the outer regions with untreated group less affected.

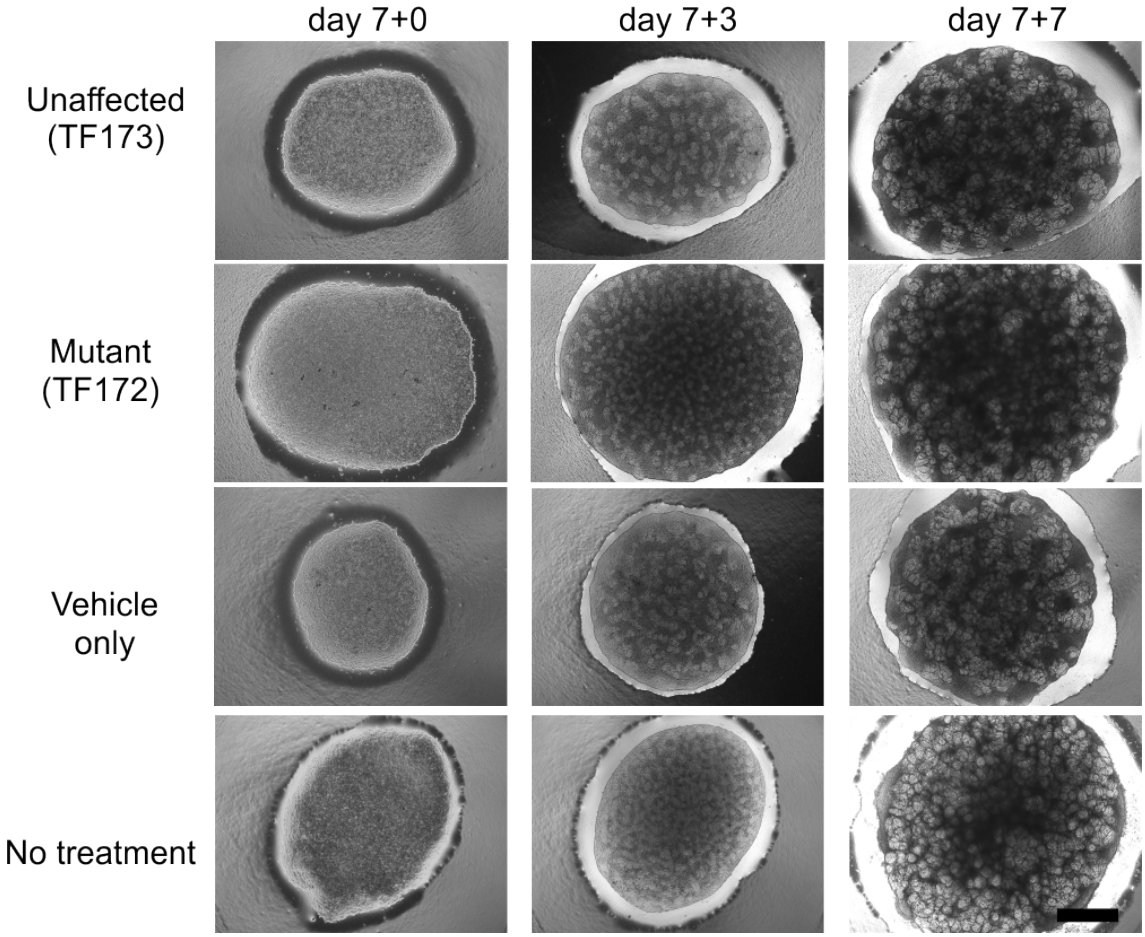

Figure 5.9 Phase contrast images of parallel differentiation to cystic morphologies before cAMP induction. Organoids increased in diameter and complexities towards day 7+7. Mutant organoids revealed slightly higher diameter as compared to other groups. No cyst was detected in any of these differentiation stages. Vehicle (PBS) only and no treatment organoids were differentiated using TF172 mutant lines. Images are representatives of 3 organoids in each line. Scale bar, 500 µm.

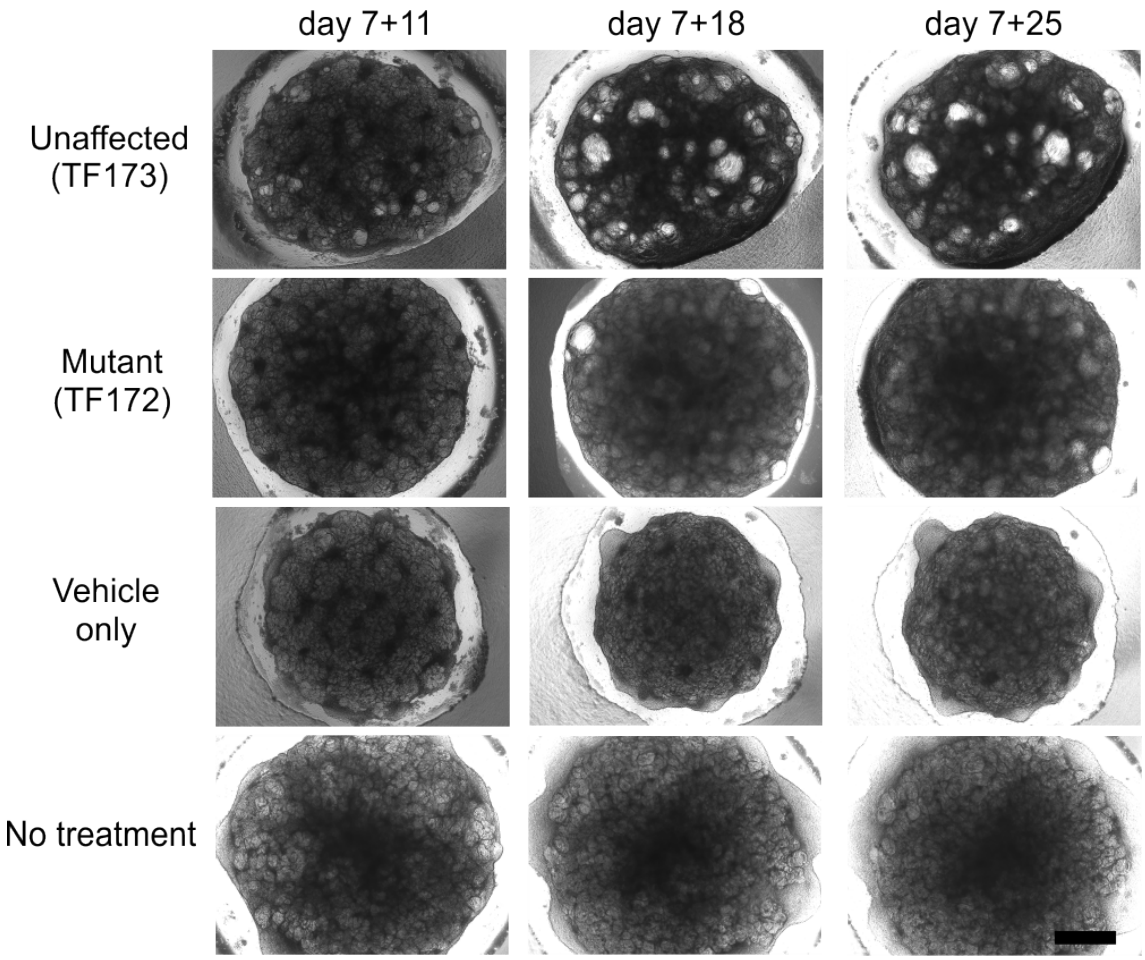

Figure 5.10 Phase contrast images of parallel differentiation to cystic morphologies after cAMP induction. Unaffected organoids revealed highest number of cyst as compared to other groups. Day 7+18 marked the optimum cyst number that was decreased in the extended culture (day 7+25). Mutant organoids showed comparable cyst-like structure at day 7+18 but these had reduced after a week. Vehicle control (PBS only) groups diminished in the total organoid diameter with no observable cyst formation. Untreated groups retained decent kidney organoid identities. Scale bar, 500 μm.

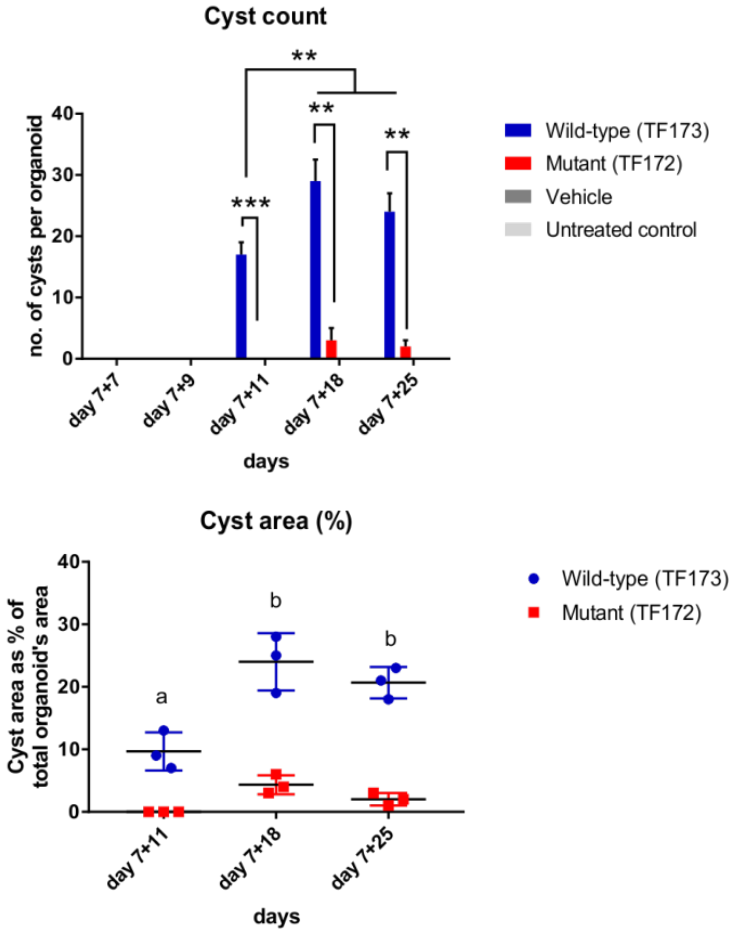

Figure 5.11 Quantification of cysts in hiPSC-derived kidney organoids. (*Top*) Average of cyst count at day 7+7 to day 7+25 of culture. No cyst formation was observed at day 7+7 or day 7+9 in both mutant and unaffected organoids. Cyst in unaffected organoids began to emerge at day 7+11, peaked at day 7+18 and degraded approaching day 7+25. No cyst formation was observed in any of vehicle (PBS only) or untreated controls. (*Bottom*) Percentage of cyst area in total organoid area at day 7+11, 7+18 and 7+25 of culture. Cysts accounted for most of an organoid's area at day 7+18 in mutant and unaffected organoids (4.3% and 24%, respectively). Analysis were performed on 3 separate organoids (N=3). Black horizontal bar indicated mean value. Statistical analysis was performed using one-way ANOVA, $^{**}p < 0.05$, $^{***}p < 0.001$, $^{a}p < 0.05$, $^{b}p < 0.001$.

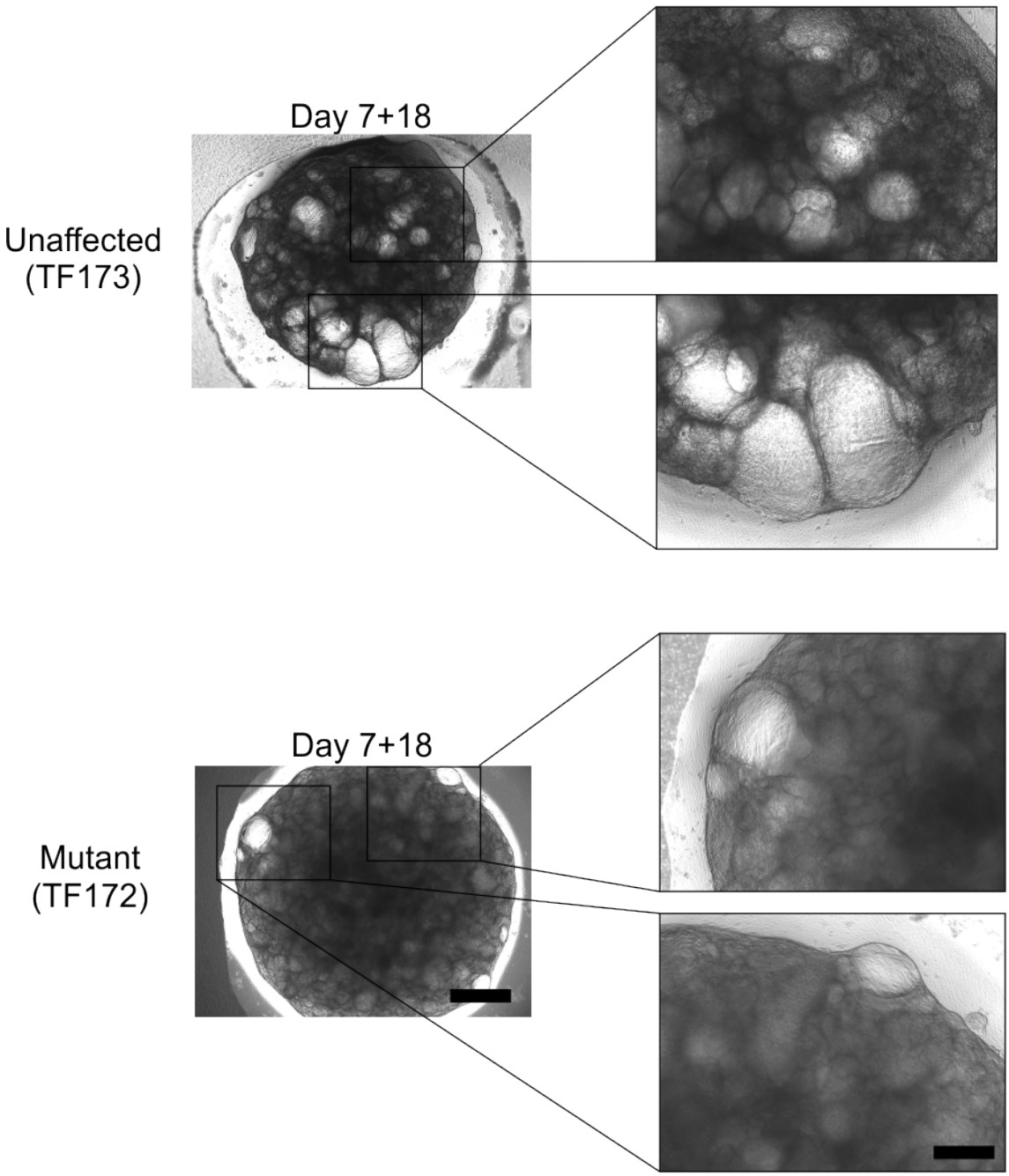

Figure 5.12 Expanded images of mutant and unaffected organoids at day 7+18. (*Top*) Unaffected organoids showed bright and bigger size of cysts that filled up the edges as well as the middle area. (*Bottom*) Mutant organoids exhibited bright cystic structures butin reduced amount and these were restricted to the outer region. Scale bars, 500 μm (low magnification), 20 μm (high magnification).

5.2.5 Transcript profiles of differentiating *HNF1B* mutant kidney organoids revealed reduced *HNF1B* downstream target expressions

To examine whether the phenotypes upon cAMP induction could reflect the transcript profiles, I analysed downstream targets of *HNF1B,* and genes associated with transport of anions into and out of the lumen. It was found that when both mutant and unaffected organoids were induced with 50 μM cAMP, PKD1 transcripts were upregulated after day 7+9 with slightly reduced expression in unaffected approaching day 7+18. Vehicle and untreated controls however revealed antagonistic PKD1 expressions at day 7+12. The similar expression patterns were observed in all of these groups and no significant differences were detected between mutant and unaffected organoids ($p<0.05$). In the PKD2 expression profiles, there were no significant differences observed between different lines in any of these groups.

In the PKHD1 transcript evaluation, it was found that the expression level gradually increased in both mutant and unaffected organoids commencing day 7+3 to day 7+12 except a slight downregulation in unaffected organoids at day 7+18. The mutant organoids revealed lower expressions as compared to unaffected in earlier timepoints. However, the expression kinetics continuously increased in mutants at day 7+12 and 7+18 thus preceded unaffected organoids expressions. None of these lines showed significant differences ($p<0.05$). From these data, it was evident that the cAMP induction does not significantly altered the *HNF1B* downstream targets expressions although mutant organoids showed slightly lower expressions of PKD1, PKD2 and PKHD1. I further hypothesised that there could be an association between delayed kidney structure formation in mutant organoids and the cyst outputs which will be discussed in the next section.

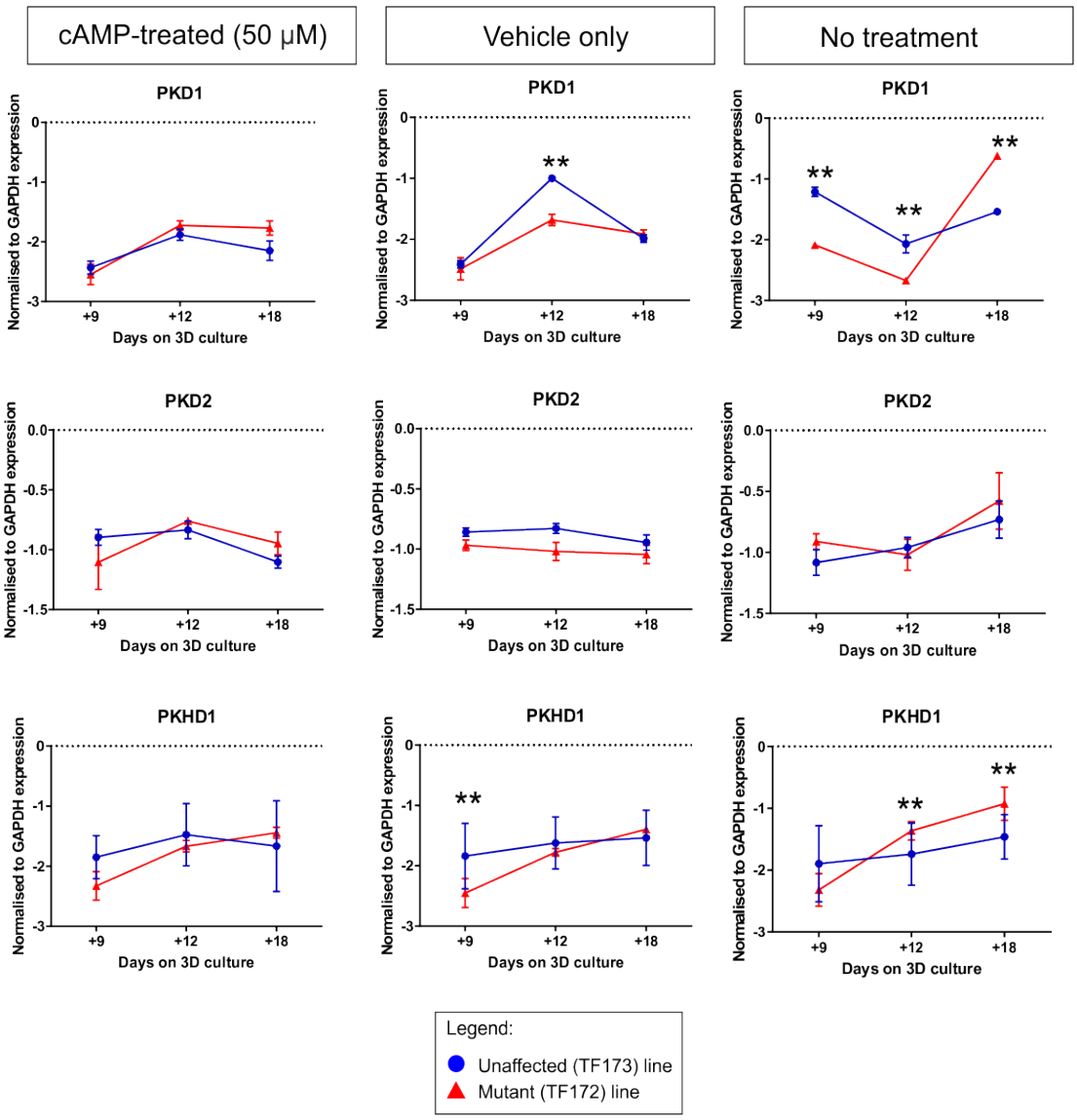

Figure 5.13 Time course of relative expression levels of cystic genes in mutant and unaffected organoids. Left panel showed transcript levels upon addition of 50 µM cAMP. Middle panel displayed vehicle (PBS only) controls and right panel demarcated transcript profiles of untreated control groups. The *HNF1B* downstream targets included *PKD1, PKD2* and *PKHD1* genes. Graph showing expression profiles of both TF172 (mutant) and TF173 (unaffected) lines depicting level of target transcripts normalised to GAPDH expression. Data are presented as mean ± SEM (n = 3 independent experiments). Statistical analysis was performed using one-way ANOVA, **p < 0.05, ***p < 0.001.

5.2.6 *HNF1B*-derived organoids diminished response to cAMP stimulation may be cased by insufficient mature tubular elements

From Chapter 4, it was evident that mutant organoids had delayed generation of kidney structures with reduced complexity. To prove whether these were replicated in the cAMP-treated organoids, I collected mutant and unaffected organoids at day 7+18 and stained with CUBN (proximal marker) as an indicator of early tubule formations. From the immunostainings (Figure 5.14), it was found that the unaffected organoids (TF173) formed relatively bigger cyst diameter, lined with a thin layer of epithelial cell that was positive for CUBN staining on the outer layer suggesting proximal tubule identity. These cyst-like structures surrounded a hollow lumen. It

was also observed that some of the developing tubules were not affected and remained elongated. On the other hand, the mutant organoids (TF172) revealed smaller cyst diameters and fewer cysts. These cysts were surrounded by CUBN+ structures that appeared to demarcate immature kidney tubules. The untreated controls revealed formation of proximal tubules without any cyst formations. It was also observed that none of these cysts were found in the developing glomeruli of either lines.

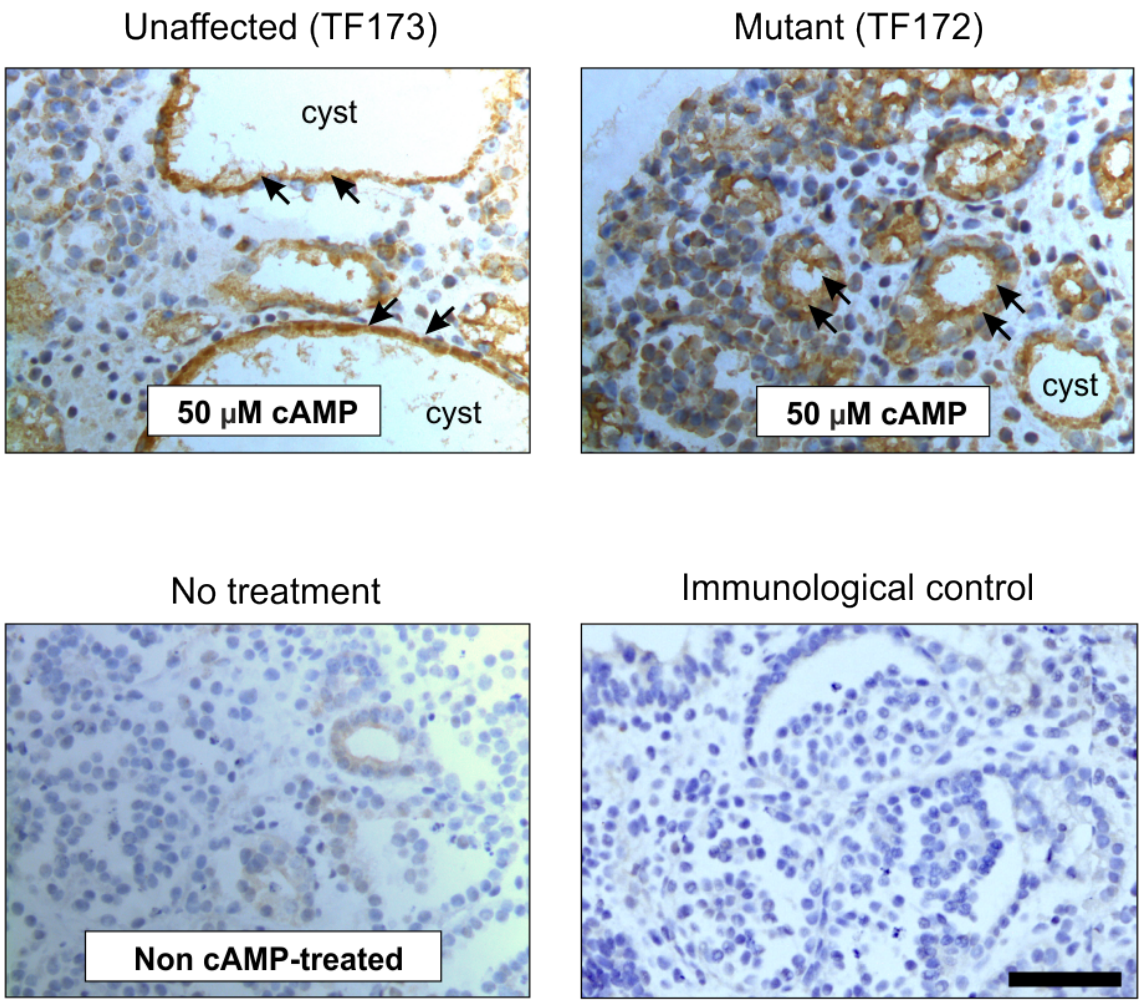

Figure 5.14 Immunostaining of day 7+18 organoids for CUBN (brown staining). Both mutant (TF172) and unaffected (TF173) organoids were treated with 50 µM 8-Br-cAMP commencing day 7+7. TF173 responded earlier to cAMP treatment and showed larger cyst diameter as compared to TF172. Non-cAMP treated organoids displayed normal tubular identities without any cyst formation. Arrows indicated cysts formation. Scale bar, 100 µm.

From the histological assessments, it was evident that the mutant organoids suffered from insufficient number and immature early tubules as compared to unaffected organoids. It was reported that the functioning tubules are essential in normal transport of electrolytes and has been shown to regulate uptake and efflux of transporters (Lawrence et al., 2018). To verify whether these developing organoids contained functional tubules, I ran qPCR analysis on the genes associated with tubular elements such as AQP1 (proximal), HNF1B (distal/collecting duct) and OAT1/OAT3 (tubular functions to transport anions). It was found that upon stimulation with cAMP, unaffected organoids increased AQP1 transcripts up to day 7+18 (Figure 5.15). The vehicle and untreated controls revealed similar expression patterns towards the end of culture without any significant differences detected between mutant and unaffected. Interestingly, HNF1B was found to be upregulated in the cAMP-treated unaffected organoids with lower expressions in mutant. However, both lines showed downregulation at day 7+12 onwards. Similarly, the vehicle and untreated controls revealed higher magnitude of HNF1B expression in unaffected organoids as compared to the mutant ($p<0.05$).

In the OAT1 and OAT3 transcript levels, it was revealed that upon cAMP treatment, mutant organoids showed reduced transcript levels as compared to unaffected organoids but at an increasing trend. Vehicle and untreated controls showed slight predomination of OAT1 expression in unaffected over mutants. OAT3 transcripts on the other hand revealed upregulation in unaffected organoids up to day 7+12 before decreased at day 7+18. Mutant organoids in vehicle group showed gradual increase to the end of culture whereas unaffected organoids revealed a sustained expression. Unlike mutant, the unaffected organoids in the untreated control groups peaked at day 7+12 but showed a sudden decrease at day 7+18. Overall, there were significant differences observed in HNF1B transcripts after addition of cAMP between mutant (TF172) and unaffected (TF173) lines, but not in other genes (AQP1, OAT1 and OAT3).

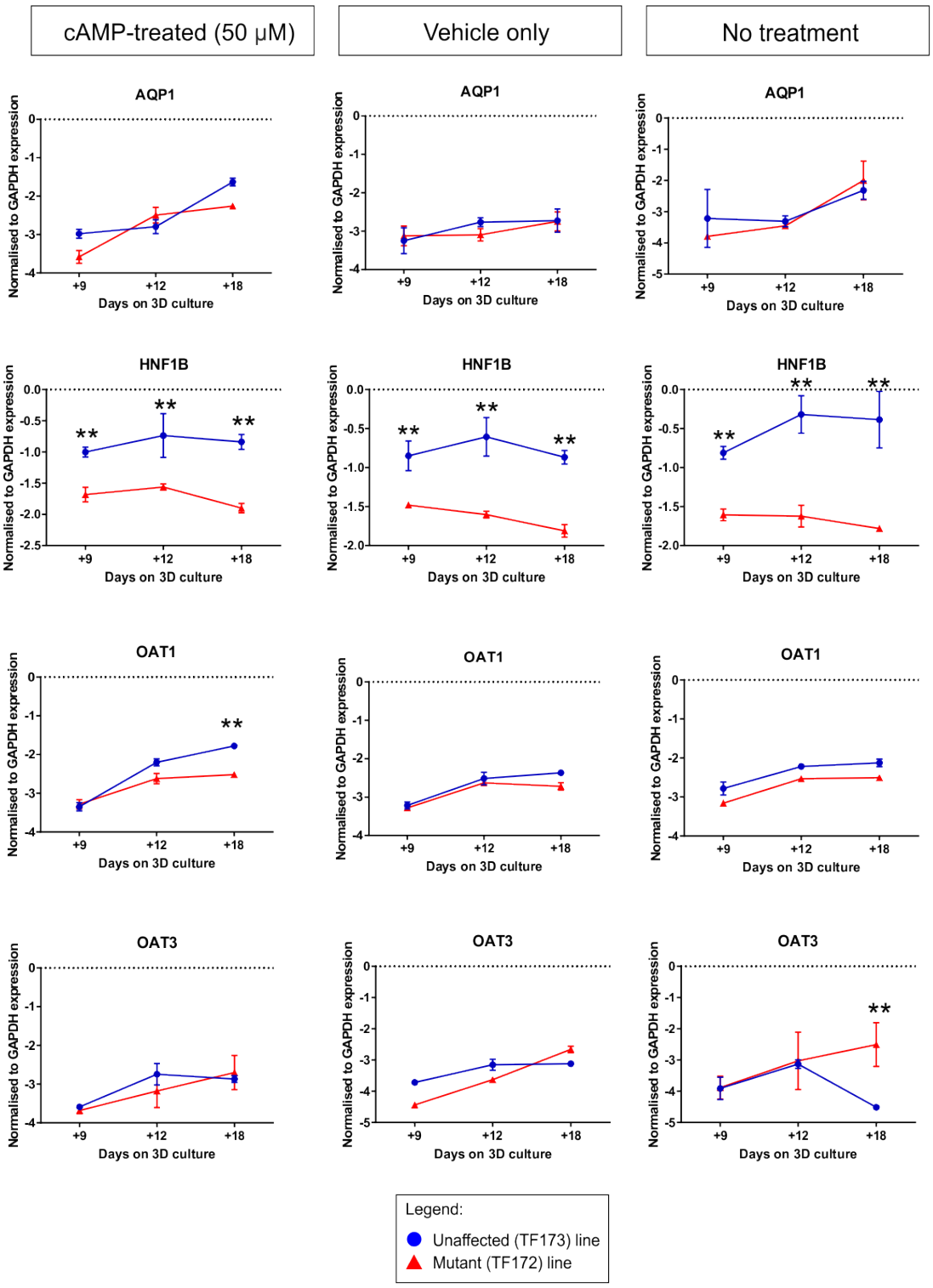

Figure 5.15 Time course of relative expression levels of associated tubular markers in mutant and unaffected organoids. Left panel showed transcript levels upon addition of 50 µM cAMP. Middle panel displayed vehicle (PBS only) controls and right panel demarcated transcript profiles of untreated control groups. Differentiation of cAMP-induced developing kidney was assessed by qRT-PCR representing key tubular genes that include AQP1 (proximal tubules), HNF1B (distal/CD) and OAT1/3 (transporters). Graphs showing expression profiles of both TF172 (mutant) and TF173 (unaffected) lines. Data are presented as mean ± SEM (n = 3 independent experiments). Statistical analysis was performed using one-way ANOVA, **p < 0.05, ***p < 0.001.

5.2.7 Functional LTL+ proximal tubules regulate uptake of exogenous 6CF

Another logical aspect to evaluate efficiency of kidney organoid differentiation is by testing functionality of tubules. To address this issue, I differentiated mutant (TF172) and unaffected organoids (TF173) towards kidney lineage and incubated them with a synthetic anion, 6-carboxyfluorescein (6-CF) to trace the uptake activity by proximal tubule (labelled with rh-PNA). Then, probenecid (an OAT inhibitor)(Lawrence et al., 2018) were added to trap 6-CF fluorophore intracellularly. It was found that when the unaffected organoids were treated with 6CF for 1 hour, the functioning tubules had taken up 6CF into the cells. After 15 min incubation with 10 mM Probenecid, the tubular cells entrapped the 6CF intracellularly. The anion 6CF was transported into rh-PNA+ tubule compartments. However, when the unaffected organoids were incubated for 1 hour in the presence of 2.5 mM Probenecid, none of the 6CF was observed in the differentiating tubules and remained outside of the tubular compartments suggesting the blocking of uptake mechanism (Figure 5.17). A similar observation was reported in the mutant organoids (Figure 5.18). However, some elements that appeared to co-exist with bright green fluorescence without rh-PNA labels were assumed to derive from non-tubular origin and remain to be identified.

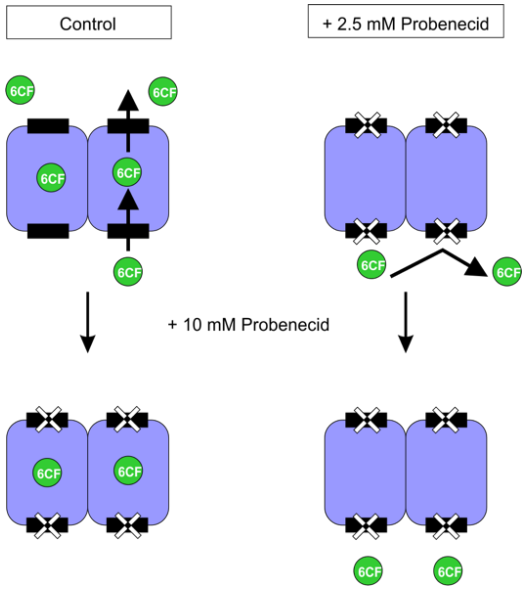

Figure 5.16 Schematic representation of OAT assay using unaffected organoids (TF173) at day 7+18. In treated group, 1 µM 6CF and 2.5 mM probenecid has been added and incubated for 1 hour at 37°C. The control group was incubated with 6CF only (indicated by green sphere). After an hour, both groups were washed and incubated with 10 mM probenecid for 15 min at 37°C to trap intracellular fluorophores. The fluorescence intensity of 6CF for both groups were quantified by inverted confocal microscope.

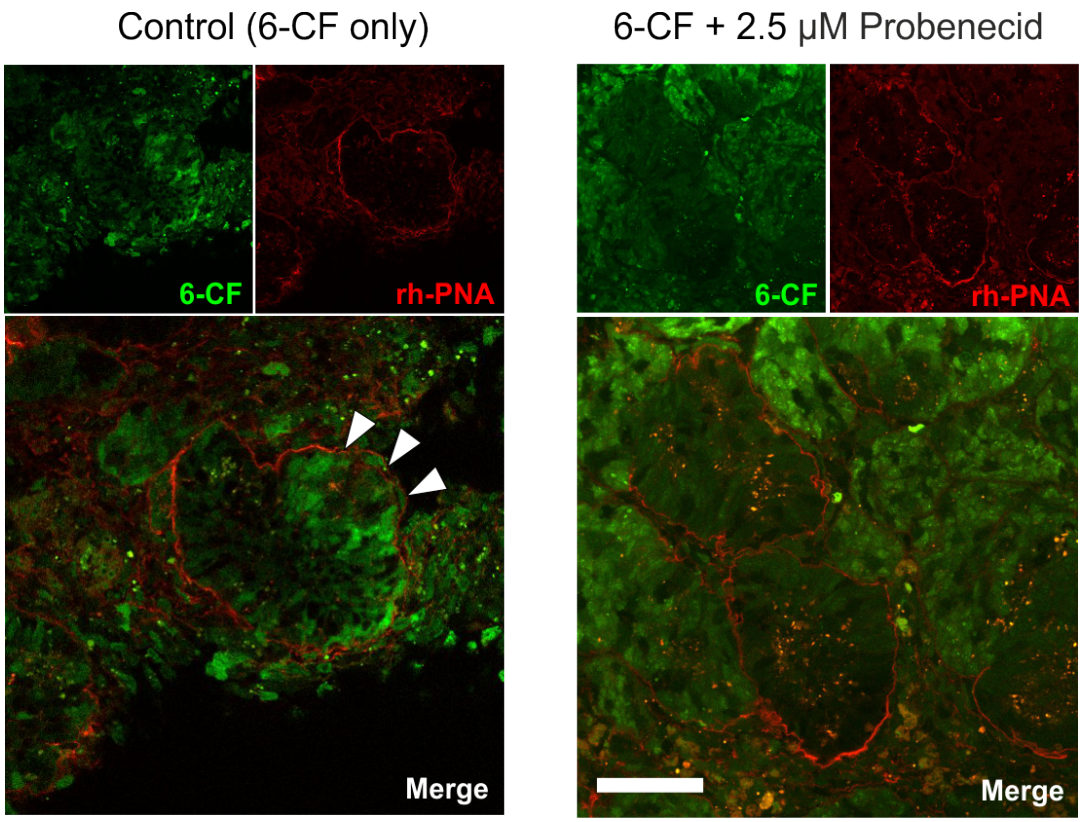

Figure 5.17 Entrapment of 6CF in unaffected organoids (TF173) at day 7+18 of differentiation. (*Left*) Control organoids were incubated with 1 µM 6CF only and incubated for 1 hour at 37°C. After addition of OAT inhibitor, probenecid, 6CF was retained in the tubular compartment indicated by green fluorescence surrounded by rh-PNA (red staining) that demarcated tubular element. (*Right*) Treated group were incubated with 6CF and 2.5 mM probenecid and incubated. After 1 hour, 10 mM probenecid were added for 15 min and the assay showed inhibitory activity that prevented influx of 6CF into tubular compartments. 6CF, carboxyfluorescein, rh-PNA, rhodamine-tagged peanut agglutinin. White arrows indicated location of OAT uptake. Scale bar, 20 μm.

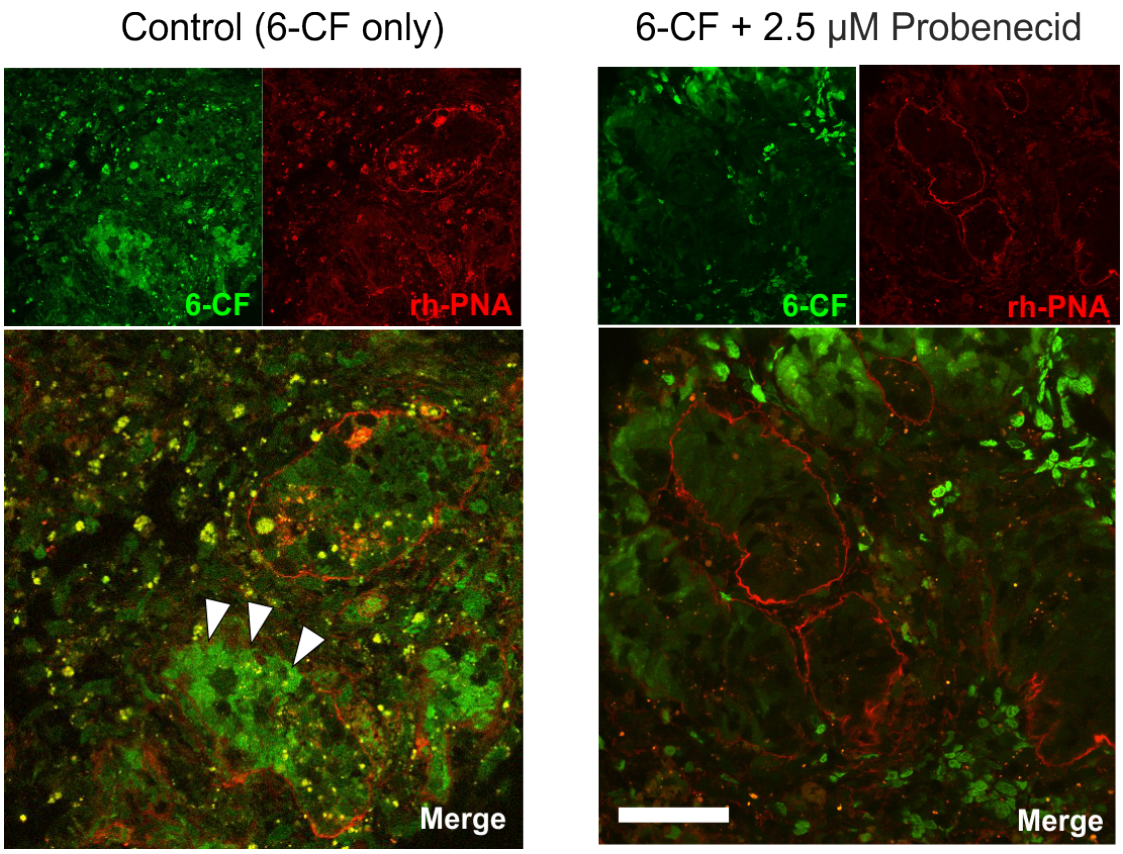

Figure 5.18 Entrapment of 6CF in mutant organoids (TF172) at day 7+18 of differentiation. (*Left*) Control organoids were incubated with 1 µM 6CF only and incubated for 1 hour at 37°C. After addition of OAT inhibitor, probenecid, 6CF was retained in the tubular compartment indicated by green fluorescence surrounded by rh-PNA (red staining) that demarcated tubular element. (*Right*) Treated group were incubated with 6CF and 2.5 mM probenecid and incubated. After 1 hour, 10 mM probenecid were added for 15 min and the assay showed inhibitory activity that prevented influx of 6CF into tubular compartments. 6CF, carboxyfluorescein, rh-PNA, rhodamine-tagged peanut agglutinin. White arrows indicated location of OAT uptake. Scale bar, 20 µm.

5.2.8 Functioning proximal tubule in unaffected organoids showed efflux of anions

After evaluation of OAT uptakes, it was shown that the unaffected organoids at day 7+18 were functioning and capable to facilitate uptake of 6CF intracellularly. To further test whether these tubules can transport the entrapped 6CF into extracellular environments, I examined the efflux of 6CF. From Figure 5.20, it was shown that after 1 hour incubation without Probenecid, tubules that were pre-loaded with 6CF was able to transport 6CF out of the tubules compartment leaving tubules free from 6CF. Interestingly, when 10 mM Probenecid were added, the pre-loaded 6CF were prevented from leaving the tubules. However, there were smaller amount of 6CF that were able to escape the tubules and remained in the non-tubular components. Figure 5.21 revealed that Probenecid blocked efflux of 6CF outside the tubules in mutant organoids, leaving bright green fluorescence in the compartments. The mutant tubules however displayed less expanded phenotypes with reduced lumen diameter as compared to control (6CF only) but does not compromise transport functions.

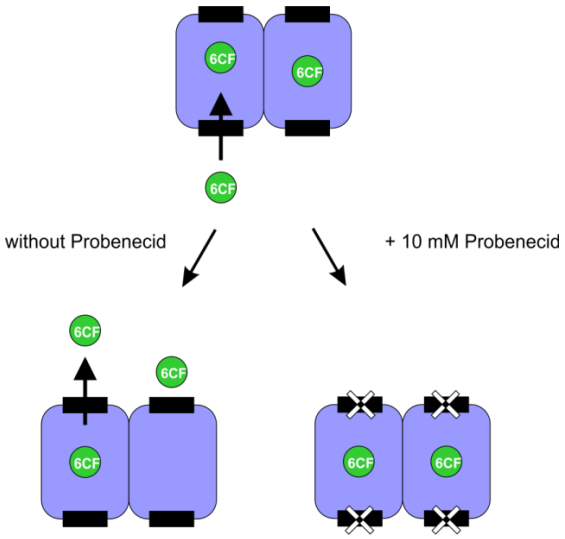

Figure 5.19 Schematic representation of OAT efflux assay using unaffected organoids (TF173) at day 7+18. Organoids were preloaded with 1 μM 6CF in kidney differentiation medium and incubated for 1 hour at 37°C. After washed, organoids were imaged to indicate uptake of 6-CF. Organoids were further incubated with/out 10 mM probenecid for another 1 hour to block anions efflux from the lumen. The fluorescence intensity of 6CF for both groups were quantified by inverted confocal microscope.

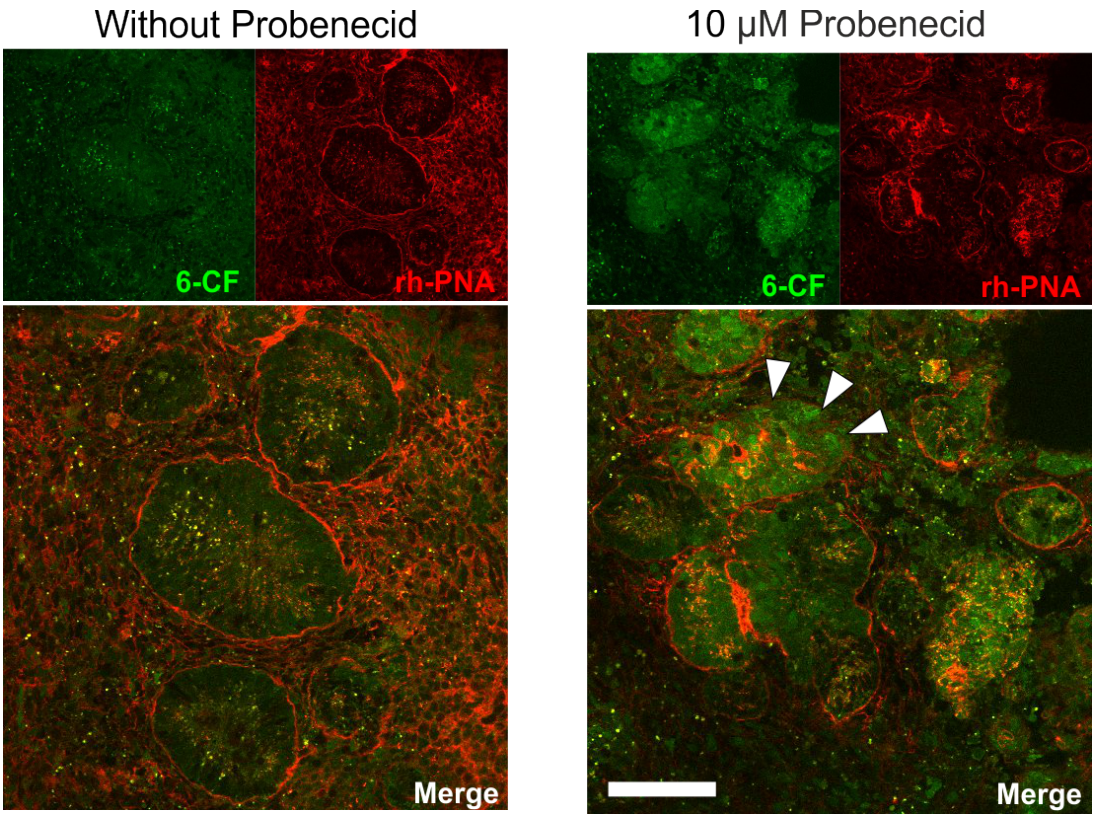

Figure 5.20 Efflux activity of 6CF in unaffected organoids (TF173) at day 7+18 of differentiation. (*Left*) Organoids were treated with 1 μM 6CF supplemented in the kidney differentiation medium and were incubated. After 1 hour, organoids were visualised to confirm uptake of 6CF. Organoids with positive uptake of 6CF were further incubated without presence of inhibitor. Merge image showed absence of 6CF in tubular compartments that suggested transport of 6CF outside the lumen (*Right*) After confirmation of 6CF uptake, organoids were further incubated with 10 mM probenecid. The organoid's tubule displayed green fluorescence inside tubule that suggested entrapment of 6CF due to inhibitory action of probenecid on OAT. 6CF, carboxyfluorescein, rh-PNA, rhodamine-tagged peanut agglutinin. White arrows indicated location of OAT uptake. Scale bar, 20 μm.

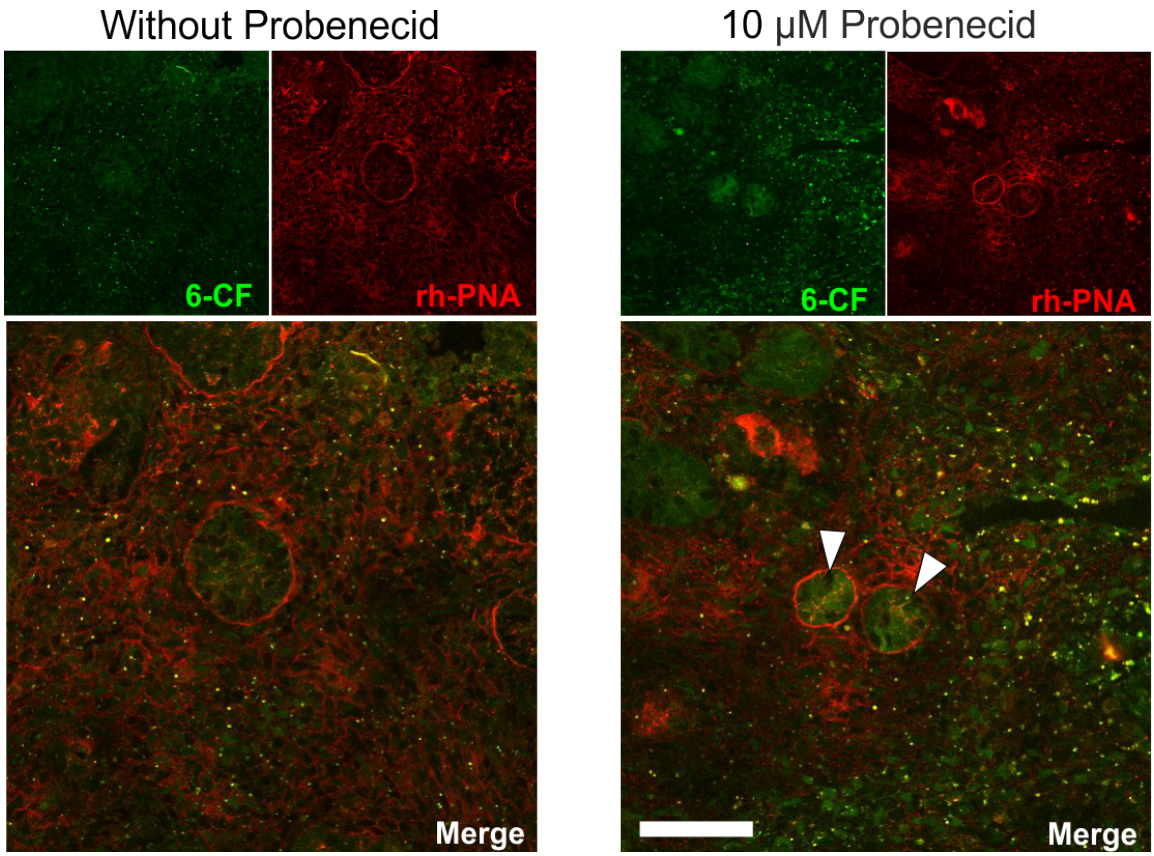

Figure 5.21 Efflux activity of 6CF in mutant organoids (TF172) at day 7+18 of differentiation. (*Left*) Organoids were treated with 1 µM 6CF supplemented in the kidney differentiation medium and were incubated. After 1 hour, organoids were visualised to confirm uptake of 6CF. Organoids with positive uptake of 6CF were further incubated without presence of inhibitor. Merge image showed absence of 6CF in tubular compartments that suggested transport of 6CF outside the lumen (*Right*) After confirmation of 6CF uptake, organoids were further incubated with 10 mM probenecid. The organoid's tubule displayed green fluorescence inside tubule that suggested entrapment of 6CF due to inhibitory action of probenecid on OAT. 6CF, carboxyfluorescein, rh-PNA, rhodamine-tagged peanut agglutinin. White arrows indicated location of OAT uptake. Scale bar, 20 µm.

5.3 Discussion

5.3.1 Mature proximal tubules effectively promote cystogenesis in cAMP-mediated culture

In the cystic experiments, a synthetic non-degradable, synthetic cAMP analogue (8-Br-cAMP) has been used to introduce swelling in the unaffected organoids. cAMP has been associated with development of cysts in PKD patients and shown to promote fluid retentions in the epithelia of non-PKD kidneys (Magenheimer et al., 2006). It was shown that the unaffected organoids revealed relatively higher cyst count as compared to mutant. This condition could be due to reduced amounts of mature tubular elements in the mutant. It was reported that the unaffected organoids can also respond to Forskolin, another powerful adenylyl cyclase agonist that was reported to induce faster generation of cyst-like appearances while retaining the shape of tubular elements (Cruz et al., 2017).

During cAMP treatments, these unaffected organoids showed greater response to the serial cAMP stimulations by forming greater diameter and earlier emergence (day 7+11) of cyst-like structures. However, the mutant-derived cysts can only be observed as early as day 7+14. This could be due to an indirect effect of *HNF1B* mutation on the generation of mature tubular elements turning cyst less pronounced. These results correlated with data reported in a previous chapter that the mutant organoids displayed less mature and delayed tubulogenesis. In fact, it was confirmed that the proximal tubules are essential target of cAMPs due to positive CUBN staining on the outer linings of cysts. However, some findings reported that the CD were regarded as the primary target in cAMP-mediated therapeutics (Gattone Ii et al., 2003) which are subjected to further examinations.

When the mutant and unaffected organoids were exposed to an increasing dose of cAMP, no differences were detected within organoids (in each line, either TF173 or TF172) in any of the dose. However, significant differences were observed in cyst count between mutant and unaffected organoids. The increasing dose neither increased nor deteriorated the cysts in either of the organoids. This showed that the dose was only slightly differed and alternative approach is required to gauge the severity of cystic features. Instead of increasing the 8-Br-cAMP concentration alone, the current protocol can be further improved by addition of other chemical agent such as dexamethasone or forskolin that can activate adenylate cyclase thus increase intracellular cAMP levels. It was reported that synergistic combination of 470 nM dexamethasone and 100 mM 8-Br-cAMP showed 50% increase in cysts per explant area in E13 metanephroi (Anders et al., 2013).

In this study, it was found that *HNF1B*-derived kidney organoids failed to dilate and expand proximal tubules upon cAMP treatments. Moreover, extending the cAMP treatments rendered them only minimally cystogenic. It was suggested that the lesser number of differentiating proximal tubules have reduced the susceptibility to cAMP-induced cystogenesis. It was shown that unaffected organoids preceded mutant with the first emergence of cyst observed after 4 days of induction although other reports suggested that the addition of 8-Br-cAMP can induce tubule expansion within 1 day of exposure (Magenheimer et al., 2006). The current findings were supported by the emergence of cysts in mouse embryonic kidney after 3-6 days of cAMP treatment affecting proximal nephron segments (Anders et al., 2013).

The delayed and less effective response to cAMP in mutant organoids suggested lack of mature developing tubules. This was in contrast to another study that reported hypersensitivity of *Pkd1* knockout mouse models to the cAMP-induced proximal tubules (Magenheimer et al., 2006). Interestingly, human ARPKD with *PKD1* mutation studies have suggested the involvement of proximal tubules in cystic formations

evidenced by positive CUBN staining on epithelial cells that surrounded cysts (Ahrabi et al., 2009; Nakanishi et al., 2000; E. Potter, 1972) which seemed to reflect the current findings. In contrast, older ARPKD and ADPKD patients tended to develop cyst in CD (Grantham et al., 1987; Nakanishi et al., 2000).

Apart from that, the number of developing glomeruli that affected by the glucocorticoids should be measured. This data can be used to estimate the maturation state of nephron segments and whether the cyst can affect glomeruli morphologies. The question however remained to be tested in an organoid model although mouse explant culture treated with 8-Br-cAMP has revealed reduced glomeruli counts (Anders et al., 2013). Furthermore, prolonged culture up to day 7+25 has confirmed that cysts in mutant organoids neither increased in number or size. In fact, an increase in the central dark area of mutant organoids treated with 200 μM cAMP suggesting increased cell death. However, the current finding can be further evaluated by apoptosis and proliferation assays that has been shown to implicate in polycystic kidney disease (PKD) (Cruz et al., 2017).

5.3.2 Regulation of anion transports in kidney organoids

It was reported that most mammalian mesonephros contain excretory functions possibly due to presence of tubules and glomeruli that are well-developed (Lawrence et al., 2018). Some earlier studies suggested direct transport across tubules but limited number of studies reported tubular functions in kidney organoids. In this study, tubular components in unaffected organoids displayed some degree of functions (uptake and efflux of synthetic anions) via inhibitable transporters (OAT1 and OAT4). Unlike unaffected, mutant showed lesser magnitude of transport and could not function efficiently due to less mature tubule structure at day 7+18 of culture. These observations reflected the transcript expression of associated transporters (basolateral OAT1) with higher upregulation seen in the unaffected line treated with 50 μM cAMP (Figure 5.15) as compared to the mutant organoids. However, none of these expression profiles indicated significant differences in OAT3 transcript profiles.

In the anion uptake study, the capabilities of unaffected tubules to transport 6CF intracellularly have suggested functional properties of developing tubular segments. This has been supported by the ability of the tubules to respond to the OAT1 and OAT3 inhibitor, probenecid that inhibit transport of 6CF into tubular cells. In the efflux study, upon treatment with probenecid, the OATs were supressed in the tubules and the efflux of 6CFs from the tubules prevented. This has shown that unaffected tubules responded effectively to blocking agents. However, neither of these observations was reported in the mutant organoids. It was evident that the current data showed active

organic anion transport across the transepithelial compartments and confirmed previous findings that suggest the similar functionalities in intact rudiments. Furthermore, this study is in agreement with a previously reported OAT assay that described functioning tubules in re-aggregated engineered kidney tissue that display transport function mimicking physiological kidney activities (Lawrence et al., 2015; Rak-Raszewska et al., 2012).

Another possibility is that the current organoids system was not be able to represent the mature kidney state as seen in human. Instead, organoids I generated are more likely to recapitulate early development and thus might lack essential transporters for uptake of ions. The upregulation of transcripts associated with uptake and efflux of transporters suggested the reabsorption across epithelial membranes, capabilities to excrete xenobiotics and endogenous materials via transporters localised on apicobasal compartments apart from glomerular filtration functions. These current findings have somehow provided evidence of early tubular transport mechanism in kidney organoids and can be further optimised to recapitulate later stages of kidney differentiations.

5.3.3 Conclusion

It was reported that heterozygous *HNF1B* mutation can phenocopy ADPKD as RCAD (Faguer et al., 2014). PKHD1 and PKD2 (ARPKD genes) are controlled by HNF1B (Gresh et al., 2004) and combination of pathogenic *HNF1B* and *PKD1* allelles may cause PKD progression *in utero* due to alterations in *HNF1B* targets and *PKD1* mutations (Bergmann et al., 2011). It was reported by Desgrange et al. (2017) that *HNF1B* mutations caused defective epithelial organisations and polarity that cause cyst formations with lesser number of cilia. Some studies have suggested that homozygous deletion of exon 2 *HNF1B* lead to failure to generate proximal tubules and TAL segments (Przepiorski et al., 2018) apart from an increase in cell proliferation of cystic epithelia and ureteric dilatations (Hiesberger et al., 2005). However, in this study, organoids that harbour heterozygous *HNF1B* mutation presented minor phenotypic alterations and the mechanism on how these variant lead to the phenotypic spectrum needed further investigation.

Mutations in *PKHD1* gene lead to ARPKD (early onset) whereas heterozygous mutation of *PKD1* and *PKD2* lead to ADPKD (late onset). Interestingly, although ADPKD patients have the same germline mutation, only small subsets were reported to become cystic. This has been explained by the two hit model of cystogenesis where the somatic second hit of the mutation to the normal allele, had cause cyst formation in ADPKD via loss of heterozygosity (Reeders, 1992). For this reason it may be challenging to observe cyst phenotypes in HNF1B-derived kidney organoids and

possibly this can be seen only after a long period of time. It was suggested that ADPKD phenotypes can be detected early in undifferentiated hPSCs or in the organoid culture because the *PKD1* and *PKD2* genes that encoded ciliary proteins were widely present (Van and Frank, 1995). Freedman et al. (2013) revealed that ADPKD-derived cell, had reduced localisation of PC2 to the primary cilium thus suggesting that the normal trafficking of PKD2 to the cilium controlled by normal PKD1 proteins. This study can be used to explain the cause of cyst formations in ADPKD patients. However, further studies needed to ascertain mechanism of cystogenesis caused by decreased PC2 in the cilium.

From the results, it was revealed that the cAMP are cystogenic in both mutant and unaffected organoids but differed greatly in terms of severity and the time of first emergence. The current data showed contradicting results to the one that suggested human (or animal) with cyst-related mutations have higher tendency to enhance and develop cyst (Anders et al., 2013). The reduced cyst in mutant organoids rather indicated the direct effect of cAMP on delayed tubular differentiation than the effect of genetic dispositions. However, the biochemical analysis can be further performed to ascertain the interaction between genetics (that elevated intracellular cAMPs) and the microenvironment factors. The data however can be used to support hypothesis that claim the adverse environmental factors aggravated cyst formations.

Studies by Cruz et al. (2017) reported that the organoid-derived cyst more likely to resemble prenatal PKD that radiated from medulla to the cortex and presented under the nephrogenic zones as seen in the PKD1 patients. However, it was found that cyst generated postnatally displayed smoother peripheral regions with multiple cell layers. This was often accompanied by inflammatory agents and interstitial nephritis which are absent in organoids or prenatal stage. The global gene expression analysis has revealed that there were significant enrichment in genes that control cell cycle progression, MYC activities and mTOR signaling in cystic organoids (Cruz et al., 2017). Another important finding is CRISPR-edited organoids showed unexpected function of myosin in PKD. The non-muscle myosin II inhibitor, blebbistatin has shown to increase cysts in PKD in a dose-dependent manner. It was also suggested that the polycystins can function normally to activate actomyosin in the tubular epithelium, tightening and strengthening tubular elements thus prevented deformation to cysts (Czerniecki et al., 2018).

It might be challenging to recapitulate clinical manifestations of renal tract malformations particularly in the formation of cysts due to expansion of tubular epithelia using hiPSC-derived kidney organoids. This is because HNF1B is thought to be affected by somatic loss of heterozygosity (second hit hypothesis)(Reeders,

1992). Due to longer time needed for HNF1B-related disease to express the phenotypes, alternative approaches such as genome editing can be used to reproduce the clinically relevant disease models. Freedman et al. (2013) showed that a biallellic, truncating mutation of PKD1/PKD2 in hESCs, generated large, free-floating cyst-like features upon differentiation to kidney organoids. These cysts tethered to the underlying matrix but easily sensitised to vibrations as compared to non-cystic tubular elements that remained fixed. The group however reported that only 6% of the CRISPR-edited kidney organoids showed cystic appearances (Freedman et al., 2015).

The current study can be used as early evidence to demonstrate the potential of hPSC to model renal tract malformations. Although the variabilities often reported between runs and lines used in the differentiation, the current data at least has provided some insights on the effects of environmental factors. In conclusion, addition of exogenous 8-Br-cAMP in an organoid model has established beneficial cell system that can model renal tract malformations. Comparison between the effects of unaffected and mutant organoids has suggested essential role of microenvironment in altering cystic pathogenesis. Although it was proposed that HNF1B mutation may intensify the cystic phenotypes, as reported by several studies, this condition however was not observed in these studies that suggested the need of further refinement of differentiation protocols. Together, these data can potentially be used in mechanistic studies and therapeutics although deeper understanding on the organoid disease model is needed before being used as a tool to develop personalised medicines.

Chapter 6 Discussion

6.1 Main findings

The kidney functions to regulate osmolality and body fluid volume through a feedback mechanism that controls blood's pH and solute concentrations apart from waste removal. Failure of kidney to maintain this homeostasis can lead to functional abnormalities thus new approach to regenerate, repair and replace faulty kidney is utmost important. In the previous 4 years, I embarked on a study attempting to generate kidney tissues from pluripotent stem cells with special focus on organogenesis and progression of HNF1B-associated kidney disease. In fact, several studies have shown that hPSC-derived kidney organoids can self-organise and morphologically resemble nephron structures as seen in mammalian kidney. The stochastic approach of differentiation towards kidney lineages, so far, however revealed mixed populations with presence of non-nephron specific cells and immature phenotypes. In this project, I showed that hPSCs can be used a cell source to recapitulate kidney development *in vitro* despite few challenges that remained to be addressed. Here, I listed the important findings generated from this study.

6.1.1 PBMCs from HNF1B affected patients can be used to derive pluripotent stem cells

Characterisation is an essential key step to clearly define hPSCs population and evaluate pluripotency. I have described characterisation of hPSCs (MAN13 and HNF1B-derived hiPSCs) in details that include hPSC genetic analysis for karyotypic integrity, differentiation potential by EB formation, integration-free hiPSCs assessment and pluripotency test using flow cytometry, immunostainings and qPCR. In the earliest phase of the study, I successfully reprogrammed 2 lines that harbour *HNF1B* mutation (TF171 and TF172) and a line with no mutation (TF173). These lines are derived from blood taken from same family. The *HNF1B* mutations lead to deletion of exon 9 that caused cystic dysplastic kidney detected antenatally. The advent of stem cell research has allowed generation of hiPSC from patient with kidney diseases thus enabled development of immunocompatible patient-specific models. In this project, I maintained and passaged these hPSC lines up to passage 20 in a defined serum-free medium. It was shown that all these 3 lines are pluripotent and capable of self-renewal. Based on the characterisations, these lines are vector-free, karyotypically normal and can differentiate into 3 germ layers. Thus, these lines were utilised in directed differentiation towards kidney lineages with the aim to generate kidney tissues that can morphologically and functionally resemble human kidney.

6.1.2 Three dimensional organoids can recapitulate early kidney developments

I reported that *de novo* generation of 3D kidney organoids *in vitro* via directed differentiation of HNF1B-derived iPS lines resulted in lesser degree of structure complexity, increased diameter per organoid and lower expression of key kidney marker genes as compared to wild type organoids that contained epithelial nephron-like structures expressing markers of podocyte (WT1, NPHS1, NPHS2 and SYNPO) and surrounded by a Bowman space and capsule that resembles nephron *in vivo*. Deeper in the generated kidney organoid, we detected a variety of tubules, often $HNF1B^{+}/ECAD^{+}$ and $PAX2^{+}/ECAD^{+}$. Some were most likely to be in the ureteric bud/collecting duct lineage (e.g. $GATA3^{+}/ECAD^{+}$, $AQP2^{+}$), while others were proximal tubules ($HNF1A^{+}/CUBN^{+}$) or loops of Henle ($UMOD^{+}$) in the nephron lineage. The hiPSC-derived kidney organoids revealed tubular functions that can transport organic anion mimic, 6CF intra- and extracellularly. Inhibition of OAT by probenecid demonstrated physiological function of developing kidney tubules generated in 3D organoids. When HNF1B-affected lines were differentiated to kidney organoids, none of them showed cyst formation even in the extended culture (up to day 7+25). Interestingly, when these organoids were challenged with cAMP, both lines can respond by generating cyst-like structure with delayed formation in the HNF1B-affected lines. This suggested that the current differentiation protocol needed to be optimised in a way that can sustain organoids at longer time before cyst can be evaluated.

6.1.3 Morphological differences between mutant and healthy organoids

The morphometric assessments have delineated unique features of mutant organoids when compared with unaffected lines. The overall organoid's architecture of mutant display lesser degree of complexity and twice the diameter of unaffected organoids. The failure of mutant organoids to vertically regionalise presumably lead to a flatter morphology. Expanded images of mutant organoids at higher magnifications revealed dilated tubules and multiple layer organisations whereas unaffected organoids comprised of extensive tubular elongations. Furthermore, it was shown that the lumen diameter of mutant-derived epithelial tubules appeared wider and could be due to expansion of cells. However, in both cases, endothelial invasions into glomerular tufts are rare occurrances. Therefore, it can be concluded that, although there are distinct morphological differences observed between mutant and unaffected organoids, whether abnormal dysmorphic glomeruli and multi-layered tubules in mutant organoids are direct consequences of delayed nephron specification due to HNF1B mutation are remain to be elucidated.

6.1.4 Effects of cAMP in cyst formation

It was shown that the mutant organoids revealed relatively lower cyst count as compared to unaffected organoids. This condition could be due indirect effect of *HNF1B* mutation leading to reduced number of mature tubular elements as seen in CUBN staining. Stimulation of organoids with cAMP analogue renders these mutant organoids by forming lesser cyst diameter, reduced cyst counts and delayed cyst emergence (day 7+14) as compared to healthy, which can be detected as early as day 7+11. It was confirmed that the proximal tubules are essential target of cAMPs due to positive CUBN staining on the outer linings of cysts and lesser number of differentiating proximal tubules have reduced the susceptibility to cAMP-induced cystogenesis. These results have supported the data reported in a previous chapter that mutant organoids comprise of less mature tubules due to delayed tubulogenesis. In fact, the mutant organoids failed to dilate and expand proximal tubules upon cAMP treatments. The increasing 8-Br-cAMP doses however do not affect any of these organoids. This showed that the dosage differences were only slightly effective and alternative approach is required to gauge the severity of cystic features. Moreover, extending the cAMP treatments rendered them only minimally cystogenic. Prolonged culture up to day 7+25 has confirmed that cysts in mutant organoids neither improve number or size of cysts but indicated greater signs of cell death.

6.2 Future work

The current study has reported essential information regarding the effects of HNF1B mutation on kidney organoids and able to answer my hypothesis. It is however noted that there are many other challenges needed to be overcome in order to generate bio-functional kidney before they can be used in clinical settings. The current study has answered few important questions associated with growing a kidney in a dish and can be further optimised to recapitulate kidney development or modeling cystic dysplastic kidney disease. It was noted that before these organoids can be used in clinical settings as a regenerative tool, few considerations need to be addressed. Here, I listed some suggested work that can be done to improve and rectify the current study.

6.2.1 Maturation of kidney organoid's structure

Maturation is a big challenge due to presence of multi-structural entities in the organoid's culture such as CD, nephrons, vascular and stroma. Mature organoids can sustain and model functional aspect of the kidney due to presence of capillaries. Kidney organoids should be differentiated in a way that promote vascularisations and able to facilitate blood flow from renal arteries to veins. Our publication revealed the

presence of CD31+ networks surrounding the outer compartment of glomeruli but these capillaries were found to rarely invade the glomerular tufts (Bantounas et al., 2018). It was also reported that hPSC-derived podocytes can promote glomeruli vascularisations when transplanted into murine renal subcapsular space (Sharmin et al., 2016). However, absence of capillary loops in the glomeruli has limited the blood filtration properties. Similar observations were discussed in some other reports (Freedman et al., 2015; Takasato et al., 2016; Takebe et al., 2015; Van Den Berg et al., 2018). Recently, Garreta et al. (2019) showed that implantation of day 16 organoids on 7 day-old chick chorioallantoic membrane (CAM) *in ovo* for 5 days revealed formation of multiple blood vessels followed by circulation of chick blood in organoids. Live imaging of FITC-dextran (fluorescein isothiocyanate) in CAM confirmed the grafting of kidney organoids. Thus, further studies are necessary to initiate, incorporate or enhance vascular systems, not only in the cortical but also considering the maturation of medullary regions.

6.2.2 Functioning proximal tubules

Proximal tubules marked as the best target for nephrotoxicity screening due to presence of anion, cation (SLC22 gene family) and multidrug resistance transporters (ABCB1, ABCG2)(Koepsell, 2013; Robinson et al., 2019). One way to test functionalities of proximal tubule was by treating organoids with nephrotoxicant such as Cisplatin. It was found that overnight treatment can induce caspase-mediated apoptosis in mature proximal tubules (Garreta et al., 2019). In fact, Bantounas et al. (2018) reported that injection of 10 kDa FITC-labeled Dextran suggested that it was filtered by glomeruli before reclaimed by proximal tubules. The current study has proved that the CUBN-positive proximal tubules were able to facilitate uptake of anions, both in the HNF1B-affected and unaffected lines. These tubules were able to retain 6CF fluorescence and transport them to the outside sub-compartments. However, the transport of cations into tubules revealed unconvincing results. When the organoids were incubated in the presence of OCT inhibitors (Cimetidine and Metformin), there were lesser degree of positive nuclear stainings retained in the tubules. Most of the DAPI+ nuclei resided on the outer surface of tubules with minimum intracellular stainings. This is an indication of immature state of proximal tubules thus further studies can focus on maturation and assessing capabilities of proximal tubules to facilitate uptake of Cisplatin via OCT.

6.2.3 Gene edit of hiPSC to create isogenic lines

The advent of CRISPR/cas9 genetic editing has allowed generation of isogenic pairs intended for disease modelling. hiPSCs has been utilised due to its unlimited expansion and clonal growth (Hockemeyer and Jaenisch, 2016). With CRISPR, the

genetic background can be replicated as in the healthy parental control lines. It was proposed that genetic background can dominate over variation in cell origin or reprogramming procedures. Thus, the best approach to analyse CRISPR modifications was to use hPSCs with the same genetic background as non-mutated controls (isogenic). In this regard, the CRISPR/Cas9 edited lines can be compared with the patient-derived HNF1B lines in order to recapitulate disease phenotypes. Also, this approach can be used to correct HNF1B mutation and rescue the phenotypes. However, in this study, HNF1B mutation has led to deletion of the last exon (exon 9). This is challenging as these lines may contain a stop codon that can send mRNA to non-sense mediated mRNA decay (NMD) thus complicated the gene editing processes (Lejeune and Maquat, 2005). Instead, CRISPR/Cas9 can be used to target earlier exons (in this case exon 2 or 4) that have been shown to be the most affected exons. In addition, CRISPR/Cas9 can be used to insert fluorescent proteins in order to assess viability, cellular identity, lineage tracing as well as functional properties (Boreström et al., 2018; Howden et al., 2018).

6.2.4 Cystic kidney model

It was noted that cysts can affect both glomeruli and tubular functions. Glomeruli that contain cyst often regarded as the result of experimental urine flow obstruction (Tarantal et al., 2001; Yang et al., 2001) and genetic factors that lead to RCAD syndrome dispositions such as RCAD (Bingham et al., 2001). It was proposed that glomeruli is susceptible to cystogenesis and worsen in the addition of glucocorticoids but this is remained to be tested in organoid culture (Anders et al., 2013). However, in the current study, no cyst were observed in the glomeruli and better model of cystic phenotypes need to be considered. In fact, cyst formations in human with *HNF1B* mutations are more likely to affect CD than proximal tubule which is not seen in this study. Also, instead of increasing the 8-Br-cAMP concentration alone, the current protocol can be further improved by addition of other chemical agent such as dexamethasone or forskolin that can activate adenylate cyclase thus increase intracellular cAMP levels. Furthermore, method to enhance CD formation that can sustain organoids for longer period of time is necessary. Alternatively, transplantation of cAMP-induced developing organoids *in vivo* would be the most practical approach to begin with.

6.3 Concluding remarks

This project has described utilisation of hPSCs to recapitulate human genetic kidney malformations caused by HNF1B. This *in vitro* culture system can be used as a tool to model early onset kidney diseases. The resulting organoids however limited to less than 100 nephron units unlike human kidney that contain 1-2 million nephrons. The

organoids length ratio is approximately 1:12 as compared to native kidney and did not show patterning of cortex or medullae region. The absence of renal pelvis or ureter further complicates urine flow. Analysis of HNF1B-affected lines in-parallel with healthy cells has concluded that there are morphological and functional differences observed apart from gene expression alterations. Given that both patients had cystic dysplastic kidneys, the current organoid model does not recapitulate that type of developmental cyst formation. Organoids probably needs a longer culture period as well as *in vivo* platforms to generate dysplastic cysts. However, challenging organoids with cAMP has revealed tubule dilatation which is a normal feature in healthy organoids and the fact that it is severely decreased in HNF1B-affected organoids which indicated that those nephron tubules, although present, are lacking in functionality.

Based on differentiation, transcript profiles and functional analysis, the current organoids possibly resembled mesonephric kidney stage or 10-20-week of human gestations. It is however recognised that pronephros and mesonephros comprised of immature nephrons during kidney development (Georgas et al., 2011) thereby transcriptional profiling of these early structures need to be compared with profiles generated from current 3D organoids apart from functional characterisations. Differentiation protocol in generating MM lineage is well established and can be used to model either tubular or glomerular diseases. However, protocol to generate UB lineage that can form functioning CD systems need to be developed in order to complement nephron functions. Although the current organoids represent an immature kidney system, understanding of molecular mechanism of organogenesis by gene expression profiling can be applied to enhance maturation and create higher order kidney structures.

In conclusion, these findings have successfully shed some light on early kidney developments although issues related to reproducibility and robustness of the protocols should be continuously highlighted. It was observed that expression profiles of organoids cultured within differentiation batch are more congruent to each other than organoids grown inter-experimentally, primarily in genes related to temporal developments. Thus, variation between experimental batches, safety concerns (tumor formation) and quality control should be addressed in disease modelling attempts before permitting utility of kidney organoids in functional genomics and regenerative medicine.

Bibliography

Adalat, S., Woolf, A. S., Johnstone, K. A., Wirsing, A., Harries, L. W., Long, D. A., Hennekam, R. C., Ledermann, S. E., Rees, L. & van't Hoff, W. (2009). 'HNF1B mutations associate with hypomagnesemia and renal magnesium wasting', *Journal of the American Society of Nephrology,* 20(5), pp. 1123-1131.

Ahrabi, A. K., Jouret, F., Marbaix, E., Delporte, C., Horie, S., Mulroy, S., Boulter, C., Sandford, R. & Devuyst, O. J. N. D. T. (2009). 'Glomerular and proximal tubule cysts as early manifestations of Pkd1 deletion', 25(4), pp. 1067-1078.

Ahrabi, A. K., Terryn, S., Valenti, G., Caron, N., Serradeil-Le Gal, C., Raufaste, D., Nielsen, S., Horie, S., Verbavatz, J.-M. & Devuyst, O. J. J. o. t. A. S. o. N. (2007). 'PKD1 haploinsufficiency causes a syndrome of inappropriate antidiuresis in mice', 18(6), pp. 1740-1753.

Alenghat, F. J., Tytell, J. D., Thodeti, C. K., Derrien, A. & Ingber, D. E. J. J. o. c. b. (2009). 'Mechanical control of cAMP signaling through integrins is mediated by the heterotrimeric Gαs protein', 106(4), pp. 529-538.

Anders, C., Ashton, N., Ranjzad, P., Dilworth, M. R. & Woolf, A. S. J. P. o. (2013). 'Ex vivo modeling of chemical synergy in prenatal kidney cystogenesis', 8(3), p. e57797.

Anders, C., Niewoehner, O., Duerst, A. & Jinek, M. (2014). 'Structural basis of PAM-dependent target DNA recognition by the Cas9 endonuclease', *Nature,* 513(7519), pp. 569-573.

Armstrong, J. F., Pritchard-Jones, K., Bickmore, W. A., Hastie, N. D. & Bard, J. B. (1993). 'The expression of the Wilms' tumour gene, WT1, in the developing mammalian embryo', *Mechanisms of development,* 40(1-2), pp. 85-97.

Aschauer, L., Carta, G., Vogelsang, N., Schlatter, E. & Jennings, P. (2015). 'Expression of xenobiotic transporters in the human renal proximal tubule cell line RPTEC/TERT1', *Toxicology In Vitro,* 30(1), pp. 95-105.

Avilion, A. A., Nicolis, S. K., Pevny, L. H., Perez, L., Vivian, N. & Lovell-Badge, R. (2003). 'Multipotent cell lineages in early mouse development depend on SOX2 function', *Genes & development,* 17(1), pp. 126-140.

Banales, J. M., Masyuk, T. V., Gradilone, S. A., Masyuk, A. I., Medina, J. F. & LaRusso, N. F. J. H. (2009). 'The cAMP effectors Epac and protein kinase a (PKA) are involved in the hepatic cystogenesis of an animal model of autosomal recessive polycystic kidney disease (ARPKD)', 49(1), pp. 160-174.

Banizs, B., Komlosi, P., Bevensee, M. O., Schwiebert, E. M., Bell, P. D. & Yoder, B. K. J. A. J. o. P.-C. P. (2007). 'Altered pHi regulation and Na+/HCO3− transporter activity in choroid plexus of cilia-defective Tg737 orpk mutant mouse', 292(4), pp. C1409-C1416.

Bantounas, I., Ranjzad, P., Tengku, F., Silajdžić, E., Forster, D., Asselin, M.-C., Lewis, P., Lennon, R., Plagge, A. & Wang, Q. (2018). 'Generation of functioning nephrons by implanting human pluripotent stem cell-derived kidney progenitors', *Stem Cell Reports,* 10(3), pp. 766-779.

Barak, H., Huh, S.-H., Chen, S., Jeanpierre, C., Martinovic, J., Parisot, M., Bole-Feysot, C., Nitschké, P., Salomon, R. & Antignac, C. (2012). 'FGF9 and FGF20 maintain the stemness of nephron progenitors in mice and man', *Developmental cell,* 22(6), pp. 1191-1207.

Barbacci, E., Reber, M., Ott, M.-O., Breillat, C., Huetz, F. & Cereghini, S. (1999). 'Variant hepatocyte nuclear factor 1 is required for visceral endoderm specification', *Development,* 126(21), pp. 4795-4805.

Barisoni, L., Kriz, W., Mundel, P. & D'AGATI, V. (1999). 'The dysregulated podocyte phenotype: a novel concept in the pathogenesis of collapsing idiopathic focal segmental glomerulosclerosis and HIV-associated nephropathy', *Journal of the American Society of Nephrology,* 10(1), pp. 51-61.

Batchelder, C. A., Martinez, M. L. & Tarantal, A. F. (2015). 'Natural scaffolds for renal differentiation of human embryonic stem cells for kidney tissue engineering', *PloS one,* 10(12), p. e0143849.

Bayley, N. & Hunt, J. V. (1974). *The Bayley Scales of Infant Development: The First Year*: Psychological Corporation.

Belk, R., Thomas, D., Mueller, R., Godbole, P., Markham, A. & Weston, M. (2002). 'A family study and the natural history of prenatally detected unilateral multicystic dysplastic kidney', *The Journal of urology,* 167(2), pp. 666-669.

Bellin, M., Marchetto, M. C., Gage, F. H. & Mummery, C. L. (2012). 'Induced pluripotent stem cells: the new patient?', *Nature reviews Molecular cell biology,* 13(11), pp. 713-726.

Benetti, E., Artifoni, L., Salviati, L., Pinello, L., Perrotta, S., Zuffardi, O., Zacchello, G. & Murer, L. (2007). 'Renal hypoplasia without optic coloboma associated with PAX2 gene deletion', *Nephrology Dialysis Transplantation,* 22(7), pp. 2076-2078.

Bergmann, C., von Bothmer, J., Brüchle, N. O., Venghaus, A., Frank, V., Fehrenbach, H., Hampel, T., Pape, L., Buske, A. & Jonsson, J. J. J. o. t. A. S. o. N. (2011). 'Mutations in multiple PKD genes may explain early and severe polycystic kidney disease', 22(11), pp. 2047-2056.

Bernstein, J. & Barajas, L. (1994). 'Renal tubular dysgenesis: evidence of abnormality in the renin-angiotensin system', *Journal of the American Society of Nephrology,* 5(2), pp. 224-227.

Bingham, C., Bulman, M. P., Ellard, S., Allen, L. I., Lipkin, G. W., van't Hoff, W. G., Woolf, A. S., Rizzoni, G., Novelli, G. & Nicholls, A. J. J. T. A. J. o. H. G. (2001). 'Mutations in the hepatocyte nuclear factor-1β gene are associated with familial hypoplastic glomerulocystic kidney disease', 68(1), pp. 219-224.

Bingham, C., Ellard, S., Cole, T. R., Jones, K. E., Allen, L. I., Goodship, J. A., Goodship, T. H., Bakalinova-Pugh, D., Russell, G. I. & Woolf, A. S. (2002). 'Solitary functioning kidney and diverse genital tract malformations associated with hepatocyte nuclear factor-1&bgr; mutations', *Kidney international,* 61(4), pp. 1243-1251.

Bingham, C., Ellard, S., van't Hoff, W. G., Simmonds, H. A., Marinaki, A. M., Badman, M. K., Winocour, P. H., Stride, A., Lockwood, C. R. & Nicholls, A. J. (2003). 'Atypical familial juvenile hyperuricemic

nephropathy associated with a hepatocyte nuclear factor-1&bgr; gene mutation', *Kidney international,* 63(5), pp. 1645-1651.
Bingham, C. & Hattersley, A. T. (2004). 'Renal cysts and diabetes syndrome resulting from mutations in hepatocyte nuclear factor-1β', *Nephrology Dialysis Transplantation,* 19(11), pp. 2703-2708.
Bock, C., Kiskinis, E., Verstappen, G., Gu, H., Boulting, G., Smith, Z.D., Ziller, M., Croft, G.F., Amoroso, M.W., Oakley, D.H. and Gnirke, A., 2011. Reference Maps of human ES and iPS cell variation enable high-throughput characterization of pluripotent cell lines. *Cell*, *144*(3), pp.439-452.
Bohn, S., Thomas, H., Turan, G., Ellard, S., Bingham, C., Hattersley, A. T. & Ryffel, G. U. (2003). 'Distinct molecular and morphogenetic properties of mutations in the human HNF1β gene that lead to defective kidney development', *Journal of the American Society of Nephrology,* 14(8), pp. 2033-2041.
Boreström, C., Jonebring, A., Guo, J., Palmgren, H., Cederblad, L., Forslöw, A., Svensson, A., Söderberg, M., Reznichenko, A. & Nyström, J. J. K. i. (2018). 'A CRISP (e) R view on kidney organoids allows generation of an induced pluripotent stem cell–derived kidney model for drug discovery', 94(6), pp. 1099-1110.
Bouchard, M., Souabni, A., Mandler, M., Neubüser, A. & Busslinger, M. (2002). 'Nephric lineage specification by Pax2 and Pax8', *Genes & development,* 16(22), pp. 2958-2970.
Boyden, E. A. (1932). 'Congenital absence of the kidney. An interpretation based on a 10-mm. human embryo exhibiting unilateral renal agenesis', *The Anatomical Record,* 52(4), pp. 325-349.
Boyer, L. A., Mathur, D. & Jaenisch, R. (2006). 'Molecular control of pluripotency', *Current opinion in genetics & development,* 16(5), pp. 455-462.
Braam, S. R., Zeinstra, L., Litjens, S., Ward-van Oostwaard, D., van den Brink, S., van Laake, L., Lebrin, F., Kats, P., Hochstenbach, R. & Passier, R. (2008). 'Recombinant Vitronectin Is a Functionally Defined Substrate That Supports Human Embryonic Stem Cell Self-Renewal via αVβ5 Integrin', *Stem Cells,* 26(9), pp. 2257-2265.
Braun, D. A. & Hildebrandt, F. J. C. S. H. p. i. b. (2017). 'Ciliopathies', 9(3), p. a028191.
Brophy, P. D., Ostrom, L., Lang, K. M. & Dressler, G. R. (2001). 'Regulation of ureteric bud outgrowth by Pax2-dependent activation of the glial derived neurotrophic factor gene', *Development,* 128(23), pp. 4747-4756.
Brown, T., Mandell, J. & Lebowitz, R. L. (1987). 'Neonatal hydronephrosis in the era of sonography', *American Journal of Roentgenology,* 148(5), pp. 959-963.
Brunskill, E. W., Aronow, B. J., Georgas, K., Rumballe, B., Valerius, M. T., Aronow, J., Kaimal, V., Jegga, A. G., Grimmond, S. & McMahon, A. P. (2008). 'Atlas of gene expression in the developing kidney at microanatomic resolution', *Developmental cell,* 15(5), pp. 781-791.
Calvet, J.P., 2015. The role of calcium and cyclic AMP in PKD. In *Polycystic Kidney Disease [Internet]*. Codon Publications.
Carroll, T. J. & Das, A. J. O. (2011). 'Planar cell polarity in kidney development and disease', 7(3), pp. 180-190.
Carroll, T. J., Park, J.-S., Hayashi, S., Majumdar, A. & McMahon, A. P. (2005). 'Wnt9b plays a central role in the regulation of mesenchymal to epithelial transitions underlying organogenesis of the mammalian urogenital system', *Developmental cell,* 9(2), pp. 283-292.
Cereghini, S. (1996). 'Liver-enriched transcription factors and hepatocyte differentiation', *The FASEB Journal,* 10(2), pp. 267-282.
Cereghini, S., Ott, M., Power, S. & Maury, M. (1992). 'Expression patterns of vHNF1 and HNF1 homeoproteins in early postimplantation embryos suggest distinct and sequential developmental roles', *Development,* 116(3), pp. 783-797.
Chamberlain, S. J., Chen, P.-F., Ng, K. Y., Bourgois-Rocha, F., Lemtiri-Chlieh, F., Levine, E. S. & Lalande, M. (2010). 'Induced pluripotent stem cell models of the genomic imprinting disorders Angelman and Prader–Willi syndromes', *Proceedings of the National Academy of Sciences,* 107(41), pp. 17668-17673.
Chambers, I., Colby, D., Robertson, M., Nichols, J., Lee, S., Tweedie, S. & Smith, A. (2003). 'Functional expression cloning of Nanog, a pluripotency sustaining factor in embryonic stem cells', *Cell,* 113(5), pp. 643-655.
Chang, S.-Y., Weber, E. J., Sidorenko, V. S., Chapron, A., Yeung, C. K., Gao, C., Mao, Q., Shen, D., Wang, J. & Rosenquist, T. A. J. J. i. (2017). 'Human liver-kidney model elucidates the mechanisms of aristolochic acid nephrotoxicity', 2(22).
Chen, D., Roberts, R., Pohl, M., Nigam, S., Kreidberg, J., Wang, Z., Heino, J., Ivaska, J., Coffa, S. & Harris, R. C. J. A. J. o. P.-R. P. (2004). 'Differential expression of collagen-and laminin-binding integrins mediates ureteric bud and inner medullary collecting duct cell tubulogenesis', 287(4), pp. F602-F611.
Cheng, H.-T., Kim, M., Valerius, M. T., Surendran, K., Schuster-Gossler, K., Gossler, A., McMahon, A. P. & Kopan, R. (2007). 'Notch2, but not Notch1, is required for proximal fate acquisition in the mammalian nephron', *Development,* 134(4), pp. 801-811.
Chi, L., Saarela, U., Railo, A., Prunskaite-Hyyryläinen, R., Skovorodkin, I., Anthony, S., Katsu, K., Liu, Y., Shan, J. & Salgueiro, A. M. (2011). 'A secreted BMP antagonist, Cer1, fine tunes the spatial organization of the ureteric bud tree during mouse kidney development', *PLoS One,* 6(11), p. e27676.
Chin, M. H., Mason, M. J., Xie, W., Volinia, S., Singer, M., Peterson, C., Ambartsumyan, G., Aimiuwu, O., Richter, L. & Zhang, J. (2009). 'Induced pluripotent stem cells and embryonic stem cells are distinguished by gene expression signatures', *Cell Stem Cell,* 5(1), pp. 111-123.
Choi, J., Lee, S., Mallard, W., Clement, K., Tagliazucchi, G. M., Lim, H., Choi, I. Y., Ferrari, F., Tsankov, A. M. & Pop, R. (2015). 'A comparison of genetically matched cell lines reveals the equivalence of human iPSCs and ESCs', *Nature biotechnology,* 33(11), p. 1173.

Choi, Y.-H., Suzuki, A., Hajarnis, S., Ma, Z., Chapin, H. C., Caplan, M. J., Pontoglio, M., Somlo, S. & Igarashi, P. J. P. o. t. N. A. o. S. (2011). 'Polycystin-2 and phosphodiesterase 4C are components of a ciliary A-kinase anchoring protein complex that is disrupted in cystic kidney diseases', 108(26), pp. 10679-10684.

Ciampi, O., Iacone, R., Longaretti, L., Benedetti, V., Graf, M., Magnone, M. C., Patsch, C., Xinaris, C., Remuzzi, G. & Benigni, A. J. S. c. r. (2016). 'Generation of functional podocytes from human induced pluripotent stem cells', 17(1), pp. 130-139.

Clissold, R. L., Hamilton, A. J., Hattersley, A. T., Ellard, S. & Bingham, C. (2015). 'HNF1B-associated renal and extra-renal disease-an expanding clinical spectrum', *Nat Rev Nephrol,* 11(2), pp. 102-12.

Colvin, J. S., Feldman, B., Nadeau, J. H., Goldfarb, M. & Ornitz, D. M. (1999a). 'Genomic organization and embryonic expression of the mouse fibroblast growth factor 9 gene', *Developmental dynamics,* 216(1), pp. 72-88.

Colvin, J. S., Feldman, B., Nadeau, J. H., Goldfarb, M. & Ornitz, D. M. (1999b). 'Genomic organization and embryonic expression of the mouse fibroblast growth factor 9 gene', *Developmental dynamics: an official publication of the American Association of Anatomists,* 216(1), pp. 72-88.

Combes, A. N., Zappia, L., Er, P. X., Oshlack, A. & Little, M. H. (2019). 'Single-cell analysis reveals congruence between kidney organoids and human fetal kidney', *Genome medicine,* 11(1), p. 3.

Costantini, F. & Kopan, R. (2010). 'Patterning a complex organ: branching morphogenesis and nephron segmentation in kidney development', *Developmental cell,* 18(5), pp. 698-712.

Crossley, P. H. & Martin, G. R. (1995). 'The mouse Fgf8 gene encodes a family of polypeptides and is expressed in regions that direct outgrowth and patterning in the developing embryo', *Development,* 121(2), pp. 439-451.

Cruz, N. M., Song, X., Czerniecki, S. M., Gulieva, R. E., Churchill, A. J., Kim, Y. K., Winston, K., Tran, L. M., Diaz, M. A. & Fu, H. (2017). 'Organoid cystogenesis reveals a critical role of microenvironment in human polycystic kidney disease', *Nature materials,* 16(11), p. 1112.

Cullen-McEwen, L. A., Kett, M. M., Dowling, J., Anderson, W. P. & Bertram, J. F. (2003). 'Nephron number, renal function, and arterial pressure in aged GDNF heterozygous mice', *Hypertension,* 41(2), pp. 335-340.

Czerniecki, S. M., Cruz, N. M., Harder, J. L., Menon, R., Annis, J., Otto, E. A., Gulieva, R. E., Islas, L. V., Kim, Y. K. & Tran, L. M. (2018). 'High-throughput screening enhances kidney organoid differentiation from human pluripotent stem cells and enables automated multidimensional phenotyping', *Cell stem cell,* 22(6), pp. 929-940. e4.

de Lázaro, I., Yilmazer, A. & Kostarelos, K. (2014). 'Induced pluripotent stem (iPS) cells: a new source for cell-based therapeutics?', *Journal of Controlled Release,* 185, pp. 37-44.

Deglincerti, A., Etoc, F., Ozair, M. Z. & Brivanlou, A. H. (2016). 'Self-organization of spatial patterning in human embryonic stem cells', *Current topics in developmental biology*: Elsevierpp. 99-113.

Desgrange, A., Heliot, C., Skovorodkin, I., Akram, S. U., Heikkilä, J., Ronkainen, V.-P., Miinalainen, I., Vainio, S. J. & Cereghini, S. (2017). 'HNF1B controls epithelial organization and cell polarity during ureteric bud branching and collecting duct morphogenesis', *Development,* 144(24), pp. 4704-4719.

Devuyst, O., Knoers, N. V., Remuzzi, G. & Schaefer, F. J. T. L. (2014). 'Rare inherited kidney diseases: challenges, opportunities, and perspectives', 383(9931), pp. 1844-1859.

Doi, A., Park, I.-H., Wen, B., Murakami, P., Aryee, M. J., Irizarry, R., Herb, B., Ladd-Acosta, C., Rho, J. & Loewer, S. (2009). 'Differential methylation of tissue-and cancer-specific CpG island shores distinguishes human induced pluripotent stem cells, embryonic stem cells and fibroblasts', *Nature genetics,* 41(12), pp. 1350-1353.

Drake, K. M., Ruteshouser, E. C., Natrajan, R., Harbor, P., Wegert, J., Gessler, M., Pritchard-Jones, K., Grundy, P., Dome, J. & Huff, V. (2009). 'Loss of heterozygosity at 2q37 in sporadic Wilms' tumor: putative role for miR-562', *Clinical Cancer Research,* 15(19), pp. 5985-5992.

Dressler, G. R. (2009). 'Advances in early kidney specification, development and patterning', *Development,* 136(23), pp. 3863-3874.

Edghill, E. L., Bingham, C., Ellard, S. & Hattersley, A. T. (2006). 'Mutations in hepatocyte nuclear factor-1β and their related phenotypes', *Journal of medical genetics,* 43(1), pp. 84-90.

Eiraku, M., Takata, N., Ishibashi, H., Kawada, M., Sakakura, E., Okuda, S., Sekiguchi, K., Adachi, T. & Sasai, Y. (2011). 'Self-organizing optic-cup morphogenesis in three-dimensional culture', *Nature,* 472(7341), p. 51.

Eliceiri, K. W., Berthold, M. R., Goldberg, I. G., Ibáñez, L., Manjunath, B. S., Martone, M. E., Murphy, R. F., Peng, H., Plant, A. L. & Roysam, B. J. N. m. (2012). 'Biological imaging software tools', 9(7), p. 697.

Evans, M. J. & Kaufman, M. H. (1981). 'Establishment in culture of pluripotential cells from mouse embryos', *Nature,* 292(5819), pp. 154-156.

Faa, G., Gerosa, C., Fanni, D., Monga, G., Zaffanello, M., Van Eyken, P. & Fanos, V. (2012). 'Morphogenesis and molecular mechanisms involved in human kidney development', *Journal of cellular physiology,* 227(3), pp. 1257-1268.

Faguer, S., Chassaing, N., Bandin, F., Prouheze, C., Garnier, A., Casemayou, A., Huart, A., Schanstra, J. P., Calvas, P. & Decramer, S. J. K. i. (2014). 'The HNF1B score is a simple tool to select patients for HNF1B gene analysis', 86(5), pp. 1007-1015.

Faguer, S., Decramer, S., Chassaing, N., Bellanné-Chantelot, C., Calvas, P., Beaufils, S., Bessenay, L., Lengelé, J.-P., Dahan, K. & Ronco, P. J. K. i. (2011). 'Diagnosis, management, and prognosis of HNF1B nephropathy in adulthood', 80(7), pp. 768-776.

Ferraz, M. L. F., Dos Santos, A. M., Cavellani, C. L., Rossi, R. C., Corrêa, R. R. M., Dos Reis, M. A., Teixeira, V. d. P. A. & da Cunha Castro, E. C. (2008). 'Histochemical and immunohistochemical study of the glomerular development in human fetuses', *Pediatric nephrology,* 23(2), pp. 257-262.

Fletcher, J., Hu, M., Berman, Y., Collins, F., Grigg, J., McIver, M., Jüppner, H. and Alexander, S.I., 2005. Multicystic dysplastic kidney and variable phenotype in a family with a novel deletion mutation of PAX2. *Journal of the American Society of Nephrology*, *16*(9), pp.2754-2761.

Forbes, T. A., Howden, S. E., Lawlor, K., Phipson, B., Maksimovic, J., Hale, L., Wilson, S., Quinlan, C., Ho, G. & Holman, K. J. T. A. J. o. H. G. (2018). 'Patient-iPSC-derived kidney organoids show functional validation of a ciliopathic renal phenotype and reveal underlying pathogenetic mechanisms', 102(5), pp. 816-831.

Freedman, B. S., Brooks, C. R., Lam, A. Q., Fu, H., Morizane, R., Agrawal, V., Saad, A. F., Li, M. K., Hughes, M. R., Werff, R. V., Peters, D. T., Lu, J., Baccei, A., Siedlecki, A. M., Valerius, M. T., Musunuru, K., McNagny, K. M., Steinman, T. I., Zhou, J., Lerou, P. H. & Bonventre, J. V. (2015). 'Modelling kidney disease with CRISPR-mutant kidney organoids derived from human pluripotent epiblast spheroids', *Nat Commun,* 6, p. 8715.

Freedman, B. S., Lam, A. Q., Sundsbak, J. L., Iatrino, R., Su, X., Koon, S. J., Wu, M., Daheron, L., Harris, P. C. & Zhou, J. (2013). 'Reduced ciliary polycystin-2 in induced pluripotent stem cells from polycystic kidney disease patients with PKD1 mutations', *Journal of the American Society of Nephrology,* 24(10), pp. 1571-1586.

Fusaki, N., Ban, H., Nishiyama, A., Saeki, K. & Hasegawa, M. (2009). 'Efficient induction of transgene-free human pluripotent stem cells using a vector based on Sendai virus, an RNA virus that does not integrate into the host genome', *Proceedings of the Japan Academy, Series B,* 85(8), pp. 348-362.

Gadue, P., Huber, T. L., Paddison, P. J. & Keller, G. M. (2006). 'Wnt and TGF-β signaling are required for the induction of an in vitro model of primitive streak formation using embryonic stem cells', *Proceedings of the National Academy of Sciences,* 103(45), pp. 16806-16811.

Gallegos, T. F., Kouznetsova, V., Kudlicka, K., Sweeney, D. E., Bush, K. T., Willert, K., Farquhar, M. G. & Nigam, S. K. J. D. b. (2012). 'A protein kinase A and Wnt-dependent network regulating an intermediate stage in epithelial tubulogenesis during kidney development', 364(1), pp. 11-21.

Garreta, E., Prado, P., Tarantino, C., Oria, R., Fanlo, L., Martí, E., Zalvidea, D., Trepat, X., Roca-Cusachs, P. & Gavaldà-Navarro, A. (2019). 'Fine tuning the extracellular environment accelerates the derivation of kidney organoids from human pluripotent stem cells', *Nat. Mater,* 18, pp. 397-405.

Gattone II, V. H., Wang, X., Harris, P. C. & Torres, V. E. J. N. m. (2003). 'Inhibition of renal cystic disease development and progression by a vasopressin V2 receptor antagonist', 9(10), p. 1323.

Geng, L., Boehmerle, W., Maeda, Y., Okuhara, D. Y., Tian, X., Yu, Z., Choe, C.-u., Anyatonwu, G. I., Ehrlich, B. E. & Somlo, S. J. P. o. t. N. A. o. S. (2008). 'Syntaxin 5 regulates the endoplasmic reticulum channel-release properties of polycystin-2', 105(41), pp. 15920-15925.

Georgas, K., Chiu, H., Lesieur, E., Rumballe, B. & Little, M. H. (2011). 'Expression of metanephric nephron-patterning genes in differentiating mesonephric tubules', *Developmental dynamics,* 240(6), pp. 1600-1612.

Georgas, K., Rumballe, B., Wilkinson, L., Chiu, H. S., Lesieur, E., Gilbert, T. & Little, M. H. (2008). 'Use of dual section mRNA in situ hybridisation/immunohistochemistry to clarify gene expression patterns during the early stages of nephron development in the embryo and in the mature nephron of the adult mouse kidney', *Histochemistry and cell biology,* 130(5), p. 927.

Goetz, R. & Mohammadi, M. (2013). 'Exploring mechanisms of FGF signalling through the lens of structural biology', *Nature reviews Molecular cell biology,* 14(3), p. 166.

Gospodarowicz, D. & Cheng, J. (1986). 'Heparin protects basic and acidic FGF from inactivation', *Journal of cellular physiology,* 128(3), pp. 475-484.

Grantham, J. J., Geiser, J. L. & Evan, A. P. J. K. i. (1987). 'Cyst formation and growth in autosomal dominant polycystic kidney disease', 31(5), pp. 1145-1152.

Green, M. D., Chen, A., Nostro, M.-C., d'Souza, S. L., Schaniel, C., Lemischka, I. R., Gouon-Evans, V., Keller, G. & Snoeck, H.-W. (2011). 'Generation of anterior foregut endoderm from human embryonic and induced pluripotent stem cells', *Nature biotechnology,* 29(3), pp. 267-272.

Gresh, L., Fischer, E., Reimann, A., Tanguy, M., Garbay, S., Shao, X., Hiesberger, T., Fiette, L., Igarashi, P. & Yaniv, M. (2004). 'A transcriptional network in polycystic kidney disease', *The EMBO Journal,* 23(7), pp. 1657-1668.

Grote, D., Souabni, A., Busslinger, M. & Bouchard, M. (2006). 'Pax2/8-regulated Gata3 expression is necessary for morphogenesis and guidance of the nephric duct in the developing kidney', *Development,* 133(1), pp. 53-61.

Gruenwald, P. (1939). 'The mechanism of kidney development in human embryos as revealed by an early stage in the agenesis of the ureteric buds', *The Anatomical Record,* 75(2), pp. 237-247.

Hains, D., Sims-Lucas, S., Kish, K., Saha, M., McHugh, K. & Bates, C. M. (2008). 'Role of fibroblast growth factor receptor 2 in kidney mesenchyme', *Pediatric research,* 64(6), pp. 592-598.

Harding, S. D., Armit, C., Armstrong, J., Brennan, J., Cheng, Y., Haggarty, B., Houghton, D., Lloyd-MacGilp, S., Pi, X. & Roochun, Y. (2011). 'The GUDMAP database–an online resource for genitourinary research', *Development,* 138(13), pp. 2845-2853.

Hartman, H. A., Lai, H. L. & Patterson, L. T. (2007). 'Cessation of renal morphogenesis in mice', *Developmental biology,* 310(2), pp. 379-387.

Harvey, S. J., Jarad, G., Cunningham, J., Goldberg, S., Schermer, B., Harfe, B. D., McManus, M. T., Benzing, T. & Miner, J. H. (2008). 'Podocyte-specific deletion of dicer alters cytoskeletal dynamics and causes glomerular disease', *Journal of the American Society of Nephrology,* 19(11), pp. 2150-2158.

Haumaitre, C., Fabre, M., Cormier, S., Baumann, C., Delezoide, A.-L. & Cereghini, S. (2006). 'Severe pancreas hypoplasia and multicystic renal dysplasia in two human fetuses carrying novel HNF1β/MODY5 mutations', *Human molecular genetics,* 15(15), pp. 2363-2375.

Heidet, L., Decramer, S., Pawtowski, A., Morinière, V., Bandin, F., Knebelmann, B., Lebre, A.-S., Faguer, S., Guigonis, V. & Antignac, C. (2010). 'Spectrum of HNF1B mutations in a large cohort of patients who harbor renal diseases', *Clinical Journal of the American Society of Nephrology,* 5(6), pp. 1079-1090.

Heliot, C., Desgrange, A., Buisson, I., Prunskaite-Hyyryläinen, R., Shan, J., Vainio, S., Umbhauer, M. & Cereghini, S. (2013). 'HNF1B controls proximal-intermediate nephron segment identity in vertebrates by regulating Notch signalling components and Irx1/2', *Development,* 140(4), pp. 873-885.

Hendry, C., Rumballe, B., Moritz, K. & Little, M. H. (2011). 'Defining and redefining the nephron progenitor population', *Pediatric Nephrology,* 26(9), pp. 1395-1406.

Hiesberger, T., Bai, Y., Shao, X., McNally, B. T., Sinclair, A. M., Tian, X., Somlo, S. & Igarashi, P. (2004). 'Mutation of hepatocyte nuclear factor–1β inhibits Pkhd1 gene expression and produces renal cysts in mice', *Journal of Clinical Investigation,* 113(6), p. 814.

Hiesberger, T., Shao, X., Gourley, E., Reimann, A., Pontoglio, M. & Igarashi, P. (2005). 'Role of the hepatocyte nuclear factor-1β (HNF-1β) C-terminal domain in Pkhd1 (ARPKD) gene transcription and renal cystogenesis', *Journal of Biological Chemistry,* 280(11), pp. 10578-10586.

Hiraoka, M., Tsukahara, H., Ohshima, Y., Kasuga, K., Ishihara, Y. & Mayumi, M. (2002). 'Renal aplasia is the predominant cause of congenital solitary kidneys', *Kidney international,* 61(5), pp. 1840-1844.

Ho, J., Ng, K. H., Rosen, S., Dostal, A., Gregory, R. I. & Kreidberg, J. A. (2008). 'Podocyte-specific loss of functional microRNAs leads to rapid glomerular and tubular injury', *Journal of the American Society of Nephrology,* 19(11), pp. 2069-2075.

Hockemeyer, D. & Jaenisch, R. J. C. s. c. (2016). 'Induced pluripotent stem cells meet genome editing', 18(5), pp. 573-586.

Homan, K. A., Kolesky, D. B., Skylar-Scott, M. A., Herrmann, J., Obuobi, H., Moisan, A. & Lewis, J. A. (2016). 'Bioprinting of 3D convoluted renal proximal tubules on perfusable chips', *Scientific reports,* 6, p. 34845.

Horikawa, Y., Iwasaki, N., Hara, M., Furuta, H., Hinokio, Y., Cockburn, B. N., Lindner, T., Yamagata, K., Ogata, M. & Tomonaga, O. (1997). 'Mutation in hepatocyte nuclear factor–1β gene (TCF2) associated with MODY', *Nature genetics,* 17(4), pp. 384-385.

Hovater, M. B., Olteanu, D., Welty, E. A. & Schwiebert, E. M. J. P. s. (2008). 'Purinergic signaling in the lumen of a normal nephron and in remodeled PKD encapsulated cysts', 4(2), pp. 109-124.

Howden, S. E., Thomson, J. A. & Little, M. H. J. N. p. (2018). 'Simultaneous reprogramming and gene editing of human fibroblasts', 13(5), p. 875.

Howe, A. K. J. B. e. B. A.-M. C. R. (2004). 'Regulation of actin-based cell migration by cAMP/PKA', 1692(2-3), pp. 159-174.

Hsieh, W.-C., Ramadesikan, S., Fekete, D. & Aguilar, R. C. J. P. o. (2018). 'Kidney-differentiated cells derived from Lowe Syndrome patient's iPSCs show ciliogenesis defects and Six2 retention at the Golgi complex', 13(2), p. e0192635.

Hu, B.-Y., Weick, J. P., Yu, J., Ma, L.-X., Zhang, X.-Q., Thomson, J. A. & Zhang, S.-C. (2010). 'Neural differentiation of human induced pluripotent stem cells follows developmental principles but with variable potency', *Proceedings of the National Academy of Sciences,* 107(9), pp. 4335-4340.

Huang, S. (2009). 'Reprogramming cell fates: reconciling rarity with robustness', *Bioessays,* 31(5), pp. 546-560.

Hubert, C. G., Rivera, M., Spangler, L. C., Wu, Q., Mack, S. C., Prager, B. C., Couce, M., McLendon, R. E., Sloan, A. E. & Rich, J. N. (2016). 'A three-dimensional organoid culture system derived from human glioblastomas recapitulates the hypoxic gradients and cancer stem cell heterogeneity of tumors found in vivo', *Cancer research,* 76(8), pp. 2465-2477.

Hughson, M., Farris, A. B., Douglas-Denton, R., Hoy, W. E. & Bertram, J. F. (2003). 'Glomerular number and size in autopsy kidneys: the relationship to birth weight', *Kidney international,* 63(6), pp. 2113-2122.

Huisken, J., Swoger, J., Del Bene, F., Wittbrodt, J. & Stelzer, E. H. J. S. (2004). 'Optical sectioning deep inside live embryos by selective plane illumination microscopy', 305(5686), pp. 1007-1009.

Iwasaki, N., Okabe, I., Momoi, M., Ohashi, H., Ogata, M. & Iwamoto, Y. (2001). 'Splice site mutation in the hepatocyte nuclear factor-1 beta gene, IVS2nt+ 1G> A, associated with maturity-onset diabetes of the young, renal dysplasia and bicornuate uterus', *Diabetologia,* 44(3), pp. 387-388.

Jain, S. (2009). 'The many faces of RET dysfunction in kidney', *Organogenesis,* 5(4), pp. 177-190.

James, R. G. & Schultheiss, T. M. (2005). 'Bmp signaling promotes intermediate mesoderm gene expression in a dose-dependent, cell-autonomous and translation-dependent manner', *Developmental biology,* 288(1), pp. 113-125.

Jenkinson, S. E., Chung, G. W., van Loon, E., Bakar, N. S., Dalzell, A. M. & Brown, C. D. A. (2012). 'The limitations of renal epithelial cell line HK-2 as a model of drug transporter expression and function in the proximal tubule', *Pflügers Archiv - European Journal of Physiology,* 464(6), pp. 601-611.

Jin, L., Kikuchi, R., Saji, T., Kusuhara, H. & Sugiyama, Y. (2012). 'Regulation of tissue-specific expression of renal organic anion transporters by hepatocyte nuclear factor 1 α/β and DNA methylation', *Journal of Pharmacology and Experimental Therapeutics,* 340(3), pp. 648-655.

Joly, D., Berissi, S., Bertrand, A., Strehl, L., Patey, N. & Knebelmann, B. J. J. o. B. C. (2006). 'Laminin 5 regulates polycystic kidney cell proliferation and cyst formation', 281(39), pp. 29181-29189.

Joly, D., Morel, V., Hummel, A., Ruello, A., Nusbaum, P., Patey, N., Noël, L.-H., Rousselle, P. & Knebelmann, B. J. T. A. j. o. p. (2003). 'β4 integrin and laminin 5 are aberrantly expressed in polycystic kidney disease: role in increased cell adhesion and migration', 163(5), pp. 1791-1800.

Karner, C. M., Chirumamilla, R., Aoki, S., Igarashi, P., Wallingford, J. B. & Carroll, T. J. (2009). 'Wnt9b signaling regulates planar cell polarity and kidney tubule morphogenesis', *Nature genetics,* 41(7), p. 793.
Kawahara, Y. (2014). 'Human diseases caused by germline and somatic abnormalities in microRNA and microRNA-related genes', *Congenital anomalies,* 54(1), pp. 12-21.
Keramari, M., Razavi, J., Ingman, K. A., Patsch, C., Edenhofer, F., Ward, C. M. & Kimber, S. J. (2010). 'Sox2 is essential for formation of trophectoderm in the preimplantation embryo', *PLoS One,* 5(11), p. e13952.
Kerecuk, L., Schreuder, M. F. & Woolf, A. S. (2008). 'Renal tract malformations: perspectives for nephrologists', *Nature Clinical Practice Nephrology,* 4(6), pp. 312-325.
Kim, D. & Dressler, G. R. (2005). 'Nephrogenic factors promote differentiation of mouse embryonic stem cells into renal epithelia', *Journal of the American Society of Nephrology,* 16(12), pp. 3527-3534.
Kim, Y. K., Refaeli, I., Brooks, C. R., Jing, P., Gulieva, R. E., Hughes, M. R., Cruz, N. M., Liu, Y., Churchill, A. J. & Wang, Y. J. S. c. (2017). 'Gene-Edited Human Kidney Organoids Reveal Mechanisms of Disease in Podocyte Development', 35(12), pp. 2366-2378.
Kimber, S. J. & Woolf, A. S. (2018). 'From human pluripotent stem cells to functional kidney organoids and models of renal disease', *Stem cell investigation,* 5.
Kip, S. N., Hunter, L. W., Ren, Q., Harris, P. C., Somlo, S., Torres, V. E., Sieck, G. C. & Qian, Q. J. C. r. (2005). '[Ca2+] i reduction increases cellular proliferation and apoptosis in vascular smooth muscle cells: relevance to the ADPKD phenotype', 96(8), pp. 873-880.
Kispert, A., Vainio, S. & McMahon, A. P. (1998). 'Wnt-4 is a mesenchymal signal for epithelial transformation of metanephric mesenchyme in the developing kidney', *Development,* 125(21), pp. 4225-4234.
Kobayashi, A., Valerius, M. T., Mugford, J. W., Carroll, T. J., Self, M., Oliver, G. & McMahon, A. P. (2008). 'Six2 defines and regulates a multipotent self-renewing nephron progenitor population throughout mammalian kidney development', *Cell stem cell,* 3(2), pp. 169-181.
Kobayashi, H., Kawakami, K., Asashima, M. & Nishinakamura, R. (2007). 'Six1 and Six4 are essential for Gdnf expression in the metanephric mesenchyme and ureteric bud formation, while Six1 deficiency alone causes mesonephric-tubule defects', *Mechanisms of development,* 124(4), pp. 290-303.
Koepsell, H. J. M. a. o. m. (2013). 'The SLC22 family with transporters of organic cations, anions and zwitterions', 34(2-3), pp. 413-435.
Kolatsi-Joannou, M., Bingham, C., Ellard, S., Bulman, M. P., Allen, L. I., Hattersley, A. T. & Woolf, A. S. (2001). 'Hepatocyte nuclear factor-1β: a new kindred with renal cysts and diabetes and gene expression in normal human development', *Journal of the American Society of Nephrology,* 12(10), pp. 2175-2180.
Kopp, J. L., Ormsbee, B. D., Desler, M. & Rizzino, A. J. S. c. (2008). 'Small increases in the level of Sox2 trigger the differentiation of mouse embryonic stem cells', 26(4), pp. 903-911.
Köttgen, M., Buchholz, B., Garcia-Gonzalez, M. A., Kotsis, F., Fu, X., Doerken, M., Boehlke, C., Steffl, D., Tauber, R. & Wegierski, T. J. T. J. o. c. b. (2008). 'TRPP2 and TRPV4 form a polymodal sensory channel complex', 182(3), pp. 437-447.
Kreidberg, J. A., Sariola, H., Loring, J. M., Maeda, M., Pelletier, J., Housman, D. & Jaenisch, R. (1993). 'WT-1 is required for early kidney development', *Cell,* 74(4), pp. 679-691.
Kumar, S. V., Pei, X. E., Lawlor, K. T., Motazedian, A., Scurr, M., Ghobrial, I., Combes, A. N., Zappia, L., Oshlack, A. & Stanley, E. G. (2019). 'Kidney micro-organoids in suspension culture as a scalable source of human pluripotent stem cell-derived kidney cells', *Development,* 146(5), p. dev172361.
Lam, A. Q., Freedman, B. S., Morizane, R., Lerou, P. H., Valerius, M. T. & Bonventre, J. V. (2014). 'Rapid and efficient differentiation of human pluripotent stem cells into intermediate mesoderm that forms tubules expressing kidney proximal tubular markers', *Journal of the American Society of Nephrology,* 25(6), pp. 1211-1225.
Lawrence, M. L., Chang, C.-H. & Davies, J. A. J. S. r. (2015). 'Transport of organic anions and cations in murine embryonic kidney development and in serially-reaggregated engineered kidneys', 5, p. 9092.
Lawrence, M. L., Smith, J. R. & Davies, J. A. J. A. J. o. P.-R. P. (2018). 'Functional transport of organic anions and cations in the murine mesonephros', 315(1), pp. F130-F137.
Lejeune, F. & Maquat, L. E. J. C. o. i. c. b. (2005). 'Mechanistic links between nonsense-mediated mRNA decay and pre-mRNA splicing in mammalian cells', 17(3), pp. 309-315.
Li, L. & Clevers, H. J. s. (2010). 'Coexistence of quiescent and active adult stem cells in mammals', 327(5965), pp. 542-545.
Li, M., Wang, X., Meintzer, M. K., Laessig, T., Birnbaum, M. J., Heidenreich, K. A. J. M. & biology, c. (2000). 'Cyclic AMP promotes neuronal survival by phosphorylation of glycogen synthase kinase 3β', 20(24), pp. 9356-9363.
Lieu, P. T., Fontes, A., Vemuri, M. C. & MacArthur, C. C. (2013). 'Generation of induced pluripotent stem cells with CytoTune, a non-integrating Sendai virus', *Pluripotent Stem Cells*: Springerpp. 45-56.
Linton, J. M., Martin, G. R. & Reichardt, L. F. (2007). 'The ECM protein nephronectin promotes kidney development via integrin α8β1-mediated stimulation of Gdnf expression', *Development,* 134(13), pp. 2501-2509.
Little, M. H., Brennan, J., Georgas, K., Davies, J. A., Davidson, D. R., Baldock, R. A., Beverdam, A., Bertram, J. F., Capel, B. & Chiu, H. S. (2007). 'A high-resolution anatomical ontology of the developing murine genitourinary tract', *Gene Expression Patterns,* 7(6), pp. 680-699.
Little, M. H. & McMahon, A. P. (2012). 'Mammalian kidney development: principles, progress, and projections', *Cold Spring Harbor perspectives in biology,* 4(5), p. a008300.

Little, M. H. & Quinlan, C. J. P. N. (2019). 'Advances in our understanding of genetic kidney disease using kidney organoids', pp. 1-12.
Louis, K. S. & Siegel, A. C. (2011). 'Cell viability analysis using trypan blue: manual and automated methods', *Mammalian cell viability*: Springerpp. 7-12.
Lovvorn III, H. N., Westrup, J., Opperman, S., Boyle, S., Shi, G., Anderson, J., Perlman, E. J., Perantoni, A. O., Wills, M. & De Caestecker, M. (2007). 'CITED1 expression in Wilms' tumor and embryonic kidney', *Neoplasia (New York, NY),* 9(7), p. 589.
Low, J. H., Li, P., Chew, E. G. Y., Zhou, B., Suzuki, K., Zhang, T., Lian, M. M., Liu, M., Aizawa, E. & Esteban, C. R. (2019). 'Generation of Human PSC-Derived Kidney Organoids with Patterned Nephron Segments and a De Novo Vascular Network', *Cell stem cell*.
Lu, B. C., Cebrian, C., Chi, X., Kuure, S., Kuo, R., Bates, C. M., Arber, S., Hassell, J., MacNeil, L. & Hoshi, M. (2009). 'Etv4 and Etv5 are required downstream of GDNF and Ret for kidney branching morphogenesis', *Nature genetics,* 41(12), p. 1295.
Ludwig, T., Riethmüller, C., Gekle, M., Schwerdt, G. & Oberleithner, H. (2004). 'Nephrotoxicity of platinum complexes is related to basolateral organic cation transport', *Kidney international,* 66(1), pp. 196-202.
Ma, Z., Gong, Y., Patel, V., Karner, C.M., Fischer, E., Hiesberger, T., Carroll, T.J., Pontoglio, M. and Igarashi, P., 2007. Mutations of HNF-1β inhibit epithelial morphogenesis through dysregulation of SOCS-3. *Proceedings of the National Academy of Sciences*, *104*(51), pp.20386-20391.
Madariaga, L., Morinière, V., Jeanpierre, C., Bouvier, R., Loget, P., Martinovic, J., Dechelotte, P., Leporrier, N., Thauvin-Robinet, C. & Jensen, U. B. (2013). 'Severe prenatal renal anomalies associated with mutations in HNF1B or PAX2 genes', *Clinical Journal of the American Society of Nephrology,* 8(7), pp. 1179-1187.
Mae, S.-I., Shono, A., Shiota, F., Yasuno, T., Kajiwara, M., Gotoda-Nishimura, N., Arai, S., Sato-Otubo, A., Toyoda, T. & Takahashi, K. (2013). 'Monitoring and robust induction of nephrogenic intermediate mesoderm from human pluripotent stem cells', *Nature communications,* 4, p. 1367.
Magenheimer, B. S., John, P. L. S., Isom, K. S., Abrahamson, D. R., De Lisle, R. C., Wallace, D. P., Maser, R. L., Grantham, J. J. & Calvet, J. P. J. J. o. t. a. s. o. n. (2006). 'Early embryonic renal tubules of wild-type and polycystic kidney disease kidneys respond to cAMP stimulation with cystic fibrosis transmembrane conductance regulator/Na+, K+, 2Cl− Co-transporter–dependent cystic dilation', 17(12), pp. 3424-3437.
Manié, S., Santoro, M., Fusco, A. & Billaud, M. (2001). 'The RET receptor: function in development and dysfunction in congenital malformation', *TRENDS in Genetics,* 17(10), pp. 580-589.
Marchetto, M. C., Carromeu, C., Acab, A., Yu, D., Yeo, G. W., Mu, Y., Chen, G., Gage, F. H. & Muotri, A. R. (2010). 'A model for neural development and treatment of Rett syndrome using human induced pluripotent stem cells', *Cell,* 143(4), pp. 527-539.
Massa, F., Garbay, S., Bouvier, R., Sugitani, Y., Noda, T., Gubler, M.-C., Heidet, L., Pontoglio, M. & Fischer, E. (2013). 'Hepatocyte nuclear factor 1β controls nephron tubular development', *Development,* 140(4), pp. 886-896.
Masyuk, T. V., Masyuk, A. I., Torres, V. E., Harris, P. C. & Larusso, N. F. J. G. (2007). 'Octreotide inhibits hepatic cystogenesis in a rodent model of polycystic liver disease by reducing cholangiocyte adenosine 3′, 5′-cyclic monophosphate', 132(3), pp. 1104-1116.
Matsuda, T., Nakamura, T., Nakao, K., Arai, T., Katsuki, M., Heike, T. & Yokota, T. (1999). 'STAT3 activation is sufficient to maintain an undifferentiated state of mouse embryonic stem cells', *The EMBO Journal,* 18(15), pp. 4261-4269.
Matsui, Y., Zsebo, K. & Hogan, B. L. (1992). 'Derivation of pluripotential embryonic stem cells from murine primordial germ cells in culture', *Cell,* 70(5), pp. 841-847.
McKee, R. & Wingert, R. (2016). 'Repopulating decellularized kidney scaffolds: an avenue for ex vivo organ generation', *Materials,* 9(3), p. 190.
Medrano, S., Monteagudo, M. C., Sequeira-Lopez, M. L. S., Pentz, E. S. & Gomez, R. A. (2012). 'Two microRNAs, miR-330 and miR-125b-5p, mark the juxtaglomerular cell and balance its smooth muscle phenotype', *American Journal of Physiology-Renal Physiology,* 302(1), pp. F29-F37.
Mefford, H. C., Clauin, S., Sharp, A. J., Moller, R. S., Ullmann, R., Kapur, R., Pinkel, D., Cooper, G. M., Ventura, M. & Ropers, H. H. (2007). 'Recurrent reciprocal genomic rearrangements of 17q12 are associated with renal disease, diabetes, and epilepsy', *The American Journal of Human Genetics,* 81(5), pp. 1057-1069.
Mekahli, D., Sammels, E., Luyten, T., Welkenhuyzen, K., Van Den Heuvel, L., Levtchenko, E., Gijsbers, R., Bultynck, G., Parys, J. & De Smedt, H. J. C. c. (2012). 'Polycystin-1 and polycystin-2 are both required to amplify inositol-trisphosphate-induced Ca2+ release', 51(6), pp. 452-458.
Mendel, D. B., Hansen, L. P., Graves, M. K., Conley, P. B. & Crabtree, G. R. (1991). 'HNF-1 alpha and HNF-1 beta (vHNF-1) share dimerization and homeo domains, but not activation domains, and form heterodimers in vitro', *Genes & development,* 5(6), pp. 1042-1056.
Meng, X., Su, R.-J., Baylink, D. J., Neises, A., Kiroyan, J. B., Lee, W. Y.-W., Payne, K. J., Gridley, D. S., Wang, J. & Lau, K. W. J. C. r. (2013). 'Rapid and efficient reprogramming of human fetal and adult blood CD34+ cells into mesenchymal stem cells with a single factor', 23(5), p. 658.
Meyer, C. J., Alenghat, F. J., Rim, P., Fong, J. H.-J., Fabry, B. & Ingber, D. E. J. N. C. B. (2000). 'Mechanical control of cyclic AMP signalling and gene transcription through integrins', 2(9), p. 666.
Miura, K., Okada, Y., Aoi, T., Okada, A., Takahashi, K., Okita, K., Nakagawa, M., Koyanagi, M., Tanabe, K. & Ohnuki, M. (2009). 'Variation in the safety of induced pluripotent stem cell lines', *Nature biotechnology,* 27(8), pp. 743-745.
Morel, N., Vandenberg, G., Ahrabi, A. K., Caron, N., Desjardins, F., Balligand, J.-L., Horie, S. & Devuyst, O. J. P. A.-E. J. o. P. (2009). 'PKD1 haploinsufficiency is associated with altered vascular reactivity and abnormal calcium signaling in the mouse aorta', 457(4), pp. 845-856.

Moretti, A., Bellin, M., Welling, A., Jung, C. B., Lam, J. T., Bott-Flügel, L., Dorn, T., Goedel, A., Höhnke, C. & Hofmann, F. (2010). 'Patient-specific induced pluripotent stem-cell models for long-QT syndrome', *New England Journal of Medicine,* 363(15), pp. 1397-1409.
Morizane, R. & Bonventre, J. V. (2017a). 'Generation of nephron progenitor cells and kidney organoids from human pluripotent stem cells', *Nature protocols,* 12(1), p. 195.
Morizane, R. & Bonventre, J. V. (2017b). 'Kidney organoids: a translational journey', *Trends in molecular medicine,* 23(3), pp. 246-263.
Morizane, R. & Lam, A. Q. (2015). 'Directed Differentiation of Pluripotent Stem Cells into Kidney', *Biomarker insights,* 10(Suppl 1), p. 147.
Morizane, R., Lam, A. Q., Freedman, B. S., Kishi, S., Valerius, M. T. & Bonventre, J. V. (2015). 'Nephron organoids derived from human pluripotent stem cells model kidney development and injury', *Nature biotechnology,* 33(11), p. 1193.
Mugford, J. W., Sipilä, P., McMahon, J. A. & McMahon, A. P. (2008). 'Osr1 expression demarcates a multi-potent population of intermediate mesoderm that undergoes progressive restriction to an Osr1-dependent nephron progenitor compartment within the mammalian kidney', *Developmental biology,* 324(1), pp. 88-98.
Nahm, A. M., Henriquez, D. E. & Ritz, E. J. N. D. T. (2002). 'Renal cystic disease (ADPKD and ARPKD)', 17(2), pp. 311-314.
Nakanishi, K., SWEENEY, W. E., Zerres, K., Guay-Woodford, L. M. & Avner, E. D. J. J. o. t. A. S. o. N. (2000). 'Proximal tubular cysts in fetal human autosomal recessive polycystic kidney disease', 11(4), pp. 760-763.
Nakanishi, K. & Yoshikawa, N. (2003). 'Genetic disorders of human congenital anomalies of the kidney and urinary tract (CAKUT)', *Pediatrics International,* 45(5), pp. 610-616.
Nakayama, M., Nozu, K., Goto, Y., Kamei, K., Ito, S., Sato, H., Emi, M., Nakanishi, K., Tsuchiya, S. & Iijima, K. (2010). 'HNF1B alterations associated with congenital anomalies of the kidney and urinary tract', *Pediatric nephrology,* 25(6), pp. 1073-1079.
Narayanan, K., Schumacher, K. M., Tasnim, F., Kandasamy, K., Schumacher, A., Ni, M., Gao, S., Gopalan, B., Zink, D. & Ying, J. Y. (2013). 'Human embryonic stem cells differentiate into functional renal proximal tubular–like cells', *Kidney international,* 83(4), pp. 593-603.
Narlis, M., Grote, D., Gaitan, Y., Boualia, S. K. & Bouchard, M. (2007). 'Pax2 and pax8 regulate branching morphogenesis and nephron differentiation in the developing kidney', *Journal of the American Society of Nephrology,* 18(4), pp. 1121-1129.
Narsinh, K.H., Plews, J. and Wu, J.C., 2011. Comparison of human induced pluripotent and embryonic stem cells: fraternal or identical twins?. *Molecular Therapy*, *19*(4), pp.635-638.
Naylor, R. W., Przepiorski, A., Ren, Q., Yu, J. & Davidson, A. J. (2013). 'HNF1β is essential for nephron segmentation during nephrogenesis', *Journal of the American Society of Nephrology,* 24(1), pp. 77-87.
Newman, A. M. & Cooper, J. B. (2010). 'Lab-specific gene expression signatures in pluripotent stem cells', *Cell Stem Cell,* 7(2), pp. 258-262.
Nichols, J., Zevnik, B., Anastassiadis, K., Niwa, H., Klewe-Nebenius, D., Chambers, I., Schöler, H. & Smith, A. (1998). 'Formation of pluripotent stem cells in the mammalian embryo depends on the POU transcription factor Oct4', *Cell,* 95(3), pp. 379-391.
Nicolaou, N., Renkema, K. Y., Bongers, E. M., Giles, R. H. & Knoers, N. V. (2015). 'Genetic, environmental, and epigenetic factors involved in CAKUT', *Nature Reviews Nephrology*.
Nieskens, T. T. G., Peters, J. G. P., Schreurs, M. J., Smits, N., Woestenenk, R., Jansen, K., van der Made, T. K., Röring, M., Hilgendorf, C., Wilmer, M. J. & Masereeuw, R. (2016). 'A Human Renal Proximal Tubule Cell Line with Stable Organic Anion Transporter 1 and 3 Expression Predictive for Antiviral-Induced Toxicity', *The AAPS Journal,* 18(2), pp. 465-475.
Nishikawa, M., Yanagawa, N., Kojima, N., Yuri, S., Hauser, P. V., Jo, O. D. & Yanagawa, N. (2012). 'Stepwise renal lineage differentiation of mouse embryonic stem cells tracing in vivo development', *Biochemical and biophysical research communications,* 417(2), pp. 897-902.
Nishinakamura, R. J. N. R. N. (2019). 'Human kidney organoids: progress and remaining challenges', pp. 1-12.
Niwa, H. (2011). 'Wnt: what's needed to maintain pluripotency?', *Nature Cell Biology,* 13(9), p. 1024.
Niwa, H., Miyazaki, J.-i. & Smith, A. G. J. N. g. (2000). 'Quantitative expression of Oct-3/4 defines differentiation, dedifferentiation or self-renewal of ES cells', 24(4), p. 372.
O'Connor, K. L., Shaw, L. M. & Mercurio, A. M. J. T. J. o. c. b. (1998). 'Release of cAMP gating by the α6β4 integrin stimulates lamellae formation and the chemotactic migration of invasive carcinoma cells', 143(6), pp. 1749-1760.
Oh, E.C. and Katsanis, N., 2012. Cilia in vertebrate development and disease. *Development*, *139*(3), pp.443-448.
Okita, K., Ichisaka, T. & Yamanaka, S. (2007). 'Generation of germline-competent induced pluripotent stem cells', *Nature,* 448(7151), pp. 313-317.
Ong, A. C., Devuyst, O., Knebelmann, B., Walz, G. & for Inherited, E.-E. W. G. J. T. L. (2015). 'Autosomal dominant polycystic kidney disease: the changing face of clinical management', 385(9981), pp. 1993-2002.
Ornitz, D. M., Xu, J., Colvin, J. S., McEwen, D. G., MacArthur, C. A., Coulier, F., Gao, G. & Goldfarb, M. (1996). 'Receptor specificity of the fibroblast growth factor family', *Journal of Biological Chemistry,* 271(25), pp. 15292-15297.
Paces-Fessy, M., Fabre, M., Lesaulnier, C. & Cereghini, S. (2012). 'Hnf1b and Pax2 cooperate to control different pathways in kidney and ureter morphogenesis', *Human molecular genetics,* 21(14), pp. 3143-3155.

Pagliuca, F.W., Millman, J.R., Gürtler, M., Segel, M., Van Dervort, A., Ryu, J.H., Peterson, Q.P., Greiner, D. and Melton, D.A., 2014. Generation of functional human pancreatic β cells in vitro. *Cell*, *159*(2), pp.428-439.

Pantoliano, M. W., Horlick, R. A., Springer, B. A., Van Dyk, D. E., Tobery, T., Wetmore, D. R., Lear, J. D., Nahapetian, A. T., Bradley, J. D. & Sisk, W. P. (1994). 'Multivalent ligand-receptor binding interactions in the fibroblast growth factor system produce a cooperative growth factor and heparin mechanism for receptor dimerization', *Biochemistry,* 33(34), pp. 10229-10248.

Park, J.-S., Valerius, M. T. & McMahon, A. P. (2007). 'Wnt/β-catenin signaling regulates nephron induction during mouse kidney development', *Development,* 134(13), pp. 2533-2539.

Patel, V., Williams, D., Hajarnis, S., Hunter, R., Pontoglio, M., Somlo, S. & Igarashi, P. (2013). 'miR-17~ 92 miRNA cluster promotes kidney cyst growth in polycystic kidney disease', *Proceedings of the National Academy of Sciences,* 110(26), pp. 10765-10770.

Perazella, M. A. & Moeckel, G. W. (2010). Nephrotoxicity from chemotherapeutic agents: clinical manifestations, pathobiology, and prevention/therapy. *In:* Seminars in nephrology, 2010. Elsevier. pp. 570-581.

Petropoulos, S., Edsgärd, D., Reinius, B., Deng, Q., Panula, S. & Codeluppi, S. (2016). Single-Cell RNA-Seq Reveals Lineage and X Chromosome Dynamics in Human Preimplantation Embryos. Cell [Internet]. Elsevier.

Pisitkun, T., Shen, R.-F. & Knepper, M. A. J. P. o. t. N. A. o. S. (2004). 'Identification and proteomic profiling of exosomes in human urine', 101(36), pp. 13368-13373.

Plisov, S.Y., Yoshino, K., Dove, L.F., Higinbotham, K.G., Rubin, J.S. and Perantoni, A.O., 2001. TGF beta 2, LIF and FGF2 cooperate to induce nephrogenesis. *Development*, *128*(7), pp.1045-1057.

Pope, J. C., Brock, J. W., Adams, M. C., Stephens, F. D. & Ichikawa, I. (1999). 'How They Begin and How They End Classic and New Theories for the Development and Deterioration of Congenital Anomalies of the Kidney and Urinary Tract, CAKUT', *Journal of the American Society of Nephrology,* 10(9), pp. 2018-2028.

Potter, E. (1972). Normal and Abnormal Development of the Kidney. Year Book Medical Publishers. Chicago.

Potter, E. L. (1972). *Normal and abnormal development of the kidney*: Year Book Medical Publishers.

Przepiorski, A., Sander, V., Tran, T., Hollywood, J. A., Sorrenson, B., Shih, J.-H., Wolvetang, E. J., McMahon, A. P., Holm, T. M. & Davidson, A. J. (2018). 'A simple bioreactor-based method to generate kidney organoids from pluripotent stem cells', *Stem cell reports,* 11(2), pp. 470-484.

Putnam, W. C., Swenson, S. M., Reif, G. A., Wallace, D. P., Helmkamp, G. M. & Grantham, J. J. J. J. o. t. A. S. o. N. (2007). 'Identification of a forskolin-like molecule in human renal cysts', 18(3), pp. 934-943.

Qian, C.-N., Knol, J., Igarashi, P., Lin, F., Zylstra, U., Teh, B. T. & Williams, B. O. J. J. o. B. C. (2005). 'Cystic renal neoplasia following conditional inactivation of apc in mouse renal tubular epithelium', 280(5), pp. 3938-3945.

Qian, Q., Hunter, L. W., Li, M., Marin-Padilla, M., Prakash, Y., Somlo, S., Harris, P. C., Torres, V. E. & Sieck, G. C. J. H. m. g. (2003). 'Pkd2 haploinsufficiency alters intracellular calcium regulation in vascular smooth muscle cells', 12(15), pp. 1875-1880.

Queisser-Luft, A., Stolz, G., Wiesel, A., Schlaefer, K. & Spranger, J. (2002). 'Malformations in newborn: results based on 30940 infants and fetuses from the Mainz congenital birth defect monitoring system (1990–1998)', *Archives of gynecology and obstetrics,* 266(3), pp. 163-167.

Radford, R., Slattery, C., Jennings, P., Blacque, O., Pfaller, W., Gmuender, H., Van Delft, J., Ryan, M.P. and McMorrow, T., 2012. Carcinogens induce loss of the primary cilium in human renal proximal tubular epithelial cells independently of effects on the cell cycle. *American Journal of Physiology-Renal Physiology*, *302*(8), pp.F905-F916.

Rak-Raszewska, A., Wilm, B., Edgar, D., Kenny, S., Woolf, A. S. & Murray, P. J. O. (2012). 'Development of embryonic stem cells in recombinant kidneys', 8(4), pp. 125-136.

Reeders, S. T. J. N. g. (1992). 'Multilocus polycystic disease', 1(4), p. 235.

Reidy, K. J. & Rosenblum, N. D. (2009). Cell and molecular biology of kidney development. *In:* Semin Nephrol, 2009. Elsevier. pp. 321-337.

Ring, K. L., Tong, L. M., Balestra, M. E., Javier, R., Andrews-Zwilling, Y., Li, G., Walker, D., Zhang, W. R., Kreitzer, A. C. & Huang, Y. J. C. s. c. (2012). 'Direct reprogramming of mouse and human fibroblasts into multipotent neural stem cells with a single factor', 11(1), pp. 100-109.

Risdon, R. (1971). 'Renal dysplasia Part IA clinico-pathological study of 76 cases', *Journal of clinical pathology,* 24(1), pp. 57-71.

Robinson, A. N., Tebase, B. G., Francone, S. C., Huff, L. M., Kozlowski, H., Cossari, D., Lee, J.-M., Esposito, D., Robey, R. W., Gottesman, M. M. J. D. M. & Disposition (2019). 'Coexpression of ABCB1 and ABCG2 in a Cell Line Model Reveals Both Independent and Additive Transporter Function', 47(7), pp. 715-723.

Rumballe, B. A., Georgas, K. M., Combes, A. N., Ju, A. L., Gilbert, T. & Little, M. H. (2011). 'Nephron formation adopts a novel spatial topology at cessation of nephrogenesis', *Developmental biology,* 360(1), pp. 110-122.

Saadi-Kheddouci, S., Berrebi, D., Romagnolo, B., Cluzeaud, F., Peuchmaur, M., Kahn, A., Vandewalle, A. & Perret, C. J. O. (2001). 'Early development of polycystic kidney disease in transgenic mice expressing an activated mutant of the β-catenin gene', 20(42), p. 5972.

Saarela, U., Akram, S. U., Desgrange, A., Rak-Raszewska, A., Shan, J., Cereghini, S., Ronkainen, V.-P., Heikkilä, J., Skovorodkin, I. & Vainio, S. J. J. D. (2017). 'Novel fixed z-direction (FiZD) kidney primordia and an organoid culture system for time-lapse confocal imaging', 144(6), pp. 1113-1117.

Saburi, S., Hester, I., Fischer, E., Pontoglio, M., Eremina, V., Gessler, M., Quaggin, S. E., Harrison, R., Mount, R. & McNeill, H. J. N. g. (2008). 'Loss of Fat4 disrupts PCP signaling and oriented cell division and leads to cystic kidney disease', 40(8), p. 1010.

Saksela, O., Moscatelli, D., Sommer, A. & Rifkin, D. B. (1988). 'Endothelial cell-derived heparan sulfate binds basic fibroblast growth factor and protects it from proteolytic degradation', *The Journal of cell biology,* 107(2), pp. 743-751.

Sakurai, H., Barros, E.J., Tsukamoto, T., Barasch, J. and Nigam, S.K., 1997. An in vitro tubulogenesis system using cell lines derived from the embryonic kidney shows dependence on multiple soluble growth factors. *Proceedings of the National Academy of Sciences*, *94*(12), pp.6279-6284.

Sanna-Cherchi, S., Caridi, G., Weng, P. L., Scolari, F., Perfumo, F., Gharavi, A. G. & Ghiggeri, G. M. (2007). 'Genetic approaches to human renal agenesis/hypoplasia and dysplasia', *Pediatric nephrology,* 22(10), pp. 1675-1684.

Santoso, N. G., Cebotaru, L., Guggino, W. B. J. C. P. & Biochemistry (2011). 'Polycystin-1, 2, and STIM1 interact with IP3R to modulate ER Ca2+ release through the PI3K/Akt pathway', 27(6), pp. 715-726.

Sanyanusin, P., Schimmenti, L. A., McNoe, L. A., Ward, T. A., Pierpont, M. E. M., Sullivan, M. J., Dobyns, W. B. & Eccles, M. R. (1995). 'Mutation of the PAX2 gene in a family with optic nerve colobomas, renal anomalies and vesicoureteral reflux', *Nature genetics,* 9(4), pp. 358-364.

Sariola, H. (2002). 'Nephron induction revisited: from caps to condensates', *Curr Opin Nephrol Hypertens,* 11(1), pp. 17-21.

Saito, S., Tampe, B., Müller, G.A. and Zeisberg, M., 2015. Primary cilia modulate balance of canonical and non-canonical Wnt signaling responses in the injured kidney. *Fibrogenesis & tissue repair*, *8*(1), p.6.

Sato, A., Matsumoto, Y., Koide, U., Kataoka, Y., Yoshida, N., Yokota, T., Asashima, M. & Nishinakamura, R. (2003). 'Zinc finger protein sall2 is not essential for embryonic and kidney development', *Molecular and cellular biology,* 23(1), pp. 62-69.

Sato, N., Meijer, L., Skaltsounis, L., Greengard, P. & Brivanlou, A. H. (2004). 'Maintenance of pluripotency in human and mouse embryonic stem cells through activation of Wnt signaling by a pharmacological GSK-3-specific inhibitor', *Nature medicine,* 10(1), p. 55.

Saxén, L. & Saxén, L. (1987). *Organogenesis of the Kidney* (Vol. 19): Cambridge University Press.

Schlaeger, T. M., Daheron, L., Brickler, T. R., Entwisle, S., Chan, K., Cianci, A., DeVine, A., Ettenger, A., Fitzgerald, K. & Godfrey, M. (2014). 'A comparison of non-integrating reprogramming methods', *Nature biotechnology*.

Scott, J. & Dorling, J. J. H. (1965). 'Differential staining of acid glycosaminoglycans (mucopolysaccharides) by alcian blue in salt solutions', 5(3), pp. 221-233.

Self, M., Lagutin, O.V., Bowling, B., Hendrix, J., Cai, Y., Dressler, G.R. and Oliver, G., 2006. Six2 is required for suppression of nephrogenesis and progenitor renewal in the developing kidney. *The EMBO journal*, *25*(21), pp.5214-5228.

Shalek, A. K., Satija, R., Shuga, J., Trombetta, J. J., Gennert, D., Lu, D., Chen, P., Gertner, R. S., Gaublomme, J. T. & Yosef, N. J. N. (2014). 'Single-cell RNA-seq reveals dynamic paracrine control of cellular variation', 510(7505), p. 363.

Shan, J., Jokela, T., Skovorodkin, I. & Vainio, S. (2010). 'Mapping of the fate of cell lineages generated from cells that express the Wnt4 gene by time-lapse during kidney development', *Differentiation,* 79(1), pp. 57-64.

Shannon, M. B., Patton, B. L., Harvey, S. J. & Miner, J. H. J. J. o. t. A. S. o. N. (2006). 'A hypomorphic mutation in the mouse laminin α5 gene causes polycystic kidney disease', 17(7), pp. 1913-1922.

Sharmin, S., Taguchi, A., Kaku, Y., Yoshimura, Y., Ohmori, T., Sakuma, T., Mukoyama, M., Yamamoto, T., Kurihara, H. & Nishinakamura, R. J. J. o. t. A. S. o. N. (2016). 'Human induced pluripotent stem cell–derived podocytes mature into vascularized glomeruli upon experimental transplantation', 27(6), pp. 1778-1791.

Shi, S., Yu, L., Chiu, C., Sun, Y., Chen, J., Khitrov, G., Merkenschlager, M., Holzman, L. B., Zhang, W. & Mundel, P. (2008). 'Podocyte-selective deletion of dicer induces proteinuria and glomerulosclerosis', *Journal of the American Society of Nephrology,* 19(11), pp. 2159-2169.

Si-Tayeb, K., Noto, F. K., Sepac, A., Sedlic, F., Bosnjak, Z. J., Lough, J. W. & Duncan, S. A. (2010). 'Generation of human induced pluripotent stem cells by simple transient transfection of plasmid DNA encoding reprogramming factors', *BMC Dev Biol,* 10(1), p. 81.

Simon-Friedt, B. R., Wilson, M. J., Blake, D. A., Yu, H., Eriksson, Y. & Wickliffe, J. K. (2015). 'The RPTEC/TERT1 Cell Line as an Improved Tool for In Vitro Nephrotoxicity Assessments', *Biological Trace Element Research,* 166(1), pp. 66-71.

Smith, L. A., Bukanov, N. O., Husson, H., Russo, R. J., Barry, T. C., Taylor, A. L., Beier, D. R. & Ibraghimov-Beskrovnaya, O. J. J. o. t. A. S. o. N. (2006). 'Development of polycystic kidney disease in juvenile cystic kidney mice: insights into pathogenesis, ciliary abnormalities, and common features with human disease', 17(10), pp. 2821-2831.

Soares, M. L., Haraguchi, S., Torres-Padilla, M.-E., Kalmar, T., Carpenter, L., Bell, G., Morrison, A., Ring, C. J., Clarke, N. J. & Glover, D. M. (2005). 'Functional studies of signaling pathways in peri-implantation development of the mouse embryo by RNAi', *BMC developmental biology,* 5(1), p. 28.

Soldner, F., Hockemeyer, D., Beard, C., Gao, Q., Bell, G. W., Cook, E. G., Hargus, G., Blak, A., Cooper, O. & Mitalipova, M. (2009). 'Parkinson's disease patient-derived induced pluripotent stem cells free of viral reprogramming factors', *Cell,* 136(5), pp. 964-977.

Song, B., Smink, A. M., Jones, C. V., Callaghan, J. M., Firth, S. D., Bernard, C. A., Laslett, A. L., Kerr, P. G. & Ricardo, S. D. (2012). 'The directed differentiation of human iPS cells into kidney podocytes', *PloS one,* 7(9), p. e46453.

Song, Z., Cai, J., Liu, Y., Zhao, D., Yong, J., Duo, S., Song, X., Guo, Y., Zhao, Y. & Qin, H. (2009). 'Efficient generation of hepatocyte-like cells from human induced pluripotent stem cells', *Cell research,* 19(11), pp. 1233-1242.
Spence, J. R., Mayhew, C. N., Rankin, S. A., Kuhar, M. F., Vallance, J. E., Tolle, K., Hoskins, E. E., Kalinichenko, V. V., Wells, S. I. & Zorn, A. M. (2011). 'Directed differentiation of human pluripotent stem cells into intestinal tissue in vitro', *Nature,* 470(7332), p. 105.
Spirli, C., Locatelli, L., Fiorotto, R., Morell, C. M., Fabris, L., Pozzan, T. & Strazzabosco, M. J. H. (2012). 'Altered store operated calcium entry increases cyclic 3', 5'-adenosine monophosphate production and extracellular signal-regulated kinases 1 and 2 phosphorylation in polycystin-2-defective cholangiocytes', 55(3), pp. 856-868.
Stadtfeld, M., Apostolou, E., Akutsu, H., Fukuda, A., Follett, P., Natesan, S., Kono, T., Shioda, T. & Hochedlinger, K. (2010). 'Aberrant silencing of imprinted genes on chromosome 12qF1 in mouse induced pluripotent stem cells', *Nature,* 465(7295), pp. 175-181.
Stark, K., Vainio, S., Vassileva, G. & McMahon, A. P. (1994). 'Epithelial transformation of metanephric mesenchyme in the developing kidney regulated by Wnt-4', *Nature,* 372(6507), p. 679.
Stoll, C., Dott, B., Alembik, Y. & Roth, M.-P. (2014). 'Associated nonurinary congenital anomalies among infants with congenital anomalies of kidney and urinary tract (CAKUT)', *European journal of medical genetics,* 57(7), pp. 322-328.
Suga, H., Kadoshima, T., Minaguchi, M., Ohgushi, M., Soen, M., Nakano, T., Takata, N., Wataya, T., Muguruma, K. & Miyoshi, H. (2011). 'Self-formation of functional adenohypophysis in three-dimensional culture', *Nature,* 480(7375), p. 57.
Sumi, T., Tsuneyoshi, N., Nakatsuji, N. & Suemori, H. (2008). 'Defining early lineage specification of human embryonic stem cells by the orchestrated balance of canonical Wnt/β-catenin, Activin/Nodal and BMP signaling', *Development,* 135(17), pp. 2969-2979.
Sun, H., Li, Q.-W., Lv, X.-Y., Ai, J.-Z., Yang, Q.-T., Duan, J.-J., Bian, G.-H., Xiao, Y., Wang, Y.-D. & Zhang, Z. (2010). 'MicroRNA-17 post-transcriptionally regulates polycystic kidney disease-2 gene and promotes cell proliferation', *Molecular biology reports,* 37(6), pp. 2951-2958.
Sun, Z. & Hopkins, N. (2001). 'vhnf1, the MODY5 and familial GCKD-associated gene, regulates regional specification of the zebrafish gut, pronephros, and hindbrain', *Genes & development,* 15(23), pp. 3217-3229.
Surani, M. A. (1999). Reprogramming a somatic nucleus by trans-modification activity in germ cells. *In:* Seminars in cell & developmental biology, 1999. Elsevier. pp. 273-277.
Sweeney, D., Lindström, N. & Davies, J. A. (2008). 'Developmental plasticity and regenerative capacity in the renal ureteric bud/collecting duct system', *Development,* 135(15), pp. 2505-2510.
Taguchi, A., Kaku, Y., Ohmori, T., Sharmin, S., Ogawa, M., Sasaki, H. & Nishinakamura, R. (2014). 'Redefining the in vivo origin of metanephric nephron progenitors enables generation of complex kidney structures from pluripotent stem cells', *Cell stem cell,* 14(1), pp. 53-67.
Takahashi, K. & Yamanaka, S. (2006). 'Induction of pluripotent stem cells from mouse embryonic and adult fibroblast cultures by defined factors', *Cell,* 126(4), pp. 663-676.
Takasato, M., Er, P., Becroft, M., Vanslambrouck, J., Stanley, E., Elefanty, A. & Little, M. (2014a). 'Directing human embryonic stem cell differentiation towards a renal lineage generates a self-organizing kidney', *Nature cell biology,* 16(1), pp. 118-126.
Takasato, M., Er, P., Becroft, M., Vanslambrouck, J. M., Stanley, E., Elefanty, A. G. & Little, M. H. (2014b). 'Directing human embryonic stem cell differentiation towards a renal lineage generates a self-organizing kidney', *Nature cell biology,* 16(1), p. 118.
Takasato, M. & Little, M. H. (2015). 'The origin of the mammalian kidney: implications for recreating the kidney in vitro', *Development,* 142(11), pp. 1937-1947.
Takasato, M., Maier, B. & Little, M. H. (2014c). 'Recreating kidney progenitors from pluripotent cells', *Pediatric Nephrology,* 29(4), pp. 543-552.
Takasato, M., Pei, X. E., Chiu, H. S. & Little, M. H. (2016). 'Generation of kidney organoids from human pluripotent stem cells', *Nature protocols,* 11(9), p. 1681.
Takasato, M., Pei, X. E., Chiu, H. S., Maier, B., Baillie, G. J., Ferguson, C., Parton, R. G., Wolvetang, E. J., Roost, M. S. & de Sousa Lopes, S. M. C. (2015a). 'Kidney organoids from human iPS cells contain multiple lineages and model human nephrogenesis', *Nature,* 526(7574), p. 564.
Takasato, M., Pei, X. E., Chiu, H. S., Maier, B., Baillie, G. J., Ferguson, C., Parton, R. G., Wolvetang, E. J., Roost, M. S. & de Sousa Lopes, S. M. C. (2015b). 'Kidney organoids from human iPS cells contain multiple lineages and model human nephrogenesis', *Nature*.
Takebe, T., Enomura, M., Yoshizawa, E., Kimura, M., Koike, H., Ueno, Y., Matsuzaki, T., Yamazaki, T., Toyohara, T. & Osafune, K. J. C. s. c. (2015). 'Vascularized and complex organ buds from diverse tissues via mesenchymal cell-driven condensation', 16(5), pp. 556-565.
Tam, P. P. & Loebel, D. A. (2007). 'Gene function in mouse embryogenesis: get set for gastrulation', *Nature Reviews Genetics,* 8(5), pp. 368-381.
Tan, A. Y., Zhang, T., Michaeel, A., Blumenfeld, J., Liu, G., Zhang, W., Zhang, Z., Zhu, Y., Rennert, L. & Martin, C. J. J. o. t. A. S. o. N. (2018). 'Somatic mutations in renal cyst epithelium in autosomal dominant polycystic kidney disease', 29(8), pp. 2139-2156.
Tarantal, A. F., Han, V. K., Cochrum, K. C., Mok, A., Dasilva, M. & Matsell, D. G. J. K. i. (2001). 'Fetal rhesus monkey model of obstructive renal dysplasia', 59(2), pp. 446-456.
Taurin, S., Sandbo, N., Qin, Y., Browning, D. & Dulin, N. O. J. J. o. B. C. (2006). 'Phosphorylation of β-catenin by cyclic AMP-dependent protein kinase', 281(15), pp. 9971-9976.
Tesar, P. J., Chenoweth, J. G., Brook, F. A., Davies, T. J., Evans, E. P., Mack, D. L., Gardner, R. L. & McKay, R. D. (2007). 'New cell lines from mouse epiblast share defining features with human embryonic stem cells', *Nature,* 448(7150), pp. 196-199.

Thomas, R., Sanna-Cherchi, S., Warady, B. A., Furth, S. L., Kaskel, F. J. & Gharavi, A. G. (2011). 'HNF1B and PAX2 mutations are a common cause of renal hypodysplasia in the CKiD cohort', *Pediatric nephrology,* 26(6), pp. 897-903.
Thomson, J. A., Itskovitz-Eldor, J., Shapiro, S. S., Waknitz, M. A., Swiergiel, J. J., Marshall, V. S. & Jones, J. M. (1998). 'Embryonic stem cell lines derived from human blastocysts', *science,* 282(5391), pp. 1145-1147.
Thomson, J. A. & Marshall, V. S. (1997). 'Primate Embryonic Stem Cells', *Current topics in developmental biology,* 38, pp. 133-165.
Thorner (1995). 'Kidneys and lower urinary tract', *In Diseases of the Fetus and Newborn.* Eds Reed GB et al. ed. London: Chapman and Hall Medicalpp. 609–661.
Tiscornia, G., Vivas, E. L. & Belmonte, J. C. I. (2011). 'Diseases in a dish: modeling human genetic disorders using induced pluripotent cells', *Nature medicine,* 17(12), pp. 1570-1576.
Torres, M., Gómez-Pardo, E., Dressler, G. R. & Gruss, P. (1995). 'Pax-2 controls multiple steps of urogenital development', *Development,* 121(12), pp. 4057-4065.
Torres, V. E. & Harris, P. C. J. J. o. t. A. S. o. N. (2014). 'Strategies targeting cAMP signaling in the treatment of polycystic kidney disease', 25(1), pp. 18-32.
Tsang, T. E., Shawlot, W., Kinder, S. J., Kobayashi, A., Kwan, K. M., Schughart, K., Kania, A., Jessell, T. M., Behringer, R. R. & Tam, P. P. (2000). 'Lim1 activity is required for intermediate mesoderm differentiation in the mouse embryo', *Developmental biology,* 223(1), pp. 77-90.
Tsiokas, L., Arnould, T., Zhu, C., Kim, E., Walz, G. & Sukhatme, V. P. J. P. o. t. N. A. o. S. (1999). 'Specific association of the gene product of PKD2 with the TRPC1 channel', 96(7), pp. 3934-3939.
Uchiyama, Y., Sakaguchi, M., Terabayashi, T., Inenaga, T., Inoue, S., Kobayashi, C., Oshima, N., Kiyonari, H., Nakagata, N. & Sato, Y. (2010). 'Kif26b, a kinesin family gene, regulates adhesion of the embryonic kidney mesenchyme', *Proceedings of the National Academy of Sciences,* 107(20), pp. 9240-9245.
Ulinski, T., Lescure, S., Beaufils, S., Guigonis, V., Decramer, S., Morin, D., Clauin, S., Deschênes, G., Bouissou, F. & Bensman, A. (2006a). 'Renal phenotypes related to hepatocyte nuclear factor-1β (TCF2) mutations in a pediatric cohort', *Journal of the American Society of Nephrology,* 17(2), pp. 497-503.
Vallier, L., Alexander, M. & Pedersen, R. A. (2005). 'Activin/Nodal and FGF pathways cooperate to maintain pluripotency of human embryonic stem cells', *J Cell Sci,* 118(19), pp. 4495-4509.
van Adelsberg, J. S. & Frank, D. (1995). 'The PKD1 gene produces a developmentally regulated protein in mesenchyme and vasculature', *Nature medicine,* 1(4), p. 359.
van den Berg, C. W., Ritsma, L., Avramut, M. C., Wiersma, L. E., van den Berg, B. M., Leuning, D. G., Lievers, E., Koning, M., Vanslambrouck, J. M. & Koster, A. J. (2018). 'Renal subcapsular transplantation of PSC-derived kidney organoids induces neo-vasculogenesis and significant glomerular and tubular maturation in vivo', *Stem Cell Reports,* 10(3), pp. 751-765.
Van Winkle, A. P., Gates, I. D. & Kallos, M. S. (2012). 'Mass transfer limitations in embryoid bodies during human embryonic stem cell differentiation', *Cells Tissues Organs,* 196(1), pp. 34-47.
Verdeguer, F., Le Corre, S., Fischer, E., Callens, C., Garbay, S., Doyen, A., Igarashi, P., Terzi, F. & Pontoglio, M. (2010). 'A mitotic transcriptional switch in polycystic kidney disease', *Nature medicine,* 16(1), pp. 106-110.
Vigneau, C., Polgar, K., Striker, G., Elliott, J., Hyink, D., Weber, O., Fehling, H.-J., Keller, G., Burrow, C. & Wilson, P. (2007). 'Mouse embryonic stem cell–derived embryoid bodies generate progenitors that integrate long term into renal proximal tubules in vivo', *Journal of the American Society of Nephrology,* 18(6), pp. 1709-1720.
Vivante, A., Kohl, S., Hwang, D.-Y., Dworschak, G. C. & Hildebrandt, F. (2014). 'Single-gene causes of congenital anomalies of the kidney and urinary tract (CAKUT) in humans', *Pediatric nephrology,* 29(4), pp. 695-704.
Wallace, D. P., Quante, M. T., Reif, G. A., Nivens, E., Ahmed, F., Hempson, S. J., Blanco, G. & Yamaguchi, T. J. A. J. o. P.-R. P. (2008). 'Periostin induces proliferation of human autosomal dominant polycystic kidney cells through αV-integrin receptor', 295(5), pp. F1463-F1471.
Wang, X., Ward, C. J., Harris, P. C. & Torres, V. E. J. K. i. (2010). 'Cyclic nucleotide signaling in polycystic kidney disease', 77(2), pp. 129-140.
Wang, X., Wu, Y., Ward, C.J., Harris, P.C. and Torres, V.E., 2008. Vasopressin directly regulates cyst growth in polycystic kidney disease. *Journal of the American Society of Nephrology*, *19*(1), pp.102-108.
Wang, Z., Oron, E., Nelson, B., Razis, S. & Ivanova, N. (2012). 'Distinct lineage specification roles for NANOG, OCT4, and SOX2 in human embryonic stem cells', *Cell Stem Cell,* 10(4), pp. 440-454.
Watanabe, T. & Costantini, F. (2004). 'Real-time analysis of ureteric bud branching morphogenesis in vitro', *Developmental biology,* 271(1), pp. 98-108.
Weber, E. J., Chapron, A., Chapron, B. D., Voellinger, J. L., Lidberg, K. A., Yeung, C. K., Wang, Z., Yamaura, Y., Hailey, D. W. & Neumann, T. J. K. i. (2016). 'Development of a microphysiological model of human kidney proximal tubule function', 90(3), pp. 627-637.
Weber, S., Moriniere, V., Knüppel, T., Charbit, M., Dusek, J., Ghiggeri, G. M., Jankauskiené, A., Mir, S., Montini, G. & Peco-Antic, A. (2006). 'Prevalence of mutations in renal developmental genes in children with renal hypodysplasia: results of the ESCAPE study', *Journal of the American Society of Nephrology,* 17(10), pp. 2864-2870.
Wei, Q., Mi, Q. S. & Dong, Z. (2013). 'The regulation and function of microRNAs in kidney diseases', *IUBMB life,* 65(7), pp. 602-614.
Wei, Z., Gao, F., Kim, S., Yang, H., Lyu, J., An, W., Wang, K. & Lu, W. J. C. s. c. (2013). 'Klf4 organizes long-range chromosomal interactions with the oct4 locus in reprogramming and pluripotency', 13(1), pp. 36-47.

Wellik, D. M., Hawkes, P. J. & Capecchi, M. R. (2002). 'Hox11 paralogous genes are essential for metanephric kidney induction', *Genes & development,* 16(11), pp. 1423-1432.
Whyte, W. A., Orlando, D. A., Hnisz, D., Abraham, B. J., Lin, C. Y., Kagey, M. H., Rahl, P. B., Lee, T. I. & Young, R. A. J. C. (2013). 'Master transcription factors and mediator establish super-enhancers at key cell identity genes', 153(2), pp. 307-319.
Wild, W., von Strandmann, E. P., Nastos, A., Senkel, S., Lingott-Frieg, A., Bulman, M., Bingham, C., Ellard, S., Hattersley, A. T. & Ryffel, G. U. (2000). 'The mutated human gene encoding hepatocyte nuclear factor 1β inhibits kidney formation in developing Xenopus embryos', *Proceedings of the National Academy of Sciences,* 97(9), pp. 4695-4700.
Wilson, P. D. J. J. o. t. A. S. o. N. (2001). 'Polycystin: new aspects of structure, function, and regulation', 12(4), pp. 834-845.
Wingert, R. A. & Davidson, A. J. (2011). 'Zebrafish nephrogenesis involves dynamic spatiotemporal expression changes in renal progenitors and essential signals from retinoic acid and irx3b', *Developmental Dynamics,* 240(8), pp. 2011-2027.
Winyard, P. J., Nauta, J., Lirenman, D. S., Hardman, P., Sams, V. R., Risdon, R. A. & Woolf, A. S. (1996). 'Deregulation of cell survival in cystic and dysplastic renal development', *Kidney international,* 49(1), pp. 135-146.
Woolf, A. & Jenkins, D. (2006). 'Development of the kidney', *Heptinstall's Pathology of the Kidney*, pp. 71-95.
Woolf, A. S. & Davies, J. A. (2012). 'Cell biology of ureter development', *Journal of the American Society of Nephrology*, p. ASN. 2012020127.
Woolf, A. S., Feather, S. A. & Bingham, C. (2002). 'Recent insights into kidney diseases associated with glomerular cysts', *Pediatric nephrology,* 17(4), pp. 229-235.
Woolf, A. S., Price, K. L., Scambler, P. J. & Winyard, P. J. (2004). 'Evolving concepts in human renal dysplasia', *Journal of the American Society of Nephrology,* 15(4), pp. 998-1007.
Wu, H., Uchimura, K., Donnelly, E. L., Kirita, Y., Morris, S. A. & Humphreys, B. D. (2018). 'Comparative analysis and refinement of human PSC-derived kidney organoid differentiation with single-cell transcriptomics', *Cell Stem Cell,* 23(6), pp. 869-881. e8.
Wu, S. M. & Hochedlinger, K. (2011). 'Harnessing the potential of induced pluripotent stem cells for regenerative medicine', *Nature cell biology,* 13(5), pp. 497-505.
Wu, W., Kitamura, S., Truong, D. M., Rieg, T., Vallon, V., Sakurai, H., Bush, K. T., Vera, D. R., Ross, R. S. & Nigam, S. K. J. A. J. o. P.-R. P. (2009). 'β1-Integrin is required for kidney collecting duct morphogenesis and maintenance of renal function', 297(1), pp. F210-F217.
Wühl, E., van Stralen, K. J., Verrina, E., Bjerre, A., Wanner, C., Heaf, J. G., Zurriaga, O., Hoitsma, A., Niaudet, P. & Palsson, R. (2013). 'Timing and outcome of renal replacement therapy in patients with congenital malformations of the kidney and urinary tract', *Clinical Journal of the American Society of Nephrology,* 8(1), pp. 67-74.
Xia, Y., Nivet, E., Sancho-Martinez, I., Gallegos, T., Suzuki, K., Okamura, D., Wu, M.-Z., Dubova, I., Esteban, C. R. & Montserrat, N. (2013). 'Directed differentiation of human pluripotent cells to ureteric bud kidney progenitor-like cells', *Nature cell biology,* 15(12), p. 1507.
Xu, C., Rossetti, S., Jiang, L., Harris, P. C., Brown-Glaberman, U., Wandinger-Ness, A., Bacallao, R. & Alper, S. L. J. A. J. o. P.-R. P. (2007). 'Human ADPKD primary cyst epithelial cells with a novel, single codon deletion in the PKD1 gene exhibit defective ciliary polycystin localization and loss of flow-induced Ca2+ signaling', 292(3), pp. F930-F945.
Yamaguchi, T., Hempson, S. J., Reif, G. A., Hedge, A.-M. & Wallace, D. P. J. J. o. t. a. s. o. n. (2006). 'Calcium restores a normal proliferation phenotype in human polycystic kidney disease epithelial cells', 17(1), pp. 178-187.
Yamaguchi, T., Nagao, S., Kasahara, M., Takahashi, H. & Grantham, J. J. (1997). 'Renal accumulation and excretion of cyclic adenosine monophosphate in a murine model of slowly progressive polycystic kidney disease', *Am J Kidney Dis,* 30(5), pp. 703-9.
Yamanaka, S. (2012). 'Induced pluripotent stem cells: past, present, and future', *Cell Stem Cell,* 10(6), pp. 678-684.
Yamazaki, T., Nalbandian, A., Uchida, Y., Li, W., Arnold, T.D., Kubota, Y., Yamamoto, S., Ema, M. and Mukouyama, Y.S., 2017. Tissue myeloid progenitors differentiate into pericytes through TGF-β signaling in developing skin vasculature. *Cell reports*, *18*(12), pp.2991-3004.
Yang, S. P., Woolf, A. S., Quinn, F. & Winyard, P. J. J. T. A. j. o. p. (2001). 'Deregulation of renal transforming growth factor-β1 after experimental short-term ureteric obstruction in fetal sheep', 159(1), pp. 109-117.
Yayon, A., Klagsbrun, M., Esko, J. D., Leder, P. & Ornitz, D. M. (1991). 'Cell surface, heparin-like molecules are required for binding of basic fibroblast growth factor to its high affinity receptor', *Cell,* 64(4), pp. 841-848.
Ye, J., Bates, N., Soteriou, D., Grady, L., Edmond, C., Ross, A., Kerby, A., Lewis, P. A., Adeniyi, T., Wright, R. J. S. c. r. & therapy (2017). 'High quality clinical grade human embryonic stem cell lines derived from fresh discarded embryos', 8(1), p. 128.
Yildirim, S. (2012). *Induced pluripotent stem cells*: Springer Science & Business Media.
Yosypiv, I. V. (2008). 'A new role for the renin-angiotensin system in the development of the ureteric bud and renal collecting system', *The Keio journal of medicine,* 57(4), p. 184.
Yu, J., Hu, K., Smuga-Otto, K., Tian, S., Stewart, R., Slukvin, I. I. & Thomson, J. A. (2009). 'Human induced pluripotent stem cells free of vector and transgene sequences', *science,* 324(5928), pp. 797-801.
Yu, J., Vodyanik, M. A., Smuga-Otto, K., Antosiewicz-Bourget, J., Frane, J. L., Tian, S., Nie, J., Jonsdottir, G. A., Ruotti, V. & Stewart, R. (2007). 'Induced pluripotent stem cell lines derived from human somatic cells', *science,* 318(5858), pp. 1917-1920.

Zaghloul, N.A. and Brugmann, S.A., 2011. The emerging face of primary cilia. *Genesis*, *49*(4), pp.231-246.

Zaika, O., Mamenko, M., Berrout, J., Boukelmoune, N., O'Neil, R. G. & Pochynyuk, O. J. J. o. t. A. S. o. N. (2013). 'TRPV4 dysfunction promotes renal cystogenesis in autosomal recessive polycystic kidney disease', 24(4), pp. 604-616.

Zeng, Y., Zhang, R., Wu, J., Liu, M., Peng, W., Yu, X., Yang, X. J. H. & toxicology, e. (2012). 'Organic anion transporter 1 (OAT1) involved in renal cell transport of aristolochic acid I', 31(8), pp. 759-770.

Zent, R., Bush, K. T., Pohl, M. L., Quaranta, V., Koshikawa, N., Wang, Z., Kreidberg, J. A., Sakurai, H., Stuart, R. O. & Nigám, S. K. J. D. b. (2001). 'Involvement of laminin binding integrins and laminin-5 in branching morphogenesis of the ureteric bud during kidney development', 238(2), pp. 289-302.

Zhang, J., Lian, Q., Zhu, G., Zhou, F., Sui, L., Tan, C., Mutalif, R. A., Navasankari, R., Zhang, Y. & Tse, H.-F. (2011). 'A human iPSC model of Hutchinson Gilford Progeria reveals vascular smooth muscle and mesenchymal stem cell defects', *Cell Stem Cell,* 8(1), pp. 31-45.

Zhang, X., Ibrahimi, O. A., Olsen, S. K., Umemori, H., Mohammadi, M. & Ornitz, D. M. (2006). 'Receptor specificity of the fibroblast growth factor family The complete mammalian fgf family', *Journal of Biological Chemistry,* 281(23), pp. 15694-15700.

Zhao, S., Nichols, J., Smith, A. G., Li, M. J. M. & Neuroscience, C. (2004). 'SoxB transcription factors specify neuroectodermal lineage choice in ES cells', 27(3), pp. 332-342.

Zhdanova, O., Srivastava, S., Di, L., Li, Z., Tchelebi, L., Dworkin, S., Johnstone, D. B., Zavadil, J., Chong, M. M. & Littman, D. R. (2011). 'The inducible deletion of Drosha and microRNAs in mature podocytes results in a collapsing glomerulopathy', *Kidney international,* 80(7), pp. 719-730.